Savannah River National Laboratory®

A U.S. DEPARTMENT OF ENERGY NATIONAL LAB • SAVANNAH RIVER SITE • AIKEN, SC • USA

Research and Development Year 1 Report for Award # 277993: Integrity Monitoring and Assessment, Prediction, Repair, and Corrosion Control of the Hanford Storage Tanks

Pavan K. Shukla
Mark Kranjc
Bruce Wiersma
Benjamin Barkai
Kiana Sykes
Kareen Blue
Nicholas Valdes
Christine Langton

October 2025

SRNL-RP-2025-01426, Revision # 0

DISCLAIMER

Printed in the United States of America

Prepared for
U.S. Department of Energy

SRNL-RP-2025-01426
Revision 0

Keywords: Corrosion, Waste Tank Integrity, Corrosion Monitoring, Reference Electrode, Cathodic Protection

Retention: Permanent

Tracking Number: SRNL-RP-2025-01426

Research and Development Year 1 Report for Award # 277993: Integrity Monitoring and Assessment, Prediction, Repair, and Corrosion Control of the Hanford Storage Tanks

Pavan K. Shukla
Mark Kranjc
Bruce Wiersma
Benjamin Barkai
Kiana Sykes
Kareen Blue
Nicholas Valdes
Christine Langton

October 2025

Savannah River National Laboratory is operated by Battelle Savannah River Alliance for the U.S. Department of Energy under Contract No. 89303321CEM000080

Reviews and Approvals

AUTHORS:

PAVAN SHUKLA (Affiliate) Digitally signed by PAVAN SHUKLA (Affiliate)
Date: 2025.10.07 13:26:49 -04'00'

P. K. Shukla, SRNL Date

MARK KRANJC (Affiliate) Digitally signed by MARK KRANJC (Affiliate)
Date: 2025.10.07 14:24:13 -04'00'

M. Kranjc, SRNL Date

BRUCE WIERSMA (Affiliate) Digitally signed by BRUCE WIERSMA (Affiliate)
Date: 2025.10.07 14:54:02 -04'00'

B.J. Wiersma, SRNL Date

BENJAMIN BARKAI (Affiliate) Digitally signed by BENJAMIN BARKAI (Affiliate)
Date: 2025.10.07 15:16:19 -04'00'

B. Barkai, SRNL Date

KIANA SYKES (Affiliate) Digitally signed by KIANA SYKES (Affiliate)
Date: 2025.10.08 09:26:46 -04'00'

K. Sykes, SRNL Date

KAREEN BLUE (Affiliate) Digitally signed by KAREEN BLUE (Affiliate)
Date: 2025.10.08 09:42:35 -04'00'

K. Blue, SRNL Date

NICHOLAS VALDES (Affiliate) Digitally signed by NICHOLAS VALDES (Affiliate)
Date: 2025.10.08 09:53:52 -04'00'

N. Valdes, SRNL Date

CHRISTINE LANGTON (Affiliate) Digitally signed by CHRISTINE LANGTON (Affiliate)
Date: 2025.10.08 10:13:39 -04'00'

C. Langton, SRNL Date

TECHNICAL REVIEWER:

MORGANA WHITESIDE (Affiliate)

Digitally signed by MORGANA WHITESIDE (Affiliate)
Date: 2025.10.08 10:56:32 -04'00'

M. Whiteside, SRNL Date

APPROVAL:

JOSEPH MANNA (Affiliate)

Digitally signed by JOSEPH MANNA (Affiliate)
Date: 2025.10.08 11:21:34 -04'00'

J. Manna, SRNL/Director, Materials Technology & Energy Sciences Division Date

MICHAEL STONE (Affiliate)

Digitally signed by MICHAEL STONE (Affiliate)
Date: 2025.10.08 12:31:10 -04'00'

M. Stone, SRNL/DOE-EM Program Manager Date

Table of Contents

List of Tables

List of Abbreviations

DOE	Department of Energy
DST	Double Shell Tank
CP	Cathodic Protection
LDR	Land Disposal Restricted
FEM	Finite Element Method
WRPS	Washington Rive Protection Solutions
H2C	Hanford Tank Waste Operations & Closure
DoE	Design of Experiments

Acknowledgments

The authors thank Dr. Ming Zhu and John Kelly for their helpful contributions and support. SRNL appreciates the opportunity to continue supporting DOE-EM in Hanford Tank Waste Mission Acceleration in FY26.

The authors thank Ms. Amy Ramsey for the project control and management and Ms. Pat Smith for helping support the subcontracting process with various industry partners.

Executive Summary

U.S. Department of Energy (DOE) launched a multi-year research program with the focus of preserving and increasing available volume for waste storage at Hanford. The Office of Environmental Management Award #277993 titled "Integrity Monitoring and Assessment, Prediction, Repair, and Corrosion Control of the Hanford Storage Tanks" is the focus of this year one report. The long-term availability and operability of the Hanford Double Shell Tanks (DST) is critical to the completion of the Hanford mission. Maintaining the integrity of the tank will involve having a technology for repair or refurbishment of a DST should the tank function be compromised by degradation, thus monitoring the tank for indications of accelerated degradation is of importance. Clearly developing a means for mitigating accelerated degradation is of high value as will be evaluating options for increasing the storage capacity in the tank farm without construction of costly new tanks. The project work was started in the middle of 2024, with significant progress being made in the following four areas: (i) Task 1 — tank refurbishment using a high-performance grout and an epoxy sealant layer system, (ii) Task 2 — developing a chemically and radiologically stable reference electrode, (iii) Task 3 — designing and implementing a cathodic protection system to mitigate underside corrosion of DST secondary shells, and (iv) Task 4 — exploring evaporation to increase waste storage capacity and cost benefit analysis of the existing tanks' refurbishment versus new tank construction.

Year 1 progress on Task 1 included identification of epoxy formulations suitable for in-tank applications, conceptualization of two-layer system to account for the potential tank bottom surface conditions, and progress with grout formulation testing. The two layer-system consists of a grout-layer at the bottom, directly in contact with the tank bottom, and an epoxy layer on top of the grout layer.

Year 1 progress of Task 2 included an exhaustive review of the literature and previous testing data to determine the failure modes of the commercially available reference electrode that have been used in the Hanford tank farm complex; the literature and data review indicated that the chemical transmission path between the reference electrode junction and the sensing wire get contaminated by the hydroxy ions, leading to failure of the reference electrodes. A design concept was developed to enhance the reference electrode performance in the Hanford waste tank chemical and radiation environments. In addition, testing was conducted to establish performance of various materials as replacements in the commercially available reference electrodes.

Year 1 progress of Task 3 included a literature review of cathodic protection (CP) methodologies in concrete structures. CP is one of the corrosion mitigation tools for controlling underside corrosion of the DSTs' secondary shells. Because each Hanford tank farm has an existing CP system to protect buried transfer lines, a finite element method (FEM) based model was needed to understand the current distribution of a combined CP system consisting of the existing and proposed CP system. The FEM model was partially built to represent tanks at the AN tank farm at Hanford. Relevant details of the tank farm were obtained and analyzed and complexities of the multitude of the buried structures were incorporated in the FEM model.

Year 1 progress on Task 4 included developing a computational framework to determine the effect of evaporation on generating additional storage with Hanford DST tanks farms. The framework was exercised on several tank supernatants and it was determined that the evaporation option can not only result in additional storage but also result in reducing land-disposal restricted (LDR) organics in the tank waste.

1.0 Introduction

Savannah River National Laboratory has been tasked to develop methods and technologies to increase storage volume for the high-level waste storage at the DOE Hanford complex. The Office of Environmental Management Award #277993 titled "Integrity Monitoring and Assessment, Prediction, Repair, and Corrosion Control of the Hanford Storage Tanks" is the focus of this year one report. To this end, the following activities with specific goals have been undertaken: (i) Task 1: refurbishing existing tanks with a combination of high-performance grout and polymeric layers for the double shell tanks (DSTs), (ii) Task 2: developing a chemically and radiologically robust reference electrode to monitor corrosive conditions of the tank waste chemistry and its propensity to cause localized corrosion in the form of pitting corrosion, (iii) Task 3: determining applicability of the cathodic protection technology to prevent underside corrosion of the secondary shells of the DST, and (iv) Task 4: evaluating evaporation and its consequences towards the end goal of increase storage and concurrently performing a cost-benefit analysis for constructing new tanks versus repairing existing tanks. The overall project team consists of:

Savannah River National Laboratory	Lead, Contracting, Program Management
Florida Internation University	High-performance grout and polymeric material
DNV Columbus	Testing for developing robust reference electrode
CorrPro Companies	Cathodic Protection Design Development
Finite Element Expert	Develop Model to Support Cathodic Protection Design Effort

This program also obtained significant support from the DOE Hanford Field Office and site contractors (WRPS and H2C).

The program was initiated in the second quarter of the calendar year 2024. Year 1 activities included subcontracting (team acquisition), kick-off and various workshop meetings to define specific activities and accomplishment of various project milestones.

2.0 Accomplishments

Research is being conducted to develop a two-layer system, consisting of a grout and an epoxy layer, for refurbishing primary tank bottoms that might have thinned by corrosion. The proposed two-layer system involves installing a 6 to 12 inch thick "false" grout layer at the bottom and laying an epoxy layer over the grout. As the system is to be delivered inside the existing underground DSTs, the constraints of risers and tank bottom surface conditions have been considered in the development and selection of the materials. For example, grout materials are to be flowable and pumpable to allow delivery into the tank through the 4-ich risers. Similarly, the workability time for the epoxy layer must be sufficiently high to be able to seal the grout layer. Numerous material testing of the epoxy formulations were carried out and grout formulations were identified to meet the various functional requirements.

Reference electrodes are used in the DSTs to indirectly measure the corrosivity of the waste in the tanks. However, the service-life of commercially available reference electrodes range from a few months to three years; failure of reference electrode can cast doubt on the validity of measured data and repeat replacements will cause operational costs and increased risks for occupational radiation dosages. Therefore, the objective is to develop a chemically and radiologically stable reference electrode with a minimum service life of 10 years. Various design concepts were developed, and reference electrode manufacturers were contacted for fabrication of the prototypes. H-cell testing was conducted for developing a down-selection of the materials that will be used in the prototypes. The prototypes will be

developed in collaboration with the reference electrode manufacturers and will undergo accelerated testing in radiation and chemical environments enveloping the DST waste chemistry.

Ultrasonic inspections have indicated that the exterior of several of the DST secondary liners have experienced significant wall thinning (up to 70% wall thinning in one case). Corrosion due to infiltration of groundwater into the region beneath the tank may be the cause of the degradation. The feasibility of applying cathodic protection (CP) to protect the exterior of the secondary liner of the DST from corrosion is being explored. CP designs for the DSTs were developed based on conventional approaches. In addition, the CP design was analyzed to determine its effects on the foundation rebars. The designs will be computationally implemented into a finite-element model to account for complexities that could arise from other components in a tank farm, such as transfer lines, risers, and pre-existing CP systems.

Approximately 211 million liters of radioactive waste are stored at the Hanford site, a large portion of which is inside the 27 in-service double-shell tanks DSTs. While the DSTs have a combined total capacity of approximately 117 million liters, only 15 million liters of free or additional space remain inside the tanks. As waste is retrieved from the single shell tanks and transferred into the DSTs, additional storage will be required. Constructing new tanks is cost prohibitive and counter to the tank closure mission. Therefore, vacuum evaporation of the water-rich, liquid-phase supernatant layer inside the DSTs was considered. Because almost 80% of all DST waste by volume appears as supernate, vacuum evaporation can lead to significant amount of added storage capacity. Simulations of the DST supernate were created and vacuum evaporation was simulated at 60 Torr and 50 °C. The simulation results indicated that roughly 11 million liters of storage volume can be obtained by concentrating the supernate among eight tanks, with minimal changes to pitting factor and solid precipitation; the storage volume obtained by evaporative treatment of the supernate is equivalent to the construction of 2-3 DSTs. The evaporation could also be applied for the removal of Land Disposal Restricted (LDR) organics in pre-treated waste, with some LDRs removal yield at up to 99 percent. A report detailing the evaporation was compiled and reviewed and referenced below.

3.0 Deliverables

Various Year 1 deliverables and their status is listed in Table 1. The deliverable documents are also appended in at the end of this report.

Table 1. Year 1 Deliverables for Award Number 277993

Deliverable	Status	Document Number	Notes
1. Complete literature review to assess alternatives for epoxy and cement/aggregates for base formula (Task 1)	Completed	SRNL-STI-2024-00627	Literature review to identify alternative materials has been documented in SRNL-STI-2024-00627 which was also presented at WM 2025. The document is appended in Appendix A.
2. Complete formulation development related to the polymer grout materials (Task 1)	Completed	SRNL-RP-2025-00085 SRNL-TR-2025-00233	Initial testing indicated that mixing and using a combination of polymer and grout

Table 1. Year 1 Deliverables for Award Number 277993			
Deliverable	**Status**	**Document Number**	**Notes**
			material is infeasible, therefore, a two-layer approach has been developed. Testing results are presented in SRNL-RP-2025-00085 and the two-layer approach is described in SRNL-TR-2025-00233 The documents are appended in Appendix A.
3. Start determination of test methodologies and Design of Experiments (DoE) (Task 1)	Completed	SRNL-RP-2025-00085 SRNL-TR-2025-00233 SRNL-RP-2025-00379	The testing methodologies are detailed in SRNL-RP-2025-00085 and the initial development of the design of experiments is described in SRNL-TR-2025-00233 and SRNL-RP-2025-00379. The first two documents for Deliverables 2 and 3 are the same. The last document (SRNL-RP-2025-00379) is appended in Appendix A.
4. Complete literature review to identify weaknesses in reference electrode materials (Task 2)	Completed	SRNL-STI-2024-00539	A comprehensive literature review related to history and technical details of the commercially available reference electrodes has been documented in SRNL-STI-2024-00539. The document is included in Appendix B.

Table 1. Year 1 Deliverables for Award Number 277993			
Deliverable	**Status**	**Document Number**	**Notes**
5. Complete identification of candidate materials, test protocols, and DoE (Task 2)	Completed	SRNL-MS-2025-00158 SRNL-RP-2025-00647	The reference electrode junction materials have been identified as the materials needing improvements to enable robust electrode development. Several candidate materials have been identified in SRNL-MS-2025-00158, and design of the experiments including the test matrix is detailed in SRNL-RP-2025-00647. The documents are included in Appendix B.
6. Start development of prototype reference electrode (Task 2)	Completed	SRNL-RP-2025-00647	Initial development approach for making more robust reference electrodes is provided in SRNL-RP-2025-00647. The document for this item is the same as the one of the documents for Deliverable 5, and is included in Appendix B.
7. Literature review of Cathodic Protection (CP) System for Concrete (Task 3)	Complete	SRNL-STI-2024-00435	The compiled literature information provided useful and critical parameters associated with the usage of CP in concrete related systems. The document is included in Appendix C.
8. Complete collection of existing CP system details for a given Hanford tank farm (Task 3)	Partially completed	SRNL-STI-2025-00209	All the relevant drawing associated with a tank farm were obtained, however, existing CP system

Table 1. Year 1 Deliverables for Award Number 277993			
Deliverable	**Status**	**Document Number**	**Notes**
			layout and the rectifier and anode output data associated with buried pipelines were not available within Year 1. The progress made in Year 1 was included in the document which is included in Appendix C.
9. Complete development of close-couple CP system design for DSTs (Task 3)	Not completed	—	The task was to be completed by the subcontractor CorrPro, however, because of subcontracting delays and resulting slow-start with the subcontractor, this task was not completed in Year 1. The task has been completed in Year 2.
10. Complete development of finite element-based model for CP systems (Task 3)	Partially completed	SRNL-STI-2025-00209	A finite-element based cathodic protection CP model for a DST was partially developed. Each DST structure has a concrete vault which has multiple layers of the reinforcing bar. Accounting for those reinforcing steel bars in the CP model was challenging. This task has been completed in Year 2, and the associated document is included in Appendix C.
11. Evaporation of Evaporation Option for DST Supernatant Liquids (Task 4)	Completed	SRNL-STI-2025-00235	A computational framework to exercise the evaporation of the DST supernatant was developed, the framework was exercised for several DST to determine feasibility of the

Table 1. Year 1 Deliverables for Award Number 277993			
Deliverable	**Status**	**Document Number**	**Notes**
			evaporation option to increase storage volume. The document is included in Appendix D.
12. Estimate cost of new tank construction (Task 4)	Completed	SRNL-STI-2025-00235	A cost estimate for construction of a new underground storage tank farm was estimated to be $200-250M/tank. The document for this activity is the same as the one for Deliverable 11.

4.0 Conclusion

The four tasks under the project progressed satisfactorily in Year 1; will all the deliverable milestones accomplished for Task 1, 2, and 4. The leftover Task 3 deliverables will be completed and accomplished in Year 2. The project is expected to yield several invention disclosures, patents, and other intellectual properties, leading to development of meaningful products and technologies which can be directly applies at the Hanford tank farm.

Appendix A. Task 1 Deliverables — SRNL-STI-2024-00627, SRNL-RP-2025-00085, SRNL-TR-2025-00233, SRNL-RP-2025-00379

Initial Progress on Tank Bottom Repair for the DOE EM Tank Waste R&D Program - 25089

Kareen Blue[1], Maxwell Alderman[1], Nicholas Valdes[1], Mark Kranjc[1]
[1]Savannah River National Laboratory

ABSTRACT

In response to the DOE National Laboratory Program Announcement Number Lab23-EM001 on Hanford Tank Waste Cleanup Research and Development a proposal titled "Integrity Monitoring and Assessment, Prediction, Repair, and Corrosion Control of the Hanford Storage Tanks" was developed, submitted, and was awarded (#277993) in April of 2024. This proposal addressed the focus area need of Tank Waste Retrieval, Transport, and Closure. This article describes only the portion of the award that addresses repair of existing Hanford storage tank bottoms. The initial intention is to refurbish Single Shell Tanks (SST) that have been taken out of service. This will increase flexibility in storage capacity and staging options. One other portion of Award 277993 addresses development of an electrode used to monitor electrochemical potentials on metal surfaces for corrosion control. A third component of the Award pertains to the use of cathodic protection for corrosion control. The latter two portions of the Award will not be discussed in this paper.

INTRODUCTION

Several years prior to the Lab23-EM001 Call Announcement, Washington River Protection Solutions (WRPS) had done a review in identifying tank repair feasibility. [1, 2] The most viable methods of repair identified for the Floor of a Primary Tank identified were Grout Stabilization and Polymer Grout. Grout Stabilization was described as a self-leveling grout which fills the entire bottom of the tank and creates a new or false bottom. These types of materials have been used at the Savannah River Site (SRS) to fill and close waste tanks as well as contaminated spaces within decommissioned reactors. No mention was made as to the chemical composition of these Stabilizing Grouts in the review, however, grouts used at SRS for the mentioned applications have always been a cementitious grout material. A thickness of approximately 12 inches was suggested in the review. It was also suggested that an additional polymeric coating could be applied to this fresh and clean grout surface.

In the Tank Repair Feasibility Report Polymer Grouts were described as similar to Stabilizing Grouts but included polymers within the cement matrix. The report goes on to describe "Polymer Grout" as low viscosity materials that can spread thinly and permeate porous surfaces such as soils making them more stable prior to excavation, create surface barriers against moisture movement through the soil, and limit mine water intrusions. This description and the specific products mentioned in the report are more accurately defined as "Chemical Grout". Chemical grouts are commonly infused in the soil as a monomer and undergo polymerization after infusion to stabilize the soil and resist water permeation. These materials did not seem suitable in the environment of our application for service life of twenty years or more.

In general, when polymers are used in concrete there are three main categories of commercial materials available: Polymer Impregnated Concrete (PIC), Polymer Modified Concrete (PMC), and Polymer Concrete (PC). [3,4] In PIC, monomer is impregnated into preformed hardened concrete objects to some depth level, either fully or partially. Monomer is polymerized after it has infused through the concrete. PIC was ruled out as a method to repair tank bottoms because it often involves processing steps that would not apply to our application such as vacuum drying of concrete preform in an autoclave.

One category of PMC is when polymer is added at levels below 5% of the final product, it is added as an admixture and acts to reduce the water content of the concrete while causing the concrete to flow as well or better than at higher levels of water. [3] Less water content used in making cement leads to lower porosity and better properties. Admixtures include lignosulfonates, naphthalene formaldehyde condensates, and polycarboxylates. The most effective of these admixtures are polycarboxylates, they are identified as superplasticizers, and can lead to self-leveling grout formulations.

Another category of PMC is when polymer is added at levels above 5% of the final product, these are identified as Polymer Cement Concrete (PCC) and are completely different from use of polymers as admixtures. For PCC, polymer is used as a partial replacement for ordinary Portland cement (OPC) and both act as the binder for aggregate in concrete., Monomer (containing polymerization initiators) or fully polymerized polymers are added as emulsion latexes or powders that form an emulsion upon mixing with water and ordinary Portland cement (OPC). They are claimed to improve flexibility, reduce cracking, and improve water permeability. The number of polymers used for PCC are vast and include acrylics, styrene-acrylics, vinyl acetate ethylene, polyvinyl acetate, styrene butadiene resin, and others.

Polymer Concrete (PC) is defined as a type of concrete where polymer has replaced OPC completely and is the binder for aggregate and other fillers. In general, properties such as strength (both tensile and compression), lower permeability to water, freeze-thaw resistance, and overall durability are superior with PC than with PCC. The cost of PC is usually greater than PCC due to the much higher cost of polymer than OPC.

The polymers most often used in PC are acrylics, vinyl esters, and epoxies. These are shown in Figure 1. The number of variations of these three materials are too numerous to discuss in this article and these chemical structures represent the most common varieties in the marketplace. Epoxy was chosen as the material of choice due to its excellent combination of properties for adhesion, radiation resistance, chemical resistance, and low uptake of water in marine environments. Epoxies are widely used in marine applications such as structural composites for offshore wind turbines, protective coatings of metal used in marine environments, and coatings used in harsh chemical environments. [5, 6]

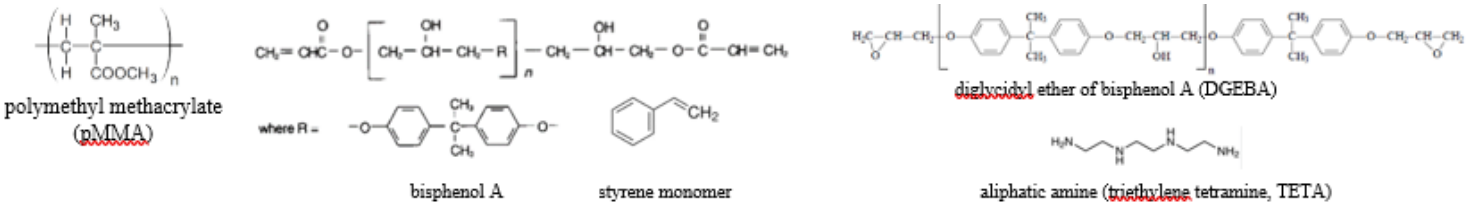

Figure 1. Typical polymers used in polymer concrete.

Table 1 shows relative radiation stabilities of select polymers. [7] Epoxies have better radiation resistance than acrylics (typically polymethyl methacrylate, pMMA) or vinyl ester. They have one of the highest radiation resistances of any polymer. Vinyl esters are a prepolymer that is about 60% the condensation reaction product of acrylic or methacrylic acid with diglycidyl ether of bisphenol A epoxy (DGEBA) plus 40% styrene monomer. Free radical polymerization is used to form a crosslinked thermoset network to polymerize the acrylic/DGEBA prepolymer and styrene monomer. It is seen in Table 1 that polystyrene retains properties quite well, however, the acrylic portion may not. In general, properties for vinyl esters are not as good as those of epoxies but their cost is lower and they are a good alternative when the service environment requirements are not as severe.

Table 1. Relative Radiation Resistance of Polymers Under Two Sets of Conditions.

Polymer	Dose Required to Reduce Mechanical Properties by 50% (In most cases physical property is %tensile elongation)			
	Gray		Mrad	
	high dose rate in inert air	low dose rate in air	high dose rate in inert air	low dose rate in air
Polyimide	100,000,000	none	10,000	none
Epoxy	50,000,000	none	5,000	none
Polystyrene	15,000,000	400,000	1,500	40
Natural Rubber	2,000,000	80,000	200	8
Low Density PolyethyeneL (LDPE)	1,000,000	90,000	100	9
Polyamide (aliphatic)	600,000	60,000	60	6
High Density Polyehtylene (HDPE)	400,000	10,000	40	1
Polymethyl methacrylate (acrylic)	150,000	none	15	none
Polytetrafluoroethylene (PTFE)	60,000	1,000	6	0.1

PCs were found that used low viscosity, uncured epoxy resins that were formulated as such by the manufacturers. Use of reactive diluents can reduce epoxy viscosity by orders of magnitude, from about 10,0000 mPa-s down to around 100 mPa-s. Low viscosity is needed to obtain proper spreading of material over the entire tank bottom. Initial testing began with commercial PC materials that used low viscosity epoxy. These were conveniently supplied with a pail of epoxy resin, a separate pail of amine type curative, and a 22 kg (50 lb.) bag of aggregate.

Several approaches to tank bottom repair are being considered. One approach is use of a self-leveling grout stabilization layer consisting solely of cementitious materials and then applying an epoxy sealant layer on top of that. A second approach is to apply the epoxy sealant layer directly onto the steel tank bottom. The third approach is to apply a single layer of PCC where a portion of the OPC has been replaced by monomer or polymer.

The first approach seems most plausible especially if residual water and/or significant levels of radionuclides are still present at the tank bottom. If residual water at the bottom of the tank cannot be totally removed then this water could be absorbed by the initial cementitious grout layer during hydration/setting. If significant radiation levels still exist at the bottom after cleaning, the initial grout layer would also act as shielding for a subsequent layer of epoxy resin sealant. This paper primarily pertains to this approach.

The second approach mentioned above may be possible if moisture is kept to a bare minimum and no significant radiation levels remain at the steel bottom surface. Methods to determine these conditions need to be developed. Data from testing by WRPS indicates that adequate adhesion of epoxy to steel can occur with minimal surface prep such as no abrasion cleaning, some visible rust, and loose sand on steel plates. In general, however, low moisture levels will be needed for adhesion.

The third approach is to use one layer of a PCC where there is partial replacement of OPC with polymer in the grout. The pros of such an approach are the cost savings of installing just one layer and decreased cost of using OPC along with polymer. In addition, there are several PCCs that are used in underwater applications. Additional personnel have recently been added to the project to further research and investigate the use of PCC, self-leveling cementitious grout formulations, and other approaches such as any interesting Chemical Grout materials. One difficulty in investigating PCC materials was the wide variety of polymers that are used and often limited information provided in manufacturer's data sheets.

Much of the effort in the first 7 months of this project has gone into researching methods to characterize an epoxy sealant layer that will be poured on top of a self-leveling grout layer. This includes literature searching, planning processing property studies of low viscosity epoxy plus generating data, planning of accelerated aging studies, planning for physical property testing, and generating required safety documentation for all this testing. These test methods could also be applied to PCC type materials and Chemical Grouts if closer inspection of those systems proves fruitful.

Characterization of the tank bottom will be critical to this program. Knowledge of these conditions is imperative and include the following: amount of residual wash water remaining; radiation levels coming from any radionuclide residuals; presence and rad levels of any saltcake; surface mapping of the tank bottom topography if saltcake thickness is significant; presence of any through wall holes; and presence of any severe wall thinning. WRPS is working diligently on programs to characterize these conditions on its own and in collaboration with laboratories like SRNL, Pacific Northwest National Laboratory (PNNL), and others.

Many of the service conditions have been identified. The following is a list of service and boundary conditions that have been determined for application and testing purposes:

- Estimated ambient tank bottom temperature during pour (30 ft. below ground): 20^{O} C.
- Maximum service temperature: 60^{O} C (see Accelerated TTS Aging section for further detail)
- Minimum glass transition temperature; 80^{O} C (20^{O} C above max service temperature)
- Maximum radiation level of liquid tank waste: 1 Ci/L
- Maximum dose rate of liquid tank waste: 750 Rads/hr. (see Accelerated Gamma Aging Section for further detail)
- Alkalinity of tank waste solution: 4% NaOH (1M, pH=14)

METHODS

Processing Properties

Modified Slump Testing

A modified version of ASTM C143 Concrete Slump Test was performed. This is a common method used to measure concrete workability or flow. These tests entailed pouring concrete and epoxy mixtures into four 2” diameter x 4” long tubes placed on a flat surface, and then lifting the tube after a set amount of time to see how well the mixture can spread out. All tubes were filled about halfway, or 2”, and lifted after 0 minutes, 15 minutes, 30 minutes, and 60 minutes. Temperature measurements using an IR laser thermometer were taken at the surface of epoxy in the 60 minute tube.

Slump testing was performed on two commercially available PC materials, As mentioned, these were conveniently supplied as a pail of epoxy resin, a separate pail of curative, and a 50 lb. bag of aggregate. These were designated as PC1, where the epoxy resin only portion had a reported viscosity of about 100 mPa-sec., and PC2, where the epoxy portion had a reported viscosity of 1,000 mPa-sec. In addition, a potting epoxy (labeled PE1) that was conveniently available in the lab and had a viscosity between those two, 500 mPa-sec, was also tested at 100% epoxy with no aggregate.

From the slump testing, it was found that using the recommended fraction of aggregate (15/85 epoxy+curative/aggregate by weight for PC1 and 12/88 for PC2) as specified by the manufacturers resulted in a grout that is far too viscous to even be poured into the slump tubes for both the PC1 and PC2

material. Additional slump testing on PC1 and PC2 was performed using a 100% epoxy mixture (epoxy+curative) with no aggregate added.

The PE1 (500 mPa-sec, viscosity) 100% epoxy mixture (epoxy resin+curative), no aggregate, proved to cure far too quickly and reached 140^{O} C after 26 minutes. At this point the test was stopped and the 30 min and 60 min slump tubes were lifted. The upper third portion of epoxy in both the 30 and 60 min. slump tube had solidified. This result shows the importance of using epoxy systems that are formulated for slow curing. The PC1 (100 mPa-sec) 100% epoxy mixture generated much less heat then the PE1 and never solidified before the 60 min tube was lifted. The PC2 performed comparably to the PC1 in terms of heat generated, however, the upper third portion of the 60 minute slump tube on the PC2 solidified in this test. Heat measured at the top of the 60 min. slump tube only reached 55^{O} C. Temperature vs time curves are plotted in Figure 2.

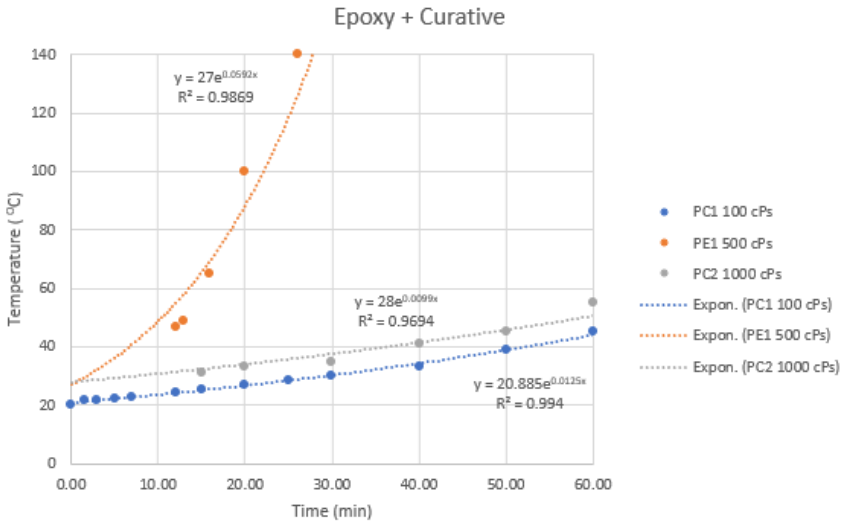

Figure 2. Heat generated at the surface of the 60 min slump tube.

One additional slump test was done using a 50/50 mixture of epoxy/aggregate with the PC1 material. Maximum temperature rise of this mix was not as high as with the PC1 100% epoxy mix. The PC1 50/50 mix reached 27^{O} C after 60 minutes whereas the maximum temperature rise of the PC1 100% epoxy mix was 45^{O} C, the aggregate acted as a heat sink. It was very difficult to keep the larger aggregate suspended during mixing of the 50/50 mixture and when the tube was lifted larger aggregate did not follow the resin front. This was not observed when the epoxy/aggregate content was in the range of 15/85. Lastly, this modified slump test for concrete and cement was not the best test to observe flow behavior differences between epoxies of low viscosity (at and below 1000 mPa-sec), no quantitative or qualitative differences were seen in flow behavior between the PC1 and PC2 material in this test. Rheology testing, discussed in the next section, is a much better method for measuring flow behavior of room temperature cured epoxy and curative with no aggregate.

Rheology Testing

Structural adhesives are usually thermosetting polymers. Generally applied to the surface as low viscosity, reactive liquids, their viscosities increase rapidly as they polymerize and crosslink in the joint to form a rigid, high strength bond. Therefore, knowing the viscosity as a function of cure time and cure temperature is important for establishing optimum cure conditions. Rheology can be used to study the formation of epoxy's crosslinked network, measuring the storage modulus, loss modulus, and complex viscosity as a function of time as shown in Figure 3a-c. The time/cure mode is an efficient way to generate viscosity profiles of a curing thermoset polymer. The viscosity profile yields the initial viscosity,

minimum viscosity, approximate gel point, and optimum heating rate of a thermoset during curing. Data obtained on the PC1epoxy from Slump Testing is shown in Figure 3a. This information can then be used to develop a production cure cycle. The crossover point of the storage and loss modulus curves (Figure 3a) is a good estimate of the gel point of a curing thermoset. But it is only an estimate, because, as the gel network structure forms, the modulus changes. So, unless measurements on the gelling system are made fast enough, the exact gel point will be obscured by changes in the modulus. The reason is, that the instant of gelation the modulus of the critical gel exhibits power law behavior and tan δ becomes frequency independent for a moment ($G' \sim G'' \sim a\omega^n$). This point can be found by making several simultaneous frequency measurements to obtain tan δ in the time scale of the developing gel shown in figure 4. Because tan δ is independent of frequency at the gel point, the curves pass through a single point and unambiguously define the instant the gel forms as shown in figure 4.

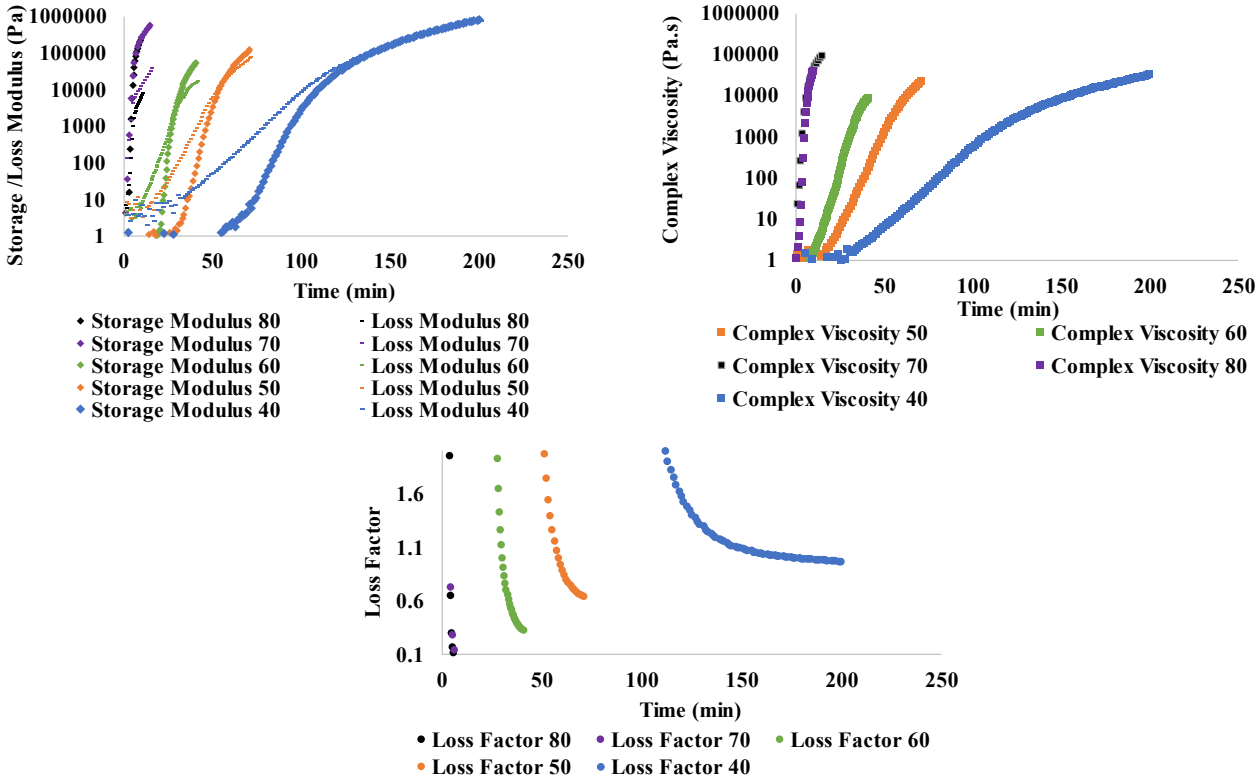

Figure 3: Rheological Isothermal analysis of an epoxy cure showing the storage modulus, loss modulus, Loss factor and complex viscosity at 40, 50, 60, 70, 80° C.

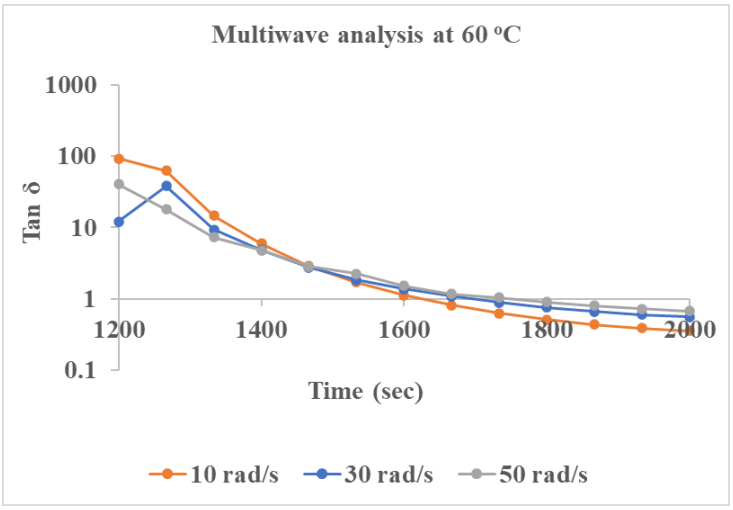

Figure 4: A rheological isothermal multiwave analysis showing the tan delta crossover for 10 rad/sec, 30 rad/sec, and 50 rad/sec frequencies of an epoxy gel-point.

Differential Scanning Calorimetry (DSC)

DSC measures the temperatures and heat flows associated with transitions in materials as a function of temperature or time in a controlled atmosphere. This technique provides quantitative and qualitative information about physical and chemical changes that involve endothermic or exothermic processes, or changes in heat capacity. Epoxy adhesives are often used for materials such as metal, glass, ceramic, and plastic. During curing, the epoxy group starts a polymerization reaction, cross-links and hardens. DSC can investigate various characteristics of epoxy adhesives, including glass transition temperatures before and after curing, as well as the temperature and reaction calories during the curing reaction. Figure 5 illustrates DSC ability to analyze the different components of the epoxy's resins, including the degree of cure.

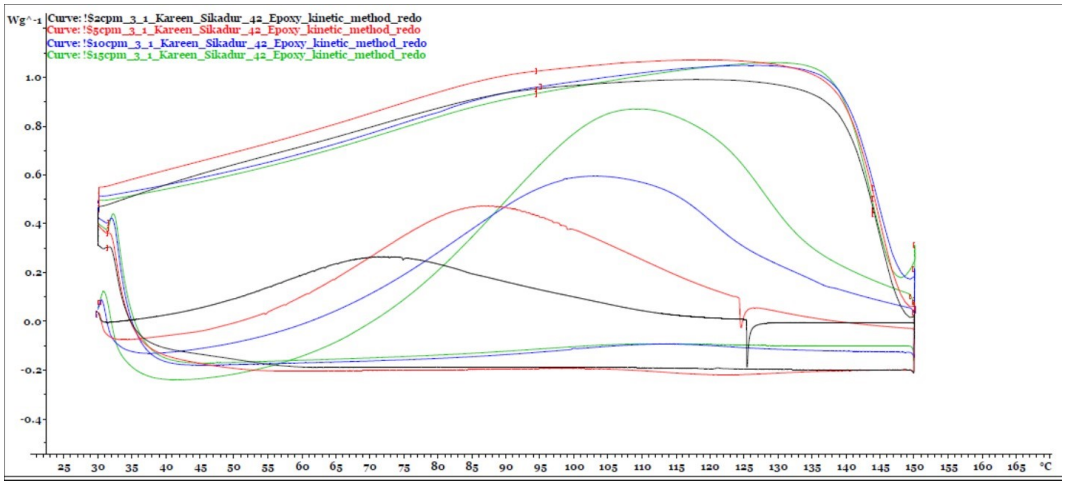

Figure 5: DSC thermogram of an epoxy cure under non-isothermal conditions ramping from 30° C – 150° C at 2, 5, 10, 15 °C/min.

Accelerated Aging Methods

There will be three methods used to accelerate aging of epoxy sealant samples: Gamma Aging, Time Temperature Superposition (TTS) Aging, and Time Temperature Chemical Superposition (TTCS) Aging. These methods are discussed below.

Accelerated Gamma Aging

The agreed upon estimated maximum radiation level that the refurbished tanks will contain is 1 Ci/L based on WRPS experience, this was considered a conservatively high radiation level. A Monte Carlo statistical dose rate software calculation was used to determine what the dose rate to the epoxy resin would be through the thickness of this epoxy sealant layer in service. To simplify the calculation, it was assumed that all radiation would be coming from Cs-137 since this would be the primary radionuclide present in the waste stored in a refurbished tank. The level of waste in the tank was assumed to be 30 feet and shielding from the waste liquid was considered. Figure 1 shows dose levels calculated near the liquid waste/epoxy sealant layer interface down to 5 inches, it is assumed that a self-leveling cementitious grout layer would not be perfectly level. The expectation is that the grout layer would be anywhere between 1.00 cm minimum depth (about 3/8 inches) to about 12 cm maximum depth (about 4¾ inches).

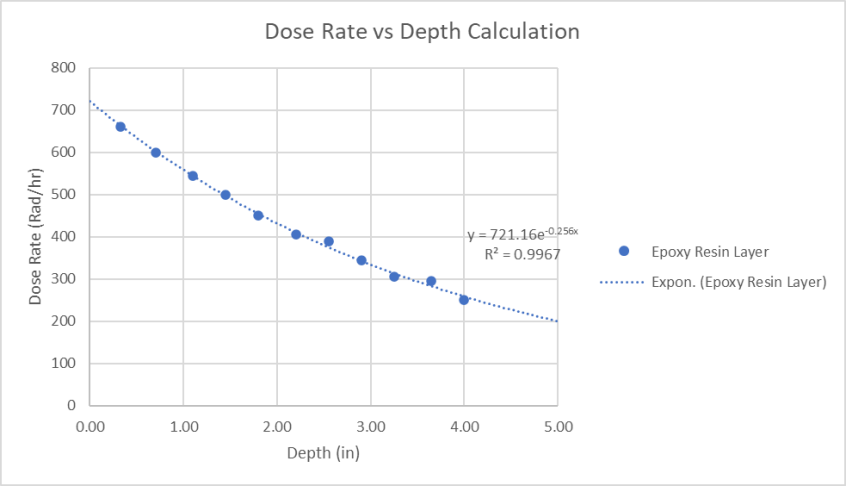

Figure 1. Dose rate versus depth of epoxy sealant layer.

The plan is to place compression strength cylinders and adhesion strength coupons into the Co-60 Irradiator at SRNL at a high dose rate of about 100,000 Rad/hr. Samples will be placed such that the absorbed dose will be uniform throughout the 2.54 cm diameter cylinders and 1 cm thick adhesive layer. Samples will be periodically removed at the total dose levels indicated in the far left column in Table 2 and the times required to attain these total dose levels are shown in columns 2, 3, and 4. These samples will be tested for compressive strength, adhesion, dimensional stability, change in weight, and change in T_g as described in the Physical Property Testing section of this paper.

Columns 5, 6, 7, and 8 show the corresponding time it will take for the in service epoxy layer to absorb the total dose in the far left column. These times assume that the entire epoxy layer in service experiences a dose rate of 750 Rad/hr. This is a high conservative assumption since only the epoxy/liquid waste interface will see this dose rate.

Table 2. Irradiator Aging Test Plan

Total Dose (Mrad)	Irradiator Time @ 100,000 Rad/h			exposure in tank @ 750 Rad/h			
	hours	days	months	hours	days	months	years
150	1500	63	2.1	200,000	8,333	278	23
300	3000	125	4.2	400,000	16,667	556	46
450	4500	188	6.3	600,000	25,000	833	68
600	6000	250	8.3	800,000	33,333	1,111	91

Dose rate effects are not expected to have a large effect in this testing. Polymer physical property degradation is known to occur more slowly at high gamma dose rates used in laboratory accelerated aging than physical property degradation observed in service at much lower dose rates. This is due to Diffusion Limiting Oxidation (DLO). [8, 9, 10, 11, 12] Oxidation reactions are a large contributor to polymer degradation in ambient conditions. At high dose rates the permeation rate of oxygen through the bulk of the polymer is not fast enough to replenish the oxygen that has reacted with highly reactive free radicals created by exposure to ionizing radiation. At elevated dose rates the concentration of oxygen in the bulk is depleted and the rate of reaction causing lower physical properties decreases. Dose rate in the irradiator is about 100,000 Rad/hr. and calculated dose rate in service is 750 Rad/hr. However, since the epoxy layer will be submerged under liquid waste in service, oxidation is unlikely to be a large contributor to property degradation.

Accelerated Time Temperature Superposition (TTS) Aging

Time, Temperature Superposition (TTS) is a common method used to predict degradation of polymeric physical properties over time. [13, 14] TTS experiments have been used to characterize service life aging of epoxies and fiber reinforced plastic (FRP) composite where the matrix resin of the composite is epoxy. [15, 16, 17, 18] This type of testing essentially uses elevated temperatures to predict long term properties. The plan is to place compression cylinders and adhesion coupons in aging ovens at several elevated temperatures, remove samples after a given time, run physical property testing on each sample group at different time and temperature, and using TTS techniques shift isothermal property degradation curves down to the lowest aging temperatures creating a master curve. The physical property testing will be the same as those mentioned in the Accelerated Gamma Aging section. An estimate of aging temperatures and times to be used are given in Table 3.

Table 3. Estimated accelerated aging temperature and time.

Temperature (^{o}C)	Time Duration					No. of Samples
75	1	30	90	180	days	12
	0.033	1	3	6	months	
	24	720	2160	4320	hours	
65	30	90	180	360	days	12
	1	3	6	12	months	
	720	2160	4320	8640	hours	
55	90	180	360	720	days	12
	3	6	12	24	months	
	2160	4320	8640	17280	hours	
45	180	360	720	1080	days	12
	6	12	24	36	months	
	4320	8640	17280	25920	hours	

The maximum service temperature spike for liquid waste in the repaired tank at any given time was estimated at 60^{O} C. The epoxy sealant layer must always be below T_g in service, the minimum T_g chosen for the epoxy was 80^{O} C. Temperature of liquid waste tanks can vary due to variations in concentration of decaying radionuclides and 60^{O} C is considered a conservatively high estimate. In TTS, test samples must all be aged at temperatures either above T_g for polymers that will be used at temperatures above their T_g (like rubbery elastomers) or below T_g for polymers that will be used at temperatures below T_g (like high modulus epoxies). This is the reason for the aging temperatures chosen.

Accelerated Time Temperature Chemical Superposition (TTCS) Aging

Since the in service epoxy sealant will be exposed to a solution of tank waste, aging will also be carried out in simulated tank waste at the same temperatures and removal times chosen for accelerated TTS aging experiments shown in Table 3. This will create an accelerated aging environment that is more like the actual use environment. The tank simulant will contain salts that are most common in tank liquid waste but without any radionuclides. The most chemically aggressive component in this mix is sodium hydroxide and the agreed upon maximum concentration that will be used in a refurbished tank is 4% NaOH or 1 M NaOH, the pH of such a solution is calculated to be 14.0. Aging under these conditions will be called Time Temperature Chemical Superposition (TTCS) and will be able to determine the effect of the highly alkaline tank waste environment. The TTS aging in ovens is being done more for comparison to literature values and comparison to the TTCS aging data generated.

Physical properties described in the Accelerated Gamma Aging section will be tested after each group is removed from solution at the same times and temperatures indicated in Table 3. Researchers have experimented with epoxy and FRP composites with epoxy matrices under moisture environments in a similar way and have referred to it as testing using Time Moisture Superposition Principles (TMSP). [15, 16]. Using TTS techniques, isothermal property degradation versus time curves will be shifted down to the lowest isothermal property degradation versus time curve and a master curve will be generated for chemical exposure.

An equation can be developed where the effects of radiation from accelerated irradiator experiments and accelerated time temperature chemical exposure effects of TTCS experiments are additive. This is an approach that was similarly used for aging experiments on liquid tank waste transfer hoses composed of a crosslinked polyethylene inner liner at the SRS. Using these techniques the recommended time to replace that transfer line Hose-In-Hose system was projected to be 25 MRad or 10 years, whichever occurs first. To date the total dose is still below 25 MRad, and the system has been in service with no issues for 8 years now. [19, 20, 21]

Physical Property Testing

Compression Strength

Compression strength will be tested according to ASTM D-695 “Compressive Properties of Rigid Plastics”. The recommended sample size is 12.7 mm in diameter and 25.4 mm in length (0. 5 in. diameter by 2.0 inch length). Silicone elastomer molds have been constructed to generate a large number of samples. When the epoxy is cured samples can be easily popped out of the rubber mold.

Adhesion Strength

Adhesion strength will be tested according to ASTM D-4541 “Pull-Off Testing of Coatings Using Portable Adhesion Testers”. ASTM D-4541 was chosen after careful consideration of several types of adhesion testing. D-4541 was chosen due to ease of use, ability to prepare and test many samples with significantly less sample and test machine preparation time, and comparison to data that has already been generated by WRPS on some epoxy systems. At the time of writing this paper a DeFelsko PosiTest AT-

A Automatic Adhesion Tester had been ordered.

Adhesion samples will consist of steel and self-leveling cementitious grout adherend plates that will be 130 mm x 130 mm square and have a thickness of 9.5 mm (3/8") for the carbon steel adherend and 25.4 mm (1.0") for the cement grout adherend. Adhesion to both a fresh self-leveling cementitious grout layer and steel tank bottom will be considered. A sample of epoxy sealant will be mixed, poured to a thickness of about 10 mm (about 3/8") on top of the steel and grout adherends. These samples will be cured at room temperature for 24 hours followed by a post cure of 120^{O} C for 2 hours. These adhesion samples composed of epoxy sealant cured onto steel and grout adherends will be placed in the accelerated aging conditions (Gamma, TTS, and TTCS). In summary, this test is a vertical pull off test of an aluminum dolly that will be glued onto the epoxy surface of adhesion samples after removing them from accelerated aging conditions. Control samples will see no aging.

The portable pull off tester and dolly fixture are shown in Figure 2. There will be four dollies glued to the samples that are 130 mm x 130 mm in area. The dolly glued surface diameter is 20 mm, therefore, the distance from sample edge to dolly and the distance between dollies will always be 30 mm. This should remove any edge effects of moisture/chemical permeation in TTCS aging and will provide four adhesion tests on one sample coupon. The instrument shown on the left in Figure 2 will record the tensile force required to pull the dolly free from the surface. The type of cohesive and/or adhesive failure will be noted.

Figure 2. Pull tester instrument shown on left. Adhesion dolly fixture on right. Z is dolly fixture, Y is glue, D thru B are successive coating layers if more than one coat is applied, A is the adherends (in our case steel and cementitious grout).

There may be adhesive failure between the dolly and glue or glue and epoxy on the Control samples if both cohesive strength of the epoxy and adhesive strength of epoxy to adherend (carbon steel or grout) is greater than the adhesive strengths between dolly/glue/epoxy. Since gluing of the dolly to epoxy occurs after aging, it is expected that after aging cohesive strength of the epoxy or adhesive strength of epoxy to adherend will drop below adhesive strengths of dolly/glue/epoxy interfaces.

Dimensional and Weight Stability

Diameters and lengths will be measured on compression cylinders before accelerated aging to the nearest 0.01 mm (0.0004 in). Three samples will be removed from the gamma irradiator, TTS, and TTCS conditions shown in Table 2 and 3 and changes in diameter and length will be recorded to the nearest 0.01 mm. The same samples will then be compression tested. For adhesion test coupons, as described in the Adhesion Test section, the thickness of the coupon will be measured before accelerated aging. It is assumed that the thickness of the carbon steel and grout adherends will not change due to irradiation, heat, or simulant exposure, therefore, the change in thickness of the epoxy layer can be determined.

Glass Transition Temperature (T_g)

T_g will be measured using DSC on 5 mg of sample taken from the compression strength cylinders after testing. All accelerated aging conditions of gamma irradiation, TTS, and TTCS will be tested. In

addition, T_g before aging will be determined on control samples that have been compression tested with no aging.

CONCLUSIONS

Currently moving forward with a cementitious false bottom with an epoxy sealant layer on top. Reasons for this are:

- Cement has better resistance to ionizing radiation than organic polymers from radionuclides that may be at the tank bottom. The cement will act as shielding to the epoxy sealant in service if radiation from any residuals prove to be greater than radiation dose from the liquid tank waste in contact with the sealant.
- Good methods to detect, characterize, and remove residual materials if needed at the bottom of the tank are currently being developed. These materials include residual water and radionuclides that may still be present after extensive cleaning.
- A Polymer Cement Concrete (PCC) type material where polymer is used as a partial replacement of ordinary Portland Cement and both act as the binder for aggregate in concrete may prove to be attractive. Advantages include reduced cost both in materials and in application since only one layer would need to be applied. If there is a significant level of radiation due to residual radionuclides still present at the bottom, however, the polymeric portion would be more susceptible to degradation than the cement.
- Characterization methods have been developed for testing of an epoxy sealant layer. Due to the large number of test samples and test iterations that would be needed only the best option is being looked at, epoxy. Similar test methodologies could be applied to other polymeric materials like vinyl ester, acrylics, styrene butadiene rubber, etc.

Lastly, a more extensive literature search of PCC, Chemical Grouts, and self-leveling grout is almost completed at the time of writing this article. This will act as a starting point for evaluating the first self-leveling grout layer that will be poured and set/cured before the second epoxy sealant layer. In addition, any other materials of interest will be identified, there may be a product that has a combination of low viscosity and radiation resistance acceptable for this application.

REFERENCES

1. WRPS Chief Technology Office, "Tank Repair Feasibility", *RPP-RPT-62020* (2020).

2. T. Wooley, K. Boomer, A. Pappas, "An Ode to Tank Repair and a Longevity Strategy for Underground Storage Tanks at the Hanford", *Proceedings of Waste Management 2022 Conference,* Phoenix, AZ, March 6-10 (2022).

3. B. SARDI, Y.D. PATEL, "Recent Research Status on Polymer Composite Used in Concrete – An Overview", *Proceedings of the International Conference of Materials Processing and Characterization*, September 10-11 (2019).

4. J. NAVISK, "Understanding Polymers in Concrete", *Concrete Construction Magazine*, September (2001).

5. A. GUEN-GEFFROY, P. LE GAC, B. HABERT, P.DAVIES, "Physical Aging of Epoxy in a Wet Environment: Coupling Between Plasticization and Physical Aging", Polymer Degradation and Stability, 168, 108947, (2019).

6. C. ANAGNOSTOPOULOS, G. SAPIDIS, E. PAPASTERGIADIS, "Fundamental Properties of Epoxy Resin-Modified Cement Grouts", *Construction and Building Materials*, 125, 184, Elsevier Ltd, Amsterdam, Netherlands, (2016).

7. R. CLOUGH, K. GILLEND, D. CLEG, G, A. COLLYER,*Irradiation Effects on Polymers*, pp110-111, Ed., Elsevier Applied Science, New York, NY, (1991).

8. K. GILLEN, R. CLOUGH, L. JONES, "Investigation of Cable Deterioration in the Containment Building of the Savannah River Nuclear Reactor", *NUREG/CR-2877, SAND81-2613*, (1982).

9. R. CLOUGH, K. GILLEN, "Combined Environment Aging Effects: Radaition Thermal Degradation of Polyvinylchloride and Polyethylene", Journal of Polymer Science, vol.19, 2041-2051, (1981).

10. H. WILSKI, "The Radiation Induced Degradation of Polymers", *Radiation Physical Chemistry,* 29, 1, (1987).

11. A. REYNOLDS, R. BELL, M. BRYSON, T. DOYLE, M. HALL, L. MASON, L. QUINTIRIC, P. Terwilliger, "Dose Rate Effects on the Radiation-Induced Oxidation of Electric Cable used in Nuclear Power Plants", *Radiation Physical Chemistry*, 45, 1, (1995).

12. A. QUINTANA, M. CELINA, "Overview of DLO Modeling and Approaches to Predict Heterogeneous Oxidative Polymer Degradation", *Polymer Degradation and Stability,* **2018**, 149, (2018).

13. J. FERRY, *Viscoelastic Properties of Polymers – 3rd edition*, pp 264-320, John Wiley and Sons Inc., New York, NY, (1980).

14. J. AKLONIS, W. MACKNIGHT *Introduction to Polymer Viscoelasticity – 2nd edition*, p44, John Wiley and Sons Inc.,New York, NY, (1983).

15. O. STARKOVA, A. GAGANI, C. KARL, I. ROCHA, J. BURLAKOVA, A. KRAUKLIS, "Modeling of Environmental Aging of Polymers and Polymer Composites – Durability Prediction

Methods", *Polymers*, 14, 907, (2022).

16. D. GIBHARDT, A. KRAUKLIS, A. DOBLIES, A. GAGANI, A. SABALINA, O. STARKOVA, B. FIEDLER, "Time, Temperature, and Water Aging Failure Envelope of Thermoset Polymers", *Polymer Testing*, 1, 18, (2023).

17. M. SILVA, B. FONSECA, H. BISCALA, "On Estimates of Durability of FRP based on Accelerated Tests", *Composite Structures*, 116, 377, (2014).

18. A. GUEN-GEFFROY, P. LE GAC, B. HABERT, P. DAVIES, "Physical Aging of Epoxy in a Wet Environment: Coupling Between Plasticization and Physical Aging", *Polymer Degradation and Stability*, 168, 108947, (2019).

19. M. KRANJC, T. SKIDMORE, R. HAWSEY, "Service Life Evaluation of the Hose-In-Hose Transfer System Between Tank 13 and 15, Final Report", *SRNL-STR-2021*, (2021).

20. M. KRANJC, B. HILL, "Update on Accelerated Aging Tests and Preparation Work for Forensics Testing After Service Life of Tank 13/14 Hose-In-Hose, Update Report", *SRNL-TR-2022*, (2022)

21. M. KRANJC, T. SKIDMORE, R. HAWSEY, "Service Life Prediction of Polymeric Hose-In-Hose Systems Used to Transfer High Level Liquid Waste Between Operations", *Proceedings of Waste Management 2022 Conference,* Phoenix, AZ, March 6-10 (2022).

Initial Progress on Tank Bottom Repair for the DOE EM Tank Waste R&D Program

Kareen Blue, PhD; Maxwell Alderman;
Nicholas Valdes, PhD; Mark Kranjc, PhD
Savannah River National Laboratory®
Materials Technology Division

Introduction

- Part of "Integrity Monitoring and Assessment, Prediction, Repair, and Corrosion Control of Hanford Tanks", Award #277993, in response to DOE Lab Program Announcement Lab23-EM001
- After a literature review of WRPS Tank Repair Feasibility Study and Materials Considered, a Two Layer approach seemed most feasible.
  - Initial Grout Layer provides a fresh surface.
  - Epoxy Sealant Layer poured on top of Grout

Tank schematic (not to scale)

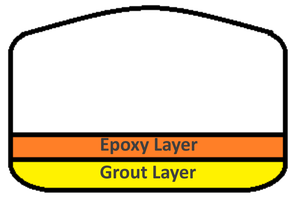

Polymers Reviewed

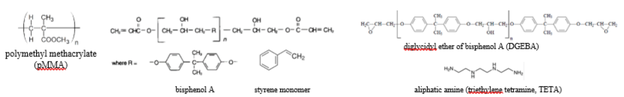

Acrylic | Vinyl ester | Epoxy (best radiation resistance)

Service Conditions Identified

- Estimated ambient tank bottom temperature during pour (30' below ground): **20 °C**
- Approximate service temperature: **15 – 27 °C**
- Minimum Epoxy T_g : **47 °C** (20 °C above service temp)
- Maximum radiation level of liquid waste tank: **1.75 mCi/L**
- Maximum dose rate of tank waste to epoxy: **< 750 Rads/hr**
- Alkalinity of tank waste solution: **4% NaOH (1M, pH=14)**
- Diameter of tank bottom to cover: **70 ft**

Processing Properties

Rheology Testing

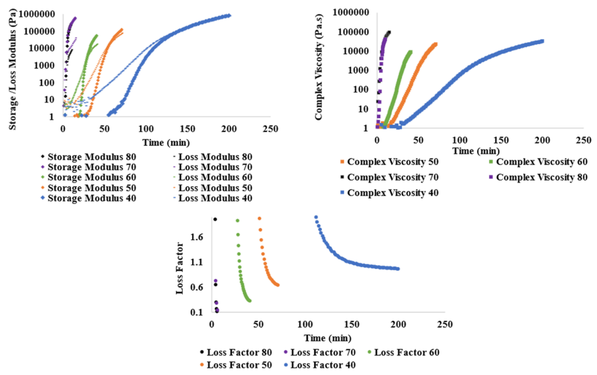

Rheological Isothermal analysis of Sikadur epoxy cure showing the storage modulus, loss modulus, Loss factor and complex viscosity at 40, 50, 60, 70, 80° C

Differential Scanning Calorimetry (DSC) Testing

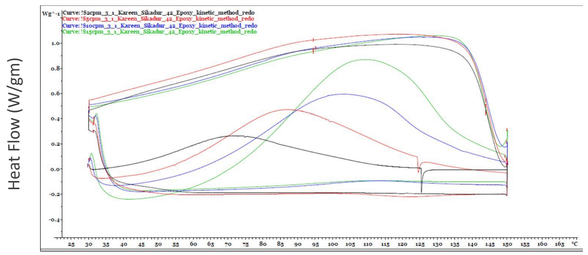

DSC thermogram of an epoxy cure under non-isothermal conditions ramping from 30° C – 150° C at 2, 5, 10, 15 °C/min.

Results

- Cure kinetics can be determined
- Workability time can be determined
- Comparison of many samples at low volumes

Accelerated Aging

Gamma

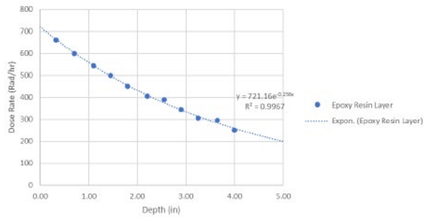

Monte Carlo calculation result to convert liquid rad level of 1 Ci/L to dose rate into epoxy layer target

Total Dose (Mrad)	Irradiator Time @ 100,000 Rad/h			exposure in tank @ 750 Rad/h			
	hours	days	months	hours	days	months	years
75	750	31	1.0	100,000	4,167	139	11
150	1500	63	2.1	200,000	8,333	278	23
300	3000	125	4.2	400,000	16,667	556	46
450	4500	188	6.3	600,000	25,000	833	68

Time Temperature Superposition (TTS)

- Common method used for accelerated aging of polymers
- Place samples in ovens at several elevated temperatures
- Remove samples and test physical properties
- Plot isothermal property degradation curves
- Shift greatest degradation at high temp to curve at low temperature and low degradation.

Time Temperature Chemical Superposition (TTCS)

- Same as TTS but soak samples in non rad tank simulant at elevated temperatures
- Aging tanks are available at FIU. Round robin testing with SRNL where Gamma and TTS testing will occur

Temperature (°C)	Time Duration					No. of Samples
75	1	30	90	180	days	12
	0.033	1	3	6	months	
	24	720	2160	4320	hours	
65	30	90	180	360	days	12
	1	3	6	12	months	
	720	2160	4320	8640	hours	
55	90	180	360	720	days	12
	3	6	12	24	months	
	2160	4320	8640	17280	hours	
45	180	360	720	1080	days	12
	6	12	24	36	months	
	4320	8640	17280	25920	hours	

Physical Property Testing after Removal from Aging

Compression Strength

ASTM D695 Compression Properties of Rigid Plastics

Stress Strain Graph of Sikadur Epoxy

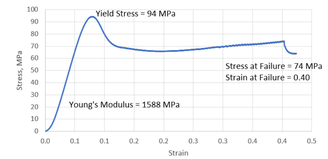

Adhesion Strength

ASTM D4541 Pull Off Strength of Coatings

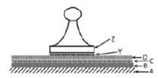

Glass Transition Temperature (T_g) by DSC

ASTM D3418 Transition Temperature by DSC

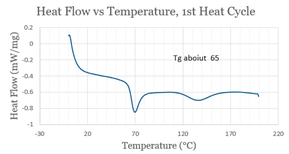

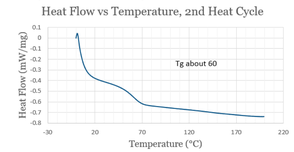

Removal of sample thermal history in 2nd heat cycle

Dimensional and Weight Stability

Measurement of diameters, lengths, and weight before and after aging

ASTM D695 compression cylinder to be used for dimensional and weight stability as well (0.5"dia x 1" length)

A U.S. DEPARTMENT OF ENERGY NATIONAL LAB • SAVANNAH RIVER SITE • AIKEN, SC • USA

Tank Bottom Refurbishment Year 1 Report

Portion of Award #277993: "Integrity Monitoring and Assessment, Prediction, Repair, and Corrosion Control of the Hanford Storage Tanks"

M. Kranjc, M. Alderman, K. Blue, N. Valdes

March 2025

SRNL-TR-2025-00233, Revision # 0

DISCLAIMER

Printed in the United States of America

Prepared for
U.S. Department of Energy

Keywords: Hanford Tank Waste

Retention: Varies

Tracking Number: SRNL-TR-2025-00233

Tank Bottom Refurbishment Year 1 Report

Portion of Award #277993:
"Integrity Monitoring and Assessment, Prediction, Repair, and Corrosion Control of the Hanford Storage Tanks"

M. Kranjc, M. Alderman, K. Blue, N. Valdes

March, 2025

Savannah River National Laboratory®

Savannah River National Laboratory is operated by Battelle Savannah River Alliance for the U.S. Department of Energy under Contract No. 89303321CEM000080

Reviews and Approvals

AUTHORS:

MARK KRANJC (Affiliate) Digitally signed by MARK KRANJC (Affiliate)
Date: 2025.05.06 13:41:35 -04'00'

Mark Kranjc, PhD, sub PI of Project #277993, L3320/Material Evaluation & NDE Date:

MAXWELL ALDERMAN (Affiliate) Digitally signed by MAXWELL ALDERMAN (Affiliate)
Date: 2025.05.07 11:01:31 -04'00'

Maxwell Alderman, L3340/Material Science & Disposition Date:

Kareen Blue Digitally signed by Kareen Blue
Date: 2025.05.07 11:33:11 -04'00'

Kareen Blue, PhD, L3320/Material Evaluation & NDE Date:

NICHOLAS VALDES (Affiliate) Digitally signed by NICHOLAS VALDES (Affiliate)
Date: 2025.05.07 11:43:46 -04'00'

Nicholas Valdes, PhD, L3330/Advanced & Energy Materials Date:

TECHNICAL REVIEWER:

MICHAEL RESTIVO (Affiliate) Digitally signed by MICHAEL RESTIVO (Affiliate)
Date: 2025.05.07 13:30:46 -04'00'

Michael Restivo, L3320/ Material Evaluation & NDE Date:

APPROVALS:

PAVAN SHUKLA (Affiliate) Digitally signed by PAVAN SHUKLA (Affiliate)
Date: 2025.05.08 10:41:22 -04'00'

Pavan Shukla, PhD, Overall PI of Project #277993, L3340/Materials Science & Disposition — Date

THOMAS SKIDMORE (Affiliate) Digitally signed by THOMAS SKIDMORE (Affiliate)
Date: 2025.05.09 09:17:16 -04'00'

Eric Skidmore, Manager, L3320/Material Evaluation & NDE — Date

JOSEPH MANNA (Affiliate) Digitally signed by JOSEPH MANNA (Affiliate)
Date: 2025.05.09 11:43:52 -04'00'

Joe Manna, PhD, Manager, L3300/Materials Technology & Energy — Date

Table of Contents

List of Tables

List of Figures

List of Abbreviations

ASTM	American Standard Test Methods
DoE	design of experiment
DOE	Department of Energy
DSC	Differential Scanning Calorimetry
DST	Double Shell Tank
FIU	Florida International University
H2C	Hanford Tank Waste Operations and Closure
M	Molar
mCi/L	milliCuries per Liter
NaOH	Sodium Hydroxide
SRNL	Savannah River National Laboratory
TTS	Time temperature Superposition
TTCS	Time Temperature Chemical Superposition
T_g	Glass Transition Temperature
WM2025	Waste Management 2025 Conference
WRPS	Washington River Protection Solutions

1.0 Introduction

This Year End Report will highlight the delivery of milestones and technical achievements for the Tank Bottom Refurbishment portion of Award #277993 "Integrity Monitoring and Assessment, Prediction, Repair, and Corrosion Control of the Hanford Storage Tanks". This portion of the project will be using the term "Refurbishment" instead of "Repair" starting in Year 2 considering that we are working in tandem with Hanford Tank Waste Operations and Closure (abbreviated H2C, formerly Washington River Protection Solutions, WRPS). H2C defines "Refurbishment" as pro-actively improving the overall condition of an item that is deemed usable, therefore, enhancing the longevity of a Double Shell Tank (DST). "Repair" is defined as reactively fixing something that is broken and no longer usable, for example patching a through wall penetration in the tank bottom.

2.0 Delivery of Year 1 Milestones

Extensive literature reviews and evaluation was performed on materials that had been first identified by WRPS for tank repair. [1, 2, 3, 4] Methods to test these materials were extensively reviewed as well. [5, 6, 7, 8] While evaluating the various components of cementitious grouts, polymer grouts, and grouts that use a mix of polymer and cement as binder for aggregate and filler it was decided to move forward with a refurbishment strategy that would involve a two layer approach. An initial layer of self-leveling cementitious grout would be poured into the tank first and when it had hardened a second epoxy sealant layer would be poured on top of that.

One purpose of the first cementitious grout layer is to provide shielding of the epoxy sealant layer if any significant residual radionuclides are still present at the bottom of the tank. In addition, if there is any water still left at the tank bottom it would become part of the cement in the hydration/drying process. The first cementitious grout layer would also provide a fresh, dry, surface for the epoxy layer to adhere to, as opposed to a decades old carbon steel bottom.

Epoxy polymer was chosen as the polymer of choice due to its excellent combination of physical properties. It has excellent adhesion to a variety of surfaces, it is one of the most radiation resistant polymers, it is resistant to degradation by sodium hydroxide, it is commonly used for applications in aqueous environments (recreational boat hulls), and has low water permeability. The Tables in Appendix A illustrate a few of these properties. A second epoxy sealant layer was chosen instead of a single grout layer composed of a mixed binder of polymer and cement due to concerns of aqueous tank waste permeability through this single layer and susceptibility of some aggregate materials to degradation by sodium hydroxide. It would be interesting to do some testing on the permeability of polymer cement grout to confirm this, however, at this time it has been determined that the two layer approach gives a higher probability of success in the short term.

A good deal of effort has been put into evaluating off the shelf epoxy grout products and off the shelf epoxies that will undergo ambient temperature cure, low maximum temperature during cure, and long cure times. Appendix B gives an evaluation of various epoxy resins, diluents, curatives, and other chemicals that go into formulating a part A epoxy and part B curative. Of all the products tested by Savannah River National Laboratory (SRNL), the Sikadur 42 epoxy/curative system was found to be the one that best fits the processing and property requirements needed for this application. In addition, the "Westlake Epoxy" which was formulated and evaluated by AVANTech was the best material evaluated by WRPS. Unfortunately, Sika Co. has discontinued Sikadur 42 sometime between SRNL obtaining

samples in June of 2024 and March of 2025 due to a merger with Master Builders and consolidation of product lines. Prior to learning this, SRNL had already been pursuing an NDA with AVANTech where AVANTech would share the Westlake Epoxy formulation.

A poster was presented at Waste Management 2025 (WM2025), March 9 through 13, and a paper was submitted for inclusion in the WM2025 Conference Proceedings that outlines material evaluation discussed above and accelerated aging tests that will be used to evaluate performance of these materials while in service as a refurbished DST bottom. [9, 10] See the paper and poster for further discussion and explanation. In summary the accelerated aging conditions that are planned include:

- ✓ Gamma Irradiation at SRNL.
- ✓ Time Temperature Superposition (TTS) at SRNL
- ❖ Time Temperature Chemical Superposition (TTCS) at Florida International University (FIU)

The methodology and scoping test plans have been completed for items above that have a check, further preparation is needed for TTCS accelerated aging. Physical Property testing of samples will be performed on samples before and after specific time periods in accelerated aging conditions, these tests are given below. Methodologies have been developed, tested, and are ready for use on items below that have a check while more development work is needed on the Adhesion Strength Testing.

- ✓ Dimensional Stability (measurement of weight, length, and diameter)
- ✓ Glass Transition Temperature (T_g) by Differential Scanning Calorimetry (DSC, ASTM D3418)
- ✓ Compression Strength (ASTM D695)
- ❖ Adhesion Strength Testing (ASTM D4541)

The following is a summary of the status of Milestones presented in the proposal. An extensive literature review has been completed and reported [4] but completion time took longer than the expected end of Quarter 1 in Year 1 due to the complexity of the task. Formulation development is almost completed but will extend into Year 2 due to the complexity of the materials evaluated for a 2 layer approach which was decide on in Year 1. Test methodologies have been decided on and will be completed in Year 2, this looks like it will be completed on time. While writing the proposal it was thought that design of experiment (DoE) testing would be used to assist in determining the epoxy formulation to place in accelerated aging. It is believed that due to the extensive research and literature study of epoxy resins, diluents, and curatives a doe is not necessary and if pursued would delay the time required to decide on an epoxy formulation to place in accelerated aging.

3.0 Technical Accomplishments

Technical Accomplishments in Year 1 include the following:

- Determined details of the path forward to evaluate the service life of a refurbished Hanford DST bottom. [9, 10]
- With the help of WRPS (now H2C), boundary conditions that the refurbished tank bottom will see in service and important properties that the epoxy layer must have are being determined. See Appendix C.
- The use of a Mettler Toledo rheometer and DSC at SRNL will greatly assist in determining processing properties needed from the epoxy sealant layer when pouring into the bottom of the DST. These properties include time after mixing that it takes for the epoxy to cure to a viscosity

where the resin front will stop flowing and the maximum temperature reached during cure. This compliments evaluations at H2C for a refurbished DST bottom by introducing small scale testing. This enables SRNL to evaluate the Sikadur 42 epoxy, AVANTech Westlake epoxy, and several different combinations of epoxies, diluents, and curatives. Ten of these components have been ordered and have recently been delivered to SRNL. See Appendix D for results.

- Determined the Accelerated Aging Conditions to place samples into. Scoping experiments are outlined in Appendix E.
- Determined the methodology for physical property testing to perform on epoxy samples before and after samples have been removed from accelerated aging. See Appendix F for results.
- A Task Technical Plan (TTP) has been put together for evaluation of the 1st Self Leveling Grout Layer. [11]
- A TTP is planned for the 2nd Epoxy Sealant Layer.

References

1. WRPS Chief Technology Office, "Tank Repair Feasibility", *RPP-RPT-62020*, 2020.
2. T. Wooley, K. Boomer, A. Pappas, "An Ode to Tank Repair and a Longevity Strategy for Underground Storage Tanks at the Hanford", *Proceedings of Waste Management 2022 Conference,* 2022.
3. R. Calmus, "Tank Repair Technology Development – Strategy, Status, and Path Forward", *Presentation at Waste Management 2022 Conference, 2022*
4. N. Valdes, "Refurbishing Hanford Waste Tanks – Overview on Grout Layers", SRNL-TR-2025-00056 Technical Report, still under editing.
5. A. Le Guen-Geffroy, P Le Gac, B. Habert, P. Davies, "Physical Aging of Epoxy in a Wet Environment: Coupling Between Plasticization and Physical Aging", Polymer Degradation and Stability, 168, 108947, 2019.
6. O. Starkova, A. Gagani, C. Karl, I. Rocha, J. Burlakova, A. Krauklis, "Modeling of Environmental Aging of Polymers and Polymer Composites – Durability Prediction Methods", *Polymers*, 14, 907, (2022).
7. D. Gibhardt, A. Krauklis, A. Doblies, A. Gagani, A. Sabalina, O. Starkova, B. Fiedler, "Time, Temperature, and Water Aging Failure Envelope of Thermoset Polymers", *Polymer Testing*, 1, 18, (2023).
8. M. Silva, B. Fonseca, H. Biscala, "On Estimates of Durability of FRP based on Accelerated Tests", *Composite Structures*, 116, 377, (2014).
9. K. Blue, M. Alderman, N. Valdes, M. Kranjc "Initial Progress on Tank Bottom Repair for the DOE EM Tank Waste R&D Program", *Poster at Waste Management 2025 Conference,* 2025.
10. K. Blue, M. Alderman, N. Valdes, M. Kranjc "Initial Progress on Tank Bottom Repair for the DOE EM Tank Waste R&D Program 25089", *Proceedings of Waste Management 2025 Conference,* 2025.
11. N. Valdes, "Task Technical Plan for Hanford Tank Bottom Refurbishment Using Grouts", Technical Report *SRNL-RP-2025-00379*, March, 2025.
12. R. Clough, K. Gillend, D. Clegg, G. Collyer, *Irradiation Effects on Polymers*, pp110-111, Ed., Elsevier Applied Science, New York, NY, (1991).
13. Chemical Compatibility Database from Cole-Parmer, 2024

Appendix A. Reasons for Choosing Epoxy

A.1 Radiation Resistance of Polymers [12]

Table 1. Generalized Radiation Resistance of Polymers Under Low and High Dose Rate Conditions

Polymer	Dose Required to Reduce Mechanical Properties by 50% (In most cases physical property is %tensile elongation)			
	Gray		Mrad	
	high dose rate in inert air	low dose rate in air	high dose rate in inert air	low dose rate in air
Polyimide	100,000,000	none	10,000	none
Epoxy	50,000,000	none	5,000	none
Polystyrene	15,000,000	400,000	1,500	40
Natural Rubber	2,000,000	80,000	200	8
Low Density PolyethyeneL (LDPE)	1,000,000	90,000	100	9
Polyamide (aliphatic)	600,000	60,000	60	6
High Density Polyehtylene (HDPE)	400,000	10,000	40	1
Polymethyl methacrylate (acrylic)	150,000	none	15	none
Polytetrafluoroethylene (PTFE)	60,000	1,000	6	0.1

A.2 Epoxy Resistance to Sodium Hydroxide [13]

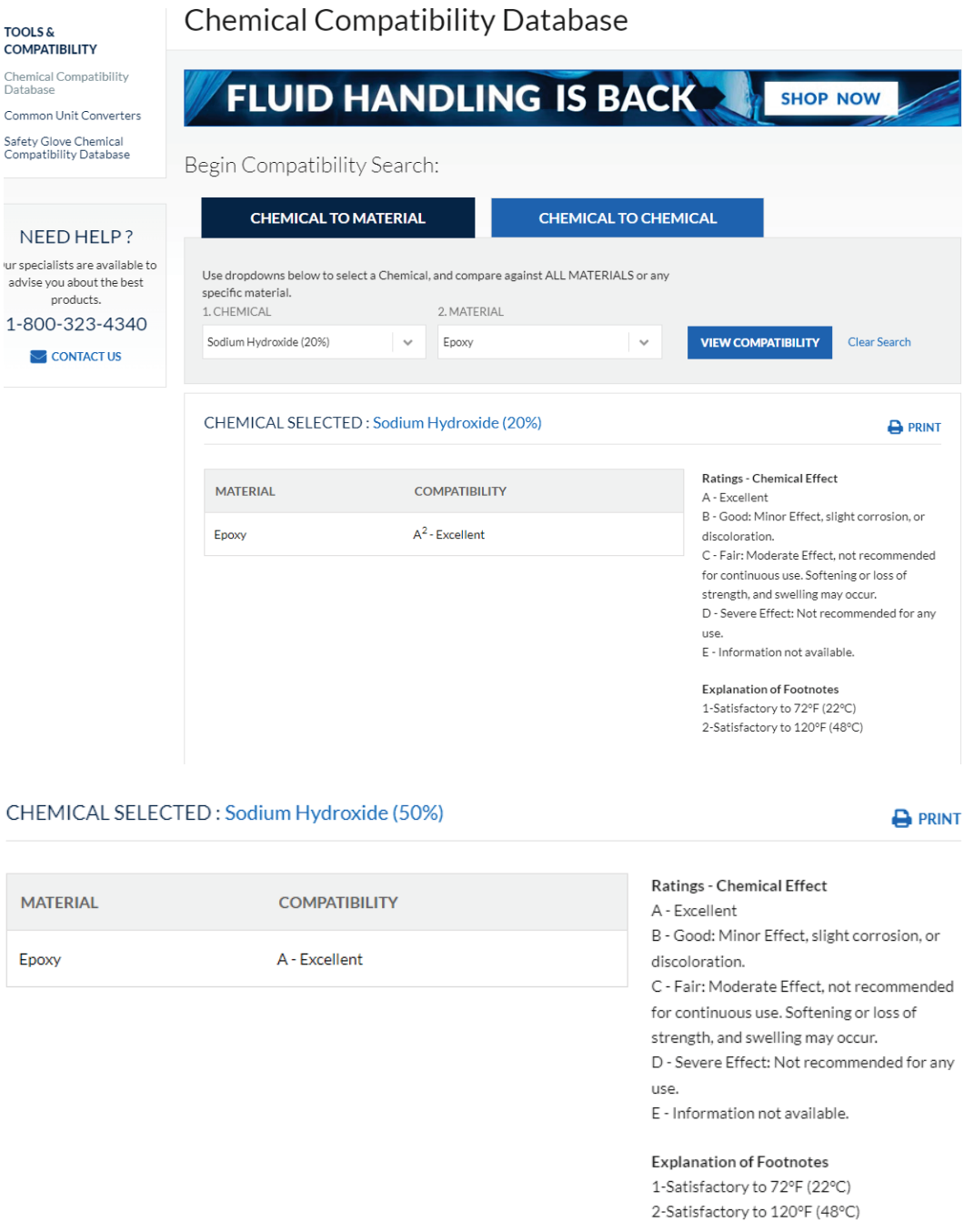

Figure 1. Sodium Hydroxide Resistance of Epoxy. [12]

Appendix B. Table of Epoxies, Diluents, and Curatives

Table 2. Table of Epoxy Resins and Diluents

Name	Structure	Source	Notes	Example Resin	Example Source	Fluid Characteristics
Bisphenol A Diglycidyl Ether (BADGE)	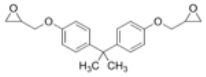		Ubiquitous epoxy resin, used in many different applications. Most commercial epoxy grouts that I looked at used this as the primary resin component.	D.E.R. 321, very low viscosity, suggested for grouting. Mix of BADGE and the monoepoxy: 1-(2-Methoxyphenoxy)-2,3-epoxypropane		Varies depending on the degree of polymerization, from a viscous liquid to a semisolid for high molecular weight resins.
Bisphenol F Diglycidyl Ether (BFDGE)	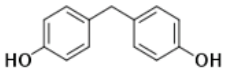		Image is of the precursor BPF. BFDGE has epoxide groups replacing the hydroxide groups. Lower viscosity than BA, and supposedly provides better chemical resistance than BA. This resin may be good both on its own, or mixed with other resins as a reactive dilutant to reduce their viscosity.	Five Star Epoxy Novolac Grout, it's called a novolac (which would make it a phenol-formaldehyde or similar resin) but it's actually ~80% BFDGE.	https://www.fivestarproducts.com/product/epoxy-novolac-grout/	Typically liquid for low MW resins.
Furan-based and benzene-based diepoxies		https://pubs.acs.org/doi/10.1021/acssuschemeng.0c09313	These resins form an epoxy with a lower Tg than that of BADGE when using the same hardener. A lower Tg often means higher toughness, but a Tg near the working temperature is undesirable.			Liquid?
Naphthalene-Based Epoxy, ex. E-DHN	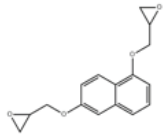	https://www.dic-global.com/pdf/products/catalog/dic_epoxy_for_composite_en.pdf	Has good mechanical properties, such as higher Tg and modulus, but resins made from this seem to be mostly solid or semisolid at room temperature.	HP-4032SS	https://www.dic-global.com/pdf/products/catalog/dic_epoxy_for_composite_en.pdf	Semisolid

Table 2 (cont'd)

Name	Structure	Source	Notes	Example Resin	Example Source	Fluid Characteristics
Epoxy Phenol Novolac (EPN)	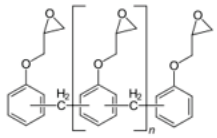	https://www.buildsite.com/pdf/fivestarproducts/Five-Star-Epoxy-Novolac-Coating-Product-Data-2230573.pdf & https://www.dic-global.com/en/products/epoxy/phenol_mn/	Unlike standard novolac resins, EPN has epoxide groups in place of the hydroxide groups, similar to the BPA-based epoxy resins. Can be cured into a highly crosslinked structure due to each monomer unit having an epoxide group. May need a solvent such as furfuryl alcohol, or a dilutant such as hexanediol diglycidyl ether, in order to become a liquid.	Epiclon N-730a	https://omnexus.specialchem.com/product/r-dic-corporation-epiclon-n-730a	Lowest provided product from the source is an exceptionally viscous liquid/semisolid (50,000+cPs viscosity). Higher M.W. products are solid with a softening point of 60+ C. Sometimes mixed with BFDGE or a solvent to reduce the viscosity.
Epoxy Cresol Novolac (EOCN)	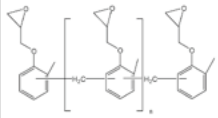	https://www.sciencedirect.com/science/article/pii/S0032386102005384 & https://www.dic-global.com/en/products/epoxy/cresol_novolac/	Very similar to EPN, but each monomer has a methyl group in the ortho position of the phenol. I haven't found any good information on the particular benefits of EOCN over EPN, but EOCN seems to be specialized for electrical applications while EPN is used more for chemical tanks and the like.	Epiclon N-660		Most pure resins made of EOCN seem to be solid or semisolid.
1,6-Hexanediol diglycidyl ether (HDDGE)	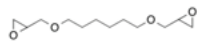	https://www.sciencedirect.com/science/article/abs/pii/S0950061820331081#:~:text=Pull%2Dout%20tests%20revealed%20that,an%20overall%20improvement%20of%20755.2%25.	Just one of a family of primary diol based epoxies. In the cited study, this compound reduces the viscosity and increases the toughness of the epoxy. It (and other diol epoxies) is commonly used as a reactive dilutant in many epoxies. However, its addition does affect the properties, and the long, aliphatic nature of this compound gives me concerns about radiation stability. It nonetheless may be a good reactive diluting agent if BFDGE does not give a low enough viscosity.			Liquid
Trimethylolpropane triglycidyl ether	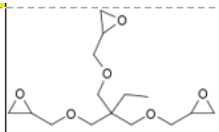	https://www.sciencedirect.com/science/article/abs/pii/S0950061820331081#:~:text=Pull%2Dout%20tests%20revealed%20that,an%20overall%20improvement%20of%20755.2%25.	Just one of a family of triglycidyl epoxies. In the cited study, this compound reduces the viscosity and increases the toughness of the epoxy. Might be a bit more resistant to radiation than the above resin and it has three reactive groups rather than two, but it likely would still be weak to radiation compared to aromatic-based resins.			Liquid

Table 3. Table of Epoxy Curatives

Name	Alternative Names(s)	Structure	Type	Solid or Liquid	# Of Acting Hydrogens	Guesstimated Relative Radiation Longevity	Melting Point	Viscosity at 25C, cps	BADGE Glass Transition Temp	Pot Life	Cure Temperature	Cure Time	Comments	Source(s)
Single Chemical Hardeners														
Isophorone Diamene	IPDA		Alicyclic Polyamine	Liquid	4	Medium	10 C	18.2	158 C	1 Hour	80 C, then 150 C	4 hours, then 1 hour	Used in at least one epoxy grout mixture. I feel like the cure temperature/time listed here could be discounted. This compound might make for a decent dilutant and pot life extender. The saturated ring structure might provide less radiation stability than an unsaturated aromatic structure.	https://www.threebond.co.jp/en/technical/technicalnews/pdf/tech32.pdf
2-Methyl-1,5-pentanediamine	2-Methylpentamethylenediamine, Dytek A, MPMD		Modified Chain Aliphatic Polyamine?	Liquid	4	Low	~ -50 o	2.63		Very short (20 minutes?)			Apparently, it cures too fast to be useful on its own.	https://webbook.nist.gov/cgi/cbook.cgi?ID=t5520-10-2&Units=SI https://explore.azelis.com/en_GB/pl_case/dytek-a-amine
Diaminodiphenylsulfone	DDS, Dapsone (as an antibiotic)	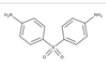	Sulfate-based aromatic amine	Solid	4	High (5e6 kRad without serious degredation)	175 C	Solid		N/A at room temperature	80C then 130 C		Used in the cited study on the radiation resistance of polymers as the curing agent for the epoxy category. This seems to be a high-temperature curing agent and therefore I think it should be ignored.	https://www.osti.gov/servlets/purl/1671937#:~:text=In%20general%2C%20most%20polymers%20can,mechanical%20properties%20and%2For%20performance.
Diethylenetriamine	DTA, DETA		Chain Aliphatic Polyamine	Liquid	5	Low (10x less than DDM)	-39C	5.6		20 Minutes	Normal to 100	30 Minutes to 4 days	Among the most ubiquitous of epoxy hardeners	
4-4'-methylenebis-cyclohexanamine	Wandamin HM, PACM		Alicyclic Polyamine	Solid	4	Medium	40 C	N/A	177 C	Not given	60 C then 150 C	3 hours then 2 hours	Structurally similar to MDA, but is non-aromatic. Since it is solid, the possibility of good room temperature curing seems unlikely.	https://www.threebond.co.jp/en/technical/technicalnews/pdf/tech32.pdf
m-xylenediamene	MXDA	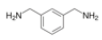	Aliphatic Aromatic amine	Liquid	4	High	14 C	6.8		20 Minutes	Normal to 60	1 Hour to 7 days	Good for solvent free epoxy mixes. Better chemical resistance than IPDA, good low temperature curing. Used in at least one novolac epoxy grout mixture. Short pot life. Has aromatic backbone and is a very low viscosity liquid. My main data source says it is not suited for casting, but is suited for bonding. May make for a good dilutant for higher viscosity hardeners. I think out of all the hardener compounds I have seen, this one has the best overall properties.	https://www.threebond.co.jp/en/technical/technicalnews/pdf/tech32.pdf, &&& http://rotafix.co.uk/wp-content/uploads/2016/01/EP3-EPOXY-GROUT-MSDS.pdf
Triethylene Tetramine	TETA, TTA	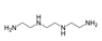	Chain Aliphatic Polyamine	Liquid	6	Low (3x less than DDM)	-35 C	19.4	~127 C?	20-30 minutes	Normal to 100	30 Minutes to 4 days	Provides for great strength, and good adhesion. A simulation found it to have lower Tg and higher mechanical properties than	https://www.sciencedirect.com/science/article/pii/S1093326315300553#sec0005
Metaphenylene Diamine	MPDA		Aromatic Amine	Solid	4	High	62 C	N/A		6 Hours	80C then 150 C	2 Hours, then 4 hours	Unfortunately, it seems to require high temperature curing, like most other aromatic amines.	https://patents.google.com/patent/US2853467A/en
Diethyl Toluene Diamene	DETD, DETDA, EPI, EDICURE W		Aromatic Amine	Liquid	4	High	-9 C	155	~200 C?	Unknown	100-200 C?	23 Minutes at 150 C	I suspect that this compound would result in a longer pot life due to stearic hindrance. That may also hinder crosslinking, however. The aromatic backbone and liquid phase of this compound are both desirable.	https://www.sciencedirect.com/science/article/pii/S0032386106012626, https://www.gantrade.com/tds/detda
Tetraethylenepentamine	TEPA	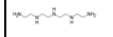	Chain Aliphatic Polyamine	Liquid	7	Low	~-35 C	51.9		30-40 minutes	Normal to 100	30 Minutes to 7 days	This compound is mixed with fatty acids to made an amidoamine hardener in at least one epoxy grout mixture. It's also found on its own in at least one other epoxy grout mixture.	https://en.wikipedia.org/wiki/Tetraethylenepentamine
Furan-Based Amines		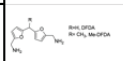	Furan-based aromatic Amine	Solid?	4	Medium	Varies, likely high	N/A	DFDA=128 C, Me-DFDA=142 C				According to the provided source, these hardeners result in a significantly lower Tg than PACM using the same resin. Furan might be less radiation stable than benzene however.	https://pubs.acs.org/doi/10.1021/acssuschemeng.0c09313
1,3-Cyclohexanebis(methylamine)	1,3-BAC		Cycloaliphatic Amine	Liquid?	4	Medium	<-25 C	9.21					Identical structure to MXDA, but the ring structure is fully saturated instead of aromatic.	https://www.euclidchemical.com/fileshare/ProductFiles/msds/TD5323122NC_c.pdf
Poly(ethylene glycol) diamine	Jeffamine (trade name)		Polyetheramine	Varies from liquid to solid depending on value of n	4	Low							According to the source, this class of hardeners has reduced reactivity due to stearic hindrance. It could potentially help as an additive to increase pot life.	https://www.pcimag.com/articles/85952-amine-curing-of-epoxy-resins-options-and-key-formulation-considerations

Appendix C. Boundary Conditions for the Refurbished Tank

- Type of Tank to Refurbish: **Double Shell Tank (DST)**
- Condition of Tank to Refurbish: **No through-wall penetration, still deemed usable**
- Activity of any Residual Radionuclides still at bottom: **Unknown at this time**
- Estimated ambient tank bottom temperature during pour (30' below ground): **20^{O} C**
- Approximate service temperature: **15 - 27^{O} C**
- Minimum Epoxy T_g : **47^{O} C (20^{O} C above service temp)**
- Maximum radiation level of liquid waste tank: **0.175 mCi/L**
- Maximum dose rate of tank waste to epoxy: **< 0.126 Rads/hr**
- Alkalinity of tank waste solution: **4% NaOH (1M, pH=14)**
- Diameter of tank bottom to cover: **75 ft**

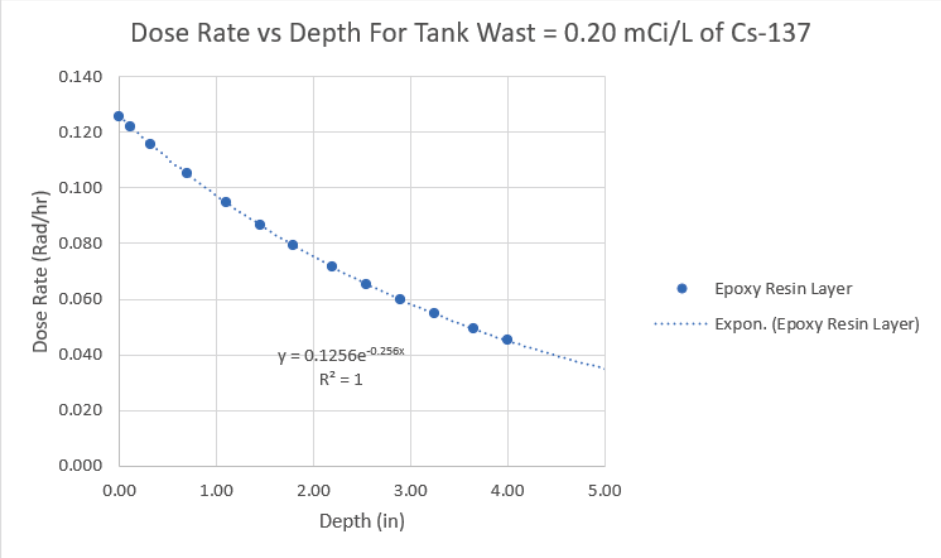

Figure 2. Calculated Radiation Dose Rate Through the Cross Section of the Epoxy Sealant Layer

Table 4. Final Epoxy Properties Needed in Epoxy Sealant Layer

No.	Property	Criterion	Method to Determine	Reasoning/Comments
1	Workability Life (or Pot Life)	TBD. Currently 1 hour to 1.5 hours?	Rheometer, DSC, large scale testing in year 2 and 3 to compliment rheometer and DSC data	- Depends on: 1. Inherent resin viscosity, which will depend on shear rate, temperature, rate of cure, etc; 2. Diameter & number of conduits; 3. Pump capacity; 4. Volume and thickness of the epoxy layer; 5. Will resin fronts from different conduits bond sufficiently
2	Required thickness of Epoxy Layer	TBD. Currently should vary between 3/8" to 2". What is reasonable for a self leveling grout	TBD	- What is a reasonable range of epoxy layer thickness considering that the self leveling grout layer will not be perfectly self leveling - What is the minimum thickness needed for sealing, is it thicker than 3/8" - The maximum thickness also depends on the mimimum temperature needed during cure (see item 3), water uptake during service and therefore expansion (will that lead to cracking?), is coefficient of expansion between service temperature range (15 to 27 C) significant, will CTE change with thickness(?), etc.
3	Low Maximum Cure Temperature	TBD	Rheometer, DSC, maybe ThermTest. Large scale testing to confirm predictions	- To prevent cracking of epoxy layer as it cures - heats up - cools after cure. - At some point polymer turns glassy (Tgel?), is bonded to the lower surface, and cannot deform any longer due to the glassy state and cracks. - What is CTE at various degrees of cure and temperature. ThermTest measures CTE on solid samples only.
4	Glass Transition Temperature (T_g)	> or = 50^{O} C approximately 20^{O} C above max service temperature (27^{O} C)	DSC	- Less degradation occurrs in the glassy state - Confirm that 15 to 27 C temp indicated by WRPS is during service (60 C was previously mentioned) NOT during the pour or pumping of epoxy to tank bottom.
5	Low moisture absorption	4% maximum.	TTCS, weighment	- Could cause expansion and cracking
6	Degree of Cure	TBD	DSC, FTIR, point of m	- May be able to minimize degree of cure and still obtain a Tg at or above 50 C - If degree of cure is low and Tg of epoxy at bottom of tank is above 50 C then applied energy (due to aging at room temp, rad from tank waste) would be expended in crosslinking reactions rather than in degradation reactions. Suspicion is that completing crosslinking would occur before degradation due to lower Ea of crosslinking than degradation
7	Cure Shrinkage	0% or a maximum that is low enough to accommodate a 75' monolith	Test on large sample	- needed so there is no gap between monolith and tank wall - robots can apply an epoxy sealant at gap between wall and monolith - could spray an epoxy layer instead of pour an epoxy layer but it will take quite a long time for robots to do this up to 3/8" thick, seems like using robots to spray coat an epoxy sealant layer at the gap would be simpler and faster (would need a study in both methods). Can we rely on the robots to get a consistent coating (use of Lidar QA method?)
8	Coefficient of Thermal Expansion (CTE	Low as possible or a low use Temp range? - Could temp of waste in tank be controlled to ensure a temp range of say 25 to 30 C?	ThermTest	- Does this depend on thickness variation? - might help to prevent cracking if the epoxy could accomodate a certain level of expansion with change in temp but temp should not change below the freeze line - some elasticity without creep could maintain adhesion
9	Toughness	TBD	Compression Stress/Strain Curve	- Could help prevent cracking - CTE may help with cracking as well

Appendix D. Processing Property Testing of Epoxies

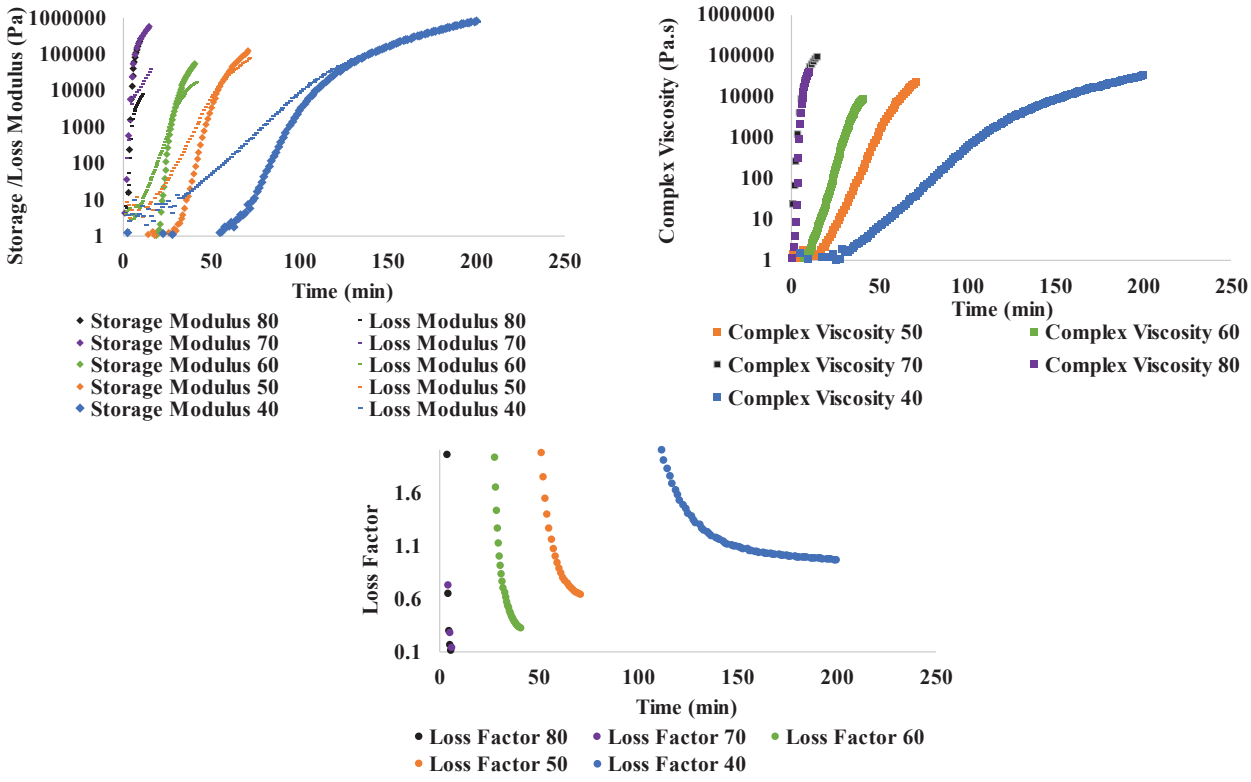

Figure 3 Rheological Isothermal analysis of Sikadur 42 epoxy cure showing the storage modulus, loss modulus, loss factor and complex viscosity at 40, 50, 60, 70, 80° C.

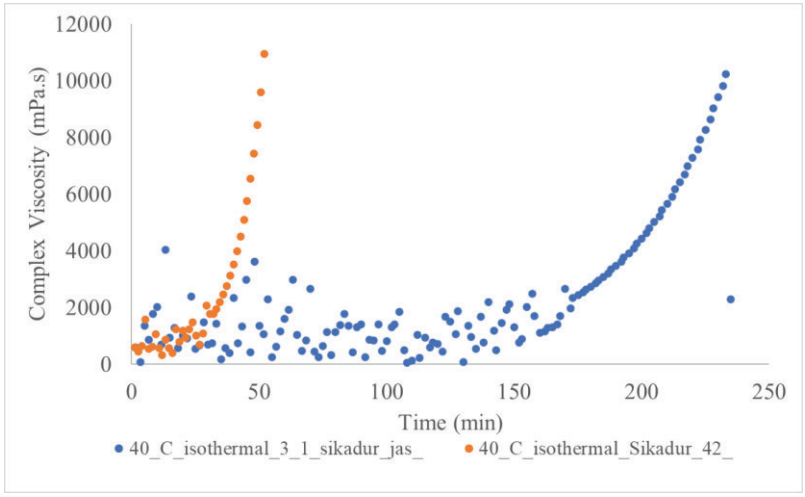

Figure 4. Change in viscosity versus time of Sikadur 42 epoxy:curative, 3:1 ratio (orange dots) and Sikadur 42 epoxy:Jeffamine curative 3:1 ratio (blue dots). Time to 10,000 mPa-s viscosity goes from 52 minutes with Sikadur 42 curative to 235 minutes with Jeffamine curative.

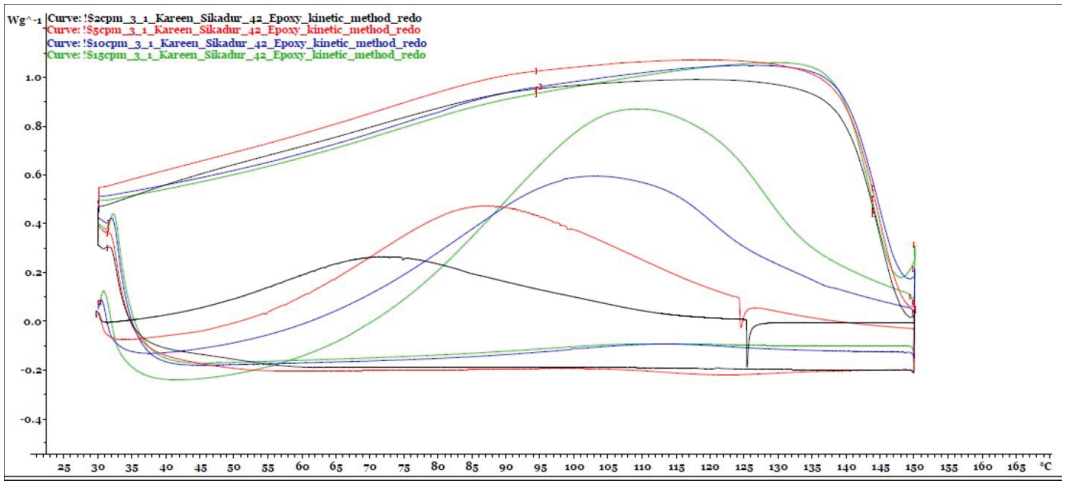

Figure 5. DSC thermogram of Sikadur 42 epoxy cure under non-isothermal conditions ramping from 30° C – 150° C at 2, 5, 10, 15 °C/min.

Appendix E. Outline of Scoping Experiments for Accelerated Aging

COMPRESSION CYLINDER SCOPING (ASTM D695)

Control samples (no aging); No. of samples = 5
Cylinders are 0.5" dia x 1.0" length

TTS Boundary

below Tg

Temp (C)	days	hours	No. of cylinders
10 C below Tg	30	720	3
10 C below Tg	60	1440	3
10 C below Tg	TBD	TBD	3
		TOTALS	9

above Tg

Temp (C)	days	hours	No. of cylinders
150 C	30	720	3
150 C	60	1440	3
150 C	TBD	TBD	3
		TOTALS	9

TTCS Boundary

Temp (C)	days	hours	No. of cylinders
100	30	720	3
100	60	1440	3
100	TBD	TBD	3
		TOTALS	9

Gamma boundary

Dose Rate (Rad/hr)	Total Dose (Mrad)	hours	days	No. of samples
400,000	100	250	10	3
400,000	200	500	21	3
400,000	TBD	TBD	TBD	2
			TOTALS	8

ADHESION SCOPING (ASTM D4541)

Control samples (no aging); No. of samples = 1 grout plate (4 dollies)
Grout/Epoxy Interface: 130mm x 130mm x 38mm (1.5") grout plate and 9.5 mm (3/8") layer of epoxy plus 9 disks between 1.53" and 1.56" dia

TTS Boundary

below Tg

Temp (C)	days	hours	No. of plates
10 C below Tg	30	720	1
10 C below Tg	60	1440	1
10 C below Tg	TBD	TBD	1
		TOTALS	3

above Tg

Temp (C)	days	hours	No. of disks
150 C	30	720	3
150 C	60	1440	3
150 C	TBD	TBD	3
		TOTALS	9

TTCS Boundary

Temp (C)	days	hours	No. of disks
100	30	720	3
100	60	1440	3
100	TBD	TBD	3
		TOTALS	9

Gamma boundary

Dose Rate (Rad/hr)	Total Dose (Mrad)	hours	days	No. of platees
100,000	100	1000	42	3
100,000	200	2000	83	3
100,000	TBD	TBD	TBD	3
			TOTALS	9

Appendix F. Results of Developing Methodologies for Physical Property Testing

Table 5. Results of Compression Strength Testing versus Days of Room Temperature Cure

Epoxy	Sample #	Diameter (inches)	Length (inches)	# Days Cured	Yield Stress (Mpa)	Graph Modulus (Mpa)	Strain at Failure	Stress at Failure (Mpa)
Sikadur	1	0.5	1	28	72.9	1419.8	0.43	69.5
Sikadur	2	0.5	1	28	74.6	1329.9	0.50	111.7
				avg	**73.7**	**1374.9**	**0.46**	**90.6**
				st dev	**NA**	**NA**	**NA**	**NA**
Sikadur	1	0.5	1	17	83.4	1736.7	N/A	N/A
Sikadur	2	0.5	1	17	82.5	1747.8	N/A	N/A
				avg	**83.0**	**1742.3**		
				st dev	**NA**	**NA**		
Sikadur	1	0.5	1	9	90.0	1730.1	N/A	N/A
Sikadur	2	0.5	1	9	91.0	1843.9	N/A	N/A
Sikadur	3	0.5	1	9	94.0	1815.1	N/A	N/A
				avg	**91.6**	**1796.4**		
				st dev	**2.1**	**59.2**		
Sikadur	Test to failure	0.5	0.9	7	78.0	1514.4	0.51	92.07
Sikadur	1	0.5	0.9	7	77.0	1517.1	N/A	N/A
Sikadur	2	0.5	0.9	7	77.4	1530.9	N/A	N/A
Sikadur	3	0.5	0.9	7	77.3	1530.6	N/A	N/A
Sikadur	4	0.5	0.9	7	74.0	1453.7	N/A	N/A
				avg	**76.7**	**1509**		
				st dev	**1.6**	**32**		
Sikadur	Test to failure	0.5	0.9	5	82.424	1669.9	0.52	128.4
Sikadur	1	0.5	0.9	5	80.17	1588.6	N/A	N/A
Sikadur	2	0.5	0.9	5	85.14	1719.3	N/A	N/A
Sikadur	3	0.5	0.9	5	78.04	1547.1	N/A	N/A
Sikadur	4	0.5	0.9	5	81.7	1665.9	N/A	N/A
Sikadur	5	0.5	0.9	5	81.67	1647.3	N/A	N/A
Sikadur	6	0.5	0.9	5	84.95	1681.7	N/A	N/A
				avg	**82.0**	**1646**		
				st dev	**2.5**	**59**		
Sikadur	Test to failure	0.5	0.9	3	66.66	1394.5	0.565	114.7
Sikadur	1	0.5	0.9	3	64.96	1354.0	N/A	N/A
Sikadur	2	0.5	0.9	3	68.63	1408.5	N/A	N/A
Sikadur	3	0.5	0.9	3	68.42	1385.3	N/A	N/A
Sikadur	4	0.5	0.9	3	67.45	1378.9	N/A	N/A
Sikadur	5	0.5	0.9	3	65.87	1338.1	N/A	N/A
Sikadur	6	0.5	0.9	3	67.79	1352.8	N/A	N/A
				avg	**67.1**	**1373**		
				st dev	**1.4**	**25**		
Sikadur	Test to failure	0.5	0.9	1	NA	37.7	NA	NA
Sikadur	1	0.5	0.9	1	NA	51.8	NA	NA
Sikadur	2	0.5	0.9	1	NA	60.2	NA	NA
Sikadur	3	0.5	0.9	1	NA	58.6	NA	NA
Sikadur	4	0.5	0.9	1	NA	58.9	NA	NA
				avg	**NA**	**53.4**		
				st dev	**NA**	**9.4**		

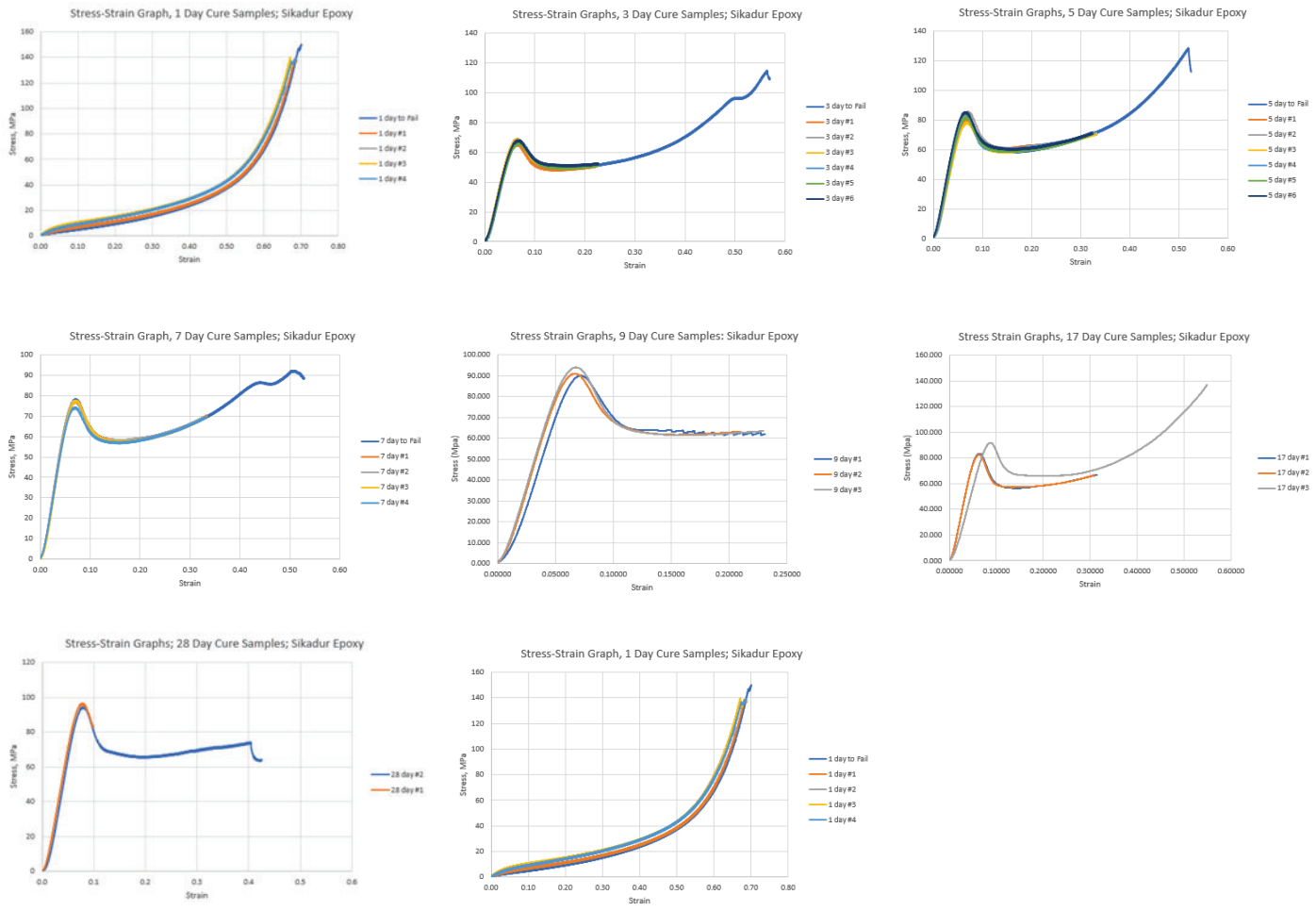

Figure 6. Stress Strain Curves for Compression Strength of 1 through 28 days of Cure.

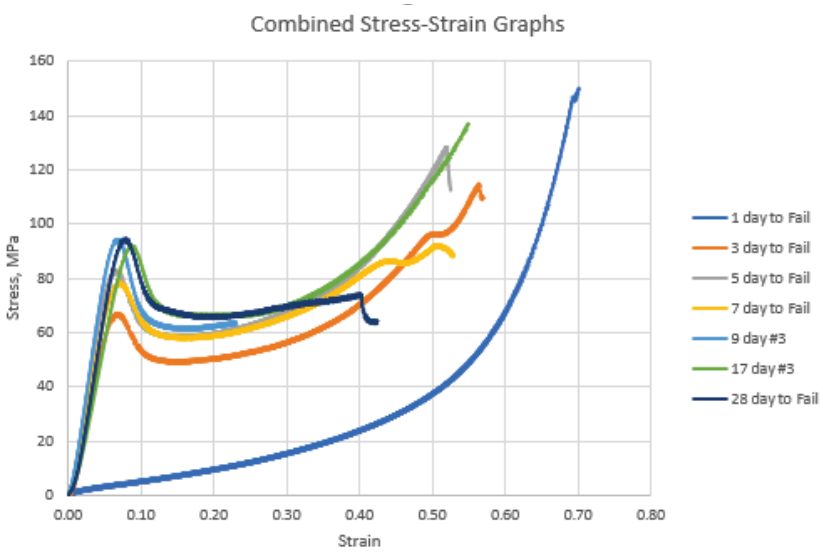

Figure 7. Combined Stress Strain Curves from Figure 4.

Table 6. Change in T_g with Cure Time

Cure Time (days)	Tg (C) 1st Heat	Tg (C) 2nd Heat	1st Heat	2nd Heat	
84	65	60			
84	55	60	60	60	**avg**
56	53	57			
56	54	54			
56	54	54			
56	55	53			
56	55	59	55	55	**avg**
56	56	53	1.0	2.5	**st dev**
28	51	58			
28	50	57			
28	49	59			
28	45	58			
28	49	58			
28	51	60			
28	49	57			
28	50	60	49	58	**avg**
28	47	57	1.9	1.4	**st dev**
7	49	72			
7	49	70			
7	50	72			
7	50	70	49	71	**avg**
7	50	71	0.5	1.2	**st dev**
5	49	72			
5	50	72			
5	51	78			
5	48	82	50	75	**avg**
5	51	73	1.1	4.3	**st dev**
3	50	76			
3	49	73			
3	48	77	49	75	**avg**
3	50	75	1.2	1.8	**st dev**
1	35	73			
1	38	73			
1	42	71			
1	46	76	41	73	**avg**
1	43	74	4.4	2.0	**st dev**

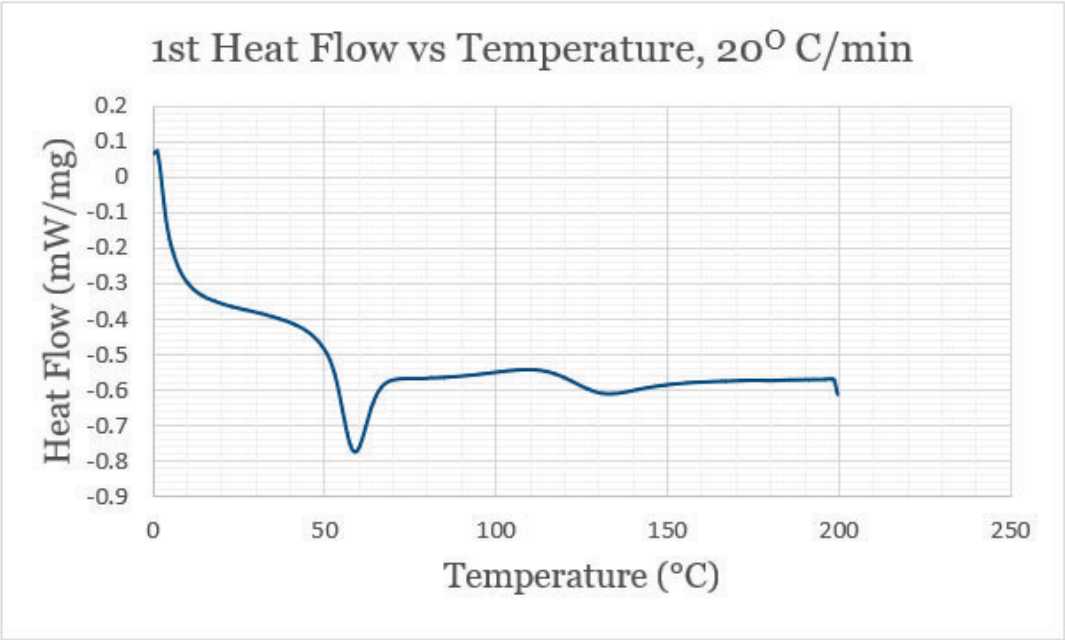

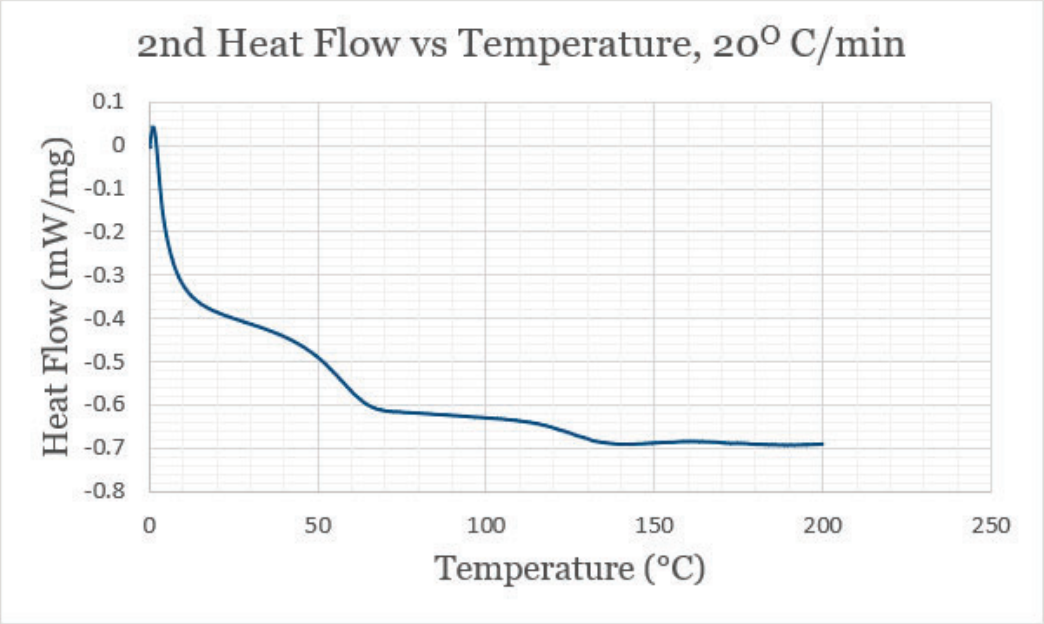

Figure 8 Determination of T_g by DSC for Sikadur 42 Epoxy after 28 days of cure at room temperature. Results from a Heat-Cool-Heat cycle on the same sample. Heat ramps were 20^O C/min. T_g after first heat ramp is 49^O C and T_g after second heat ramp is 59^O C.

Distribution:

Camden Chatham
Benjamin Barkai
Charles W. James
Haley Jones
Will Jolin
Kiana Sykes
Morgan Whiteside
Bruce Wiersma
Cade Willis

Savannah River National Laboratory®

A U.S. DEPARTMENT OF ENERGY NATIONAL LAB • SAVANNAH RIVER SITE • AIKEN, SC • USA

Task Technical Plan for Hanford Tank Bottom Refurbishment Using Grouts

N. Valdes

April 2025

SRNL-RP-2025-00379, Rev. 0

srnl.gov

Task Technical Plan for Hanford Tank Bottom Refurbishment Using Grouts

N. Valdes

Savannah River National Laboratory is operated by Battelle Savannah River Alliance for the U.S. Department of Energy under Contract No. 89303321CEM000080.

Savannah River National Laboratory®

1.0 APPROVALS/TASK TECHNICAL REQUEST IDENTIFICATION

Task Lead: N. Valdes	**Signature/Date:** NICHOLAS VALDES (Affiliate) Digitally signed by NICHOLAS VALDES (Affiliate) Date: 2025.04.01 09:18:35 -04'00'	**Organization:** **SRNL – ELM and Materials Technology & Energy Sciences**
Technical Reviewer: K. Hill	**Signature/Date:** KATIE HILL (Affiliate) Digitally signed by KATIE HILL (Affiliate) Date: 2025.04.01 16:15:22 -04'00'	**Organization:** **SRNL – ELM and Materials Technology & Energy Sciences**
Technical Reviewer: B. Wiersma	**Signature/Date:** BRUCE WIERSMA (Affiliate) Digitally signed by BRUCE WIERSMA (Affiliate) Date: 2025.04.02 13:25:25 -04'00'	**Organization:** **SRNL – ELM and Materials Technology & Energy Sciences**
Approver: C. Langton	**Signature/Date:** CHRISTINE LANGTON (Affiliate) Digitally signed by CHRISTINE LANGTON (Affiliate) Date: 2025.04.02 12:18:24 -04'00'	**Organization** **SRNL – ELM and Materials Technology & Energy Sciences**
Principal Investigator: M. Kranjc	**Signature/Date:** MARK KRANJC (Affiliate) Digitally signed by MARK KRANJC (Affiliate) Date: 2025.04.02 12:56:19 -04'00'	**Organization:** **SRNL – ELM and Materials Technology & Energy Sciences**
Lead Principal Investigator: P. Shukla	**Signature/Date:** PAVAN SHUKLA (Affiliate) Digitally signed by PAVAN SHUKLA (Affiliate) Date: 2025.04.02 13:54:59 -04'00'	**Organization:** **SRNL – ELM and Materials Technology & Energy Sciences**
Manager: C. James	**Signature/Date:** CHARLES JAMES (Affiliate) Digitally signed by CHARLES JAMES (Affiliate) Date: 2025.04.02 14:27:46 -04'00'	**Organization:** **SRNL – ELM and Materials Technology & Energy Sciences**
Division Director: J. Manna	**Signature/Date:** JOSEPH MANNA (Affiliate) Digitally signed by JOSEPH MANNA (Affiliate) Date: 2025.04.02 14:55:16 -04'00'	**Organization:** **SRNL – ELM and Materials Technology & Energy Sciences**

Technical Task Request Title: *Hanford Tank Waste R&D Award (277993)*	**Document Number:** **2024-58 BSRA FP # 45 REV 0** **Work Authorization 277993** **Revision: 0**	**Approved Date:** **03/15/2024**

LIST OF REVISIONS

Revision Number	Summary of Changes	Date
0	Initial	04/03/2025

2.0 INTRODUCTION

The Hanford site has interest in refurbishing Hanford double shell waste tanks to address cracking and thinning at the bottom of their carbon steel tanks. The objective is to prevent liquid nuclear waste from leaking into the annulus space which separates the tanks from the external environment. Hanford Tank Waste Operations and Closure (H2C), the operating contractor for the Hanford site, plans to use one or more of the leaking tanks to store decontaminated supernate which will be generated as waste is removed from tanks and processed for final disposal. The tanks identified for refurbishing and extended use range in size from 30,000-gallon tanks to 1M gallon tanks that are 23 m (75 ft) in diameter.

In 2024 Savannah River National Laboratory (SRNL) received funding from Department of Energy Environmental Management (DOE EM) for EM001 Hanford Tank Waste R&D Work Authorization 277993, "Integrity Monitoring and Assessment, Prediction, Repair, and Corrosion Control of the Hanford Storage Tanks" [1].

2.1 Task Definition

This Technical Task Plan (TTP) addresses the following technical needs:

- Developing and implementing a conceptual plan for refurbishing Hanford waste tanks that provides a clean working surface that can be sealed to prevent aqueous leaks into the annulus space.
- Identifying potential cementitious grouts that can be installed in the tank through a central or other risers on the tank top. The purpose of the grout is to serve as a "false bottom"[1] that is chemically compatible with tank residuals and can be placed by existing technology used for tank closure at SRS and the tank closure demonstration for Hanford tanks [2, 3]. The cementitious grout layer must also be capable of being coated with a sealant which includes materials such as an epoxy [4]. See the SRNL conceptual model for the proposed refurbishing strategy, Figure 1. At this time, refurbishing cementitious grouts will not have steel fibers in the mix.
- Identifying / proposing attributes and properties for the false bottom grout, e.g., layer thickness, grout volume, grout production options for candidate grouts (trucks from ready mix plant), grout placement rate and placement method for self-leveling in tank, flowability, chemical compatibility with tank residuals, sealant material, and decontaminated supernate generated as the result of removing and processing tank waste.
- Determining relevant grout layer features and measuring grout performance parameters.
- Testing grout performance for the relevant properties.
- At this time, epoxies have been selected as the sealant. Assist the project team to perform scoping tests for grout-epoxy and/or other coating compatibility [4].

[1] RPP-RPT-62020 defines stabilization grout as flowable Portland cement-type grout that would be used as a false bottom similar to tank closure at the Savannah River Site, and Polymer Grout as similar to stabilizing grout but includes polymers within the cement matrix.

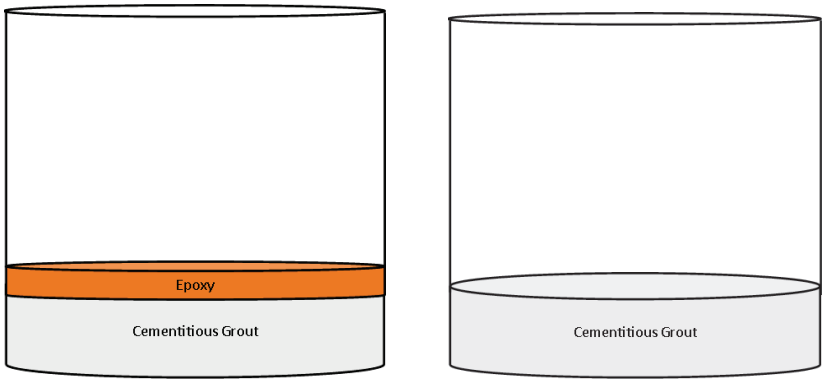

Figure 1. Schematic of the bottom repair layers, first layer being cementitious followed by second layer of an epoxy. A single cementitious grout layer may also be considered if the epoxy sealant layer proves to be too difficult to apply over a 75 ft (23 m) diameter. Drawing is not to scale.

This work will be performed in phases starting with Phase 1, Bench-scale Testing of grout and sealant followed by Phase 2, Engineering-scale Testing. Phase 3 will provide recommendations for Full-scale Testing, but the actual testing is outside this task plan.

2.2 Customer/Requester

DOE EM funded this work under the Hanford Tank Waste R&D Work Authorization 277993. The end user is H2C, the Hanford site contractor.

2.3 Task Responsibilities

Researchers in the Environmental and Legacy Management (ELM) Directorate, Materials Technology and Energy Sciences Division will be the primary performers of this task. Their responsibilities include:

- Preparing this TTP, and other documentation for example addressing documentation required in the SRNL Hazard Analysis System (HAS).
- Planning and executing laboratory activities, ordering materials, preparing samples, and characterizing samples.
- Interacting with vendors to acquire sample products for testing.
- Establishing non-disclosure agreements with other companies as needed.
- Ensuring hands on workers have the proper training to perform lab work.
- Ensuring tasks are completed in a timely manner, on schedule.
- Ensuring instrumentation is calibrated.
- Providing project updates as requested.
- Participating in pre-job briefings and performing lab work safely.
- Following directions or instructions for lab tasks.
- Maintaining records of lab activities and sample generation in the ELN (Electronic Laboratory Notebook).
- Compiling, analyzing, and interpreting data generated by sample preparation and testing.
- Interacting with the Hanford site and H2C regarding solutions for the project goals.
- Dispositioning all waste generated by the task through appropriate channels and documentation.

Additional support may be needed from other groups at SRNL for experimental setup and execution.

2.4 Task Deliverables

Monthly status updates will be prepared. Reports after each phase of work will be written, completed by SRNL personnel.

Table 1. Deliverables and estimated due dates.

Deliverable	Review	Date*
Task Technical Plan (TTP)	M. Kranjc, P. Shukla, C. James	4-3-2025
Monthly progress updates	M. Kranjc, P. Shukla	First week of each month
Report 1: Bench-scale Results	M. Kranjc, P. Shukla, C. James	12-1-2025
Report 2: Engineering-scale Results	M. Kranjc, P. Shukla, C. James	4-1-2026 Part A 12-1-2026 Part B
Report 3: Recommendations for Full-scale Testing	M. Kranjc, P. Shukla, C. James	4-1-2027

*Dates for Report deliverables are estimated.

3.0 TASK ACCEPTANCE CRITERIA

SRNL personnel will review the TTP and three technical reports for technical adequacy and appropriate content and the final documents/reports will be signed by the authors and approvers certifying accuracy and completeness of the information provided. The final technical reports will be reviewed per SRS Manual E7, Procedure 2.60 [5]. Acceptance shall be indicated by approval of the final technical reports.

4.0 TASK ACTIVITIES

Phase 1. False-bottom grout testing.

- Literature Review: Obtain and review flowable low porosity cementitious grout designs and test data.
    - Low water : cementitious materials grouts,
    - Self-healing grouts,
    - Grouts containing pore plugging ingredients.
- Identify options and material for modifying these cementitious grouts to achieve better flow and order products that are used for increasing flowability and decreasing porosity/permeability for concrete.
    - Screen samples based on fresh properties of the modified grouts.
    - Test cured properties if fresh properties are acceptable.
- Prepare samples of cementitious grouts selected for testing.
- Perform *initial bench-scale scoping* evaluation of selected cementitious grouts for processibility and fresh properties, for example bleed water, wet density, set time, flowability, entrapped air, surface characteristics relevant to bonding, epoxy or coating adhesion.
- Down Select and Measure Cured Properties: Measure cured properties on selected grouts for example, strength as a function of curing time up to 28 days, porosity, hydraulic conductivity, leachability, and diffusivity.
- Pour cementitious grouts into forms that are approximately 2 ft x 1.5 ft wide and 2 in x 4 in cylinders for 1) use in property testing and 2) fresh property / flow evaluation at pre-Engineering-scale. Work

with project team to pour epoxy over cured cementitious grout to test flow, grout-epoxy adhesion, and prepare samples for durability testing.

- Work with project team to test methods to evaluate epoxy-grout properties using 1-3 cementitious grouts and relevant epoxies such as the ones tested by AVANTech, LLC [6].
    - Adhesion and interfacial features, screen composite samples for accelerated aging
    - Interfacial characterization: options include bond strength, microstructure, microhardness, permeability.
    - Durability and dimensional stability of cementitious grout samples and epoxy coated grout samples in the tank environment during use for expected conditions and accelerated aging (increased temperature). Evaluate permeability of simulant through grout/epoxy to underlying bottom.

Phase 2. Engineered-scale testing.

- Perform small-scale mock up tests to identify mixing and pumping parameters that are needed to specify equipment and design operating conditions for the larger scale testing.
- Select best grout and epoxy candidates from Phase 1 and obtain materials.
- Testing will first be performed with 3-4 ft diameter forms, then afterwards will proceed to 10-20 ft diameter forms.
- For reference, the volume of materials required for a various diameter forms are listed in the tables below.

Table 2. Approximate Cement Grout Volume.

Diameter (ft)	Diameter (m)	Thickness (in)	Volume (ft^3)	Volume (yd^3)	Volume (m^3)
3	0.9	3	1.8	0.1	0.1
3	0.9	6	3.5	0.1	0.1
10	3.0	3	20	0.7	0.6
10	3.0	6	42	1.6	1.2
20	6.1	3	79	2.9	2.2
20	6.1	6	160	6.0	4.5

Table 3. Approximate Epoxy Volume.

Diameter (ft)	Diameter (m)	Thickness (mil)	Thickness (mm)	Volume (ft^3)	Volume (yd^3)	Volume (m^3)
3	0.9	20	0.5	$1*10^{-2}$	$4*10^{-4}$	$3*10^{-4}$
3	0.9	100	2.5	0.1	$2*10^{-3}$	$2*10^{-3}$
3	0.9	500	12.7	0.3	$1*10^{-2}$	$1*10^{-2}$
10	3.0	20	0.5	0.1	$5*10^{-3}$	$4*10^{-3}$
10	3.0	100	2.5	0.7	$2*10^{-2}$	$2*10^{-2}$
10	3.0	500	12.7	3.3	$1*10^{-1}$	$1*10^{-1}$
20	6.1	20	0.5	0.5	$2*10^{-2}$	$1*10^{-1}$
20	6.1	100	2.5	2.6	$1*10^{-1}$	$1*10^{-1}$
20	6.1	500	12.7	13.1	$5*10^{-1}$	$4*10^{-1}$

- Identify equipment to procure and determine location to perform the initial small scale placement demonstration for Phase 2. Figure 2 shows a schematic of the proposed Engineered-scale setup for pumping and placing grout and epoxy in the 10-20 ft form from a central discharge location. Equipment and materials that need to be acquired or assembled are listed below:
    - Cylindrical form of steel or plastic, 10-20 ft in diameter.
    - Ingredients for tank refurbishing grout
    - Grout mixer or grout ordered from a local batch plant and delivered to the test location via concrete transit mixer (8 cubic yd).
    - Mixer for epoxy
    - Grout Pump
    - Epoxy Pump
    - Tremies or hard pipe (depending on drop height of the grout).
    - Scaffolding to support hardware going over the cylindrical form.
- Construct scaffolding to support delivery system at the designated location.
- Obstacles should also be added into forms to simulate potential issues for grout and epoxy flow. This includes the condition of the tank floor (residual salts) and if the bottoms of the air lift circulators are close enough to the tank floor.
- Determine and optimize grout and epoxy pump / discharge rates.
- Mix cement and epoxy and pump into the form.
- Evaluate the following:
    - Grout and epoxy's ability to flow and cover the entire diameter.
    - Thickness of the cementitious grout and epoxy across the diameter.
    - Adhesion to the sidewalls of the cylinder form.
    - Collect samples from the engineered-scale test for characterization of fresh and cured properties.

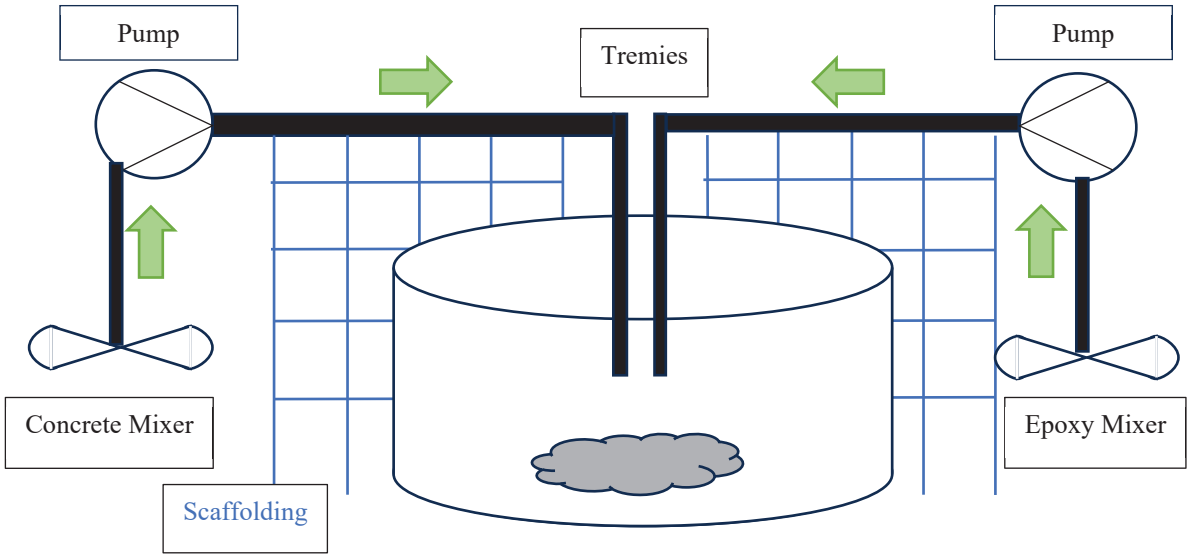

Figure 2. Schematic of setup and components for the medium scale testing. The epoxy section in the drawing assumes a single component product, however, two component epoxies are more likely, and thus would require sub-sections with 2 lines and an in-line mixer.

Phase 3. Full scale considerations

- Analyze findings from Phase 2 and provide recommendations on how they could be employed at full scale or discuss the challenges that still need to be resolved before such execution.

5.0 TASK SCHEDULE

Table 4 shows the task schedule of activities. It should be noted that some activities can be performed simultaneously, for example as some samples go through durability testing, the effect of additional admixtures on grout properties can also be studied.

Table 4. Task Schedule.

Quarter (Calendar Year)	Phase 1	Phase 2	Phase 3
Q1 2025	Complete TTP. Order additional materials.	Plan for first Engineering-scale test at 3 ft diameter.	
Q2 2025	Prepare additional cement grout samples and start curing. Measure cured properties. Begin durability testing.	Continue planning for first Engineering-scale test at 3 ft diameter.	
Q3 2025	Complete durability testing and characterize durability results of the cement grouts and grout/epoxy.	Set up 3 ft grout-sealant placement test.	
Q4 2025	Additional experiments and analysis as needed. Draft Report 1 on material property testing.	Perform 3 ft grout-sealant placement test. Characterize 3 ft test samples.	
Q1 2026	Additional experiments and analysis as needed. Issue Report 1.	Prepare for second Engineering-scale test at 10 ft diameter. Write report for first 3 ft placement testing (Part A).	
Q2 2026		Set up second Engineering-scale test at 10 ft diameter.	
Q3 2026		Perform second Engineering-scale test at 10 ft diameter. Characterize Engineering Scale samples.	
Q4 2026		Finish any Engineering-scale testing tasks. Write Report for second small scale placement testing (10 ft Part B).	
Q1 2027		Finalize and issue Report 2, including both Parts A and B.	Write Report 3.
Project Conclusion Under Current Funding			

6.0 RESEARCH FACILITY PLANNING

6.1 Effects of Task on Equipment, Personnel, and Facilities' Physical Plant:

The cementitious grout property testing of Phase 1 will be performed in the Aiken County Technology Laboratory (ACTL, 999-1W) in Lab 122. The space is designed specifically for grout preparation. Some work may occur in A-Area as well, one location being 777-A which has the IMER mixer. Work with epoxies and chemical testing will occur in 723-A. Additional locations (non-rad) may be identified as the work progresses. All experiments in Phase 1 will not affect equipment, other personnel, or the facility.

In Phase 2, the first 3-4 ft diameter tests will be performed in 777-A., 786-A, ACTL High Bay, or Engineering Development Lab (EDL). For testing of 10-20 ft diameter forms, a large area location will be required and need to be identified. Locations for this testing are still being discussed. Several candidate locations include:

- 777-A
- 786-A
- N area
- AMC High Bay
- AVANTech's Richland location
- Other Location in Richland WA

Phase 3 does not involve laboratory work as it is mainly a recommendation and reporting phase. The application of the findings is for the double shell waste tanks at the Hanford site.

6.2 Sample Storage and Disposition of Products and By-products of the Task:

An Environmental Evaluation Checklist was previously completed for similar tasks. It was sent to the SRNL Environmental Compliance Authority (ECA) and was approved. It will be modified for additional chemicals to be added. Samples will be sealed and stored on the bench. Samples and chemicals will be stored in appropriate cabinets and not mixed with any incompatible chemicals, if any. Disposition of samples generated in this study will be properly stored or discarded. Disposition of waste generated as the result of this work will be discarded as directed by the EEC or ECA.

6.3 Disposition of Test Equipment:

Equipment will be cleaned, reused when possible, and stored properly.

6.4 Exposure of Personnel to Various Materials or Conditions:

Phase 1 work will be performed in chemical hoods to prevent personnel exposure. Personal protective equipment was or will be identified in each HAS and will be worn. Informal Pre-Job Briefings will occur prior to work. Workers will be added as "Hands-On Workers" to relevant HAS. Phase 2 work may require additional personnel to be brought on who are more experienced setting up and performing work at larger scale.

7.0 PROGRAMMATIC RISK REVIEW

Table 5. Risk Review.

Risk	Impact	Mitigation
SRNL M&TE	Inaccurate results	Check calibration and operation before use. M&TE shall be calibrated in advance of expiration and lab work. Have all equipment ready and identify spares.
Readiness Safety	Personnel injury, damage to equipment, or delay in future work.	Workers shall be signed on to the HAS and informal Pre Job briefings shall be performed prior to work. Workers should thoroughly understand all task directions. PPE will be worn.
Materials	Not enough to complete experiments, can delay work.	Materials will be received prior to work. Align schedule with material arrival, aim to be on schedule but adjust as necessary. Identify alternative suppliers, back up equipment, have spares if necessary.
Personnel Unavailability	Can delay work	Understand associate's schedule and availability ahead of time and reschedule tasks in advance as necessary. Identify alternate workers if needed.
Facility Outages	Can delay work	Anticipate any known or scheduled outages. Reschedule tasks as necessary. Work in another lab if needed.
Analytical teams unavailable	Can delay work	Understand analytical teams' schedule. Adjust prioritization with management if needed.
Insufficient funding	Unable to perform or complete tasks	Estimate work needed and adjust work scope as necessary. Work with funding source / customer to obtain additional funding or reduce scope.

8.0 R&D HAZARDS SCREENING

Hazards associated with activities in this TTP will be evaluated in accordance with the latest revisions of SRNL Manual L1, Procedure 7.02, *SRNL Research and Development (R&D) – Hazard Analysis* using the electronic Hazard Analysis System (HAS). The electronic HAS includes an assessment of the hazards by the Task Lead followed by identification of the mitigation methods. The hazards review and mitigation methods are reviewed and approved by relevant subject matter experts for each hazard identified. The electronic Hazards Analysis System also includes an assessment of the environmental hazards and controls for the task with review and approval by relevant subject matter experts. Prior to performing work, personnel are required to review and sign the Hazards and Controls Summary.

9.0 REFERENCES

[1] P. Shukla, "Integrity Monitoring and Assessment, Prediction, Repair, and Corrosion Control of the Hanford Storage Tanks (Work Authorization 277993)."
[2] "Tank Repair Feasibility Study (RPP-RPT-62020)," Washington River Protection Solutions, 2020.
[3] M. Hendrickson, C. Langton, and J. Wu, "Concrete Testing Case for Closure of Hanford's 241-C Underground Storage Tanks," 2023.
[4] K. Blue, M. Alderman, N. Valdes, and M. Kranjc, "Initial Progress on Tank Bottom Repair for the DOE EM Tank Waste R&D Program," in *Waste Management Symposia*, Phoenix, 2025 (to be submitted).
[5] "SRS Manual E7, Conduct of Engineering, Procedure 2.60, Technical Reviews."
[6] N. Campbell, "Epoxy Sealant Self-Leveling and Adhesion Test Report (TR-23302-00)," 2024.
[7] "4M Sodium Simulant Recipe for Bottom Sealant Testing."
[8] S. Doll, "Bottom Sealant Assumptions for SRNL (Personal Communication)," 2025.

Attachment 1. Hanford Tank Conditions and Simulant Recipe

Table 6 below lists SRNL's understanding of characteristics/conditions in the Hanford double shell waste tanks.

Table 6. Hanford Tank Conditions.

Characteristics	Original Understanding Pre-February 2025	Current Understanding February 2025
Tanks to Refurbish	Double Shell	Same
Shell Materials	Carbon steel	Same
Temperature at Bottom	55F or warmer	Same
Service Temperature	60C Note 70-90F in [2]	60-80F (now cooler)
Max Radiation Level	1 Ci/L	1.75 mCi/L (3 orders of magnitude lower)
Max Dose Rate of Tank Waste	750 Rad/hr Note 1000 rad/hr in [2]	Likely less due to above
Alkalinity of Tank Waste Solution	4% NaOH (1M, pH = 14) pH 10 or greater [2]	Similar, note simulant recipe in next table
Diameter of Tank	75 ft	Same
Sludge/Salts at Bottom	Yes	Same
Humidity	5-100% [2]	Same
Water at Bottom	Yes	Same
Curvature at Bottom	Yes	Same
Columns (Support)	Yes, but unknown number	Same
Risers	Yes, but unknown number	Same

Table 7 below lists a simulant recipe distributed to SRNL for this project [7].

Table 7. Simulant Recipe.

Chemical	Concentration (M)
NaOH (50% solution, w/w)	1.09
NaCl	0.09
$Na(NO_2)$	0.74
$Na(NO_3)$	1.30
$Na_3(PO_4)$-$12H_2O$	0.03
$Na_2(CO_3)$-H_2O	0.34

Figure 3. Picture of the bottom of double shell tank AY-102 [8].

Attachment 2. Additional Experimental Details

The following cementitious grouts are being considered as the (first) false bottom layer:

- Sika/Lafarge Ductal
- Steelike
- Hanford 2.0
- Hanford Pipe Grout
- SikaGrout-928 (MFlow-928)
- Other cementitious grouts to be identified

The following epoxies are being considered as the sealant layer:

- Sikadur 42 / SikaFlow 648
- Westlake Epoxy [6]
- Other epoxy grouts to be identified

The above prepackaged cementitious grouts will be investigated for properties such as below for

- Fresh grout: bleed water, wet density, set time, flowability, entrapped air
- Cured grout: strength, porosity, hydraulic conductivity, leachability, diffusivity

The prepackaged products may have acceptable fresh and cured properties that would allow for further testing of epoxy coating and/or durability testing. However, the table below shows certain metrics that must be met and if needed, potential ways to improve the metric. Additional metrics and methods/products for improvement may be identified during the course of the project.

Table 8. Metrics to Evaluate for Cementitious Grout.

Metric	If metric not met, potential ways to improve
Slump > 3x diameter of slump cone/cylinder, no mounding	Increased water/cement ratio DOW Rhoplex AS-48 (flexibility and leveling benefits) Increased amount of superplasticizer or viscosity modifying admixtures
Low porosity hydraulic conductivity Value TBD	Waterproofing admixture Kryton Krystal Integral Membrane Water resistance from DOW Rhoplex AS-48
No bleed water visible or segregation	Reduced water/cement ratio Increased superplasticizer or viscosity modifying admixtures
Strength, shrinkage, surface roughness, leachability, release of chemicals as the result of leaching, changes as the result of immersion in DI water and Hanford specified tank solution Bonding of sealant to grout	TBD

Samples that have fresh or cured properties that cannot be made acceptable will not proceed to steps of epoxy coating and/or durability testing.

DISTRIBUTION LIST

nicholas.valdes@srnl.doe.gov
katie.hill@srnl.doe.gov
bruce.wiersma@srnl.doe.gov
christine.langton@srnl.doe.gov
mark.kranjc@srnl.doe.gov
pavan.shukla@srnl.doe.gov
charles.james@srnl.doe.gov
joseph.manna@srnl.doe.gov
kareen.blue@srnl.doe.gov
maxwell.alderman@srnl.doe.gov
eric.skidmore@srnl.doe.gov
jennifer.wohlwend@srnl.doe.gov
morgana.whiteside@srnl.doe.gov

Appendix B: Task 2 Deliverables — SRNL-STI-2024-00539, SRNL-MS-2025-00158, SRNL-RP-2025-00647

A U.S. DEPARTMENT OF ENERGY NATIONAL LAB • SAVANNAH RIVER SITE • AIKEN, SC • USA

Design and Materials of Reference Electrodes for Radioactive Waste Tank Service – A Literature Review

K.S. Sykes, J. Jiang, and B. J. Wiersma, SRNL

S. Chawla, N. Sridhar, K. Evans, and J. A. Beavers, DNV

November 2024

SRNL-STI-2024-00539, Revision 0

DISCLAIMER

Printed in the United States of America

Prepared for
U.S. Department of Energy

SRNL-STI-2024-00539
Revision 0

Keywords: Corrosion, Waste Tank Integrity, Corrosion Monitoring

Retention: Permanent

Tracking Number: 10560

Design and Materials of Reference Electrodes for Radioactive Waste Tank Service – A Literature Review

K. S. Sykes, J. Jiang, and B. J. Wiersma
SRNL

S. Chawla, N. Sridhar, K. Evans, and J. A. Beavers

DNV

November 2024

Savannah River National Laboratory is operated by Battelle Savannah River Alliance for the U.S. Department of Energy under Contract No. 89303321CEM000080

Reviews and Approvals

AUTHORS:

Bruce Wiersma — Digitally signed by Bruce Wiersma
Date: 2024.12.03 12:25:46 -05'00'

B. J. Wiersma, SRNL/Advisory Engineer — Date

Materials Science and Disposition

Chawla, Sandeep — Digitally signed by Chawla, Sandeep
Date: 2024.12.09 05:11:34 -05'00'

S. Chawla, DNV /Principal Engineer — Date

Electrochemistry and Alternative Energy

TECHNICAL REVIEWER:

PAVAN SHUKLA (Affiliate) — Digitally signed by PAVAN SHUKLA (Affiliate)
Date: 2024.12.03 14:23:14 -05'00'

P.K. Shukla, SRNL/Advisory Engineer — Date

Materials Science and Disposition

APPROVAL:

JOSEPH MANNA (Affiliate) — Digitally signed by JOSEPH MANNA (Affiliate)
Date: 2024.12.04 17:11:06 -05'00'

J. Manna, SRNL/Director — Date

Materials Technology & Energy Sciences Division

MICHAEL STONE (Affiliate) — Digitally signed by MICHAEL STONE (Affiliate)
Date: 2024.12.05 07:57:13 -05'00'

M. E. Stone, SRNL/DOE-EM Program Manager — Date

Environmental and Legacy Management

Acknowledgements

The authors acknowledge the U.S. Department of Energy-Environmental Management for the funding and support to conduct this research. The development of more robust reference electrodes for in-situ monitoring of tank corrosion is under the umbrella of a program that was initiated as part of the “R&D Roadmap for Hanford Tank Waste Mission Acceleration” (NNLEMS-2022-00005). The title of the awarded program within the roadmap is, “Integrity Monitoring and Assessment, Prediction, Repair, and Corrosion Control of the Hanford Storage Tanks” (Award #277993). The Principal Investigator for the program is Dr. P.K. Shukla of the Savannah River National Laboratory.

The new reference electrodes will ultimately benefit the Hanford waste tank farm facility. K.D. Boomer of the Chief Technology Office (CTO), Washington River Protection Solutions (WRPS) provided a letter of support for this investigation. J. S. Page, Tank and Pipeline Integrity (TAPI), WRPS, has provided useful reference documents for this review.

Executive Summary

The Hanford site stores approximately 55 million gallons of radioactive and chemically hazardous wastes from the production of weapons materials. The wastes are stored in 177 underground, carbon steel storage tanks, 149 of these are single shell tanks (SSTs) and 28 of these are double shell tanks (DSTs). The DSTs provide critical retrieval and interim storage before the waste is vitrified in the Waste Treatment and Isolation Plant (WTP). The DSTs have been in service for 38 to 56 years and current plans indicate that WTP operations will be completed in 2075. Thus, the tanks will need to remain in service far beyond the initial 40-year life expectancy. For life extension of the tanks, effective corrosion control practices must remain in force. This effort includes direct measurements of the extent of corrosion (e.g., ultrasonic measurements and corrosion coupons) and electrochemical processes (e.g., linear polarization measurements).

Tank corrosion and stress corrosion cracking (SCC) may also be monitored by the use of electrochemical techniques such as measurement of the open circuit potential (OCP) of the tank. Attempts to measure the OCP in waste tanks have been made at both Hanford and SRS. A reference electrode is typically utilized for these measurements. Failures of the reference electrodes in the chemically and radiolytically harsh environments in the tanks have occurred after relatively short term exposures, encumbering long-term surveillance efforts. Therefore, DOE-EM has undertaken a research program to develop reference materials that are capable of surviving the waste tank environment for longer periods of time.

The first phase of this program was to perform a literature review. The purposes of the literature review were two-fold. First, summarize the performance of reference electrodes in both field applications and laboratory testing. From this summary, the types of commercial electrodes that have been utilized, the environments to which they have been exposed, the durability of the electrodes, and failure mechanisms could be categorized, such that weaknesses in materials of construction and electrode design could be defined. Second, identify and recommend materials of construction and electrode designs that will overcome these weaknesses, such that a robust reference electrode is available to provide accurate potential measurements for an extended period of time.

The literature review was organized in the following manner:

Section 1: A discussion of the key corrosion information and performance characteristics that may be gathered from reference electrode data is presented.

Section 2: A summary of the performance of commercial reference electrodes that have been deployed in waste tanks at both Hanford and the Savannah River Site is presented. Additionally, a summary of laboratory studies that investigated the failure mechanisms of the electrodes in the waste environments is discussed.

Section 3: Reference electrodes are made from a variety of materials for a multitude of applications. The literature review highlighted and recommended materials that may survive the harsh chemical and and radioactive environment of the Hanford waste tanks.

Section 4: Reference electrode design was another factor in the failure of commercial electrodes in the waste tanks. The literature presents several alternative designs that will be considered for the development of a new robust reference electrode.

Section 5: Once the materials and design for the reference electrode have been selected and a prototype reference electrode fabricated, a series of tests are necessary to verify functionality. Testing that has been utilized to investigate functionality of commercial reference electrodes were reviewed. Similar tests will be employed for the recommended reference electrode.

This literature review provides the following key observations about the utilization and testing of reference electrodes:

- Measurement of the OCP provides a fundamental basis for predicting long-term performance of a waste tank. This approach provides a conservative estimate of the occurrence of failure modes such as pitting corrosion and SCC.
- Key characteristics of an effective reference electrode system include: lack of sensitivity to redox species, lack of sensitivity to pH, non-polarizability, resistance to chemical species in the waste, low impedance, electrolyte communication, chemical and radiation resistance of the electrode body, and mechanical integrity.
- Long-term (~3 years) testing of commercial Ag/AgCl under laboratory conditions show that the degradation/failure modes could be broadly classified into two types: (1) monotonic positive drift from the initial potential, and (2) sharp drop to negative potentials after a period of relative stability. The degradation was attributable to diffusive intermixing of the internal fills of the Ag/AgCl reference electrodes with the external simulant solutions over time through the porous frit junctions. This process leads to extensive KCl depletion and contamination of the fills, causing loss of potential stability.
- The potential drift trends were correlated to Cl^- activity changes in the fill and the effects of various contaminant species originating from the waste simulants.
- Long-term studies on single junction (SJ) Ag/AgCl reference electrodes in actual supernatant waste samples drawn from various DSTs also indicated that degradation of electrodes was found to be primarily due to the intrusion of aggressive chemicals causing clogging, physical and chemical degradation of AgCl, and alteration of the internal electrolyte. Radiation had less impact on electrode degradation compared to the chemicals, though radiolytic species such as H_2O_2 and HNO_3 could possibly have contributed to Ag wire degradation.
- Reference electrodes have been utilized at both Hanford and SRS in the past to make instantaneous measurement and for long term monitoring of the corrosion behavior of tanks. However, reference electrode failures have typically occurred within 2-3 years of installation. Trends in the potential drift that were indicative of failure an electrode during laboratory tests correlate with those observed in the field.
- Electrochemical noise systems, another electrochemical technique, were also deployed in Hanford waste tanks to monitor for localized corrosion and SCC. Although, the technique had modest success, the utilization of the system was discontinued due to many issues related to interpretation of noise signals and interference from a variety of ambient electrical noise.

This literature review provides the following recommendations on materials, design and testing of future reference electrodes:

- Alternate materials of construction for the internal fill of the reference electrode include solid state Ag/AgCl carbon nanotube (CNT) thread reference electrode or a solid state reference electrode using CNT.

- Alternate materials of construction for the reference electrode frit include ion-conducting composite, porous polymer frits, and Teflon frits.
- Alternate materials of construction for the body of the electrode include polymer composites doped with sizeable amounts of high atomic number (high-Z) materials, epoxy resins, non-oxide and oxide ceramics, and carbides of transition metals.
- Additive manufacturing can use several different materials of interest for the development of the reference electrode such as ceramics, metals, and thermoplastics. It can potentially reduce the cost because it can consolidate multiple parts into one and minimize material usage by building objects up rather than cutting, molding, and combining materials.
- Various type of alternative design concepts for reference electrodes have been discussed in the literature to overcome the limitations of traditional reference electrodes. These can be broadly classified into the following categories: reference electrodes with extended diffusion lengths, reference electrodes with improved liquid junction designs, reference electrodes with flowless junction designs, ionic liquid reference electrodes, solid-contact reference electrodes, and Field Effect Transistor (FET) based reference electrodes.
- Reference electrode design development should focus on increasing the lifespan of reference electrodes by increasing the diffusion length of the internal and frit sections. Additive manufacturing may allow more flexibility and reproducibility to accomplish this objective.
- Testing protocols for the accuracy and functionality of the reference electrodes were presented. Electrochemical Impedance Spectroscopy (EIS) has been utilized in previous laboratory studies and may provide a baseline for comparison between the commercial electrodes and the newly developed electrodes.

Table of Contents

List of Tables

List of Figures

List of Abbreviations

Ag/AgCl	Silver-Silver Chloride
DJE	Double Junction Electrode
DNV	Det Norske Veritas
DOE	Department of Energy
DST	Double Shell Tank
EIS	Electrochemical Impedance Spectroscopy
EM	Environmental Management
EN	Electrochemical Noise
MPCMS	Multi-Probe Corrosion Monitoring System
OCP	Open Circuit Potential
RCMP	Retractable Corrosion Monitoring Probe
SCC	Stress Corrosion Cracking
SCE	Saturated Calomel Electrode
SJE	Single Junction Electrode
SRNL	Savannah River National Laboratory

1.0 Introduction

The Hanford site stores approximately 55 million gallons of radioactive and chemically hazardous wastes from the production of weapons materials. The wastes are stored in 177 underground, carbon steel storage tanks, 149 of these are single shell tanks (SSTs) and 28 of these are double shell tanks (DSTs)[1]. The DSTs provide critical retrieval and interim storage before the waste is vitrified in the Waste Treatment and Isolation Plant (WTP). The DSTs have been in service for 38 to 56 years and current plans indicate that WTP operations will be completed in 2075[2]. Thus, the tanks will need to remain in service far beyond the initial 40-year life expectancy. For life extension of the tanks, effective corrosion control practices must remain in force[1].

DOE Order 435.1-1 contains the following corrosion control requirements[3]:

- Identify corrosion, fatigue and other critical degradation modes.
- Adjust the chemistry of tank waste and implement other necessary corrosion protective measures.
- Identify additional controls necessary to maintain an acceptable operating envelope.

Corrosion control of the waste chemistry in the DSTs relies on ensuring that there is sufficient concentration of chemical species to inhibit the aggressive species that are present. Until the late1990s corrosion control was accomplished by waste modeling, waste sampling, and corrosion testing in laboratories with tank waste or simulants. However, assumptions regarding how representative the waste samples are result in uncertainties as to the degree of corrosion that may be occurring. The samples also provide a “lagging” indicator as to when corrosion of the tank may have initiated.

An alternative approach to assessing tank corrosion and SCC is the use of electrochemical techniques. Attempts have been made to monitor tank corrosion and SCC using an electrochemical noise technique[4] but these have not been successful due to many issues related to interpretation of noise signals and interference from a variety of ambient electrical noise. A simpler and more robust approach is to monitor the corrosion potential (E_{corr}) of the tank. The fundamental basis for predicting long-term performance using the tank E_{corr} (also called Open-circuit Potential, OCP) is illustrated schematically in Figure 1-1. The onset of localized corrosion or SCC occurs when the OCP exceeds the repassivation potential for localized corrosion (E_{rp}) or the critical cracking potential for SCC (CCP), respectively, in the same tank waste. This approach ignores the gestation time for initiation and stable growth of localized corrosion or SCC and thus is a conservative estimate for the occurrence of these failure modes. The OCP, E_{rp}, and CCP are measured using laboratory tests in tank waste simulants or real wastes extracted from the tanks. However, the OCP can also be measured

[1] C. L. Girardot, RPP-7574, Rev. 8, “Double-Shell Tank Integrity Program Plan”, August 10, 2021.
[2] Parsons, *Final Report: Waste Treatment and Immobilization High Level Waste Treatment Analysis of Alternatives.* Richland: Office of River Protection, 2023.
[3] DOE M Order 435.1-1, Chapter II, Section Q.2.a., “Radioactive Waste Management Manual”, U. S. Department of Energy, July 9, 1999.
[4] G. L. Edgemon, *Electrochemical Noise Based Corrosion Monitoring: Hanford Site Program Status*, Corrosion/2005, AMPP, 2005, Paper 05584.

directly in the tank. The measurement of OCP in the tank is an attractive method to monitor tank corrosion and SCC integrity because it is less subject to interference from ambient electronic noise and the measurement system is simpler.

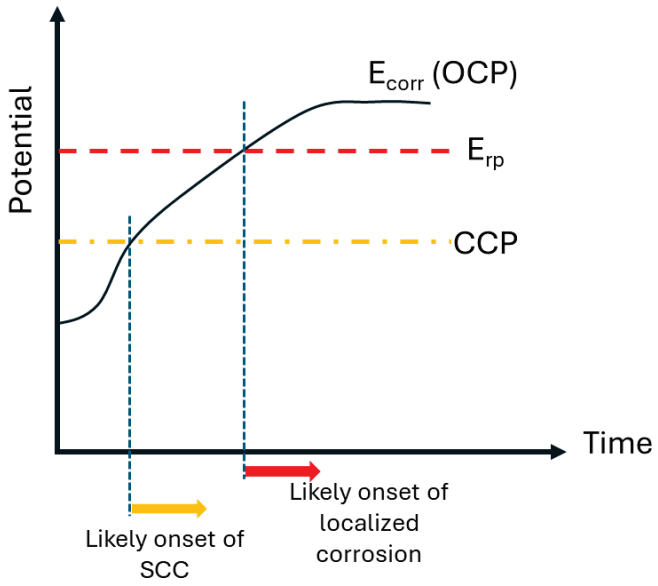

Figure 1-1. Schematic illustration of conditions for the onset of localized corrosion and SCC and their use in tank integrity prediction.

The measurement of OCP involves the use of reference electrodes. The OCP of a metal in an electrolyte is a combination of thermodynamic and kinetic effects of a variety of electrochemical reactions occurring at the interface. This is illustrated in Figure 1-2.

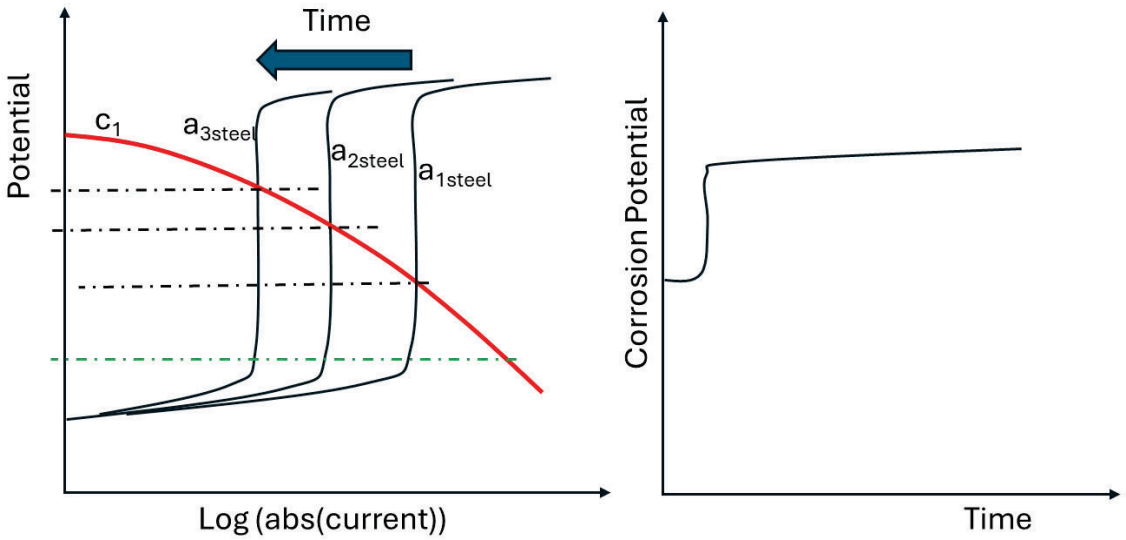

Figure 1-2. Schematic illustration of the change in corrosion potential (OCP) versus time

The anodic currents, shown as "a_{1steel} to a_{3steel}" are governed by the electrochemical response of the steel to the waste chemistry over time. In Figure 2, the passive current is shown to decrease with time, but this is not necessarily the case for all systems. The cathodic current, shown by c_1, is governed by the redox reactions occurring in the waste solution. This cathodic current has an opposite sign to the anodic current, but the absolute value of this current is plotted in Figure 1-2. The intersection of the anodic and cathodic currents provides the zero net charge condition representative of OCP (ignoring the ohmic potential drop in the solution). This diagram, called the Evans diagram, shows that the OCP increases with time. However, other electrochemical reactions in a tank may influence changes in OCP over time. Thus, measurement of OCP is important for monitoring the tank performance and relating it to changes in waste chemistry.

1.1 Electrochemical Potential and Reference Electrodes

It is instructive to step back from the complex kinetic processes leading to OCP and consider the thermodynamic aspects of this interface first. The classic definition of chemical potential involves a change in free energy of a chemical species with changes in molar composition at any given temperature and pressure. By this definition, the chemical potential of a single ion cannot be measured, because the addition of only one ionic component is not possible without the charge balancing addition of a counter ion. Thus, the definition of the chemical potential of a single ion, and by extension the activity of a single ion, is only a matter of convenience and cannot be measured directly. Electrochemical potential of a solid (electrode) in equilibrium with an electrolyte is defined as the sum of chemical potential of the electrode in equilibrium with the electrolyte, the chemical potential of the ion of the electrode in the electrolyte, and the electrostatic potential associated with the work involved in bringing a unit charge from infinity to just inside the surface of a solid. However, the work involved in bringing the charge into a solid cannot be measured because the act of bringing the charge through the electrolyte-solid interface will involve changes in surface charges, which cannot be measured. Thus, the electrochemical potential of an electrode/electrolyte interface is indeterminate. A practical approach for determining an electrode potential is to define the potential difference of a system consisting of the electrode/electrolyte interface of interest, a reference system consisting of a reference electrode in a controlled electrolyte, the interface between the two electrolytes, and the external measurement system. Thus, even a thermodynamic definition of an electrode potential involves a reference electrode, with the proviso that any measurement of the voltage difference between the electrode of interest and a reference electrode is performed with minimum of disturbance of the equilibrium of the total system. By convention, the potential of the standard hydrogen electrode (SHE) system, H^+ (activity of H^+= 1)|H_2 (1 atm. Pressure), is assumed to be 0 V at all temperatures. The SHE is inconvenient in practice as the electrode (typically a platinized Pt) is subject to the influence of redox species in solution and can be poisoned easily by impurities. Thus, practical reference electrode systems are tailored for specific environments and their potentials referenced to the SHE.

It is obvious from the above discussion that the use of a reference electrode system implies that its electrode potential must be insensitive to the act of measurement (even the most sensitive voltage measurement must involve the passage of a small current) and to the composition of the electrolyte in which the measurement is made. In their magisterial work on reference

electrodes, Ives and Janz[5] state the issue thus: “If an electrode does not work properly, its failure to do so presents a physicochemical problem outside the scope of thermodynamics. It must be examined in such terms as the chemical purity and physical states of the essential phases and interfaces”. This perspective will be explored in subsequent sections.

1.2 Characteristics of a Reference Electrode System

A simple schematic of an electrode potential measurement is shown in Figure 1-3.

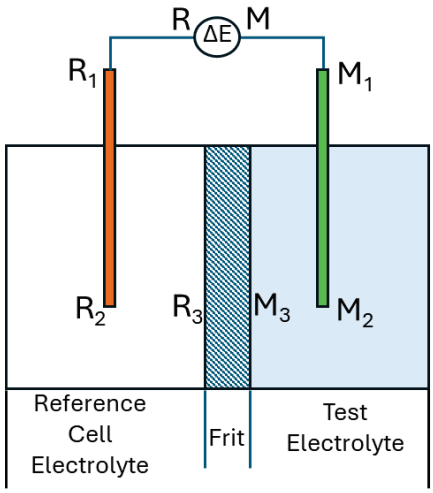

Figure 1-3. A simple schematic of an electrode potential measurement at a metal (M) using a reference electrode (R).

This simple cell consists of an electrode of interest, M, reference electrode, R, the test solution containing M, a reference solution containing R, a membrane or frit that separates the two solutions, and the external circuits consisting of wires and a high input impedance voltmeter. In reality, this arrangement may be more complex consisting of other intermediate solutions between the reference electrode and the test electrode and other barriers to protect the reference cell. The measured potential difference consists of several voltage drops:

$$\Delta E_{measured} = (E_M - E_R) + i \times \{(Z_{R_1-R}) + (Z_{M_1-M}) + (Z_{M_1-M_2}) + (Z_{M_2-M_3}) + (Z_{M_3-R_3}) + (Z_{R_3-R_2}) + (Z_{R_2-R_1})\} \quad (1)$$

The Z_{R_1-R}, etc. refer to the complex impedances of various parts of this system. The current drawn by the measuring system is given by:

$$i = \Delta E_{measured}/Z_{voltmeter} \quad (2)$$

Thus, the actual potential difference is related to the measured potential difference by:

$$(E_M - E_R) = \Delta E_{measured} \times \left[1 - \frac{\{(Z_{R_1-R})+(Z_{M_1-M})+(Z_{M_1-M_2})+(Z_{M_2-M_3})+(Z_{M_3-R_3})+(Z_{R_3-R_2})+(Z_{R_2-R_1})\}}{Z_{voltmeter}}\right] \quad (3)$$

[5] D.J.G. Ives and G.J. Janz, Reference Electrodes – Theory and Practice, 1961, Academic Press, Inc. (reprinted in 1996 by NACE International, Inc.).

Where, $Z_{voltmeter}$ is the input impedance of the voltage measuring instrument. If the voltage measurement system has a high input impedance compared to the impedances of the various interfaces, the desired potential, $(E_M - E_R)$ is not significantly different from the measured voltage. Thus, a large input impedance voltmeter is critical for accurate potential measurements. However, if blockage of the frit or electrolyte communication within the reference electrode system occurs, then its impedance may increase sufficiently to affect the measured potential difference. Additionally, air pockets or other discontinuities in the electrolytic communication between interfaces may cause increased measurement noise due to electromagnetic interference and small changes in the actual OCP may not be easy to resolve.

A second important aspect of the OCP measurement is the changes in the reference potential, E_R. As mentioned in the previous section, the E_R is affected by: (1) the presence of redox species in the system that may influence the reference electrode potential, (2) the electrochemical polarization of the reference electrode due to the current drawn by the measurement system, and (3) the change in potential due to changes in species involved in the equilibrium reaction of the reference electrode. The general criteria for good reference electrode performance are shown in Table 1-1.

1.2.1 Sensitivity to Redox Species

All reference electrodes operate on the basis of heterogeneous redox equilibria. The hydrogen electrode uses the H^+/H_2 redox system as its basis, but this reaction occurs at the surface of a solid catalyst metal (e.g., Pt). If there are other redox species in solution, such as O_2 and Fe^{3+}, they also set up redox equilibria at the Pt surface and the resulting potential will be dictated by the kinetics of the reaction with higher redox potential reaction. This is illustrated for Fe^{3+}/Fe^{2+} redox reactions at different dilutions in a solution of 4% NaCl on Pt (Figure 1-4).

Table 1-1. Criteria for reference electrode performance.

Criterion	Performance issue
Lack of Sensitivity to Contamination with Other Redox Species	The reference electrode potential is typically increased by redox species in solution
Lack of Electrochemical and Chemical Sensitivity to pH (buffering, precipitation)	Change in solution pH alters the redox reactions at the electrode. Extreme pH values affect the speciation in the reference electrode and electrode surface
Non-polarizability	The potential should not be affected by current passed
Resistance to Other Chemical Species	The chemistry of buffer solution may change or electrode surface may change
Low impedance	High impedance will alter measured potential and induce electronic noise
Electrolyte Communication	Plugging will reduce electrolyte communication and increase impedance. Loss of internal electrolyte will result in dry out and failure of the electrode. Free communication with external electrolyte will alter chemistry.
Chemical and Radiation Resistance of Electrode Body	The body of the electrode may be adversely affected. Radiolytic products may alter electrochemical reactions
Mechanical Integrity	The body of the electrode may fail

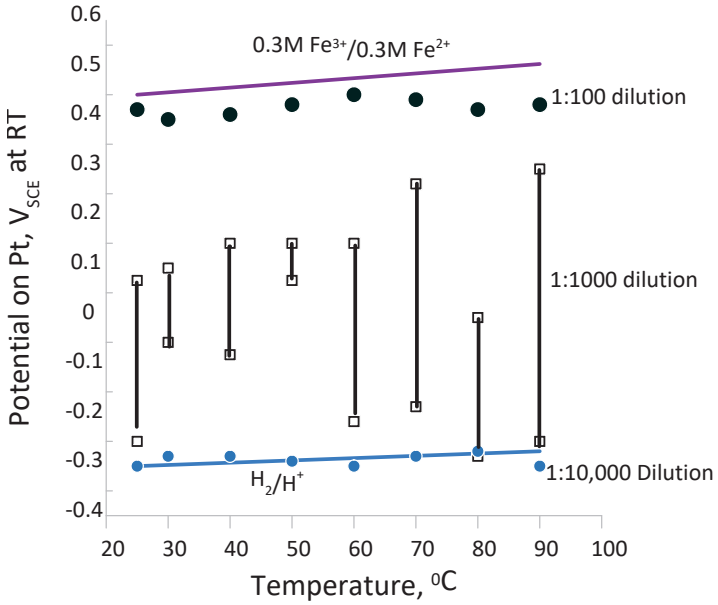

Figure 1-4. Effect of ferrous/ferric redox couple at different dilutions on the measured potential on Pt at room temperature[6]

Only at very low concentrations of impurities (less than about $3x10^{-5}$M Fe^{3+}/Fe^{2+}) does the potential correspond to the H^+/H_2 reaction. Similar effects were found on other corrosion resistant alloys, such as Alloy 22[4], which have been used as pseudo-reference electrodes. Redox species can be present in the test solutions or enter into solutions from corrosion reactions, radiolysis, or exposure to air. Most primary reference electrodes are insensitive to other redox reactions in the system, provided they do not alter the chemistry of the reference electrode.

1.2.2 Sensitivity to pH

The hydrogen and Quinone electrodes are examples of reference electrodes that are extremely sensitive to pH because they operate on the basis of H^+ reduction reactions. However, metal oxide electrodes, such as Ir/IrO_2 and W/WO_3 electrodes and glass electrode are also sensitive to pH and are used as pH electrodes. These electrodes can be used as reference electrodes when the surrounding solution is pH-buffered.

1.2.3 Non-Polarizability

Ideal reference electrodes operate under essentially equilibrium conditions. This means that their potential does not change significantly upon passage of a small current across their interface. For example, in the case of the hydrogen electrode, Pt has a large exchange current density that enables it to undergo very little polarization upon passage of a small current.

[6] J. Kolts and N. Sridhar: 'Temperature Effects in Localized Corrosion', Corrosion of Nickel-Base Alloys, Cincinnati, Ohio, 1984, ASM International, 191-197.

Similarly, Ag/AgCl electrode operates under near equilibrium conditions between Ag and AgCl, whereby a small anodic current dissolves a small concentration of Ag that then precipitates as a AgCl salt film, whereas a small cathodic current dissolves AgCl to replate Ag. Thus, this electrode is essentially a non-polarizable electrode. However, when the AgCl layer completely dissolves and bare Ag wire is exposed to solution, significant anodic polarization can occur. When passive metals are used as reference electrodes, even a small anodic current can increase the potential significantly (see Figure 1-2). In the case of valve metals such as Ti and Zr, the resulting oxide films can be either semi-conductive or insulating, resulting in large ohmic potential drops in the film. Such electrodes are highly polarizable and are poor reference electrodes.

1.2.4 Resistance to Other Chemical Species

Many anionic species can attack the reference electrodes and change the surface equilibria. For example, exposure of Ag/AgCl electrode to highly alkaline solution can result in the conversion of AgCl to Ag_2O, resulting in significant change in the reference potential. Some species such as sulfur or sulfides can also form sulfides or poison the surface catalytic reactions, as in the case of Pt used in the Hydrogen electrode. The ability of some species to form sulfides can be used in some systems, as in the case of the Ag/Ag_2S electrode.

Radiolytically generated free radicals may also affect chemical reactions and must be evaluated. Early studies of reference electrode performance in radiation environment used high energy radiation from a linear accelerator simulating that in the core of a nuclear reactor[7]. Danielson[8] evaluated the effect of gamma irradiation on the performance of reference electrodes using a Co^{60} source to generate Gamma radiation around a non-radioactive waste simulant consisting of a mixture of 3.0 molal NaOH, 0.5 molal $NaNO_2$, and 1.0 molal $NaNO_3$ at ambient temperature. The study showed that the performance of Ag/AgCl and Saturated Calomel Electrodes (SCE) did not degrade up to a total fluence of $9.4x10^8$ Rads. Marsh et al.[9] evaluated the effect of Gamma radiation from Co^{60} source on SCE at an absorbed dose rate of $2x10^3$ Sv/h for 100 hours and found no effect on SCE potential in comparison to another SCE that was shielded from radiation using 10 cm of lead (Pb).

1.2.5 Low Impedance

The impedance is affected by the semi-permeable membrane or frit used at the interface between the reference electrode solution and test solution. If this frit is blocked, the effective diffusivity of ionic species is reduced. The effective diffusivity is given by

$$D_{eff} = D \times \rho \times (1 - \tau) \quad (4)$$

Where, ρ is the porosity and τ is the tortuosity. If the porosity is low and tortuosity is high, then the effective diffusivity becomes low and increases the impedance. In solid-state or gel

[7] D.F. Taylor, *Response of Electrochemical Sensors to Ionizing Radiation in High-Temperature Aqueous Environments.* Corrosion, 1991, **47**(2): 115–122.
[8] M. J. Danielson, *Effect of Gamma Radiation on Stability of Silver-Silver Chloride and Mercury-Calomel Commercial Reference Electrodes*, Corrosion, 1995, **51**(6): 450–455.
[9] G.P. Marsh, K.J. Taylor, G. Bryan, and S.E. Worthington, *The influence of radiation on the corrosion of stainless steel.* Corrosion Science, 1986. **26**(11): 971-982.

electrodes, the impedance is also affected by changes in the gel layer or polymer fill. In the case of reference electrodes used in non-aqueous systems, the impedance may also be affected by the reference fill solutions. In such cases, suitable supporting electrolytes must be used to reduce electrolyte impedance. Another source of high impedance is poor electrical connections (e.g., corroded contacts) and long electrical leads to the measurement system. Long leads also introduce electromagnetic noise in the system and should be minimized if at all possible. As shown in Eq. 3, the impedance of the reference electrode plays an important role mainly when a low-input impedance measurement system is used. Unfortunately, this may often be the case in field measurements.

1.2.6 Electrolytic Communication

Electrolyte (ionic and gaseous) communication is essential for the functioning of the reference electrode. However, if the communication is free flowing, the reference electrode compartment solution is replaced by the external test solution and the reference electrode potential drifts significantly. Typically, multiple junctions may be used to increase the diffusion path. However, if there is significant impediment to flow of species, the interface impedance will increase altering the measured potential (Eq. 3).

1.2.7 Chemical and Radiation Resistance of Electrode Body

Many reference electrode bodies are made of polymers that can be affected by certain chemical species, such as hydroxide or oxidizing compounds. Radiation can also affect the integrity of the reference electrode body through change in glass transition temperature, crazing, or softening. Finally, chemicals and radiation can affect elastomeric seals through volumetric swelling or embrittlement resulting in leakage.

1.2.8 Mechanical Integrity

The mechanical robustness of reference electrodes is key for field application, where they can be seldom handled with the same gentleness as in the laboratory. Often shear forces from moving liquids or from solids entrained in liquids can crack or erode the reference electrode body or the tip.

2.0 Reference Electrode Performance in DOE-Complex Waste Tanks

Electrochemical techniques have been utilized to monitor corrosion in waste tanks at both Hanford and the Savannah River Site (SRS). The performance of these corrosion monitoring systems was reviewed and is presented. As will be discussed, these systems frequently fail after relatively short-term exposure to the chemically and radioactively harsh environments of the waste tanks. Recently, there has been extensive laboratory testing to understand the failure modes of the reference electrodes in both simulated and actual waste environments. This testing was also reviewed below.

2.1 Electrode Performance in Waste Tanks in the DOE Complex

2.1.1 Early Reference Electrodes at SRS and Hanford

Prior to 1996, the use of reference electrodes within the DOE complex to measure the tank potential was limited. SRS in the 1970's utilized a saturated calomel electrode (SCE) to measure the tank potential in four waste tanks to determine if at the current waste compositions and temperatures these tanks were susceptible to SCC. Similar tanks had previously experienced SCC in supernates with these compositions[10]. Tank potentials were measured by immersing both a working SCE and an inactive SCE (emptied of electrolyte to measure any spurious signal from strong electrical fields) in the waste supernate and attaching the tank lead to a cooling coil supply line that was welded to the tank. Potentials were measured at various locations in the tank by connecting the tank lead to five different cooling coils (some extending into both supernate and sludge and some into supernate only). The largest range of potentials in any tank was 5 mV. The potentials were monitored for approximately 30 days.

Table 2-1 shows the composition, temperature and potential data obtained during the month-long exposure. In general, the data followed expected trends (i.e., higher pH wastes resulted in more negative (active) potentials)[11]. On the other hand, the effect of an oxidizing species, such as mercury, is also exhibited as potentials of tanks that contained mercury were more postive (noble). Although two of the tanks had experienced cracking previously, it was concluded that the measurements demonstrated that the tanks were in a passive condition. However, it is now recognized that SCC typically occurs under passive conditions, where the passive film breaks down locally. The tank potential measurements in the table also suggest that the potentials were similar to those observed in actual wastes and simulants with carbon steel coupons, which were performed in the laboratory. Differences were attributed to the use of fresh coupon surfaces in the laboratory versus the thick oxide that likely exists on the tank walls.

In the 1980's, SRS demonstrated feed preparation processes for the waste vitrification facility in two of the waste tanks[12]. The degradation concern in this case was pitting in dilute wastes due to chlorides either at the liquid air interface or at the interface between liquid and solid waste layers. The method for determining tank potential was similar to that used in the 1970s, except that a sleeve-type, double junction Ag/AgCl (DJE) was deployed in addition to an SCE. The sleeve type junction was considered to be more resistant to pluggage by slurries than the normal frit junctions. The double junctions allowed the outer junction to be filled with sodium rather than potassium chloride solutions, which may have resulted in precipitation in the tetraphenylborate waste. The additional concerns of localized redox and aggressive species required multiple probes, movement of the probes through the depth of the tank contents and a means of determining probe elevation. In addition to the reference electrode probe, pH, Eh and chloride laboratory probes were attached to 50 ft. waterproof leads. Probes that contained fill

[10] R. S. Ondrejcin, S.P. Rideout, J. A. Donovan, *Control of Stress Corrosion Cracking in Storage Tanks Containing Radioactive Waste*, Nuclear Technology, 1979, **44**(2): 297-306.
[11] N. Sridhar, J.A. Beavers, B.C. Rollins. S. Chawla, K. Evans and X. Li, *Stress Corrosion, Cracking and Localized Corrosion of Carbon Steel in Nitrate Solutions,* Corrosion, 2016, **72** (7): 927-942.
[12] D. F. Bickford, J. W. Congdon, and S. B. Oblath, *"Corrosion of Radioactive Waste Tanks Containing Washed Sludge and Precipitates"*, Materials Performance,1988, **27**(5),16-21.

solutions were completely filled, and vent holes were closed with polyvinylchloride electrical tape and sealed with silicon rubber. ASTM A537 carbon steel coupons, the tank material of construction, were attached to waterproof leads and the coupon junctions were potted in silicone rubber.

Table 2-1. Composition, Temperature and Potential Data for SRS Tanks in the 1970s.

	Tank Designation			
	F-4	F-8	H-11	H-15
Nitrate (M)	2.4	1.7	3.5	3.6
Nitrite (M)	3.1	0.5	0.8	1.1
Hydroxide (M)	2.8	1.1	0.79	1
Chloride (M)	0.032	0.03	0.03	0.016
Sulfate (M)	0.032	0.18	0.03	0.05
Carbonate (M)	0.18	0.1	0.1	0.1
Mercury (ppm)	12	40	240	100
Supernate Temperature (°C)	56	40	49	48
Tank Leakage	No	No	Yes	Yes
Tank Potential (mV vs. SCE)	-440	-0.12	-0.085	-0.065
Carbon steel coupon potential in simulant (mV vs. SCE, 2 mo.)	-460	NA	-140	NA

The probes were calibrated in the field immediately prior to use. They were then bundled together with PVC electrical tape inside 2-inch diameter by 1.5-ft long, schedule 40 PVC pipe. The pipe was attached to a 50-ft steel tape measure, which permitted determination of the relative elevation of the probes in the tanks. Probe readings were taken at various elevations. After the tanks had been scanned in this manner, periodic readings were taken at constant elevations to determine the drift of tank potentials and changes in the passive films on the coupons during aging. Aged coupons were shorted to the tanks though a nanoammeter to determine the risk of galvanic corrosion. An example of the reference electrode data is shown in Figure 2-1.

As shown in the figure, the tank contained approximately 4 feet of waste, and it contained both sludge solids and a clear solution. The tank potential did not vary with elevation or the presence of solids. However, the potentials of the carbon steel (Fe) coupons did change depending on the elevation and presence of the solids. These potentials were similar to those observed in both actual wastes and simulants, which suggested minimal effect of irradiation.

The potentials were monitored for 40 days in two tanks. The composition, temperature and potential for each tank are shown in Table 2-2. In general, the data again followed expected trends (i.e., higher pH results in more negative potentials). However, the presence of mercury in the solids phase may also have contributed to the more noble potential observed in Tank H-42. Based on these results and laboratory tests it was concluded that this test demonstrated that the tanks were in a passive condition.

Both SRS tests provided “snapshots” of the tank conditions and, in neither case, was deterioration of the reference electrode probe noted. The probes were not intended for long-term trending purposes and, thus, no precautions were taken to improve the design or materials for the electrodes.

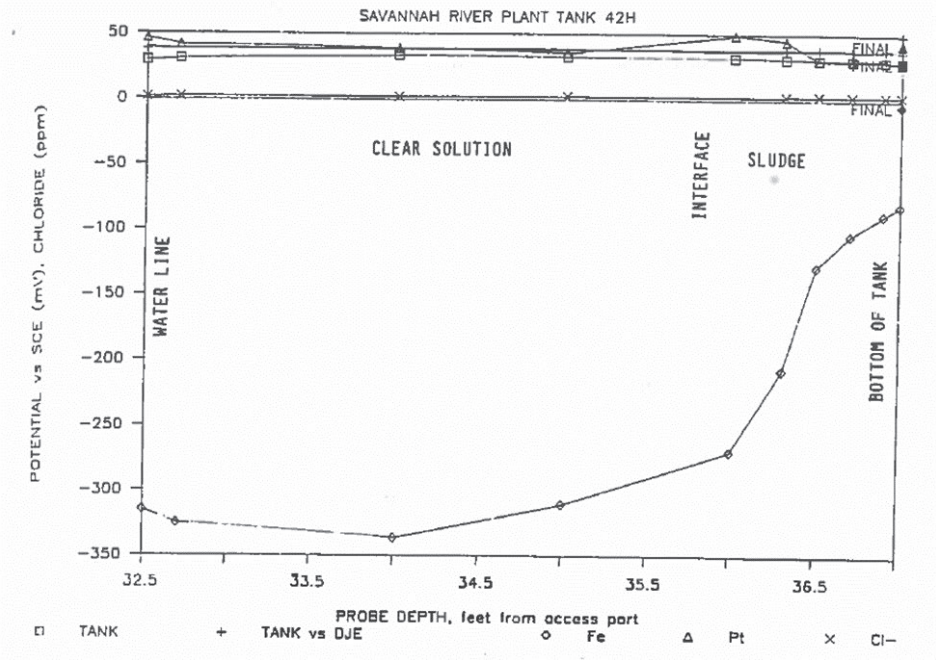

Figure 2-1. Reference electrode results in an SRS tank[12]

Table 2-2. Composition, Temperature and Potential Data for SRS Tanks in the 1980s[12]

	Tank Designation	
	H-42	H-48
Nitrate (M)	0.0014	0.09
Nitrite (M)	0.026	0.24
Hydroxide (pH)	9.5	11.5
Chloride (M)	0.0001	0.0004
Sulfate (M)	0.0003	0.009
Carbonate (M)	0.064	0.29
Supernate Temperature (°C)	< 40	< 40
HgO (wt% in solids)	0.53	0
Tank Potential (mV vs. SCE)	40	-290

The reference electrodes in the tanks are challenging to deploy and extract, as demonstrated by these early attempts. The difficulties encountered with radiological exposure and disposal constraints make long-term performance of a reference electrodes desirable. Furthermore, the

long-term potential of the tank may drift with time depending on the waste simulant. This was evident in many of the waste simulant tests in the laboratory. The actual in-tank potential of the tank steel is the net result of the drifts in the corrosion potential of the tank steel and the reference electrode. Therefore, it is imperative to determine the drift in the reference electrode potential to determine whether the corrosion potential of the tank is attaining values that may necessitate corrective actions.

At the Hanford site, longer term monitoring was attempted early on. A corrosion monitoring probe, designed by Pacific Northwest Laboratories (PNL), was also installed in Tank AN-107 between 1987-1990[13]. At the time, the waste chemistry was outside the corrosion control specification (i.e., pH 10.8). Laboratory polarization scans performed in simulants and actual AN-107 waste indicated that the tank potential was near the active/passive transition, which could lead to failure by SCC. The purpose of the probe was to measure the potential and polarization resistance to assess the general corrosion rate. The probe consisted of a reference electrode, working electrodes fabricated from A537 carbon steel, and a thermocouple (see Figure 2-2). An Ag/AgCl electrode (with a teflon tip) was used as the reference electrode. The body of the probe was made of “Scotchcast”, a 3M resin. A PVC tube was used for the outer wall and probe mold. Stainless steel shot was placed in the probe body to increase the overall weight and overcome buoyancy forces. A stainless-steel aircraft cable was attached to maneuver the probe. A standard shielded cable was used for electrical connections. The anticipated life of the probe was 90 days; however, the probe functioned for approximately 3 years.

Figure 2-3 shows the potential measurements approximately 6 months after the probe had been inserted into the tank. Neglecting the time when the probe lead was cut, the tank wall potential was approximately –0.300 V vs. Ag/AgCl, while the A537 samples were at –0.44 V vs. Ag/AgCl. The potential was very stable over a seven-day period. Figure 2-4 shows the potential measurements after 3 years of exposure. The tank potential at this time was also around -0.300 V; however, the potential of the A537 coupon had increased to approximately –0.325 V. The increase was attributed to the build-up of oxide film on the surface of the sample. For both electrodes, the potential was relatively stable. After 1990, the data from the electrode was not utilized as much. The reasons are not clear for the suspension of measurements, and there are no indications that it was due to probe failure. However, the data from the polarization resistance electrode, as expected, indicated a low corrosion rate. There was a desire to develop techniques that provided information on localized corrosion mechanism (e.g., pitting). Thus, the focus turned to techniques, such as electrochemical noise.

[13] J. I. Mickalonis, SRT-MTS-92-3022, *Trip Report: Informational Meetings on the PNNL Probe for Corrosion Monitoring,*1992.

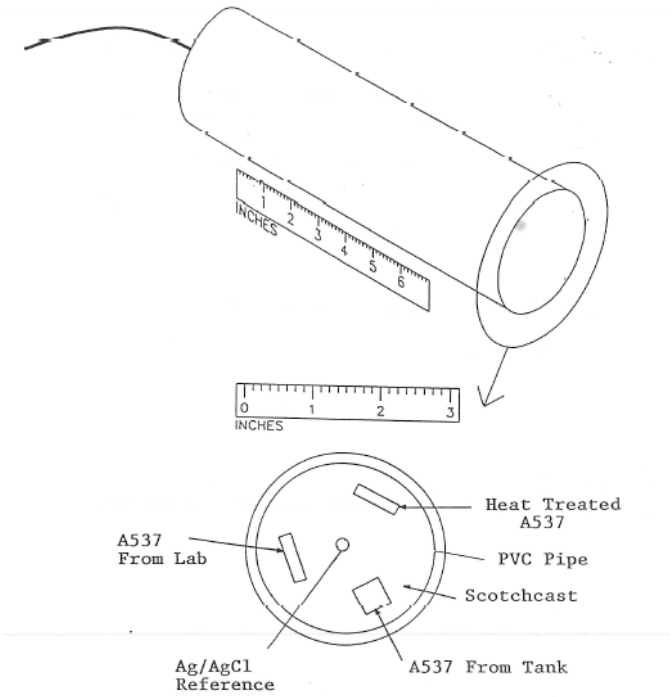

Figure 2-2. Schematic of PNL Probe ca. 1989.[13]

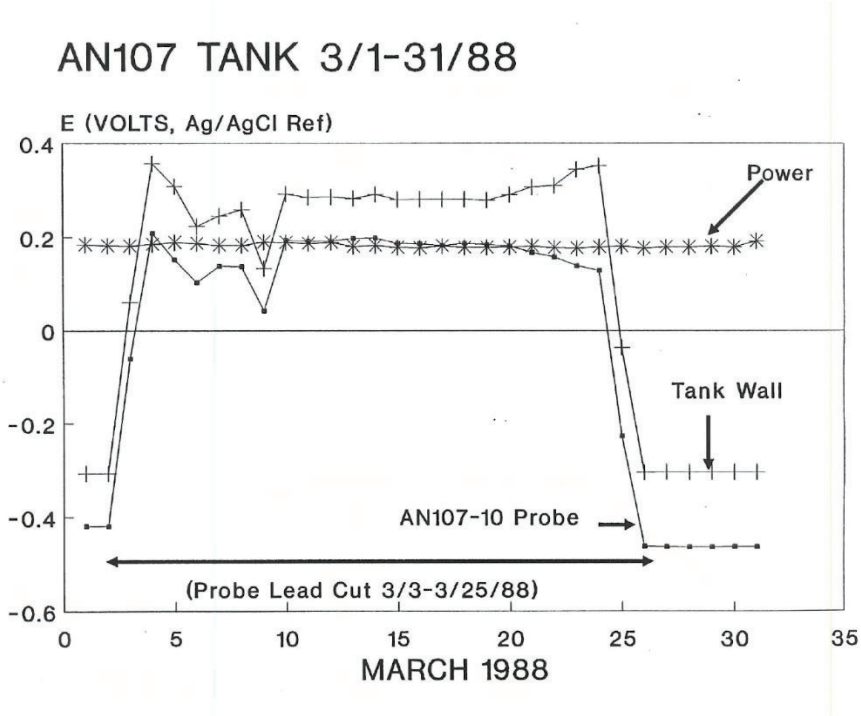

Figure 2-3. OCP measurements of A537 coupon for probe in Tank AN-107, March 1988.[13]

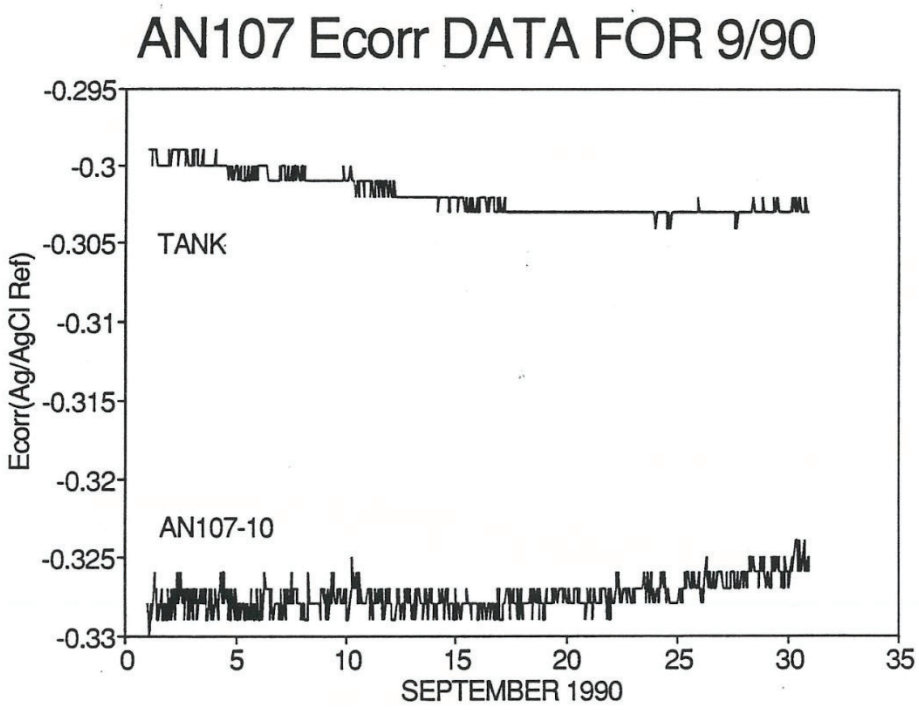

Figure 2-4. OCP measurements of A537 coupon for probe in Tank AN-107, September 1990.[13]

2.1.2 Electrochemical Noise Probe at Hanford

Beginning in 1995 corrosion monitoring in DST began a new phase, that is an emphasis on electrochemical noise (EN) systems[14]. There were three primary reasons for the new approach.

- Previous corrosion monitoring systems had utilized general corrosion techniques such as electrical resistance (ER) and linear polarization resistance (LPR). The results merely demonstrated the expected low general corrosion rates for carbon steel in high pH solution. This did not address primary degradation mechanisms of concern, which were localized corrosion mechanisms such as pitting and stress corrosion cracking.
- Previous monitoring systems did monitor the potential, however, there was not an extensive database that provided information on the critical potentials for cracking and pitting, which could be compared to the potential measurement. Given the wide variety of waste chemistry, there was the possibility that meaningful comparisons could not be made even if the potential was measured.
- Previous monitoring systems did not emphasize long-term monitoring. There was a concern regarding the durability of the systems at that time.

EN was seen as an opportunity to provide information on the localized corrosion behavior of the tanks. Given that EN utilized electrodes made from carbon steel, the stability of a reference electrode in the waste environment was not as great of a concern.

[14] G. L. Edgemon, V. S. Anda, M. M. Dahl, and K. D. Boomer, *The Evolution of Corrosion Monitoring in Hanford High-Level Waste Tanks*, Journal of Nuclear Materials Management, July 2013, **41** (4), 48-60.

The EN systems were implemented from 1997 through 2005. However, due to many issues related to interpretation of the signals and interference from other electrical noise signals the monitoring system did not provide information that was actionable (i.e., actions such as when to add chemicals such as hydroxide). As stated previously, EN instrumentation does not directly measure corrosion occurring on the internal surfaces of the tank or monitor the open circuit potential of the tank wall. Tank wall corrosion must be inferred from the measurements made on the EN electrodes.

2.1.3 Multi-Probe Corrosion Monitoring System at Hanford

In 2004, a group of corrosion and nuclear waste chemistry experts from industry, academia, and other DOE Sites, evaluated proposed initiatives to optimize the waste chemistry specification requirements for a small set of DSTs with waste chemistries that were particularly difficult to adjust[15]. This panel was referred to as the Expert Panel Oversight Committee (EPOC). The experts concluded that optimized waste chemistry control limits could likely be established by conducting laboratory tests to determine the range of corrosion potentials conducive to SCC for a given DST waste type, then monitoring the corrosion potential of the associated DST(s) with relatively simple in-tank corrosion monitoring systems[15]. Thus, one of the weaknesses of previous potential monitoring attempts was addressed.

In 2005 and 2006, researchers performing laboratory corrosion testing, identified the relationship between corrosion potential and the initiation of pitting and SCC in the DST 241-AN-102 and DST 241-AN-107 waste types[16]. Once the range of potentials for pitting and SCC were defined in the laboratory testing for the DST 241-AN-102 and 241-AN-107 waste types, focus shifted to measuring the corrosion potential of those tanks. In 2007, the functions and requirements were completed for the first new corrosion monitoring system associated with this program, known as the Multi-Probe Corrosion Monitoring System (MPCMS). The first MPCMS was installed in 241-AN-102 in May 2008. In addition to these DST, probes were planned for Tank AY-102, AY-101, and AW-104. These DST represented a wide variety of chemistries present in the tank farm.

Figure 2-5 shows the reference electrode configuration and tank-top terminal box for the MPCMS. The reference electrodes that were utilized in the MPCMS are described in Table 2-3[17]. The anticipated life expectancy of the probe was 10 years[18]. All three electrodes were installed on

[15] M.T. Terry, RPP-RPT-22126, *Expert Panel Workshop for Hanford Site Double-Shell Tank Waste Chemistry Optimization*, January 1, 2004.

[16] C.S. Brossia, F. Gui, C. Scott, RPP-RPT-31680, *Final Report, Hanford Tanks 241-AN-I 07 and 241-AN-102: Effect of Chemistry and Other Variables on Corrosion and Stress Corrosion Cracking,* October 30, 2006.

[17] S. Philo, RPP-RPT-44463 Rev.0, *Effects of Temperature and Contamination on MPCMS Electrodes I 241-AY-101 and 241-AN-107 Tank Waste Simulants*, March 26, 2010.

[18] M. M. Dahl and R. J. Crosswhite, RPP-RPT-51766, Rev. 41, *Corrosion Probe Monitoring Systems: January through March 2024 Quarterly Report*, May 2024. (Note: Multiple revisions of this report were reviewed and provided information for this report)

Tanks AN-102 and AY-102. The Ag/AgCl reference electrode proved to be the most robust electrode. The SCEs failed after between 33-55 months of use, while the Cu/$CuSO_4$ electrodes failed after 24-48 months. Therefore, in the remaining three tanks (AN-107, AW-104, and AY-101) only Ag/AgCl electrodes were installed.

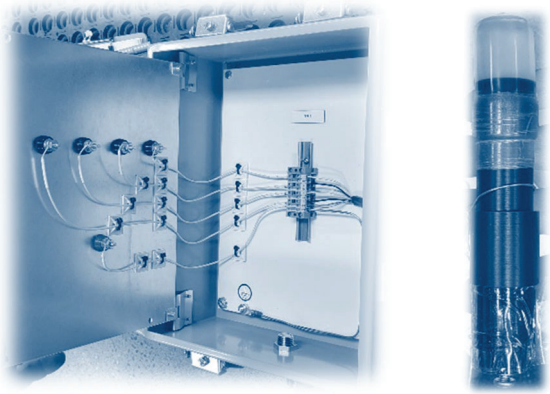

(a) (b)

Figure 2-5. (a) Tank-top Terminal Box, and (b) Reference electrode utilized for MPCMS.[17]

Table 2-3. Description of Reference Electrodes Utilized for MPCMS.[17]

Reference Electrode	Description
Schiff Associates® Model RE-AGAGCL-65 MPCMS-Style Ag/AgCl Reference Electrode.	A specifically-designed Ag/AgCl electrode for the MPCMS application with a Kynar body and porous Kynar frit (for radiation resistance), uses a 1 M potassium chloride filling solution
Schiff Associates Model RE-HGHGCL-65 MPCMS-Style SCE.	A specifically-designed SCE for the MPCMS application with a Kynar body and porous Kynar frit (for radiation resistance)
Schiff Associates Model RE-SCUCUSO4-65 MPCMS-Style Cu/$CuSO_4$ Reference Electrode.	A specifically-designed Cu/$CuSO_4$ electrode for the MPCMS application with a Kynar body and porous Kynar frit (for radiation resistance), uses a saturated copper sulfate filling solution

An example of the data that has been obtained in Tank AN-102 is shown in Figure 2-6. The data shown includes the tank potential vs. a Ag/AgCl electrode and two tank material electrodes that are mounted on the MCPMS mast. The potentials shown in the figure are adjusted to the SCE reference electrode scale. The temperature of the supernate is also shown in the figure. As

expected, the potential oscillated inversely with the change in temperature. The two tank material electrodes produced similar values, while the tank potential was typically 5-10 mV more positive than the tank materials. During the first four years after installation, the potential drifted in the positive direction by approximately 20 mV, however, there was no indication of a failure of the electrode.

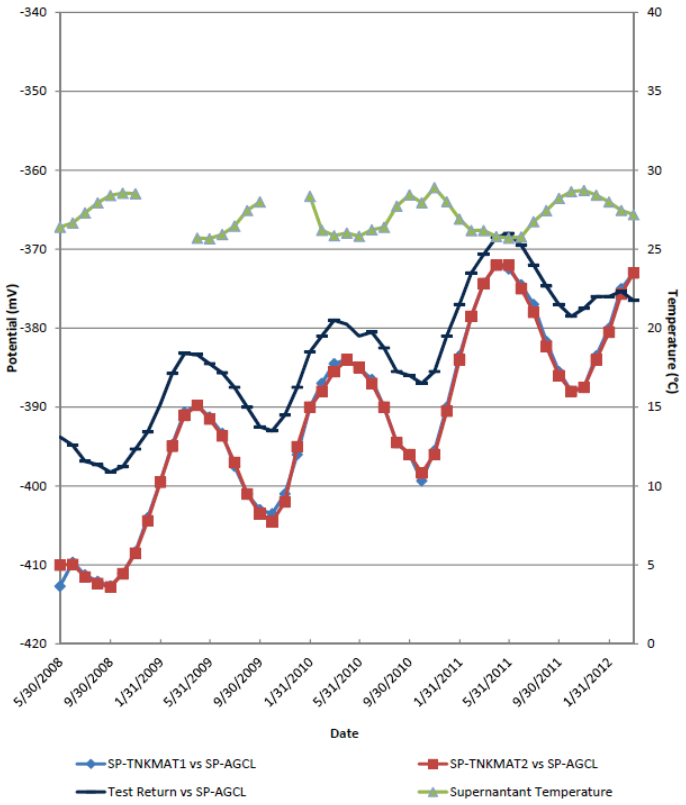

Figure 2-6. 241-AN-102 MPCMS Average Monthly Tank and Supernate Tank Material Electrode Potentials from May 2008 to January 2012.[18]

This was the last operable electrode in Tank AN-102 as most of the reference electrodes in this tank failed within 3 years. Table 2-4 shows the average lifespan of a reference electrode as a function of the type of electrode and the tank. The data from the remaining four tanks indicate that reference electrodes tended to fail in approximately 3 years or less. The two longest lasting electrodes were in the supernate that had a relatively low hydroxide concentration (0.5 to 0.6 M) and contained significant quantities of organics. The performance of the Ag/AgCl electrode in Tank AN-102 was significantly better than the SCE and $CuSO_4$ electrodes. Based on this result, only Ag/AgCl reference electrodes were installed in tanks AN-107, AW-104 and AY-101.

Table 2-4. Average life span of reference electrodes attached to an MPCMS

	Tank	Average Lifetime Ag/AgCl (months)	Average Lifetime SCE (months)	Average Lifetime $CuSO_4$ (months)
MPCMS	AN-102	158	44	36
	AN-107	138 (6**)	NA	NA
	AY-102*	32	26	36
	AW-104	6	NA	NA
	AY-101	30	NA	NA

*Status when tank leakage detected in August 2012. Only 39 months of operation.

**Lifetime of electrode in the sludge solids; Other lifetime was in the supernate

Table 2-5 shows the condition of the reference electrodes in 2019, approximately 10 years after installation. Recall that 10 years was the desired lifetime for these reference electrodes. Discounting the performance of the electrodes in Tank AY-102 (because of the tank failure in 2012), only 2 of the 20 original reference electrodes remained operational in 2019.

Table 2-5. Status of Reference Electrodes in MPCMS Probes in 2019.

	Tank	Installation Date	Operational	Suspect	Failed	Total
MPCMS	AN-102	May-08	1	0	5	6
	AN-107	Jun-10	1	0	3	4
	AY-102*	Mar-09	2	0	4	6
	AW-104	Jul-10	0	0	4	4
	AY-101	Apr-09	0	0	6	6
Total			4	0	22	26

* Status when tank leakage detected in August 2012. Only 39 months of operation.

2.1.4 Retractable Corrosion Monitoring Probe System at Hanford

A significant problem with the MPCMS, was that once installed in a DST it was challenging to troubleshoot, inspect, repair, or replace any of the in-tank electrodes or other waste-contacting components. In 2011, MPCMS designers and equipment engineers began to make changes in

the design of the deployment system. In 2012, a set of design requirements for a new Retractable Corrosion Monitoring Probe (RCMP) were issued[19].

As with the MPCMS, the primary purpose of the RCMP is to facilitate the measurement of the DST corrosion potentials. However, instead of using a large, fixed, in-tank probe to hold electrodes at various elevations in the DST, the RCMP assembly consists of a small replaceable cable reel assembly and associated housing. The entire assembly is approximately 3 ft. x 3 ft. x 2 ft. and can be carried and installed by hand. The cable reel assembly consists of a simple reel wound with cable leading to a probe head containing the required electrodes. The probe head can be raised and lowered in the tank via the cable reel assembly.

The primary reference electrode currently used for potential monitoring in DSTs in the RCMP system is a single-junction Ag/AgCl type manufactured by Van London Co[20]. A photograph of the electrode is shown in Figure 2-7. The body and frit of the Van London reference electrode are made of Kynar (PVDF or Polyvinylidene fluoride), an inert thermoplastic fluoropolymer with a combination of thermal, alkali, and radiation resistance. The Van London single junction (VLSJ) electrode contains a fill of 4-M KCl and is identical to the reference electrode type currently installed in DSTs that are outfitted with RCMPs.

Figure 2-7. Photograph of a VLSJ Ag/AgCl reference electrode type that is currently used in Hanford DSTs (manufactured by Van London Co.).[21]

A schematic of the internal design of the VLSJ Ag/AgCl electrode currently used in Hanford DST corrosion probes is shown in Figure 2-8. The Kynar body of the electrode is approximately 4 inches long and 0.75 inches in diameter at the largest section. The internal element is made from a 0.01-inch diameter, fine Ag wire that is connected to a stainless-steel screw terminal in the end cap for electrical connection. The Ag wire extends into the middle of the electrode cavity and is sealed into the inner diameter of the body with polymeric sealing pads. The end of the Ag wire inside the electrode cavity is coated with an AgCl layer that is approximately 0.5-inch long and has an average thickness of about 0.008 inches. The electrode cavity is filled with a 4-M KCl gel of proprietary composition. The other end of the electrode body is sealed with an end cap that contains a cylindrical porous frit made of natural Kynar. The porous frit provides a low-

[19] C. A. Sumner, RPP-SPEC-49792, *Procurement Specification for the 241-AW-105 Retractable Corrosion Monitoring Probe Assembly*, May 17, 2012.

[20] Van London Co.,10540 Rockley Rd, Houston, TX 77099. Part No. VL8604201.

resistance liquid junction between the electrode and the external waste solution, while restricting intermixing and cross contamination of the electrode fill with the waste.

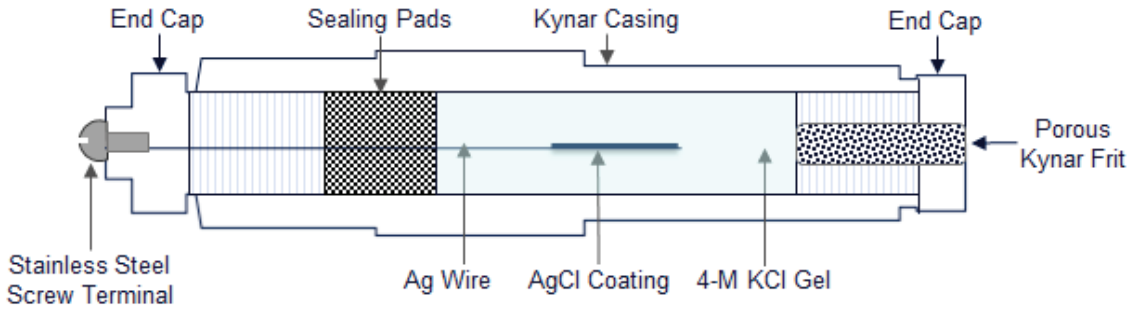

Figure 2-8. Schematic of the internal design of the VLSJ Ag/AgCl electrode currently used in Hanford DST corrosion probes.

Up to four electrodes of this Van London design can be mounted and potted into the head of the Retractable Corrosion Monitoring Probe (RCMP) for installation in the tank, as shown in the photographs in Figure 2-9.

Figure 2-9. Four VLSJ Ag/AgCl reference electrodes mounted in RCMP probe head (top) and installation via riser in Tank 241-AP-106 (bottom)[21].

[21] M.J. Feldmann, RPP-RPT-63666, Rev.0, *Construction Acceptance Test Report for the 241-AP-106 Retractable Corrosion Monitoring Probe (RCMP)*, Prepared by Sargent & Lundy for Washington River Protection Solutions, LLC, October 2022.

An example of the data that has been obtained in Tank AW-105 is shown in Figure 2-10. Note that only the tank potential is measured (i.e., there are no tank material coupons with this arrangement). The potentials shown in the figure are adjusted to the SCE reference electrode scale. The temperature of the supernate is also shown in the figure. The potential has been relatively stable for nearly 18 months and the two reference electrodes are in good agreement. However, two of the four reference electrodes in this tank failed after 15 months.

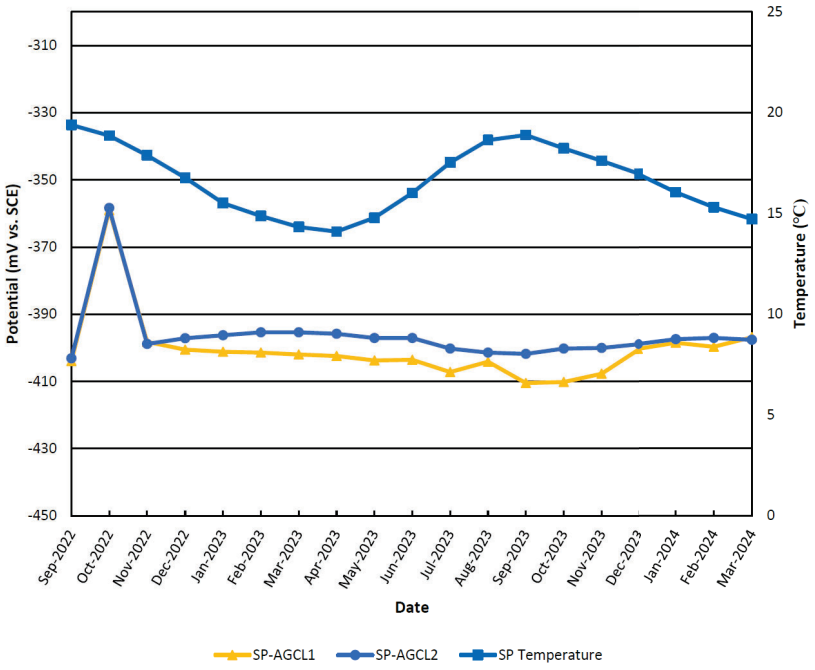

Figure 2-10. Corrosion potential data collected from RCMP installed in Tank AW-105 from September 2022 to March 2024[18].

Figure 2-11 presents the potential data from Tank AP-102. All four of the original reference electrodes had either failed or were suspect within 15 months of being installed. In this situation failure was detected by a sharp 400 mV increase in the potential that occurred within a three-to-six month period. If this were true, the tank potential would be in a range where the steel would be susceptible to localized corrosion or SCC.

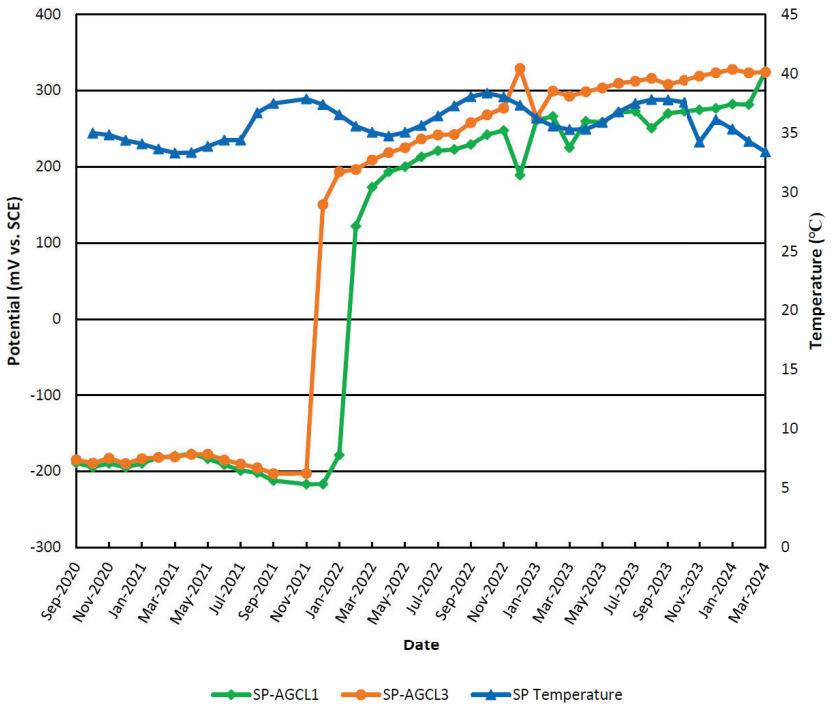

Figure 2-11. Corrosion Potential data collected from RCMP installed in Tank AP-102 from September 2020 to March 2024[18].

Figure 2-12 presents the potential data from Tank AW-105. Both of the original reference electrodes had either failed or were suspect within 9 months of being installed. In this situation, failure was a bit more subtle. The tank potential had drifted slowly in the negative direction approximately 80 mV. Between 2013 and 2020, the potential had drifted in the negative direction approximately 150 mV. If this were accurate, this indicates that the tank wall may be experiencing active corrosion. Four new reference electrodes were installed in 2022. Already, two of the reference electrodes have failed within 15 months.

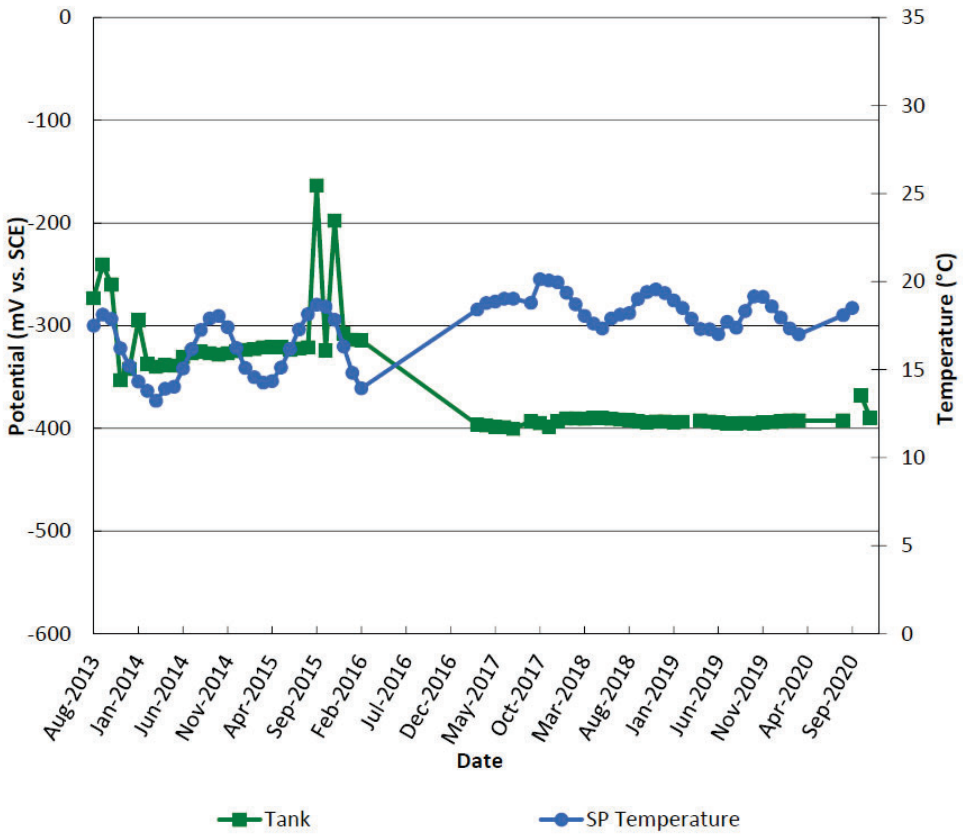

Figure 2-12. Corrosion potential data collected from RCMP installed in Tank AW-105 from August 2013 to September 2020[18].

Table 2-6 shows the average lifespan of a Ag/AgCl reference electrode that has been installed in a DST. With the exception of Tank SY-101, the reference electrodes tended to fail in approximately 2 years or less. The hydroxide concentration in the supernate in Tank SY-101 is also relatively low (i.e., between 0.5 to 1 M). The performance of the Ag/AgCl electrode in Tank AN-102 was significantly better than the SCE and $CuSO_4$ electrodes. Based on this result, only Ag/AgCl reference electrodes were installed in Tanks AN-107, AW-104 and AY-101.

Table 2-6. Average life span of reference electrodes attached to an RCMP.

	Tank	Average Lifetime Ag/AgCl (months)
RCMP	AW-105 #1	9
	AW-105 #2	15
	SY-101	66
	AY-101	19
	AP-102	13
	AP-106	NA
	AZ-101	11

Table 2-7 shows the condition of the reference electrodes in 2024, approximately 2-11 years after installation. Excluding Tank SY-101, 14 of the 22 reference electrodes have failed or are suspect within two years of installation.

Table 2-7. Performance of Reference Electrodes in RCMP.

	Tank	Installation Dates	Operational	Suspect	Failed	Total
RCMP	AW-105 #1	Aug-13*	0	1	1	2
	AW-105 #2	Sep-22	2	0	2	4
	SY-101	Jul-14	0	1	2	3
	AY-101	Sep-19	2	0	2	4
	AP-102	Sep-20	0	2	2	4
	AP-106	Sep-22	4	0	0	4
	AZ-101	Oct-20	0	3	1	4
			8	7	10	25

2.2 Testing in Simulants at DNV

Accurate measurements of tank-wall potentials are important, especially in mission-critical tanks (e.g., AP farm tanks related to DFLAW, 242-A Evaporator feed tank, etc.), where the impacts of waste transfers and other operations are to be monitored. Starting in FY2018, DNV performed long-term testing and evaluation of various types of commercial primary reference electrodes, including the VLSJ Ag/AgCl electrodes, in nonradioactive simulants of the supernatant liquid waste in various tanks to better predict field performance in the DST environments.

The wastes stored in the Hanford DSTs are highly alkaline in nature and span a wide range of chemistries. To test the long-term performance of the reference electrodes, nonradioactive simulants of the supernatant liquids stored in various DSTs were formulated. Table 2-8 shows the calculated pHs, test temperatures, and some compositional features of the simulants tested. The OH^- concentrations of the simulants ranged from 0.53 M to 5.76 M and the sodium concentrations ranged from 3.66 M to 12.4 M. Metal analytes with reported concentrations exceeding 5×10^{-4} M were included in the simulant formulations.

For testing, a stainless-steel reducing union with PTFE ferrules was used to seal around the PTFE tube and the electrode body, shielding the electrical connection from the test environment (Figure 2-13). The tests were performed in 1-L vessels made of chemically resistant perfluoroalkoxy (PFA) polymer. Many simulants were tested at room temperature while a few, such as the AW-101, AW-105, and AZ-101 simulants, were tested at elevated temperatures corresponding to in-tank waste temperatures. For elevated temperature tests, the test vessel was equipped with a heating tape, temperature controller, and thermocouple to provide controlled heating. Various electrode types, including the incumbent VLSJ Ag/AgCl type, were exposed to each waste simulant (Figure 2-13).

Table 2-8. Calculated pHs, test temperatures, and some compositional features of the supernatant liquid simulants tested in the DNV reference electrodes studies.

Tank Simulant ID (Year of Formulation)	pH at 25˚C	Test Temp (˚C)	Waste Features
AY-101 (2018)	13.6	RT	No TIC
AY-101 (2019)	13.9	RT	High TIC
AP-102 (2019)	14.1	RT	High TIC
AZ-101 (2019)	14.3	70	High temperature
AN-102 (2018)	14.4	RT	High TIC, TOC, complexants, heavy metals
AW-105 (2018)	14.8	RT	High fluoride
AW-105 (2019)	14.5	35	Full TOC makeup
SY-103 (2018)	15.3	RT	High aluminum, nitrite, nitrate
AW-101 (2018), 35C	15.6	35	High aluminum, nitrite, nitrate, hydroxide
RT: Room Temperature TIC: Total Inorganic Carbon TOC: Total Organic Carbon			

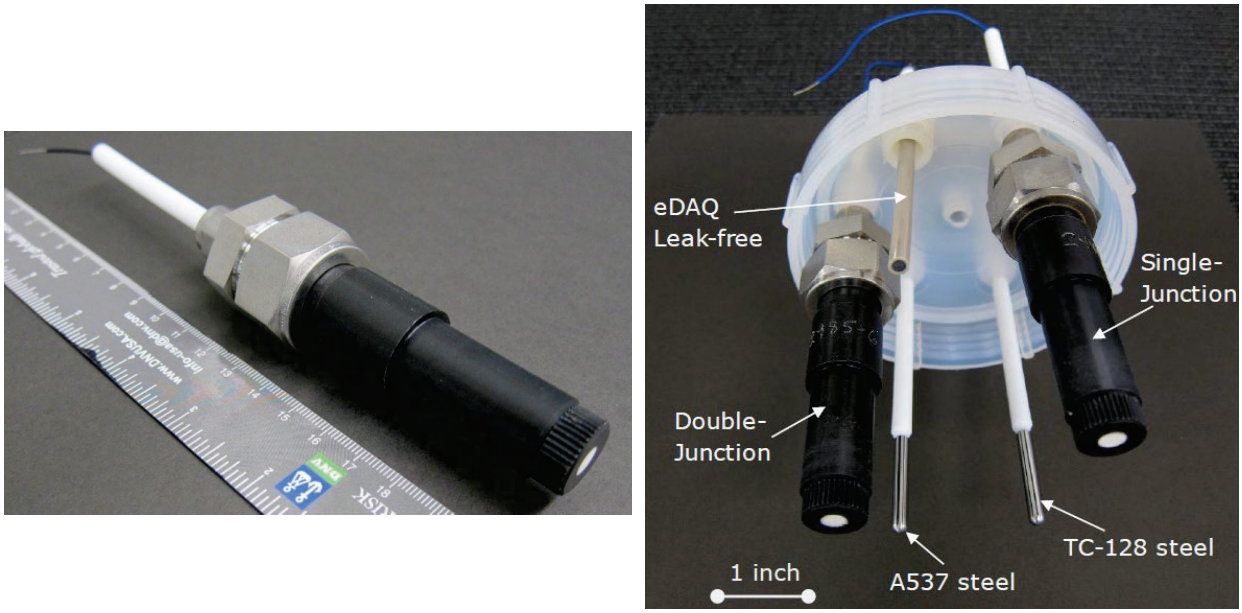

Figure 2-13. Left: Photograph of VLSJ Ag/AgCl reference electrode with compression fitting and wire connection tested at DNV (Ruler scale in cm and inches). Right: Photograph of a PFA test vessel lid showing various Ag/AgCl reference electrodes and tank steel electrodes, prior to insertion in a test vessel for long-term performance testing in a waste simulant[22].

A photograph of the test setup is shown in Figure 2-14. Each test vessel was filled with approximately 800 mL of waste simulant to fully immerse the electrodes. PTFE tubes containing the electrical leads from the electrodes were inserted through ports in the PFA lid of the vessel

[22] S. Chawla, et al., RPP-RPT-63781, Rev. 0, *FY2021 DST Chemistry Testing Report, Prepared by DNV GL USA*, Inc. for Washington River Protection Solutions, LLC, May 2022.

and sealed with compression fittings. One port in the lid was used for inserting a Pt-Nb counter electrode for periodic impedance measurements. Another capped port was reserved for inserting a laboratory reference electrode or Luggin probe to make electrochemical measurements on the test reference electrodes.

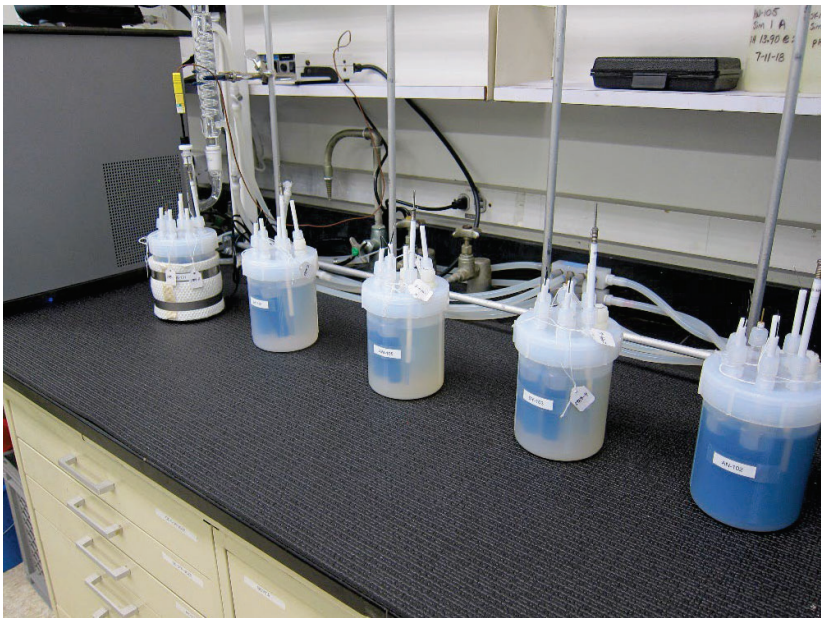

Figure 2-14. Photograph of a DNV test setup for long-term reference electrode study in various DST waste simulants[22].

A standard laboratory SCE was used as the reference electrode for potential measurements. To avoid contamination of the laboratory SCE and damage to its glass body and frit from the high-pH simulants, the laboratory SCE was not kept continuously immersed but inserted in the test cells only when potential or electrochemical impedance spectroscopy (EIS) measurements were to be made. Before and after each use, the potential of the laboratory SCE was verified against a master SCE, which was maintained in a saturated KCl solution.

For the simulants tested at elevated temperatures, a Luggin capillary filled with the simulant was used. Potential measurements were made against the laboratory SCE maintained at room temperature during measurements. A potentiostat in a 2-electrode configuration was used for EIS, with the test reference electrode as the working electrode. The EIS measurements were performed under potential control using a sinusoidal AC voltage perturbation of 5 mV_{rms} around the open-circuit potential of the test electrode. Impedance measurements were carried out in the 5 kHz to 100 Hz frequency range. The high-frequency impedance nearest 0° phase shift was recorded as the electrolytic impedance. This term represents the combined resistive impedances from the test reference electrode fill, porous frit junction, laboratory reference-electrode fill and frit junction, and waste simulant solution. Some EIS scans were performed over a wider frequency range of 10 kHz to 2 mHz using a 3.5 mV_{rms} sine wave excitation. The low-frequency response in these scans was used to study interfacial changes on the Ag/AgCl wire elements of electrodes that exhibited either a large positive drift or a large negative potential drop.

Long-term tests of VLSJ Ag/AgCl reference electrodes were carried out over periods ranging to about 3 years. Figure 2-15 summarizes the potential trends that were observed for continuously immersed and retracted (i.e., periodically immersed, either weekly (“w”) or monthly (“m”)) electrodes as a function of time in various waste simulants.[23]

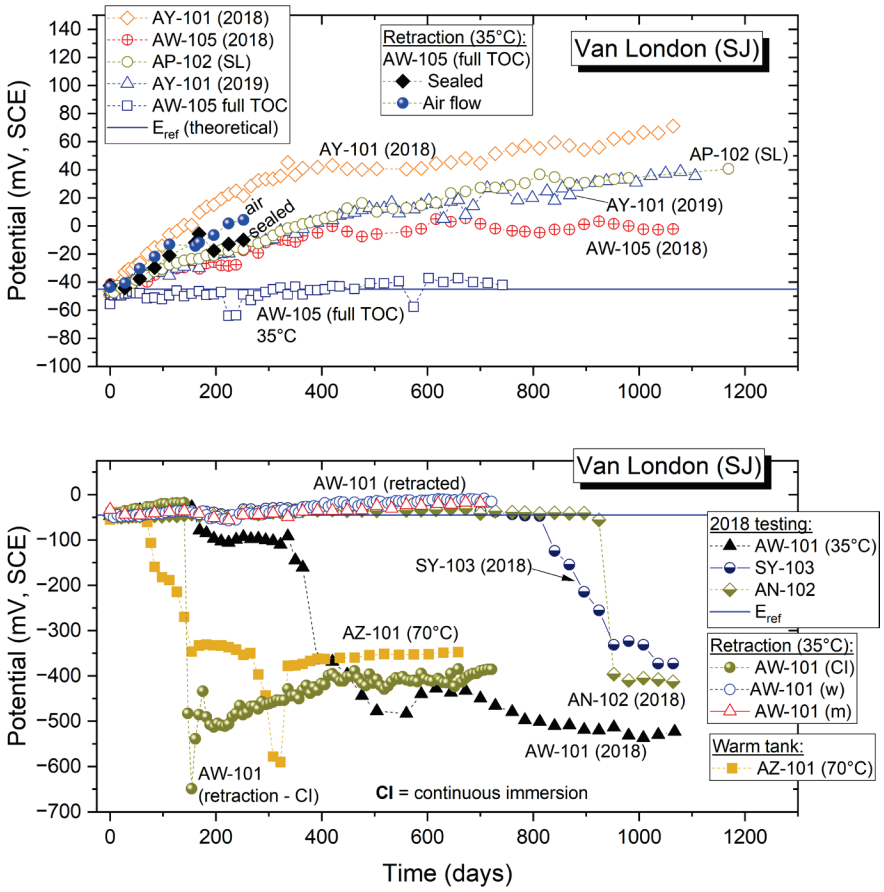

Figure 2-15. Potential trends observed in DNV long-term studies of continuously immersed and retracted VLSJ reference electrodes in various DST supernatant liquid waste simulants.[23]

From the potential trends, the degradation/failure modes for Ag/AgCl electrodes could be broadly classified into two types: (1) monotonic positive drift from the initial potential, and (2) sharp drop to negative potentials after a period of relative stability. The degradation was attributable to diffusive intermixing of the internal fills of the Ag/AgCl reference electrodes with the external simulant solutions over time through the porous frit junctions leads to extensive KCl depletion and contamination of the fills, causing loss of potential stability. All of the simulants in which the reference electrodes exhibited positive drifts had pHs, calculated using OLI software, that were below about 14.8. On the other hand, the simulants in which the electrodes exhibited a sharp potential drop either had pHs greater than 14.9 (AW-101 and SY-103) or a high temperature (AZ-101. 70ºC). The period of relative stability prior to the sharp potential drop was

[23] K. Evans, et al., *In-Tank Corrosion Probes: DNV laboratory evaluations of reference electrodes, Presentation at the Tank Integrity Expert Panel Corrosion Subgroup Meeting*, Denver, CO, March 2023.

shorter at higher pH or higher temperature. The exception to these trends was the AN-102 simulant, which had a pH of 14.4, exhibited a relatively stable potential over about 900 days and then exhibited a large potential drop.

During the long-term tests, EIS measurements were also periodically performed on the electrodes. The EIS measurements were performed under potential control using a sinusoidal AC voltage perturbation of 5 mV_{rms} around the open-circuit potential of the test electrode in a frequency range of 5 kHz to 100 Hz. Figure 2-16 shows the high-frequency impedance, nearest 0° phase shift, of VLSJ Ag/AgCl electrodes as a function of time in various DST supernatant liquid waste simulants. This term represents the combined resistive impedances from the test reference electrode fill, porous frit junction, laboratory reference-electrode fill and frit junction, and waste simulant solution. The high-frequency impedances of the electrodes tested in the SY-103, AN-102, and AW-101 simulants exhibited some increase with time compared to their initial values but, in general, the impedances of all of the electrodes remained low (<600 Ω). Furthermore, no correlation was observed between the large potential drops that were observed for the SY-103, AN-102, and AW-101 electrodes (Figure 2-16) and the changes in their high-frequency impedances.

After completion of the long-term exposures to various waste simulants, various methods were used to analyze some of the tested SJ Ag/AgCl electrodes and compare them with a fresh, unused electrode ("Exemplar") of the same type to understand the reasons for degradation. These methods included visual examination to identify physical damage, and internal investigations, after cutting the electrodes open, by chemical analysis and FTIR spectroscopy of the fill, and Raman spectroscopy and scanning electron microscopy (SEM) with energy dispersive x-ray spectroscopy (EDS) of the Ag/AgCl wire elements.[24]

No damage was observed on the PVDF bodies of the electrodes after the long-term exposures. However, the fills in all the electrodes had transformed from colorless gels into light brown, viscous liquids or jelly-like, wet semi-solids. Chemical analysis of electrode fills (Figure 2-17) revealed significant depletions in the K^+ and Cl^- concentrations of all of the tested SJ Ag/AgCl electrodes compared to the Exemplar. Significant contamination by Na^+, OH^-, NO_3^-, and NO_2^- ions was observed due to intrusion from the respective waste simulants through the electrode frits. The pHs of the fills had increased to 13 or higher compared to about 6 in the Exemplar.

Samples of fills extracted from the SJ Ag/AgCl Exemplar and AW-101 electrodes were analyzed by FTIR. The IR spectrum of the Exemplar gel showed two major absorbance bands close to those of water, indicating the presence of water-related O-H stretch and H_2O molecule bending vibrations. After subtracting the water spectrum, the Exemplar fill's IR peaks closely matched those of sodium carboxymethylcellulose (NaCMC), a common hydrogel former used to reduce ionic mobility and leakage in reference electrode fills. The AW-101 fill showed significant changes including the absence of the O-H stretch band, indicating water loss, and heavy nitrate and nitrite contamination from the AW-101 waste simulant (Figure 2-18). It is possible that structural changes such as cross-linking also occurred in the NaCMC structure.

[24] S, Chawla, K. Evans, S. Feng, and N. Sridhar, *Long-Term Performance of Reference Electrodes in Alkaline Radioactive Waste Storage Environments*, Corrosion, 2024, **80**(5): 472-488.

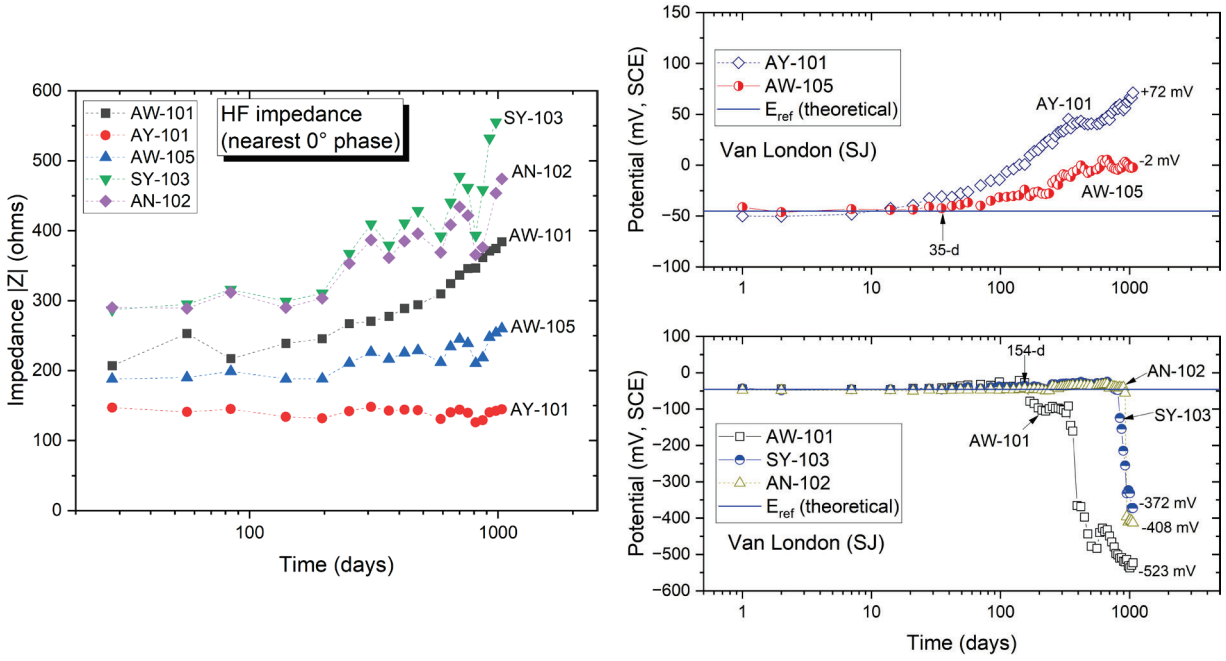

Figure 2-16. Left: High-frequency impedance, nearest 0° phase shift, of VLSJ Ag/AgCl electrodes as a function of time in various DST supernatant liquid waste simulants. Right: Corresponding potential trends of the electrodes over the same exposure period.[23]

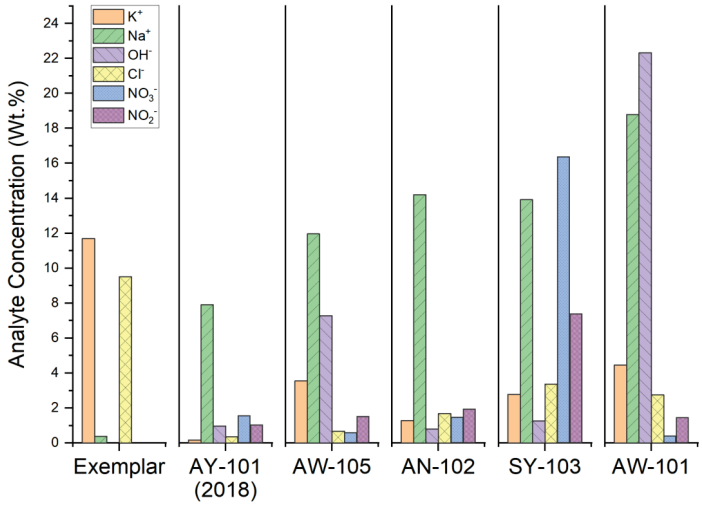

Figure 2-17. Concentrations of selected analytes measured in the fills of SJ Ag/AgCl electrodes after ~1064 days of immersion in various waste simulants, compared to an Exemplar.

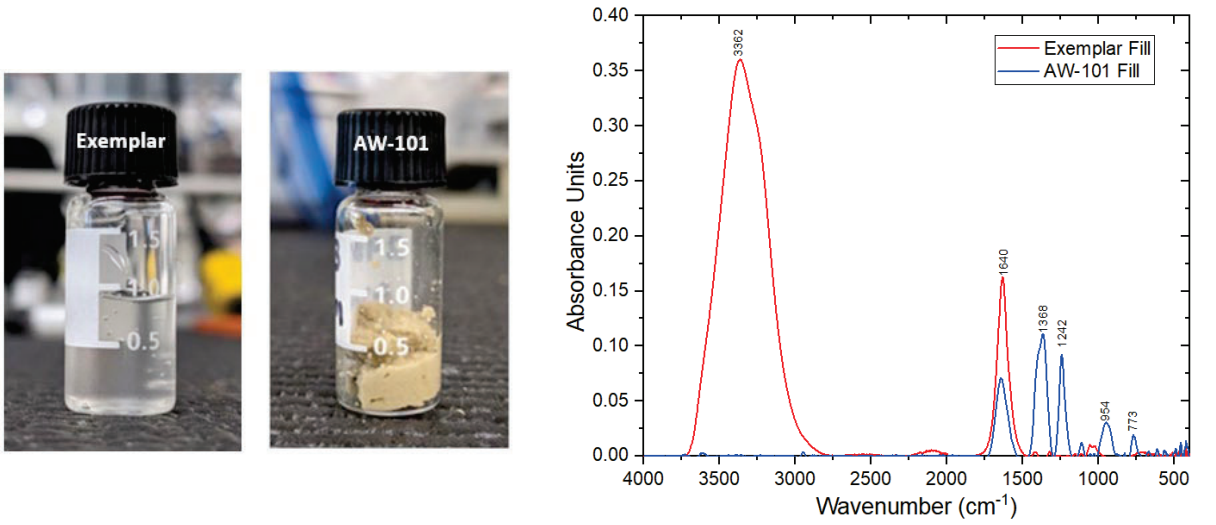

Figure 2-18. Left: Photographs of fill samples extracted from an Exemplar VLSJ Ag/AgCl electrode and the AW-101 electrode (after ~1064 days of immersion in waste simulant). Right: FTIR spectra from the two electrode fills.

An SEM examination of SJ Ag/AgCl wire elements showed varying degrees of chemical attack on the AgCl layers due to waste simulant intrusion, with specific observations for different electrodes (Figure 2-19). The SEM images revealed that the AgCl layers on electrodes tested in AN-102 and SY-103 simulants experienced deep intercrystalline attack; whereas the electrode tested in AY-101 simulant showed only superficial surface roughening. The AgCl coating on the AW-101 wire was the thinnest amongst all the wires. Except for two large (~2-mm) accretions, the coated region on the AW-101 wire was uniformly thin and smooth. EDS analysis indicated that the AgCl layers on the examined electrodes contained high concentrations of elements like C, N, O, F, Na, Al, and K, originating from waste simulants, with significant deviations in Ag/Cl ratios compared to the Exemplar electrode.

Full spectrum EIS scans, in a wider frequency range of 10 kHz to 2 mHz and using a 3.5 mV_{rms} sine wave excitation, were performed on two VLSJ Ag/AgCl reference electrodes and compared to an Exemplar to study their potential trends and frequency responses (see Figure 2-20). The first electrode, exposed to AY-101 simulant, showed a positive monotonic drift of 76 mV over 918 days, while the second electrode, exposed to AW-101 simulant, exhibited a large negative potential drop of about 377 mV over 529 days. The low-frequency impedance, which is representative of the polarization resistance, was slightly higher for the positively drifted electrode (AY-101) and more than an order of magnitude higher for the negatively drifted electrode (AW-101) compared to the Exemplar, as shown in Figure 2-20. The large increase in low-frequency impedance in the AW-101 electrode was attributable to loss of the AgCl layer due to chemical attack by the intruded waste. Significant differences in phase shift were observed below 1 Hz, with the negatively drifted electrode (AW-101) showing higher phase angles. At frequencies above 1 kHz, the impedance magnitudes of both drifted electrodes were only slightly higher than the Exemplar, and the phase angles were close to 0°, indicating resistive response.

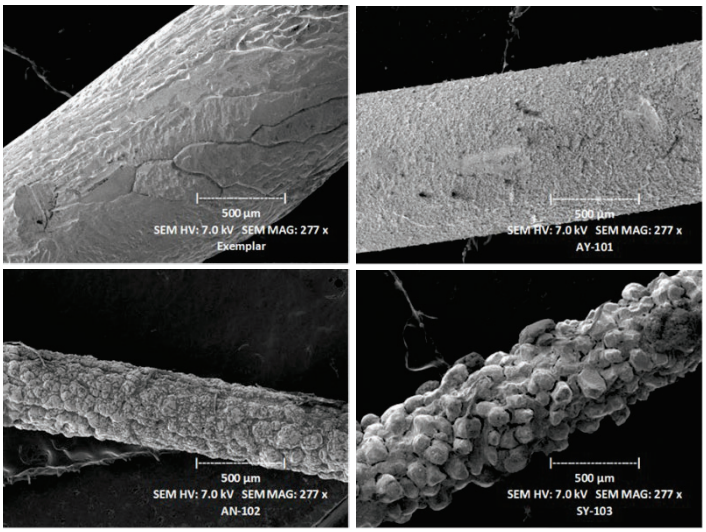

Figure 2-19. SEM secondary electron images of wire elements of SJ Ag/AgCl electrodes; clockwise from top left: Exemplar, AY-101 (2018), SY-103, and AN-102.

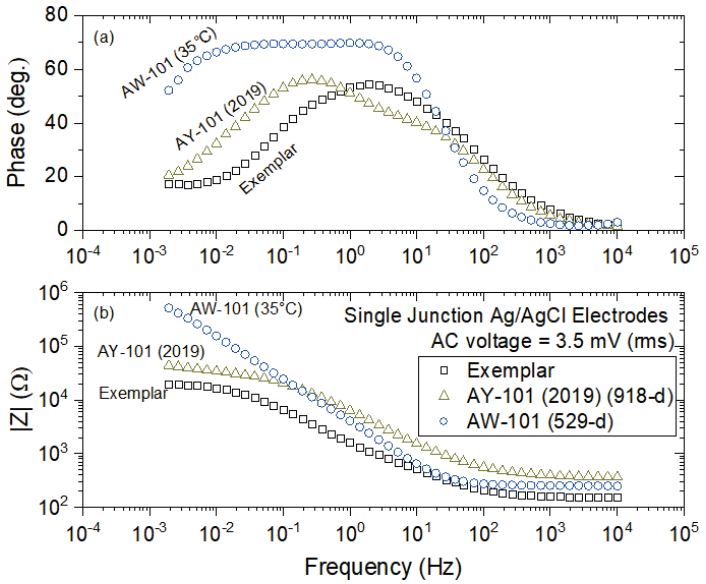

Figure 2-20. Phase angle (top) and magnitude of impedance (bottom) obtained from EIS of VLSJ Ag/AgCl electrodes after long-term exposures in AY-101 and AW-101 waste simulants, compared to an Exemplar tested in 4M KCl.

The potential response of a fresh SJ Ag/AgCl electrode to intentional contamination with AY-101 (2019) simulant showed a positive drift in potential over 11 contamination steps, with a final drift

of about 60 mV (Figure 2-21). This behavior was similar to that observed in long-term natural contamination.

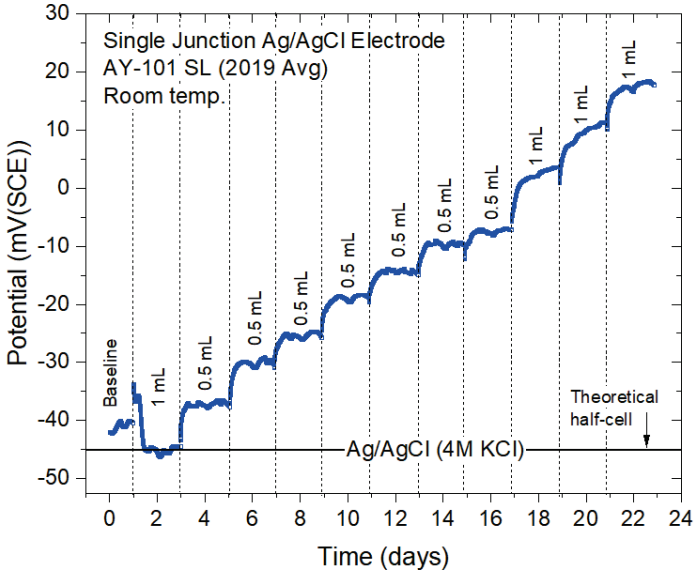

Figure 2-21. Potential change of SJ Ag/AgCl reference electrode in response to incremental intentional contamination of fill solution with AY-101 (2019) waste simulant at room temperature.

In summary, the long-term testing of VLSJ Ag/AgCl reference electrodes in various DST waste simulants showed the following:

- Over time, the porous frit junctions caused extensive KCl depletion and contamination of the electrode fill, resulting in a loss of potential stability.
- The main degradation modes for the reference electrodes were monotonic, positive potential drift, and sharp drops to negative potentials.
- Electrode failure by large potential drop occurred in waste simulants with very high pHs. This type of failure was accompanied by a large increase in polarization resistance and attack and thinning of the AgCl layer by the intruded waste simulant.

2.3 Testing in Actual Wastes at 222-S

A long-term study on Ag/AgCl reference electrodes in radioactive supernatant waste samples drawn from various DSTs was performed in hot cells at the Hanford 222-S Laboratories.[25] Three different Ag/AgCl reference electrode designs from Manufacturers A, B, and C were

[25] S. Feng, S. Chawla, D. Frye, K. Evans, and N. Sridhar, *Long-Term Performance of Ag/AgCl Reference Electrodes for Corrosion Potential Monitoring in Radioactive Tank Waste at the Hanford Site*, Corrosion, 2024, **80**(6): 660-672.

tested, each with distinct materials and geometries. The main features of the electrodes from the three manufacturers are summarized in Table 2-9.The electrodes from Manufacturer A (Van London Co.) contained a gel fill and were the same type currently deployed in Hanford DSTs. The electrodes from Manufacturer B (eDAQ Inc) contained a liquid fill, and the electrodes from Manufacturer C (BORIN Manufacturing) contained a wet solid fill.

Table 2-9. Main features of the single junction Ag/AgCl reference electrodes tested in DST wastes.

Manufacturer		A	B	C
Size	Diameter (cm)	1.9	0.5	3.1
	Length (cm)	10	13	21
Body material		PVDF[(A)]	PEEK[(A)]	ABS[(A)]
Junction	Material	Porous PVDF	Polymer	Ceramic
	Surface Area (cm^2)	0.28	0.13	6.02
Electrolyte		4 M KCl in aqueous gel	3.4 M KCl in water	NaCl loaded in solid fill
Measured potential of as-received electrodes at 25°C (mV_{SCE})		−41±3	−27±3	−49±5

[(A)] PVDF: Polyvinylidene fluoride; PEEK: Polyether ether ketone; and ABS: Acrylonitrile butadiene styrene

The reference electrodes were tested in supernatant from various tanks, including AN-106, AP-102, AW-101, AW-105, AY-101, and AZ-101, under different temperatures and radiation levels. The Ag/AgCl reference electrodes from different manufacturers were tested in 500-mL glass jars containing tank waste supernatants at temperatures representative of the tank conditions, primarily at 35°C and ambient hot cell temperature. Weekly measurements involved monitoring potentials of Ag/AgCl reference electrodes and tank liner carbon steel against a laboratory SCE using a Luggin tube. EIS was used to characterize changes in electrolytic resistivity and polarization processes of Ag/AgCl reference electrodes due to exposure to tank wastes, with measurements performed bi-weekly. Dose rates were measured and calculated for the test cells and actual tanks, with the highest dose rate inside the test cell observed in the AZ-101 waste due to a high Cs-137 concentration. Failed electrodes were analyzed using x-ray microtomography (XMT), SEM/EDS, and Raman spectroscopy to examine conditions and changes in the electrodes.

Ag/AgCl electrodes from Manufacturer A showed a general increase in potential over time, with significant drops indicating failure, especially in AW-101, AN-106, and AP-102 tank wastes (Figure 2-22). Electrodes from Manufacturer B also failed, exhibiting sudden potential drops in various tank wastes, with the most significant drop being 900 mV in AW-105. Electrodes from Manufacturer C were more stable compared to A and B, with only minor fluctuations and potentials remaining close to the initial values.

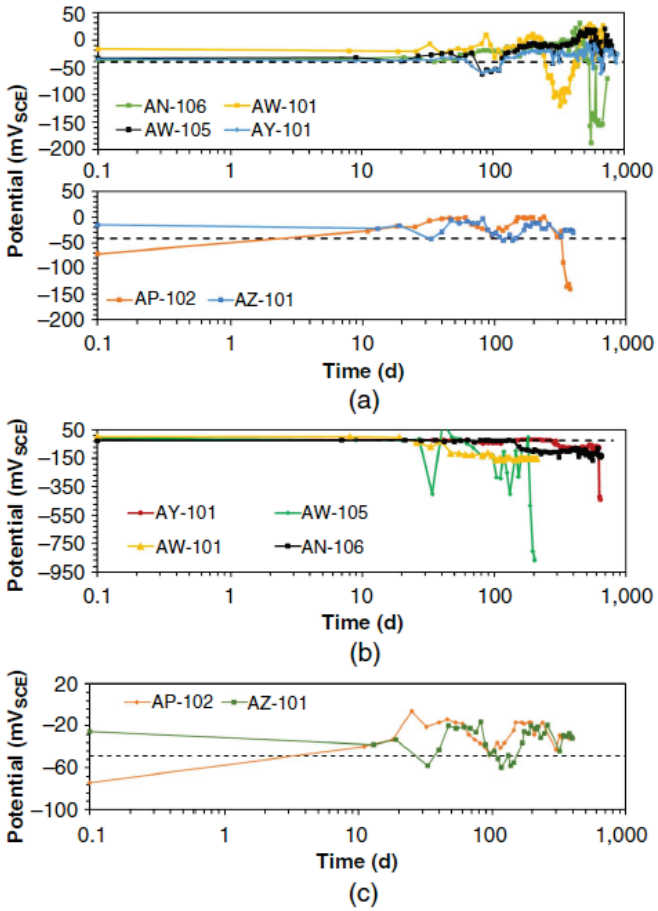

Figure 2-22. Potentials of Ag/AgCl Reference electrodes from Manufacturers (a) A, (b) B, and (c) C collected over different durations in various tank waste samples.

Impedance measurements (Figure 2-23) indicated that the polarization resistance (Rp) increased significantly over time, correlating with potential changes, especially for electrodes exposed to AN-106, AW-101, and AP-102.

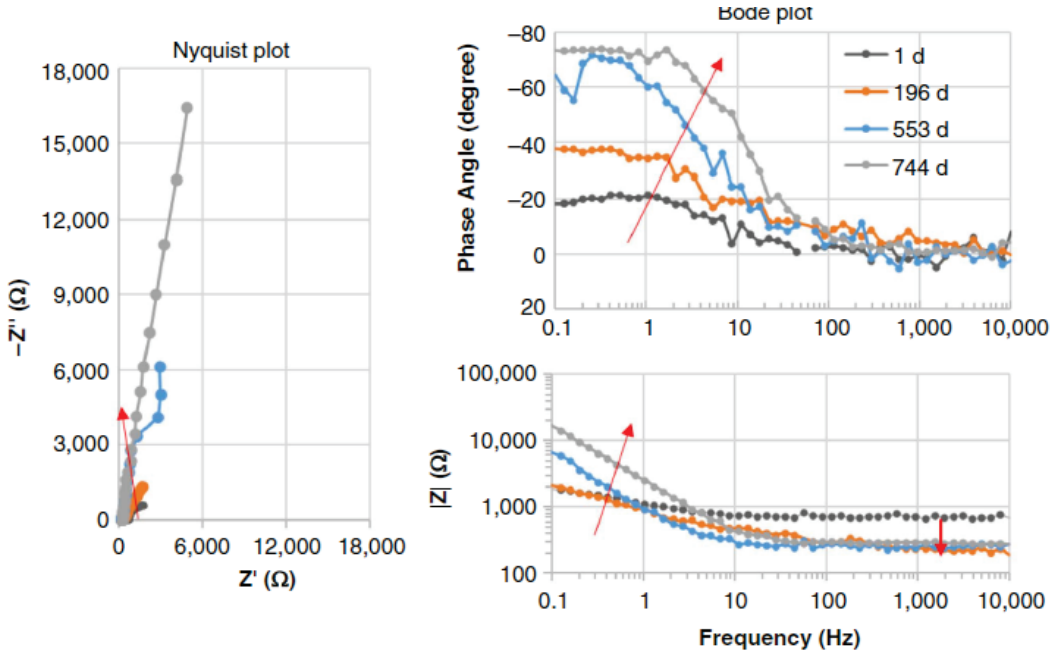

Figure 2-23. Time-evolution of EIS spectra of electrode from Manufacturer A exposed to Tank AN-106 supernatant waste sample at 35°C.

Radiography and computed tomography scans (Figure 2-24) showed significant degradation inside the electrode from Manufacturer A, including thinned Ag wires, loose AgCl layers, and clogged frit materials. Electrodes remained radioactive even after cleaning, indicating tank waste intrusion into the electrode body.

SEM/EDS analysis revealed the formation of new compounds on Ag wires, including elements like C, O, Na, Al, and Si, indicating chemical reactions with tank waste. Analysis of the frit junction materials showed clogging by materials from tank waste, with elements like Na, Al, and Si being predominant. Raman spectroscopy showed peaks indicating the presence of Ag-Cl bonding and new chemical phases formed during tank waste exposure.

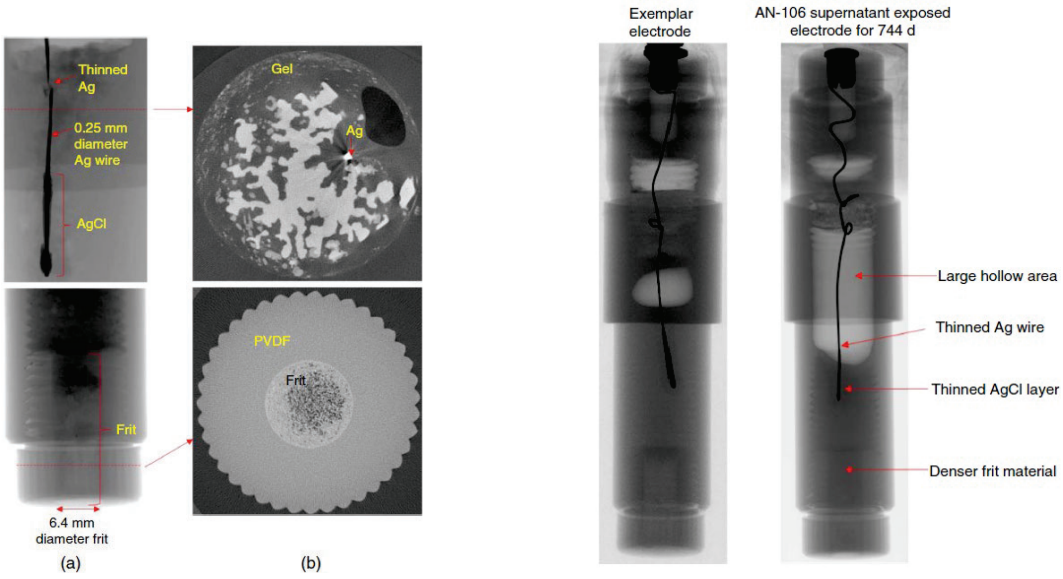

Figure 2-24. Left: Radiographs and XMT cross sections of Manufacturer A electrodes after testing in Tank AW-101 supernatant waste. Right: Radiographs of an exemplar electrode from Manufacturer A and an electrode exposed in Tank AN-106 supernatant waste sample at 35°C for 744 days.

In summary, the long-term testing of the reference electrodes in radioactive waste samples from various DSTs showed the following:

- The primary degradation mechanisms included the intrusion of aggressive chemicals through porous frit materials, leading to clogging, physical and chemical degradation of the AgCl, and alteration of the internal electrolyte. The chemical composition of the tank waste, including the presence of aggressive anions, significantly influenced the degradation and performance of the electrodes.
- Radiolytic species such as H_2O_2 and HNO_3 may have contributed to the degradation of the Ag wire, but chemical effects were more significant than radiation in long-term performance.
- Gradual potential drift, electrolyte resistance decrease, and increased polarization resistance indicated degradation, while a sudden potential drop of over 100 mV signified electrode failure.
- Electrode design and environmental conditions significantly affect the performance and failure probability of Ag/AgCl electrodes, with chemicals having a stronger impact than radiation.
- The studies concluded that electrode design and environmental conditions significantly affect performance, with solid-state electrodes showing the most promise for future deployment.

3.0 Chemically and Radiation Resistant Materials

The previous sections have demonstrated that the commercial electrodes, particularly the internal junction materials, are susceptible to contamination and degradation due to the waste chemistry. Radiolysis may also factor into the degradation of the Ag wire. In this section, candidate materials for the reference electrode that are chemically robust and radiation resistant are considered.

3.1 Degradation of Ag/AgCl Reference Electrodes

When a conventional Ag/AgCl reference electrode is deployed in a tank supernatant, significant contamination by Na^+, OH^-, NO_3^-, and NO_2^- ions may occur due to intrusion from the waste supernatant through the electrode frit. In addition to various ions, organics ligands are also likely to diffuse through the frit into the electrode chamber, contributing to the contamination. The potential of the reference electrode is strongly dependent upon the microenvironment for the Cl^-containing solution (usually potassium chloride or sodium chloride to minimize the liquid junction potential) in contact with Ag/AgCl. Contact of this electrode solution with the external environment occurs through an ion conducting bridge (porous membrane or frit). Dilution of the Cl^- solution or contamination with an incompatible external environment can cause large shifts in the generated reference electrode potential.

In the tank supernatant, OH^-, NO_3^-, NO_2^- and CO_3^{2-} ions are considered dominant. The potential response of the OH^- concentration can be estimated as follows[26]. The redox half-cell reaction of the Ag/AgCl reference electrode is:

$$AgCl + e^- = Ag + Cl^- \qquad (4)$$

The potential of the Ag/AgCl reference electrode is governed by the activity of Cl- ions in the fill and is given by the Nernst Equation:

$$E = E^o - \frac{2.303RT}{F} log a_{Cl^-} \qquad (5)$$

Changes in Cl^- ion activity and the chemical environment around the Ag/AgCl element inside the reference electrode shift the electrode potential. The results showed significant contamination and KCl depletion in the fills that was attributable to long exposure time, large concentration gradients of chemical species across the frit, and various other physicochemical factors.

Metathesis reactions can occur on the AgCl surface when Cl^- ions are exchanged with other anions present in the waste, forming sparingly soluble silver compounds that alter the electrode's response. The formation and solubility products of these silver compounds, along with the activities of the anions, influence the electrode potential. The potential response of the electrode due to foreign ion contamination was analyzed in terms of the Nikolskii-Eisenman Equation:

[26] S, Chawla, K. Evans, S. Feng, and N. Sridhar, *Long-Term Performance of Reference Electrodes in Alkaline Radioactive Waste Storage Environments*, Corrosion, 2024, **80**(5): 472-488.

$$E_{obs} = E^o + \frac{2.303RT}{z_i F} log\left(a_i + \sum_{j \neq i} K_{i-j} a_j^{z_i/z_j}\right) \quad (6)$$

where E_{obs}, is the electrode potential; E^o is a term that includes all potential contributions that are independent of ionic activities, a; subscripts i and j represent the primary (analyte) ion (i.e., Cl^- for the Ag/AgCl electrode) and an interferant ion, respectively; z is the ionic charge; and K_{i-j} is the potentiometric selectivity coefficient, which determines the effect of the interferant ion. Potentiometric selectivity coefficients quantify the effects of interferant ions on the potential response of ion-selective electrodes, including the Ag/AgCl electrode. The Nikolskii-Eisenman Equation is empirical in nature and assumes a Nernstian potential response to the primary ion as well as the interferant ions, with K_{i-j} being a weighting factor for the latter. When no interferants are present or the selectivity coefficients of the interferants' activities are very low, the Nikolskii-Eisenman Equation (Equation 6), reduces to the Nernst Equation (Equation 5) for the primary ion. Hydroxide ion was identified as a dominant interferant for the Ag/AgCl electrode in alkaline media, forming insoluble AgOH and potentially transforming into more stable Ag(I) oxide. A selectivity coefficient for hydroxide ion, K_{Cl-OH}, was estimated from the intentional contamination study and used to calculate the long-term potential drifts for various combinations of Cl^- and OH^- activities in the fills of contaminated Ag/AgCl reference electrodes.

The organic species are also likely to interact with these Ag species and affect the solubility of Ag/AgCl in the supernatant. These organic species can pose challenges when designing a reference electrode to minimize the internal contamination and interaction with the Ag species. To maximize the performance reference electrodes, careful consideration of materials for the internal and outer components are a necessity.

3.2 Internal Reference Electrode Materials

The degradation of the internal materials of Ag/AgCl reference electrodes provides a challenging obstacle to overcome in complex sample matrixes such as tank waste. Throughout this section, several materials will be reviewed to maximize the performance of the internal components of the Ag/AgCl reference electrodes to allow for accurate, reliable, and continuous measurements.

Several documents from DNV and Hanford indicate that the failure of the reference electrode has been thought to be due to containments attached to the silver wire, or the silver wire deteriorating over time.[27] Upon development of a degradation resistant reference electrode the material of the wire should be considered to decrease the amount of degradation. In a patent Alvarez et al., developed and demonstrated the use of a solid state Ag/AgCl carbon nanotubes (CNT) thread reference electrode. A bare CNT thread was plated with 0.3 M $AgNO_3$ in 1M NH_3 to form Ag on the CNT and then AgCl was formed on the surface using $FeCl_3$. They found during the testing that the Ag/AgCl coated CNTS are comparable to the commercial Ag/AgCl reference electrodes. While they did not include long term stability tests, the physical and chemical characteristics of carbon nanotubes could provide interesting results when

[27] K. Evans, S. Chawla, K. Sherer, B. Rollins, and J. Beavers. DNV. *In-Tank Corrosion Probes: DNV Laboratory Evaluations of Reference Electrodes*. March 2023.

incorporated into reference electrodes.[28] In another example employing carbon nanotubes, Rius et al., developed a solid-state reference electrode using carbon nanotubes as the transducer layer between a polyacrylate membrane to entrap the Ag/AgCl system.[29] They found that the performance of the solid-state reference electrode was best (insensitivity to changes in KCl, NaCl, $NaNO_3$ and pH) with photo-nBA reference membrane single walled carbon nanotubes. Generally, carbon nanotubes have been shown to exhibit carrier mobility, chemical stability, and offer chemical functionalization for tunability for various applications. Therefore, employing carbon nanotubes to be used for some of the internal components of the reference electrode could offer higher chemical resistance in the event the tank waste leaches into the compartments.

Moreover, because of the tank waste supernatant's intrusion through the frit, the frit of the reference electrode can be the largest limitation of the accuracy and viability provided by the reference electrode. For example, the Van London reference electrodes currently employed in waste tanks to monitor the potential have a porous frit type and the junction material is Kynar with a fill solution of 4 M KCl gel. After forensic investigation of the Van London reference electrodes, DNV found that several of them have failed due to the intrusion of tank waste through the porous frit junction by analyzing the gel filling and silver wire. Both the gel filling solution and the silver wire were affected by the tank waste and led to the failure of the electrodes.[30] Therefore, the search for alternative materials for the frit/junction type are vital to the development of a stable and accurate reference electrode.

Bühlmann et al. performed several studies on various porous glass frits and porous polymer frits. They found that, while increasing the pore size of the glass frits, the sample dependence of the potential decreases. While this improves the performance of the electrode, the disadvantage of the larger pores allows for intermixing of the solution with the internal solution due to higher flow rates through the frit. In comparison to porous glass frits, they looked at porous polymer frits. They used porous polyethylene and Teflon frits and found that they had more stable potentials over time; however, because the pores are larger, they still cause internal contamination of the reference solution.[31] In an example by Rafea et al., to alleviate cross contamination from the frit, mesoporous borosilicate glass-ceramic compositions were used as frits in reference electrodes. They found that the mesoporous glass-ceramic frit-based reference electrodes exhibited a lower flow rate compared to available microporous frit based reference electrodes such as Teflon, KT-glass, and polyethylene. The average pore size for the mesoporous glass-ceramic frits were around 2.2 nm while other reference electrode frits such as Teflon, KT-glass and polyethylene had pore sizes of 1 µm, 0.5 -1 µm, and 10 µm, respectively. Teflon, KT-glass, and polyethylene also had a significantly larger documented

---

[28] U.S. Pat. Appl. 2017; US 20170363563 A1 20171221 Carbon nanotube based reference electrodes and all-carbon electrode assemblies for sensing and electrochemical characterization 2. N. T. Alvarez; D. Zhao; W. Heineman; V. Shanov; D. Siebold

[29] F. Xavier Rius-Ruiz, A. Kisiel, A. Michalska, K. Maksymiuk, J. Riu, and F. Xavier Rius, Solid-state reference electrodes based on carbon nanotubes and polyacrylate membranes, Analytical and Bioanalytical Chemistry, 2011, **399**: 3613-3622

[30] S. Feng. *Tank Deployable Reference Electrode Testing at 222-S Laboratory*. TIEP Corrosion Subgroup Meeting. March 23, 2023.

[31] M. P. S. Mousavi, S. A. Saba, E. L. Anderson, M. A. Hillmyer, and P. Bühlmann, *Avoiding Errors in Electrochemical Measurements: Effect of Frit Material on the Performance of Reference Electrodes with Porous Frit Junctions*, Analytical Chemistry, 2016, **88**: 8706-8713

potential drift of 200 µV/h compared to -2.4 µV/h from the mesoporous glass-ceramic reference electrodes.[32]

Additionally, inorganic glass composites with good ionic conduction have been studied as solid electrolytes in electrochemical systems. Two interesting materials $Na_{1+x}Zr_2Si_xP_{3-x}O_{12}$ (NASCION) and $Na_2Zn_2TeO_6$ (NETO). An extensive literature study of doped $Na_{1+x}Zr_2Si_xP_{3-x}O_{12}$ shows that the materials exhibit highest conductivities when containing 3–3.5 sodium ions per formula unit, M cation with an ionic radius close to r = 0.72 Å as well as silicon ions substituting phosphorous ions. The ion-conductivity of $Na_2Zn_2TeO_6$ is a novel solid sodium-ion conductor. For likely deployment in the waste tanks, the long-term stability of these ion-conducting composites needs to be evaluated.

In another instance involving stability of reference electrodes, Shen and coworkers studied the degradation of Ag/AgCl reference electrodes in choline chloride based deep eutectic solvents, and developed a Pt $[Fe(CN)_6]^{3-}/[Fe(CN)_6]^{4-}$ reference electrode to combat the challenges.[33] In many studies, the Ag/AgCl reference electrode has been found to be incompatible with deep eutectic solvents because of the anhydrous nature and high concentration of chloride ions. To demonstrate the instability of the Ag/AgCl reference electrode, they performed a cyclic voltammetry study over 800 cycles, 14 hours, and exhibited a dramatic shift of the redox potential of ferrocene. Ferrocene is a common internal standard to test redox potentials. As shown in Figure 3-1, the shift of the potential is attributed to the shift of the reference potential of the Ag/AgCl reference electrode due to the degradation. After two weeks of heavy usage of the FCN reference electrode it was used in a cyclic voltammetry study to determine the stability of the redox potential of ferrocene (Figure 3, right).

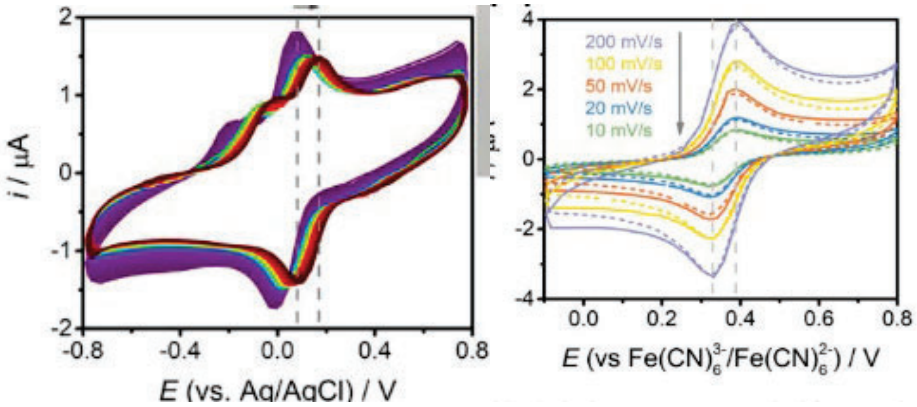

Figure 3-1. Cyclic Voltammetry curves for Ag/AgCl reference electrode over 800 scans in ferrocene (left), FCN reference electrode in ferrocene after 2 weeks of vigorous use (right).[33]

It is thought that the FCN reference electrode would be highly stable for this particular system because the high viscosity of ethaline leads to low diffusivity of $[Fe(CN)_6]^{3-}/[Fe(CN)_6]^{4-}$ and

[32] I. H. A. Badr and O. A. S. Rafeaa, *Evaluation of mesoporous borosilicate glass–ceramic composites as frits in reference electrodes*, Royal Society of Chemistry, 2022, **12**: 28878-28885
[33] X. Shen, et.al., *Evaluating and Developing a Reliable Reference Electrode for Choline Chloride Based Deep Eutectic Solvents,* Journal of the Electrochemical Society, May 2020, **167**(8).

minimizes the diffusion of ions across the porous frit.[33] While the degradation of the Ag/AgCl is notable, the reason for the degradation is something that Shen and coworkers wanted to investigate further. They found a correlation between the stable time (t_s) and the film thickness of the AgCl film (Figure 3-2). This suggests that over time the AgCl is constantly being lost from the Ag wire.[33] Since there were no documented solids, it was thought the AgCl was dissolving in the ethaline. Many previous studies have suggested the AgCl dissolving from the Ag wire to form other complexes, such as dissolving in concentrated hydrochloric acid or in non-aqueous solutions dissolving in acetonitrile containing high concentrations of chloride.[33] Seemingly, the Ag/AgCl reference electrode can be problematic with the AgCl becoming unstable and dissolving over time in a variety of solutions.

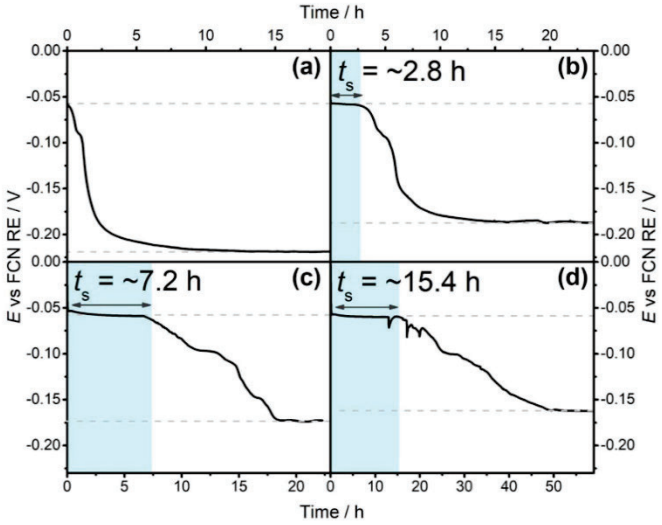

Figure 3-2. The correlation of the stable time with the thickness of the AgCl film. A)5, B)20, C),50, D)100. *The numbers indicate the amount of square wave cycles to thicken the film.[33]

While the longevity of this study[33] is still not where the reference electrode for the waste tank systems should be, it gives more thought to controlling and tuning the reference electrodes for a given application. More specifically, controlling the film thickness of the AgCl offers tuneability and the idea of using the viscosity of the solution to minimize the diffusion of ions through the frit is a creative way to use the contents to their advantage.

Overall, by optimizing the materials for the internal components of the reference electrode, the aim is to lessen the cross contamination from the tank waste and the internal components of the reference electrode. By achieving this, the reference electrode will be more robust in a high activity environment and have longer lifetime stability.

3.3 Irradiation effects on Ag/AgCl reference electrodes and tank composition

While maximizing the internal components of the reference electrode by material selection and optimization, another challenging aspect of designing a reference electrode for tank waste is the irradiation effects on Ag/AgCl reference electrodes.

Radiation creates high-energy, transient redox species that may cause the RE potential to drift from the thermodynamic value when they recombine upon the electrode surface. Radiolysis of water generates active species such as hydrated electrons and hydroxyl radicals as follows[34]:

$$H_2O \rightarrow e_{aq}^-, H^\bullet, OH^\bullet, H_2, H_3O^+, \ldots \quad (13)$$

$$Ag^+ + e_{aq}^- \rightarrow Ag^0 \quad (14)$$

Hydrated electrons directly reduce Ag^+ precursor to Ag^0 nuclei (Reaction V), which progressively coalesce into clusters. To prevent hydroxyl radicals from oxidizing nascent Ag^0 clusters, scavengers such as alcohols are usually added prior to the irradiation process to react with the hydroxyl radicals. This results in the formation of hydroxyalkyl radicals, which, in turn, react with other molecules in solution to produce new radicals for the reduction of Ag^+ to Ag^0.[35] Reactions (I)~(V) indicate that the chemicals and radioactivity in the tank supernatant can cause the degradation of Ag/AgCl reference electrodes, characteristic of the electrode potential shift and the changes of the electrode structures.

In Hanford waste supernatants, numerous chemicals and radionuclides have been detected.[36] The major non-radioactive chemicals include but are not limited to: NaOH, $NaNO_2$, $NaNO_3$, NaF, NaCl, NH_4Cl, HCOONa, NaAc, Na_2CO_3, acetonitrile, uranium, lead, chromium, benzene, butanol, Hg, biphenyls, trichlorophenol, Na_4EDTA. Major radionuclides are listed in Table 3-1.[37]

Table 3-1. List of radionuclides in tank wastes

Radionuclides	Type of Radioactivity	Half-life
Hydrogen-3 (tritium) (^3T)	β decay	12.3 years
Carbon-14 (^{14}C)	β decay	5730 years
Strontium-90 (^{90}Sr)	β decay	29 years
Technetium-99 (^{99}Tc)	β decay	210000 years
Iodine-129 (^{129}I)	β, γ decay	16 million years
Cesium-137 (^{137}Cs)	β, γ decay	30 years
Uranium isotopes (^{233}U, ^{234}U, ^{235}U, ^{238}U)	α decay	703.8 million years for ^{235}U
Neptunium-237 (^{237}Np)	α, γ decay	2144000 years
Plutonium isotopes (^{239}Pu, ^{240}Pu, ^{241}Pu)	α decay	24,100 years for ^{239}Pu
Americium (^{241}Am)	α, γ decay	432 years

[34] P. Uttayarat, J. Eamsiri, T. Tangthong, P. Suwanmala, *Radiolytic Synthesis of Colloidal Silver Nanoparticles for Antibacterial Wound Dressings, Advances in Materials Science and Engineering*, Advances in Materials Science and Engineering, **2015**: 376082.
[35] B. Soroushian, I. Lampre, J. Belloni, M. Mostafavi, *Radiolysis of silver ion solutions in ethylene glycol: solvated electron and radical sea venging yields*, Radiation Physics and Chemistry, 2005, **72**(2-3): 111-118.
[36] J. Marcial, B. Riley, A. Kruger, C. Lonergan, J. Vienna, *Hanford low-activity waste vitrification: A review*, Journal of Hazardous Materials, 2024, **461**: 132437.
[37] M. J. Kupfer, A. L. Boldt, K. N. Hodgson, L. W. Shelton, B. C. Simpson, R. A. Watrous, M. D. LeClair, G. L. Borsheim, R. T. Winward, B. A. Higley, R. M. Orme; N. G. Colton, S. Lambert, D. Place, W. W. Schulz, HNF-SD-WM-TI-740, *Standard Inventories of Chemicals and Radionuclides in Hanford Site Tank Wastes*, February 1999.

3.4 Irradiation penetration factor and radiation shielding

Ionizing radiation is electromagnetic radiation that carries higher energy than nonionizing radiation; ionizing radiation radionuclides are capable of ejecting electrons from atoms and produce negatively charged free electrons and positively charged ionized atoms. Ionizing radiation consists of any types of photons (X- and γ-rays) or particles (alpha, beta, and neutrons). The three most common types of radiation are[38]:

- Alpha – A particle consisting of two protons and two neutrons emitted from the nucleus of an atom. These charged particles lose their energy very rapidly in matter and are easily shielded by small amounts of material, such as a sheet of paper or the surface layer of skin. Alpha particles are only hazardous when they are internally deposited.

- Beta – An electron emitted from the nucleus of an atom. These charged particles lose their energy rapidly in matter, although less so than alpha radiation. Beta radiation is easily shielded by thin layers of metal or plastic. Beta particles are generally only hazardous when they are internally deposited.

- Gamma – Electromagnetic radiation, or photons, emitted from the nucleus of an atom. Gamma radiation is best shielded by thick layers of lead or steel. Gamma energy may cause an external or internal radiation hazard. (X-rays are similar to gamma radiation but originate from the outer shell of the atom instead of the nucleus.)

The more material the radiation can pass through, the greater the penetration power and the more dangerous they are. In general, the greater mass presents the greater the ionizing power and the lower the penetration power.

Shielding has merits such as it has independent efficacy in safe working conditions over the time of exposure and distance that require continued managerial regulation. Thus, an appropriate shielding against nuclear radiation is constantly in demand for a secure life and a healthy environment as the radiation uses are consistently viable in various human activities. A good radiation shield is one that can attenuate, absorb, or block the maximum part of incident gamma radiation. The nature and mechanism of interaction between gamma rays and materials is a critical issue to study to determine the ability of these radiations to diffuse and crack in the medium that according to the mechanism of interaction helps to choose the more applicable radiation shield.

Table 3-2. Comparison of penetrating power, ionizing power, and shielding of α and β particles, and γ rays.

Particle	Symbol	Mass	Penetrating power	Ionizing power	Example shielding
Alpha	α	4 amu	Very Low	Very High	Paper skin
Beta	β	1/2000 amu	Intermediate	Intermediate	Aluminum
Gamma	γ	0	Very High	Very Low	2 inches lead

[38] J. Shultis, R. Faw, *Radiation Shielding and Radiological Protection* in Dan Gabriel Cacuci (ed.), Handbook of Nuclear Engineering, Springer Science, 2010, 1311-1448.

The radiation protection efficiency (RPE) of a material is an important parameter to know material's shielding ability and is determined as follows[39]:

$$RPE = (1-I/I_0) \times 100 \quad (15)$$

where I_0 and I are the un-attenuated and attenuated photon intensities respectively. Their relation follows the Lambert–Beer law as follows:

$$\ln(I/I_0) = (\mu/\rho) \times \rho t \quad (16)$$

where t (cm) is the sample thickness, μ (cm^{-1}) is the linear attenuation coefficient, and ρ (g/cm^3) is a measured density of the sample. The mass attenuation coefficient (μ/ρ) for any chemical compound or mixture of elements is given by

$$(\mu/\rho)_c = \sum_i w_i (\mu/\rho) \quad (17)$$

where w_i is the weight fraction and $(\mu/\rho)_i$ is the mass attenuation coefficient of the ith constituent element.

3.5 Outer Cover Reference Electrode Materials

The outer cover materials for the reference electrode provide a protective barrier of the internal components from the tank waste. As previously mentioned, the internal components of the reference electrode can fail if the tank waste leaches into the internal compartment, causing a failure of the Ag wire, frit, and/or contaminate the filling solution. Additionally, the outer cover materials can provide protection against radiation as a shield and protection against high alkaline solutions. Here, several irradiation resistant materials and alkaline resistant materials are discussed to be used for the outer cover of the reference electrode.

3.5.1 Irradiation Resistant Materials

Many types of materials have been used as radiation shielding barriers to keep a safe environment for everyday practice in all radiation facilities.[40] Customarily, lead, multiple layers of single slabs of pure elements such as barium (Ba), lead (Pb), copper (Cu), iron (Fe), and concrete are reliable, efficient, materials. However, lead and concrete are discarded from consideration; concrete, due to its heterogeneous nature and moisture variation, to predict radiation protection, and lead due to insidious hazards to human health and the environment. On the other hand, polymer and its composites offer promising suitable alternative candidates to lead and concrete in the field of radiation shielding due to its lightweight, durability, flexibility along with superior physical, mechanical, optical, and radiation resistance properties. Besides, polymers can easily be doped with sizeable amounts of high atomic number (high-Z) materials to form their composites that are more competent radiation shields.

Polymers in the form of bonded molecules are proposed in the radiation shielding industry due to their significant properties such as elasticity, compatibility, low cost, and low density, which nominate them as good candidates for radiation attenuation. Furthermore, polymers are materials containing elements with a low atomic number such as carbon (C), hydrogen (H),

[39] Y. Harima, *An approximation of gamma-ray buildup factors by modified geometrical progression*, Nucl. Sci. Eng, 1983, **83**(2): 484-491.
[40] Y. Wu, Z. Wang, *Progress in Ionizing Radiation Shielding Materials*, Adv. Eng. Mater., **2024**:2400855.

oxygen (O), and nitrogen (N). In polymers, radiation resistance depends on the oxygen concentration present in the material. Organic polymer materials are characterized by low density, corrosion resistance, and a low dielectric constant, which allow their application in many fields containing radiation hazard. The interaction of a polymer material with radiation determines their applicability in radiation environments. Usually, materials having dense structures are better in radiation resistance due to a high degree of symmetry.[41]

For example, Kacal et al., studied various polymers and their gamma radiation attenuation. They found that polyacrylonitrile, natural rubber, and polyvinylidene chloride have the highest attenuation coefficient values of the polymers tested.[42] Similar results were found by Mann et al., that polyvinylidene chloride (PCV) has the highest attenuation to gamma radiation. Among the other polymers tested, PCV has the highest equivalent atomic number of the polymers tested, which is directly related to the attenuation of gamma radiation indicating it is the best at shielding.[43] To improve the polymer performance, different fillers can be added to form a polymer composite. Polymer composites are convenient because they retain the characteristics of the polymer in addition to the filler. When forming a polymer composite to be radiation resistant, it is important to think of the type of radiation that should be shielded **(**Table 3-2), the rate of the adsorbed dose, and size of the material.

Epoxy resins are a class of reactive prepolymers and polymers that contain epoxide groups.[44] They can react with hardeners or curing agents, form a strong, durable substance used in a variety of commercial and industrial applications. Because they have many desirable properties, including high strength, low cost, flexibility, low toxicity, good chemical resistance, low shrinkage, and good adhesive strength, they have recently been used in radiation shielding. Epoxy resins are often used as a matrix for composite materials that can be used to shield against X-rays, gamma rays, and neutrons. The properties of epoxy resins can be further improved by adding micro- and nanoparticles to the matrix. For example, bismuth oxide (Bi_2O_3) nanoparticles are often used in radiation shielding because they are effective at absorbing radiation. Al-Dhuhaibat et al., studied the shielding capabilities of pure epoxy, aluminum oxide epoxy, and ferric oxide epoxy. The epoxy composites showed higher shielding capabilities than the epoxy alone. While the polymer composite with inorganic materials provides enhanced performance, polymer composites using nanofillers have a stronger molecular interaction via chemical bonding, thus leading to further enhancement in terms of overall stability.[45]

---

[41] C. More, Z. Alsayed, M. S. Badawi, A. Thabet, P. Pawar, *Polymeric composite materials for radiation shielding: a review*, Environmental Chemistry Letters, 2021 **19**(2):2057–2090.
[42] M.R. Kaçal, F. Akman, M.I. Sayyed, F. Akman, *Evaluation of gamma-ray and neutron attenuation properties of some polymers*, Nuclear Engineering and Technology, 2019, **51**(3):818-8124.
[43] K. S. Mann, A. R., M. S. Heer, *Shielding behaviors of some polymer and plastic materials for gamma-rays*, Radiation Physics and Chemistry, 2015, **106**(1): 247-254.
[44] N. Moonkum, C. Pilapong, K. Daowtak, G. Tochaikul, *Radiation Protection Device Composite of Epoxy Resin and Iodine Contrast Media for Low-Dose Radiation Protection in Diagnostic Radiology*, Polymers, 2023, **15**(2): 430 (1-10).
[45] M.J.R. Aldhuhaibata, M. S. Amanaa, N.a J. Jubiera, A.A. Salimb, *Improved gamma radiation shielding traits of epoxy composites: Evaluation of mass attenuation coefficient, effective atomic and electron number*, Radiation Physics and Chemistry, 2021, 179(2): 109183.

To improve the polymer performance and characteristics, a stiff material called filler can be added to the polymer matrix to form a polymer composite.[46] The combination between filler and polymer matrix provokes the formation of a mixture that influences the polymer–composite properties by retaining the properties of both the filler and the polymer. The composite materials are named according to the re-inforcement and the matrix material constituting them. There are many types of matrix materials such as metal matrix composites, polymer matrix composites, ceramic matrix composites, and epoxy resin matrix composites. The availability of radiation shielding materials that can be molded into specific shapes and used even at high temperatures is quite significant for medical and industrial procedures.

Investigators working in the field of radiation protection have focused and reported numerous polymer matrices that can be used as gamma-ray shields like high-density polyethylene (HDPE) composite loaded with tungsten (W), molybdenum sulfide (MoS_2), and boron carbide (B_4C); micro- and nanosized tungsten oxide (WO_3) dispersed emulsion polyvinyl chloride (EPVC) polymer composites; lead oxide filled isophthalic resin polymer composites; silicone rubber composites containing bismuth content; polymer bricks; polyester composites re-inforced with zinc; composites of high-density polyethylene with zinc oxide; lead oxide; Gd_2O_3/PEEK composites; and ultra-high-molecular-weight polyethylene (UHMWPE) composites containing varying contents of surface-treated samarium oxide (Sm_2O_3) or gadolinium oxide (Gd_2O_3) particles as dual thermal neutron- and gamma-shielding materials.[47]

3.5.2 Alkaline resistant materials

Non-oxide and oxide ceramics (SiC, YSZ, Li_2ZrO_3, $LiAlO_2$, and $SrZrO_3$) are generally stable in hydroxide media at low and elevated temperatures.[48] However, SiC, YSZ, Li_2ZrO_3 and $LiAlO_2$ may undergo structural and chemical changes due to dissolution of the ceramic particles in the hydroxide media followed by precipitation. The $SrZrO_3$ powder is both chemically and structurally stable. They are considered as promising separator materials in molten hydroxide for intermediate temperature water electrolysis system. Several metal oxides such as CeO_2 and TiO_2 also exhibit good alkaline stability.

Additionally, several engineering plastics exhibit high resistance to concentrated acids and alkalis.[49] Fluoropolymers are a distinct class of per- and polyfluoroalkyl substances (PFAS), high molecular weight (MW) polymers with fluorine attached to their carbon-only backbone. Fluoropolymers possess a unique combination of properties and unmatched functional performance critical to the products and manufacturing processes they enable and are irreplaceable in many uses. Fluoropolymers are thermally, biologically, and chemically stable, negligibly soluble in water, nonmobile, nonbioavailable, nonbioaccumulative, and nontoxic.

---

[46] S. Nambiar, J. Yeow, *Polymer-Composite Materials for Radiation Protection*, ACS applied materials & interfaces, 2012, **4**(11): 5717-5726.
[47] P. Zhang, C. Jia, J. Li, W. Wang, *Shielding composites for neutron and gamma-radiation with Gd2O3@W core-shell structured particles*, Materials Letters, 2020, **276**(10):128082.
[48] M. Anisur, A. Aphale, M. Reisert, P. Dubey, S. Heo, J. Hong, K. Patil, H. Xu, C. Yuh, P. Singh, *Stability of ceramic matrix materials in molten hydroxide under oxidizing and reducing conditions*, Inter. J. Hydrogen Energy, 2021, **46**(28): 14898-14912.
[49] J. Sheng, *Critical review of alkaline-polymer flooding*, J Petrol Explor Prod Technol, 2017, **7**(1):147–153.

Fluoropolymers have been widely used in different chemical applications including alkaline-chlorine processes.

Polyether ether ketone (PEEK) material, has excellent alkali resistance and can be used in environments with a pH of 14. Its excellent chemical stability, mechanical properties and processing properties make it an ideal material for the manufacture of high corrosion resistance, high strength, and high durability equipment. PEEK is a thermoplastic special engineering plastic, has excellent chemical resistance, high temperature resistance and oxidation resistance. It can be used at high temperatures and pressures for long periods of time and has excellent mechanical and electrical properties.

Polyvinylidene fluoride (PVDF) is a semi-crystalline thermoplastic fluoropolymer. It is readily melt-processible. It can be fabricated by injection and compression molding. It combines high mechanical strength with good processability. Because of its good alkali resistance, PVDF membranes have been examined to extend membrane life and expand membrane applications in alkaline environments.

UHMW (ultrahigh molecular weight polyethylene) is a low-cost, versatile plastic with resistance to a broad range of chemicals, including concentrated acids and alkalis as well as many organic solvents. Its high molecular weight makes it extremely tough, with excellent resistance to abrasion and impact.

Zirfon® is a porous composite separator material composed of a polysulfone matrix and ZrO_2 which is present as a powder.[50] The manufacturing is based on the film-casting technique. The separator is very stable in concentrated KOH solutions at elevated temperatures. The ZIRFON PERL UTP 500 membrane is composed of an open mesh polyphenylene sulfide fabric which is symmetrically coated with a mixture of a polymer and zirconium oxide.

Another class of alkaline resistant materials are superhard materials.[51] These include but are not limited to carbon allotropes, with the hardest possible material being diamond, followed by carbon nitrides, cubic boron nitride, boron allotropes, and borides, nitrides, and carbides of transition metals as such chromium, rhenium, molybdenum, tungsten. Some of these carbides (WC) and nitrides (TiN) are widely used in machining tools and mining.

3.6 Additive Manufacturing

Additive manufacturing (AM) has several advantageous properties when developing a reference electrode.[52] For example, additive manufacturing can potentially reduce the cost because it can consolidate multiple parts into one and minimize material usage by building objects up rather than cutting, molding, and combining materials. AM offers an ease of modifying the designs to fit the experimental needs and can rapidly produce the designs accurately and precisely. Additionally, additive manufacturing can use several different materials of interest for the

[50] D. Henkensmeier, W. Cho, P. Jannasch, J. Stojadinovic, Q. Li, D. Aili, J. Oluf Jensen, *Separators and Membranes for Advanced Alkaline Water Electrolysis*, Chem. Rev., 2024, **124**(10):6393−6443.
[51] J. Haines, J. Léger, G. Bocquillon, *Synthesis and Design of Superhard Materials*, Annual Review of Materials Research, 2001, **31**:1-23.
[52] M. Whittingham, R. Crapnell, E. Rothwell, N. Hurst, C. Banks, *Additive manufacturing for electrochemical labs: An overview and tutorial note on the production of cells, electrodes and accessories*, Talanta Open, 2021, **4**:100051.

development of the reference electrode such as ceramics, metals, and thermoplastics.[53] For example, Lewenstam et al., developed a solid-state reference electrode using a polymer/inorganic salt composite with an Ag/AgCl wire embedded in the polymeric matrix as the reference element.[54] The reference electrode was found to be insensitive to several changes to pH, concentration, and mobility of ions. The stability of the reference electrode was found to be exceptional with a shift of +/- 0.5 mV and lasted for greater than two months. The solid-state composite reference electrode was mechanically robust and was simple to manufacture. In another example, Girault et al., performed a large-scale fabrication of a solid-state reference electrode on a flexible substrate by using inkjet printing to print the silver patterns on a flexible PET substrate and then chemically transform it into Ag/AgCl electrodes. The method proved to be low cost, simple, and effective, showing exceptional reproducibility using large scale production.[55] Moreover, Kochan et al., developed the fabrication of a solid contact reference electrode by 3D printing using a PVC based composite. They discussed the benefits of the reproducibility and accuracy of the manufacturing process using 3D printing. The fabrication can be integrated and controlled from a PC screen, which eliminates any lab errors when fabricating the reference electrode by injection molding or other fabrication methods.[56]

Overall, additive manufacturing provides an ease of fabrication, greater accuracy and precision, cheaper cost, and less material usage when considering the development of a reference electrode for tank waste. The flexibility of design and material usage with additive manufacturing could provide a unique way to fabricate a reference electrode to maximize the performance while minimizing slight changes in the fabrication if it is developed in a lab based environment.

4.0 Design Features

Traditional reference electrode designs consist of a reference element immersed in a reservoir of electrolyte or fill with a known ionic activity, housed within a casing. The internal electrolyte can be in the form of liquid, gel, semisolid, or solid and has three main functions: (1) provide a known ionic activity of a redox species, (2) support ion-to-electron transduction via a redox reaction on the surface of the reference element, and (3) support a small ionic current flow across a salt bridge or liquid junction with the external environment, preferably through anion and cation species with similar mobilities to minimize junction potentials.

The casing of the electrode isolates the internal electrolyte from the external environment. The junction between the internal electrolyte and the external environment provides ionic communication, thus completing the electrochemical circuit. To minimize intermixing between the internal and external solutions, the junction in traditional reference electrode designs typically consists of a microcapillary, ground sleeve, frit or porous plug, or sealed fiber wick in

[53] N. Dossi, R. Toniolo, F. Terzi, F. Impellizzieri, G. Bontempelli, *Pencil leads doped with electrochemically deposited Ag and AgCl for drawing reference electrodes on paper-based electrochemical devices*. Electrochimica Acta, 2014, **146**(11): 518-524
[54] Z. Mousavi, K. Granholm, T.Sokalski and A.Lewenstam, *An analytical quality solid-state composite reference electrode*, Analyst, 2013. **138**(18): 5216-5220
[55] A. Bananezhada, M. Jovićb, L. F. Villalobosc,K. V. Agrawalc ,M. R. Ganjalia, H. H. Girault, *Large-scale fabrication of flexible solid-state reference electrodes*, Journal of Electroanalytical Chemistry, 2019, **847**(8): 113241
[56] A. Lewenstama, B. Bartoszewicza, J. Migdalskia, A. Kochanb, *Solid contact reference electrode with a PVC-based composite electroactive element fabricated by 3D printing*, Electrochemistry Communications, 2019, **109**(10): 106613

the casing (see Figure 4-1[57]). While traditional reference electrodes are suitable for many applications, they have significant drawbacks. These include electrolyte leakage, contamination of the external environment, and intrusion of the external environments into the electrolyte. Electrode contamination in long-term exposures affects the ionic activity of the redox species in the internal electrolyte, introduces extraneous species, which disturbs the equilibrium on the reference element and causes changes in the electrode potential. Furthermore, certain intrusive species can react with the internal element through metathesis, complexation, or dissolution reactions and alter the electrode response.

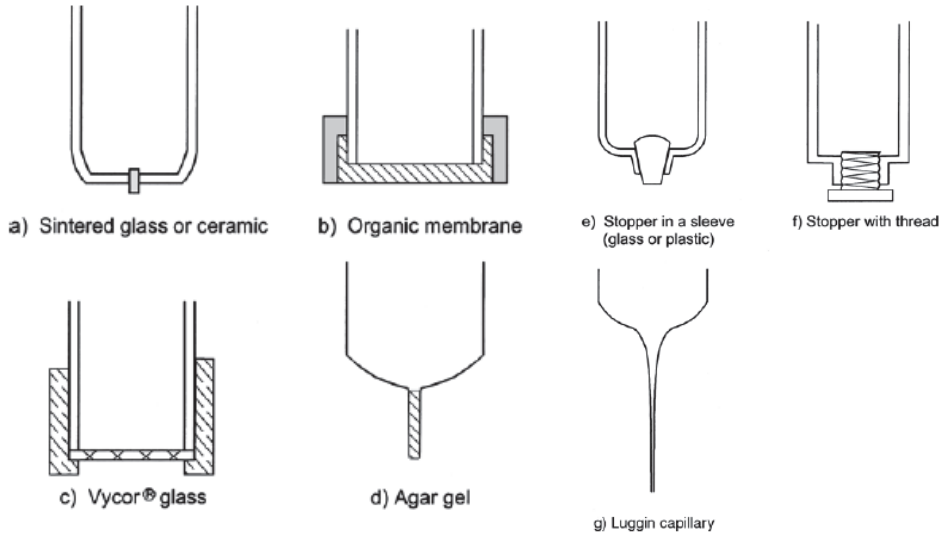

Figure 4-1. Commonly used reference electrode junction designs. From Kahlert[57].

Guth et al.[58] summarized the improvements in classical rod-shaped reference electrode design and the evolution of planar and solid-state designs for potentiometry. Troudt et al.[59] reviewed recent advancements in reference electrodes for electrochemistry, emphasizing the need for improved stability, reproducibility, and compatibility with modern electrochemical sensors.

Various type of alternative design concepts for reference electrodes are discussed in the literature to overcome the limitations of traditional reference electrodes. These can be broadly classified into the following categories:

1. Reference electrodes with extended diffusion lengths
2. Reference electrodes with improved liquid junction designs
3. Reference electrodes with flowless junction designs

[57] H. Kahlert, Electroanalytical Methods: Guide to Experiments and Applications, 2010, Eds: F. Scholz, et al. Springer, Berlin, Heidelberg. 291-308.
[58] U. Guth, F. Gerlach, M. Decker, W. Oelbner, and W. Vonau, *Solid-state reference electrodes for potentiometric sensors*, J Solid State Electrochem., 2009, **13**:27–39.
[59] B. K. Troudt, C.R. Rousseau, X.I.N. Dong, et al., *Recent progress in the development of improved reference electrodes for electrochemistry*. Anal. Sci., 2022, **38**: 71–83. https://doi.org/10.2116/analsci.21SAR11

4. Ionic liquid reference electrodes
5. Solid-contact reference electrodes
6. Field Effect Transistor (FET) based reference electrodes

4.1 Reference Electrodes with Extended Diffusion Lengths

Duffy and coworkers[60] explored the idea of enhancing the lifespan of reference electrodes by increasing the diffusion length. Their work includes a mathematical model, experimental validation, and practical applications using 3D printing and CNC machining. The stability of reference electrodes is determined by the open circuit potential (OCP), which is related to the concentration of redox-active species and can be quantified using the Nernst equation. Deviation of the OCP from its initial value in an environment can be indicative of concentration changes in the redox-active species due to diffusion. The authors modeled the lifetime of the reference electrode based on a 1D representation of Fick's law of diffusion and developed reference electrodes based on this model. The OCP is directly related to the concentration of redox active species, thus the Nernst equation can be employed. [1]

$$C(x,t) = \frac{C_0 - C\infty}{\sqrt{\pi t}} H(x,t) + C_\infty \qquad (18)$$

$$E_{OCP} = E_{RE}(t) - E_{Test} = -2.303 \frac{RT}{nF} log_{10} \left[\frac{C(0,t)}{C\infty}\right] \qquad (19)$$

Duffy and coworkers used the Nernst Equation (Eqn. 2) to compare the OCP of a reference electrode to an identical electrode in a test solution to demonstrate how the reference electrode changes regarding diffusion. C(0,t) should remain constant one the reference electrode is immersed in the test solution until the electrolytes diffusion reaches the reference couple. Here, the reference electrode lifetime, $t_{lifetime}$, is quantified at some point where the OCP deviates significantly from the initial value.[60]

$$P = \frac{E_{OCP}\,(t_{lifetime})}{E_{OCP}\,(0)} = log_{10}\left[\frac{C(0,t_{lifetime})}{C\infty}\right] / \, log_{10}\frac{C_0}{C\infty} \qquad (20)$$

$$C(0, t_{lifetime}) = \frac{C_0}{C\infty}^{P} C\infty \qquad (21)$$

By using equation 18, equation 20 can be solved for $t_{lifetime}$ using the design parameters and the solution to the 1D diffusion problem given in equation 1. Using a percentage is more accurate than doing so with only shifts in the potential. A change in percent will be more easily noticed in similar concentration reservoirs than a 10 mV shift.

By using a mathematical analysis, they were able to observe a large change on the stability of the reference electrode based on the filling solutions length (Figure 4-2). They demonstrate that the diffusion front takes longer to reach the reference couple once the distance is increased and that the rate of diffusion is slowed down.

[60] . S. Duffy, D. M. Hall, and S. N. Lvov, *Increasing the lifespan of reference electrodes by increasing the diffusion length*, Electrochimica Acta, 2023, **438**: 141562.

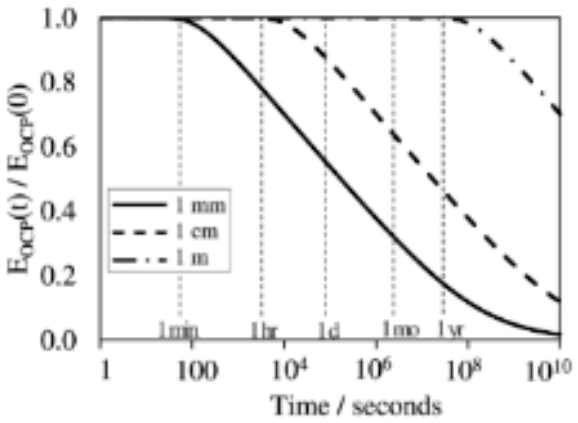

Figure 4-2. Influence of time and the filling solution length on the stability of a reference electrodes OCP.[60]

Additionally, their lifetime model predictions were confirmed experimentally. Reference electrode housings with long, serpentine, and narrow filling solution channels, made by 3D printing and CNC machining, were used to produce small reference electrodes with enhanced lifetimes; these electrodes outperformed conventional designs (see Figure 4-3). Housings with serpentine cavities 2 mm x 2 mm in cross-section and up to 75 cm long were produced by the 3D printing process. A small Ag/AgCl couple element was introduced through an opening in the top end of the channel and the bottom end of the channel formed the junction with external solution. The channel was filled with an agar gel containing 1-mol/Kg KCl + saturated AgCl salt. Their study suggested that increasing the length of the filling solution channel is more effective than changing the diffusion coefficient of the filling solution material for extending the lifespan of reference electrodes.

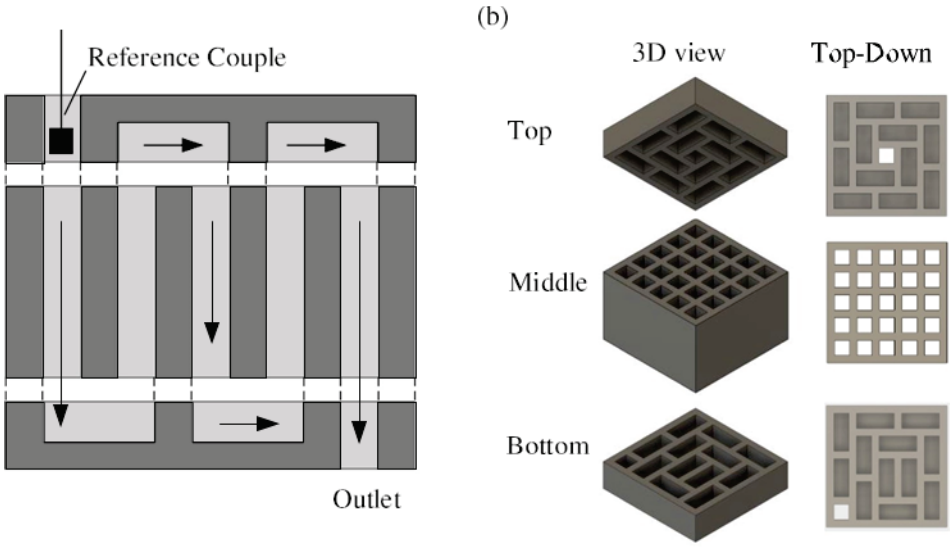

Figure 4-3. Reference electrodes design concepts based on long, serpentine fill channels produced by 3D printing and CNC machining. From Duffy et al.[60].

The results show that the longer channels maintain a constant potential for a longer period (Figure 4-4). While these experiments were carried on for < 240 days, the overall thought process could be beneficial to optimizing a reference electrode designed to implement into waste tanks.

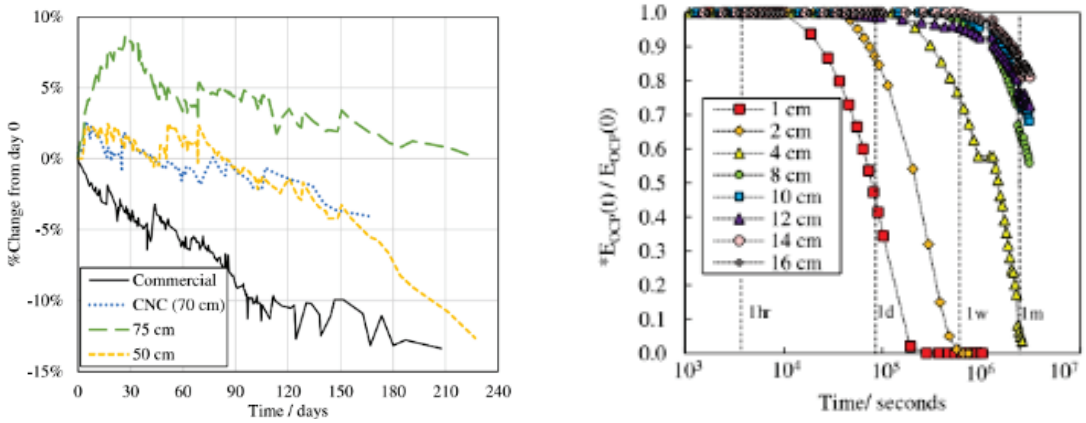

Figure 4-4. Experimental results showing change in percent over time with different lengths (left). Change in the OCP over time for the glass tube RE (right).[60]

The concept of an increased diffusion length to extend electrode life is also being investigated through customized design modifications in a commercial Ag/AgCl reference electrode, manufactured by BORIN Manufacturing. The standard, off-the-shelf version of this electrode is 8.25-in. long x 1.25-in. diameter and features a ceramic frit junction. The electrode body in the customized electrode design, is only one inch longer than the standard version. However, the diffusion path length between the junction and the Ag/AgCl element inside the modified electrode is 4 inches, which is about 8 times longer than the path length in the standard version.[61] This modification is accomplished by compressing the coil-shaped Ag/AgCl element thereby increasing the distance between the ceramic junction of the electrode and the tip of the coil. Another advantage of the BORIN electrode design is that it contains a wet-solid fill consisting of gypsum saturated with NaCl. Diffusion of contaminating ionic species through the wet solid is expected to be slower than in liquid or gel fills that are found in other commercial reference electrode designs. The standard and customized Borin electrodes are currently undergoing long-term performance testing and evaluation at DNV in various Hanford waste simulants and in radioactive waste samples at the Hanford 222-S Laboratory.

4.2 Reference Electrodes with Improved Liquid Junction Designs

The junction or salt bridge in a reference electrode must maintain ionic contact between the external solution and the internal fill while having relatively low impedance. Free-flowing junctions that allow a small amount of fill electrolyte to stream out at a constant flow rate through a single leak path have the advantage of a constant and reproducible junction potential.

[61] S. Chawla, et al., DNV Test Plan & Status Report- 04102024, WRPS FY2024 Hanford Waste Chemistry and Corrosion Testing (10475418), Tank Integrity Expert Panel Corrosion Subgroup Meeting (Virtual), April 10, 2024.

However, these junction designs are impractical for field applications because the fill electrolyte needs to be periodically replenished. Additionally, a high flow rate from the junction can contaminate the external environment, while too low a flow rate may make the junction susceptible to clogging by suspended matter resulting in erratic junction potentials.[62]

Higuchi et al.[63] described a valve-actuator integrated Ag/AgCl reference electrode junction design to overcome these problems and provide a stable reference potential for pH measurement over long periods. This design incorporates a valve actuator based on a shape memory alloy wire to control the liquid junction, allowing it to open only during measurements, which helped in reducing the outflow of internal electrolyte. Figure 4-5 shows the operating principle of the intermittently opened liquid junction, the valve actuator design, and a schematic of the 70 mm long x 20 mm diameter pH probe assembly containing the valve actuator reference electrode, control circuit, and a battery.

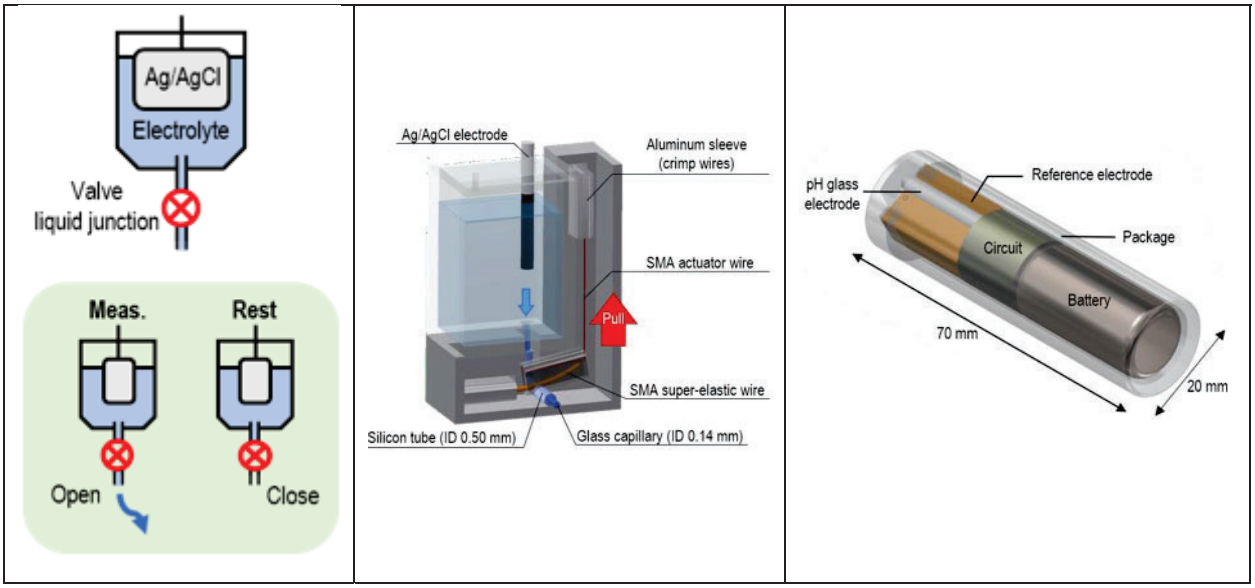

Figure 4-5. Left: Operating principle of valve-actuator reference electrode; Middle: Valve-actuator design using shape memory alloy wire; Right: Conceptual design of the valve-actuator integrated reference and pH electrode. From Higuchi et al.[63]

The Ag/AgCl element was contained inside a small reservoir of KCl fill solution. A silicone tubing of 0.5-mm ID was connected to a bottom outlet in the KCl reservoir. The other end of the tubing was connected to a 0.14-mm ID glass capillary, which served as the liquid junction. The valve design was similar to a normally closed (NC) pinch valve. When no electrical current was flowing in the shape-memory actuator wire, the silicone tube was pinched, and the valve was in the NC position. The actuator wire contracted when a voltage was applied, which allowed the tubing bore to open and release a small amount of KCl through the capillary junction and enabled a potential measurement to be made with respect to the Ag/AgCl electrode. The valve-

[62] D.T. Sawyer and J.L. Roberts, Experimental Electrochemistry for Chemists, 1974, John Wiley & Sons.
[63] S. Higuchi, H. Okada, S. Takamatsu, and T. Itoh, *Valve-Actuator-Integrated Reference Electrode for an Ultra-Long-Life Rumen pH Sensor*, Sensors 2020, **20**: 1249; doi:10.3390/s20051249.

actuator reference electrode design exhibited stable potential values, with errors of 0.5 mV or less relative to the theoretical potential, and a response time of less than 0.083 seconds when the liquid junction was switched open. The lifetime could be greatly extended by intermittent operation of the junction. Calculations showed that starting with an electrolyte volume of 500 µL in the valve and applying a differential pressure of 20 kPa inside the electrolyte container by injecting air before use, the reference electrode lifetime would be 2 years assuming that the valve was opened for 5 s every hour to make a measurement.

In practice, flow-restricted junction designs are more commonly used to minimize intermixing and contamination between the internal fill and external solution, especially in long-term potential monitoring. These junctions are typically made of porous glass, polymeric or ceramic frits, hydrophilic gels, membranes, capillaries, sealed quartz or asbestos fiber, or sealed Pt wire (see Figure 4-1).[62] Improvements in the designs of salt-bridge reference electrodes include incorporation of nanoporous and capillary junctions. These bridge designs help maintain a stable reference potential by minimizing ion exchange and contamination of the electrode fill from the external test environment. Reference electrodes with nanoporous glass frits are commonly used in laboratory work. However, it was shown that the use of glass frits with very fine pore sizes (4-10 nm diameter) can introduce errors in the reference electrode potential due to electrostatic charge screening, particularly in low ionic strength solutions.[64] A later study by Anderson et al.[65] showed that increasing the pore size to 100 nm eliminates the charge screening effect. However, it was found that, even with a 100-nm pore size, the flow rate of reference electrode fill solution through the frit was low enough that diffusion remained the main transport mode through the frit. Therefore, cross-contamination of the fill and external solution could result from the diffusive exchange of ionic and neutral chemical species. It should also be noted that glass frits are incompatible with highly alkaline environments such as Hanford waste.

Polymeric frits made of Teflon and polyethylene generally exhibit low charge screening effects due to the absence of ionic surface groups but have relatively large pore sizes (1 to10 µm) and pore walls that are hydrophobic, which make them electrically resistive.[59] It was shown that these problems could be overcome by using polymeric frits of these materials that had electrically neutral pore sizes of around 10 nm size and functionalizing the pore walls to improve wettability.[66] These frits exhibited very low leak rates of around 0.007 ± 0.003 µL/h.

Porous ceramic frits are commonly used in constricted-flow junctions of reference electrodes. Bosch et al.[67] investigated the porosity of magnesia-stabilized zirconia plugs for use in electrochemical sensors. The plugs were produced by cold isostatic pressing and sintering at various temperatures to achieve different porosities and pore sizes. High porosity and small pores were identified as key factors for optimal plug performance. It was found that the flow rate

[64] M. P. S. Mousavi, S. A. Saba, E. L. Anderson, M. A. Hillmyer, and P. Bühlmann, *Avoiding Errors in Electrochemical Measurements: Effect of Frit Material on the Performance of Reference Electrodes with Porous Frit Junctions*, Anal. Chem., 2016, **88**: 8706–8713.
[65] E.L. Anderson, B.K. Troudt, and P. Bühlmann, *Critical Comparison of Reference Electrodes with Salt Bridges Contained in Nanoporous Glass with 5, 20, 50, and 100 nm Diameter Pores*, Anal. Sci., 2020, **36**: 187–191.
[66] E.L. Anderson, S.A. Saba, D.J. Loomi. P. Bühlmann, and M.A. Hillmyer, *Functionalized Mesoporous Polymers with Enhanced Performance as Reference Electrode Frits*, ACS Appl. Nano Mater. 2018, **1**(1): 139–144.
[67] R. W. Bosch, S. Straetmans, and S. Van Dyck, *Characterizations of porous ceramic plugs for use in electrochemical sensors*, Journal OF Materials Science 2002, **37**: 3973–3979.

of electrolyte through the plugs, ranging from 0.2 to 25 µL/h, was controlled by the pore size. For plugs with similar pore sizes, electrical conductance was higher for the plug with a higher porosity since it offered more electrolytic pathways.

Badr et al.[68] describe the preparation and evaluation of mesoporous glass–ceramic composite frits using low-cost materials like borosilicate and kaolin, sintered at relatively low temperatures (750–850 °C), for use in reference electrode junctions. Reference electrodes based on these composite frits exhibited flow rates as low as 0.002 ± 0.001 µL/h, improved potential stability, and reduced potential drift compared to existing reference electrodes based on glass or polymeric frits.

Suzuki et al.[69] developed a microfabricated liquid-junction Ag/AgCl reference electrode. The structure of the miniature liquid-junction Ag/AgCl reference electrode, shown in Figure 4-6 , included a glass substrate with a 7 µm deep recess where the thin-film Ag/AgCl element was formed. A 4.5 µm thick polyimide layer was used as an intermediate layer to promote adhesion, and a 200 nm thick gold backbone layer was formed on top of the polyimide layer. A 300 nm thick silver pattern was then formed on the gold layer. The Ag/AgCl element was formed by chemically converting approximately 50% of the silver layer, in situ, to AgCl by immersing the chip in a 1.0 M $FeCl_3$ solution. The container for the internal electrolyte solution was formed by anisotropically etching a (100) silicon substrate using an SiO2 mask and a 35 wt% KOH etchant. A rectangular groove for the electrolyte solution and a long narrow groove for a pin-hole liquid junction were etched into the silicon substrate. The glass and silicon substrates were aligned and bonded using a photocurable adhesive. The internal electrolyte solution, saturated with both KCl and AgCl, was introduced into the cavity by immersing the chip in the electrolyte solution and evacuating the chamber. Leakage of the electrolyte solution was also restricted by plugging the pin-hole liquid junction with cellulose acetate The potential of the electrode was tested against a commercially available Ag/AgCl reference electrode in various KCl solutions. The electrode with an unrestricted pin-hole junction exhibited positive potential drift due to KCl effusion. The electrode with a cellulose-acetate-plug junction was insensitive to KCl concentration in the range of 10 mM to 1.0 M, maintaining a stable potential level within ±1 mV for several hours. While such a design may not be suitable for a long-term potential monitoring application, it could be possibly used for a short-term potential measurement, e.g., when co-deployed with tank grab sampling equipment.

In considering the use of improved liquid junction designs and materials, such as those discussed above, for reference electrode in the Hanford tank application, the following are some general concerns: (1) long-term reliability of moving parts in active operation designs such as the intermittently actuated, free-flow junction, (2) compatibility of new polymeric or ceramic junction materials with the highly alkaline, radioactive waste environment, and (3) the possibility of plugging of nano-/meso- porous frit materials with nonconductive solids, leading to high electrode impedance.

[68] H. Ibrahim, A. Badr, and O. A. S. Rafea, *Evaluation of mesoporous borosilicate glass– ceramic composites as frits in reference electrodes*, RSC Adv., 2022, **12**: 28878–28885.
[69] H. Suzuki, T. Hirakawa, S. Sasaki, and I. Karube, *Micromachined liquid-junction Ag/AgCl reference electrode,* Sensors and Actuators B, 1998, **46**: 146–154.

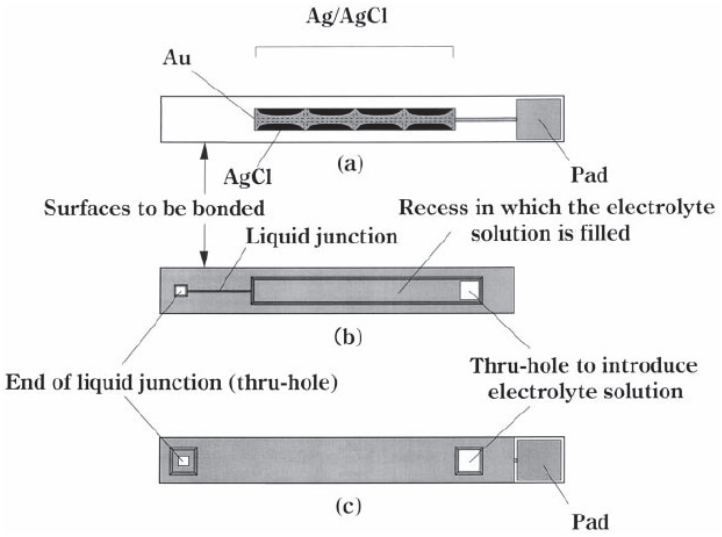

Figure 4-6. Structure of microfabricated liquid-junction Ag/AgCl reference electrode developed by Suzuki et al.[55]

4.3 Ionic Liquid Reference Electrodes

Reference electrodes based on ionic liquids, also known as room temperature molten salts (RTMS), utilize these unique salts as the salt bridge component. Ionic liquids are nonpolar water-immiscible (lipophilic) organic compounds composed of a large organic cation and a smaller inorganic or organic anion and remain in a liquid state at room temperature. Morawska and Wardak[70] list the common types of cations and anions that form ionic liquids. The low melting points of ionic liquids are due to the size discrepancy between the cation and anion, which hinders the formation of a homogeneous crystal structure. Ionic liquids also have large ionic radii and low symmetry, with cation charge distributed over a large space.

An ionic liquid salt bridge maintains electrical neutrality by allowing ions to move between the reference electrode fill and the external solution being measured. Ionic liquids are chemically stable and have low volatility, which enhances the durability and reliability of the reference electrode.

Ionic liquid-based salt bridges avoid several deficiencies of conventional salt bridges, such as the need to replenish the bridge electrolyte and fluctuations of the liquid junction potential due to contamination. Physical robustness of the junction can be increased by incorporating ionic liquids into polymeric support membranes such as plasticized PVC, PMMA, fluoropolymers and silicones (see Troudt[59] for cross-references). Morawska and Wardak[70] discuss the uses of ionic liquids as components of ion-selective membranes, both polymeric ones based on PVC and membranes in carbon paste electrodes. The liquids perform various functions in these

[70] K. Morawska and C. Wardak, *Application of ionic liquids in ion-selective electrodes and reference electrodes: A review*, Chem. Phys. Chem 2024, e202300818.

membranes, including acting as lipophilic ionic additives, ionophores/ion exchangers, plasticizers, transducer media, and matrix components.

The transfer of sample ions into the ionic liquid phase can affect the phase-boundary potential, especially when the concentration of sample ions is high. Research by Kakiuchi et al[71] focused on the phase boundary potential at the interface between ionic liquids and aqueous electrolyte solutions. They studied an RTMS mixture of 1-methyl-3-octylimidazolium salts of bis(trifluoromethylsulfonyl)imide and of bis(pentafluoroethylsulfonyl)imide that are immiscible with water. They found that ionic liquids can transfer, to some extent into the aqueous phase, resulting in an equilibrium distribution across the interface. This transfer does not significantly affect the interfacial phase boundary if other ions present do not transfer substantially into the ionic liquid phase.

Despite their potential benefits, ionic liquid reference electrodes have not seen widespread adoption due to challenges such as the purity of the ionic liquid and the complexity of their implementation.[72]

4.4 Reference Electrodes with Flowless Junction Designs

Reference electrodes with flowless junctions differ from traditional reference electrodes by using a solid-state interface instead of a liquid junction, which makes them more robust and less prone to leakage or contamination. The solid junction is typically made of a hydrophobic polymeric or other solid conductive material, which is in direct contact with the electrolyte solution. Lindner et al.[73] discuss the materials used, which include polyvinyl resin, pressed Al_2O_3-PTFE, urea formaldehyde, poly methyl methacrylate-propylene carbonate, and polyester resin. The solid material is made ionically conductive by doping or dispersing an equitransferent salt such as KCl or lipophilic tetrabutyl ammonium tetrabutyl borate. These junction materials offer improved stability and reproducibility compared to liquid junctions. The solid junction design also makes the electrode more resistant to external pressure.

Diamond et al[74] discussed the performance and properties of an ionically conducting polymeric junction material, Refex™, highlighting its advantages over conventional materials. Refex (RepHex) was made of polyvinyl acetate with a high loading of KCl (1:1 ratio by weight of PVA to KCl) and designed for use in reference electrode junctions. Their studies showed that the Refex junction gave very stable potentials in buffer solutions in the pH 2 to pH 11.9 range, outperforming conventional ceramic frit junctions in terms of leakage rates. Impedance studies revealed that the high KCl loading in Refex results in low electrical resistance and efficient charge transfer, which are essential for stable potentiometric measurements.

---

[71] T. Kakiuchi, N. Tsujioka, S. Kurita, and Y. Iwami, *Phase-boundary potential across the nonpolarized interface between the room-temperature molten salt and water*, Electrochem. Commun., 2003, **5**(2): 159–164.
[72] E. Lindner, M. Guzinski, T. A. Khan, and B.D. Pendley, *Reference electrodes with ionic liquid salt bridge: When will these innovative novel reference electrodes gain broad acceptance?* ACS Sensors, 2019, **4**(3): 549–561.
[73] P. Lingenfelter B. Bartoszewicz, J. Migdalski, T. Sokalski, M. M. Bucko, R. Filipek, and A. Lewenstam, *Reference Electrodes with Polymer-Based Membranes—Comprehensive Performance Characteristics, Membranes*, 2019, **9**, 161; doi:10.3390/membranes9120161.
[74] D. Diamond, E. McEnroe, M. McCarrick, and A. Lewenstam, *Evaluation of a New Solid-State Reference Electrode Junction Material for Ion-Selective Electrodes*, Electroanalysis, (1994), **6**: 962–971.

A recent study[75] by DNV evaluated the long-term performance of a commercially available Refex Ag/AgCl electrode[76] in supernatant waste simulants of Tanks AY-101 and AW-101. This electrode is 4.7-in. long x 0.47-in. diameter and contains a fill of 2.8-M KCl (see photograph in Figure 4-7). The entire electrode barrel is made from the patented ionically conductive Refex polymer. The Refex electrode showed high stability at a potential near its theoretical half-cell potential of -37 mV(SCE) in the AY-101 waste simulant at room temperature, with a minimal positive drift of less than 5 mV over 6 months, compared to a 25 mV drift in a Van London electrode. While the Refex electrode was promising in the AY-101 simulant, it failed by a large decline in potential after 6 weeks in the highly alkaline (5.76 M NaOH) AW-101 simulant. There was no perceptible damage or change in color of the Refex electrode at the end of the 6-month test in AW-101 simulant. Subsequently, the electrode was immersed for 8 weeks in 4-M KCl, but the degradation was found to be irreversible as the electrode remained at a low potential near -175 mV(SCE).[77]

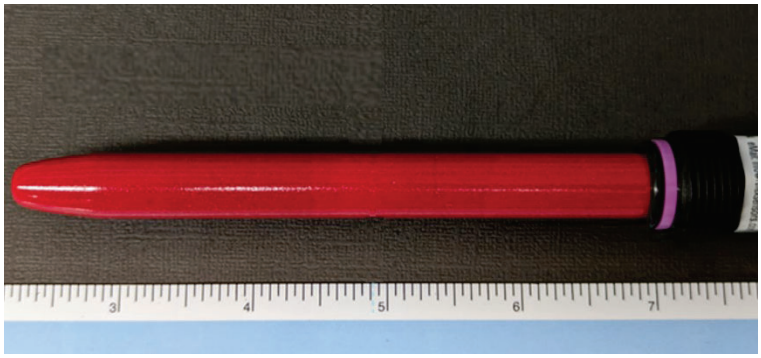

Figure 4-7. Photograph of a commercially available Refex Ag/AgCl reference electrode.

Another commercially available electrode with an ionically conductive polymeric junction that was evaluated at DNV in various waste simulants is the eDaq Electrode. This Ag/AgCl electrode features a cylindrical body, 5.1 in. long x 0.47-in. diameter, made of PEEK and contains a fill of 3.4-M KCl. A proprietary conductive polymer plugs the bottom of the electrode barrel forming a flowless junction. These electrodes failed by exhibiting a large drop in potential after a few weeks of continuous immersion in various waste simulants. Investigation showed that the electrodes failed due to degradation of the conductive polymer junction, which allowed intrusion of the alkaline test solution into the electrode and attack on the Ag/AgCl element.[78]

The main concerns with these flowless junction designs are the chemical and radiological compatibility of the polymeric junction materials with the waste environment and the lifetime limitations due to leaching of the ionic dopant (KCl) from the polymer matrix.

---

[75] S. Chawla, et al., RPP-RPT-64916, Rev. 0, FY2023 Hanford Waste Chemistry and Corrosion Testing Report, Prepared by DNV GL USA, Inc. for Washington River Protection Solutions, LLC, May 2024.
[76] Manufactured by REFEX Sensors Ltd, Part No. S8-5710-120.
[77] S. Chawla, et al., DNV Test Plan & Status Report- 03132024, WRPS FY2024 Hanford Waste Chemistry and Corrosion Testing (10475418), Tank Integrity Expert Panel Corrosion Subgroup Meeting (Virtual), March 13, 2024.
[78] S. Chawla, et al., RPP-RPT-64282, Rev. 0, FY2022 Hanford Waste Chemistry and Corrosion Testing Report, Prepared by DNV GL USA, Inc. for Washington River Protection Solutions, LLC, May 2024.

4.5 Solid-Contact Reference Electrodes

Efforts to address the challenges of traditional reference electrodes have led to the development of solid-state reference electrodes (SSREs) without an internal electrolyte and a liquid-liquid junction. Solid-state reference electrodes aim to eliminate liquid components, using materials like mixed ionic electronic conductors to maintain a stable potential. Collins[79] defines an SSRE as “any material in direct contact with the test solution that maintains a constant or predictable interfacial potential difference despite changing type and concentration of chemical species in the test electrolyte” and discusses practical limits and challenges in developing solid-state reference electrodes.

4.5.1 Electrodes with Solid Fills

Efforts to improve conventional reference electrodes include the use of gel-solidified electrolytes, which offer advantages like pressure resistance and position independence.[58] Other attempts include embedding the Ag/AgCl element in a solidified KCl melt inside a hollow casing with a porous ceramic frit at one end for making ionic contact with the external solution. Vonau et al.[80] described a sintered Ag/AgCl reference element embedded in a solidified melt of KCl, enclosed within a chemical-resistant, porous, ceramic cylinder, and sealed in a chemically resistive casing with a small opening (see Figure 4-8). The porous ceramic layer at the opening forms a junction to modulate ionic communication between the inner electrode and the analyte, limiting KCl dissolution into the analyte. Another design involved a second solid salt mixture added to the lower part of electrode to serve as a bridge electrode. While these designs improve potential stability and extend electrode lifetime compared to a conventional electrode, the use of a porous junction between the interior salt fill and the analyte allows dissolution of the KCl fill over time. In some designs, the electrode body is made of a conductive polymer, eliminating the need for a porous junction.[79,80]

Kwon et al.[81] described a solid-state Ag/AgCl electrode design that was fabricated by layering a silicone rubber film containing KCl on an AgCl surface, followed by a perfluorinated ionomer film, and finally a polyurethane-based membrane containing an H^+-ion-selective ionophore, a lipophilic ionic additive, and a plasticizer. The electrode exhibited little potential variation even with the addition of very high concentrations of various salts and was stable over two years.

Lewenstam[82] discussed two types of polymeric solid contact designs: those employing conducting polymers and those using redox polymers. Conducting polymers such as poly(pyrrole), poly(thiophene), and poly(aniline) are used in solid contacts due to their mixed conductivity and ability to support ion-to-electron coupling. Historical developments in solid contact technology include the use of poly(vinylferrocene) and composites like PMMA with modified graphite, as well as the introduction of carbon nanostructures.

---

[79] S. D. Collins, *Practical limits for solid-state reference electrodes*, Sensors and Actuators B, 1993, **10**: 169–178.
[80] W. Vonau, W. Oelßner, U. Guth, and J. Henze, *An all-solid-state reference electrode*, Sensors and Actuators B, 2010, **144**: 368–373.
[81] N. Kwon, K. Lee, M. Won, and Y. Shim, *An all-solid-state reference electrode based on the layer-by-layer polymer coating*, Analyst, 2007, 1**32**: 906–912.
[82] A. Lewenstam, Handbook of Reference Electrodes, 2013, Eds. G. Inzelt, A. Lewenstam, F. Scholz, Springer Heidelberg, New York, Dordrecht, London, 279–288.

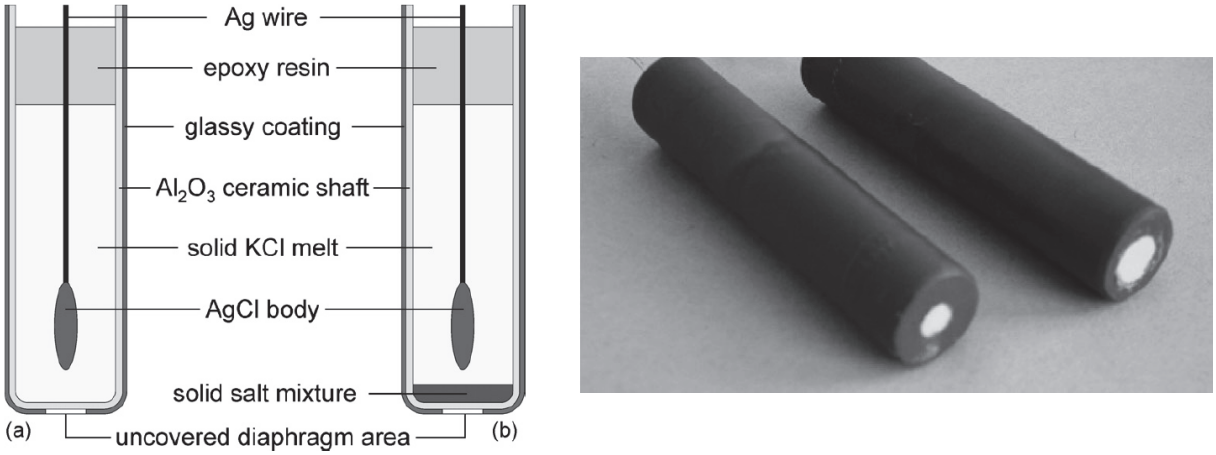

Figure 4-8. Left: Schematics of reference electrodes containing solidified KCl fill. Right: Photographs of electrodes prepared using Design (a). From Vonau et al.[80]

Mousavi et al.[83] developed Ag/AgCl reference electrodes embedded in polyvinyl acetate (PVAc) loaded with KCl, which showed good potential stability across various analytes. However, these electrodes may have poor resistance to chemical and mechanical degradation in corrosive or abrasive environments.

In Patent WO 2018/201200 A1[84], Vepsalainen et al. describe methods for making an SSRE featuring an Ag/AgCl reference element within an electrochemically active composite. The composite includes a polymeric matrix loaded with a solid inorganic chloride salt. The matrix is a cross-linked vinyl polymer made from a copolymer of vinyl acetate and/or vinyl caprolactam and a cross-linking agent chosen from ethylene glycol di(meth)acrylate, poly(ethylene glycol) di(meth)acrylate, and glycerol propoxylate triacrylate.

Nolan et al.[85] developed solid state reference electrodes by dip coating Ag/AgCl wires with a solution of NaCl and polyvinylchloride (PVC) to create an immobilized electrolyte. They then coated the wire with a protective layer of permeable polyurethane or Nafion to prevent NaCl leaching into the analyte. However, these electrodes experienced significant drift due to low electrolyte loading and were not stable enough for many electrochemical applications.

Crisculo et al.[86] evaluated different fabrication strategies for solid-state Ag/AgCl reference electrodes, including membranes made of KCl- (or NaCl/KCl-) doped Agar, Polyvinyl Butyral (PVB), Polyvinyl Chloride (PVC), and Ionic-Liquid-doped PVC, for their stability in varying chloride concentrations and pH levels. The study found that PVC-based reference electrodes exhibited the highest stability with PVB and IL-PVC also showing promising results.

---

[83] Z. Mousavi, K. Granholm, T. Sokalski, and A. Lewenstam, *An analytical quality solid-state composite reference electrode*, Analyst, 2013, **138**: 5216–5220.
[84] International patent WO 2018/201200 A1, Solid state reference electrode, WIPO, 2018.
[85] M. Nolan, S. Tan, and S. Kounaves, *Fabrication and Characterization of a Solid-State Reference Electrode for Electroanalysis of Natural Waters with Ultramicroelectrodes*, Anal. Chem., 1997, **69**(6): 1244-1247.
[86] F. Criscuolo; M. Galfione, S. Carrara; G. De Micheli, *All-solid-state Reference Electrodes for analytical applications*, 2019 IEEE 8th International Workshop on Advances in Sensors and Interfaces, 13-14 June 2019.

As discussed in Section 4.1, the commercially available BORIN electrode, that is currently undergoing testing at DNV and the Hanford 222-S Laboratory, contains a wet-solid fill consisting of gypsum saturated with NaCl. The use of a wet-solid fill reduces the diffusive loss of Cl^- ion from the fill and the diffusive contamination of the fill from extraneous chemical species, which improves the stability and longevity of the electrode.

4.5.2 Miniature Screen-Printed Reference Electrodes

Sophocleous[87] reviewed the significant amount of effort that has gone into the development of solid-state screen-printed microelectrodes, which are alternatives to conventional liquid- or gel-filled reference electrodes for use in potentiometric applications. Screen-printed Ag/AgCl reference electrodes consist of three functional layers: a conductor layer for electron transfer, an ion-to-electron layer (silver/silver chloride), and a KCl layer for controlling chloride ion concentration. Figure 4-9 shows some examples of screen-printed solid-state Ag/AgCl reference electrode configurations developed by various researchers. However, challenges remain in maintaining a stable chloride concentration around the Ag/AgCl element, cross-sensitivity, and lifetime. Researchers are trying to address these through innovative materials and fabrication techniques.

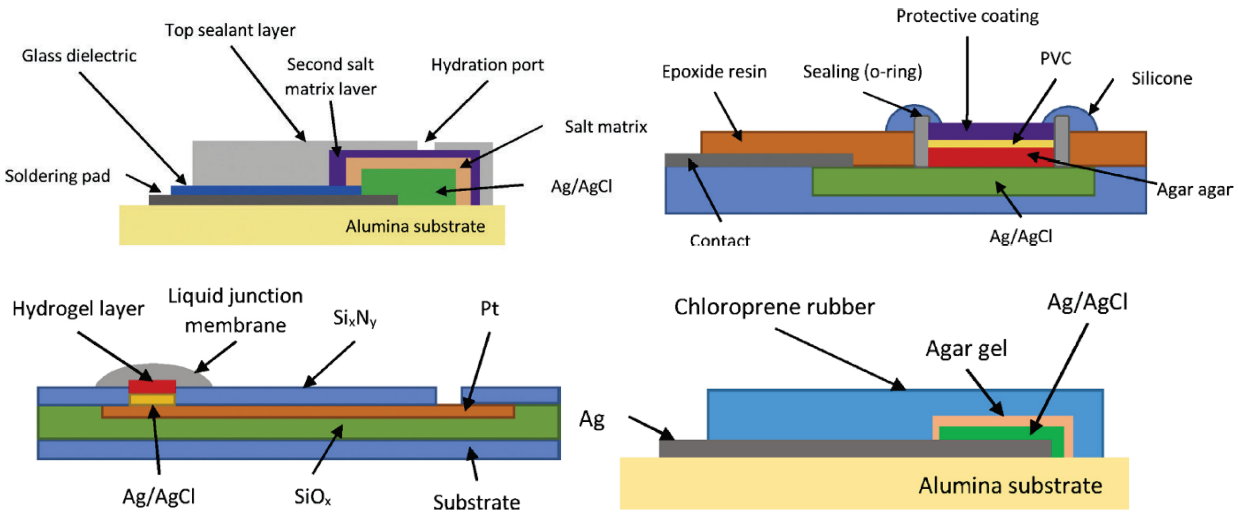

Figure 4-9. Some examples of screen-printed solid-state Ag/AgCl reference electrode configurations developed by various researchers. See Sophocleous[87] for details and cross-references.

The previously reported solid-state reference electrodes generally fail to provide a satisfactory balance of properties, particularly in terms of resistance to chemical and mechanical degradation, rapid conditioning and response, low impedance, and longevity. For long-term service in nuclear waste tanks, radiation stability of the solid contact materials is also

[87] M. Sophocleous and J. K. Atkinson, *A review of screen-printed silver/silver chloride (Ag/AgCl) reference electrodes potentially suitable for environmental potentiometric sensors*, Sensors and Actuators A, 2017, **267**: 106–120.

important.[88] There is an ongoing need to develop solid-state reference electrodes that offer an improved balance of these properties.

4.5.3 Perovskite-Based Electrodes

Gabel et al.[89] developed reference electrodes based on tungsten-substituted alkali molybdenum oxide bronzes that showed promising results for use as solid-state reference electrodes due to their stability and insensitivity to pH, Na^+ concentration, and redox potential changes. The bronzes were synthesized via solid state reaction under inert conditions and had a perovskite-like structure with a composition, $Li_xMo_{0.95}W_{0.05}O_3$, where x = 0.3-0.4. Electrodes were made from polycrystalline samples of the synthesized bronze powders mixed with unsaturated polyester resin, cast into molds, and connected to a copper wire using electrically conductive adhesive, and the entire coated with epoxy for shielding. The electrical resistance of the electrodes fabricated this way was high (about 1–500 MΩ). Cyclic voltammograms for a $Li_xMo_{0.95}W_{0.05}O_3$ electrode in 0.1-M $FeCl_2$ showed no discernable oxidation-reduction peaks in comparison to a Pt electrode (see Figure 4-10). The behavior of the material could not be explained from the theory of cation exchange and intercalation and the exact mechanism of operation was unclear.

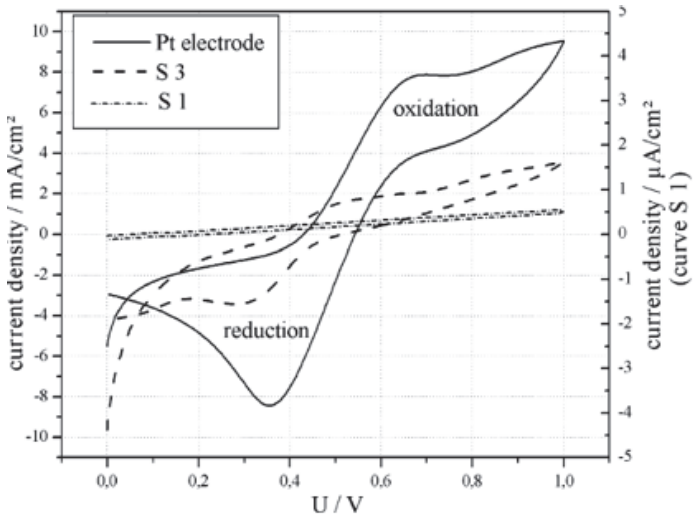

Figure 4-10. Cyclic voltammograms of a $Na_{0.9}Mo_6O_{17}$ (S 3) and $Li_xMo_{0.95}W_{0.05}O_3$ (S 1) in comparison to Pt in 0.1 M $FeCl_2$ (50 mV/s) from Gabel et al.[89]

Lorant, et al.[90] studied an all-solid-state reference electrode using lithium lanthanum titanium oxide (LLTO) perovskite, $Li_{0.3}La_{0.56}TiO_3$, for electrochemical measurements in harsh environments, providing robustness, resistance to high temperatures and pressures, and no

[88] J. Savosina, M. Agafonova-Moroz, M. Khaydukova, A. Legin, V. Babain, P. Tolstoy, and D. Kirsanov, *On the Radiolytic Stability of Potentiometric Sensors with Plasticized Polymeric Membranes*, Chemosensors 2021, **9**: 214.
[89] J. Gabel, W. Vonau, P. Shu, U. Guth, *New reference electrodes based on tungsten-substituted molybdenum bronzes*, Solid State Ionics, 2004, **169**: 75–80.
[90] S. Lorant, C. Bohnke, M. Roffat, and O. Bohnke, *New concept of an all-solid-state reference electrode using a film of lithium lanthanum titanium oxide (LLTO)*, Electrochim. Acta, 2012, **80**: 418–425.

clogging (see Figure 4-11). The LLTO electrodes were manufactured using a dip-coating technique, followed by heat treatments, resulting in thick ceramic films on alumina substrates. The electrodes were tested in various pH buffer solutions, ranging up to pH 10 and demonstrated low impedance and stability over several days, as shown in Figure 4-11.

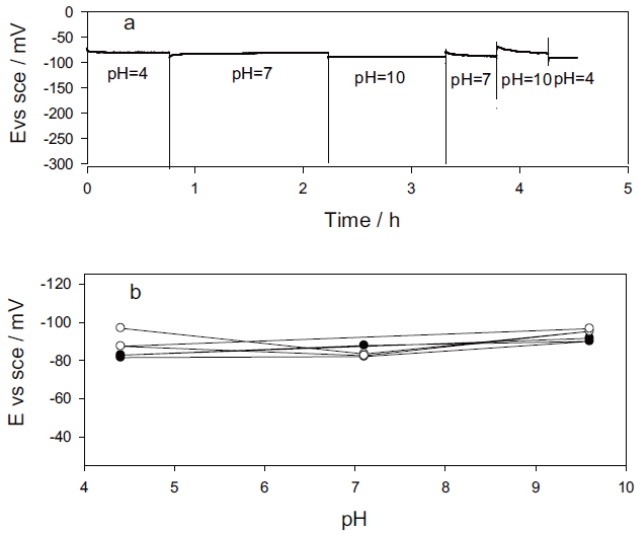

Figure 4-11. Potential of the solid state LLTO reference electrode as a function of time in buffer solutions of different pH at room temperature; and stabilized potentials of two LLTO electrodes as a function of pH from Lorant et al.[90]

Although the mechanism by which perovskite type materials maintain stability of potential in various environments remain unclear, these materials should be explored further to evaluate compatibility, potential stability, interference from common ions and redox-active species, and lifetime in alkaline waste simulants.

4.6 Field Effect Transistor (FET) Based Reference Electrodes

Various approaches to integrate reference systems with Field Effect Transistors (FETs) have been explored. These miniature FET-based reference electrodes, also called REFETs (Reference Field-Effect Transistors), are designed to provide a stable reference potential in potentiometric measurements. They are intended to be integrated with on-chip sensors for various applications such as medical diagnostics, environmental monitoring, and chemical analysis.

The basic architecture of the REFET is the same as a metal-oxide-semiconductor FET (MOSFET). Silicon is commonly used as a substrate for semiconductor devices, particularly in the creation of MOSFETs, which have three terminals: source, drain, and gate. The gate terminal, separated by a dielectric layer, modulates the current flow between the source and drain by applying a bias voltage. Various configurations of FETs exist, including back, top gate, dual gate, and electrolyte-gated FETs. REFETs typically consist of an FET with a reference

electrode material deposited on the gate. This material is chosen to be insensitive to the analyte of interest, ensuring a stable reference potential.

Comte and Janata[91] first described the construction and performance of an integrated on-chip reference REFET used with ion-sensitive FETs (ISFETs) for pH and K^+ measurements. To make a REFET, a small epoxy well was cast and cured around one of the ISFETs on the chip (see Figure 4-12). A buffered gel made of 1% agarose was packed into the well and a glass microcapillary was inserted into the gel to serve as an ionic conduit. The ion-sensitive gate of the second ISFET was used for ionic or pH measurements. The drain current of both transistors was measured with a differential current follower. The reference gate's performance was evaluated based on pH response, temperature, and noise sensitivity, demonstrating good stability and minimal drift.

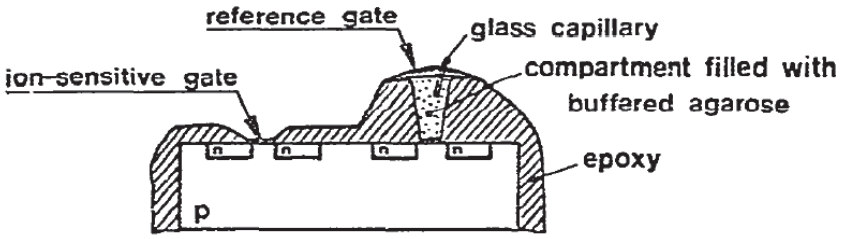

Figure 4-12. Schematic a chip with and ISFET and REFET from Comte and Janata[91].

Chudy et al.[92] applied a membrane containing a highly lipophilic complex, which showed insensitivity to pH changes and various metal cations and chlorides, on the gate oxide surface of an ISFET. The response of this REFET was measured using an ISFET amplifier in a constant drain-current mode. The REFET demonstrated pH insensitivity over a range of pH 2 to 10 and maintained this performance over 100 days of continuous exposure to aqueous electrolyte. The REFET showed no significant response to sodium and potassium ions in specific concentration ranges, although higher concentrations of potassium cations did affect the sensor.

REFETs offer several advantages over traditional liquid-based reference electrodes, including improved stability, reduced size, and compatibility with microfabrication techniques. However, despite their advantages, REFETs face the same challenges as other solid-state reference electrodes such as drift over time, sensitivity to environmental conditions, and concerns about long-term durability.

5.0 Verification Protocols

During the development of the new reference electrodes, it will be critical to assess the performance of the prototypes. Electrochemical techniques have been utilized in the laboratory to assess the condition or performance of an electrode. Two of these methods, half-cell potential verification and electrochemical impedance spectroscopy, will be discussed below.

[91] [91] P.A. Comte and J. Janata, *A Field Effect Transistor as a Solid-State Reference Electrode*, Analytica Chimica Acta, 1978, **101**: 247–252.
[92] M. Chudy, W. Wroblewski, Z. Brzozka, *Towards REFET*, Sensors and Actuators B, 1999, **57**: 47–50.

5.1 Half-cell Potential Verification

Reference electrodes that are commercially procured may come with a certificate of some type but there is no requirement or standardized practice in the industry for verifying the half-cell potential of manufactured reference electrodes. Most manufacturer certificates indicate that the reference electrode was checked versus another "Master" reference electrode (typically saturated calomel electrode) and they report the measured potential versus the expected potential and the acceptance criterion. However, there are typically no details on the manufacturer's certificate to validate or justify the use of the master reference electrode as a trustworthy standard.

5.1.1 Master Reference Electrodes for Verification

It is common practice to check the potential of a reference electrode against an "in-house" master reference electrode before and after using it for laboratory or field measurements. The master reference electrode can be of any half-cell type (e.g., Ag/AgCl, $Cu/CuSO_4$, etc.), but generally speaking, the saturated calomel electrode (SCE) is considered one of the most stable half-cell chemistries that is readily available from most commercial vendors.

In order to maintain its status as master reference electrode, it should be kept and stored properly, and never used in experiments. Master reference electrodes should be replaced or verified every few years if possible.

5.1.2 Quinhydrone Electrode for Verification

Verification of a master reference electrode or any received batch of commercial reference electrodes can be accomplished with the quinhydrone electrode, which is based on the reversible redox system consisting of p-benzoquinone (quinone) and hydroquinone:

$$C_6H_4O_2 + 2H^+ + 2e^- \leftrightarrows C_6H_4(OH)_2 \qquad (22)$$

Under defined conditions, the quinhydrone electrode provides fast response times and highly reproducible potentials to within a few microvolts. Its main drawback is that it is less permanent than traditional glass electrodes such as SCE.

In addition to being highly accurate, the quinhydrone electrode has the advantage of being easily prepared in most laboratory settings. Quinhydrone can be readily procured as a reagent in equal molar ratio (1:1 complex) of hydroquinone and p-benzoquinone. By simply saturating pH 4 buffer solution with this 1:1 reagent and inserting an inert metal electrode, the quinhydrone redox half-cell can be established to serve as a verification potential. Nitrogen sweeping of the buffered solution is also recommended since hydroquinone is a reducing agent that undergoes aerial oxidation. Further details about the quinhydrone electrode and its limitations are thoroughly addressed by Ives and Janz[93].

[93] D.J.G. Ives and G.J. Janz, Reference Electrodes – Theory and Practice, 1961, Academic Press, Inc. (reprinted in 1996 by NACE International, Inc.).

5.2 Electrochemical Impedance Use for Functional Verification

Electrochemical impedance spectroscopy (EIS) is a powerful tool for characterizing electrical properties of materials and their interfaces with electronically conducting electrodes. It normally involves a small sinusoidal voltage excitation to the system at discrete frequencies while the resulting current response is measured. Alternatively, EIS measurements can consist of a sinusoidal current as the stimulus while the voltage response is measured. The frequency range that is typically surveyed in aqueous electrochemical systems is between 100 kHz and 1 mHz.

EIS data are commonly analyzed using an equivalent circuit to represent the physical system, which allows fundamental parameters such as electrolyte resistances, interfacial capacitances, and charge-transfer resistances to be obtained. However, the utility of these circuit models is restricted by the ability of the experimenter to construct an analog that is physically accurate. Despite the challenges of creating suitable circuit models, EIS still finds wide use in many applications where direct current (DC) techniques fall short of providing vital information. For example, EIS has been widely adopted in the evaluation of polymeric coating performance since it can resolve changes in the impedance as an electrolyte penetrates the coating. When EIS is used for ranking polymeric coatings, the low frequency impedance can be used as the primary figure of merit rather than trying to fit the data to an equivalent circuit.

In a similar way, EIS could be used as a diagnostic tool to detect or confirm when a reference electrode is experiencing degradation that compromises its ability to maintain a proper half-cell potential. The low frequency and high frequency impedances could simply be examined for magnitude changes rather than implementing an equivalent circuit approach to analyzing the data.

5.2.1 High Frequency (HF) Impedance Response

Performing impedance measurements on a reference electrode shifts its role to that of the working electrode, which introduces additional high frequency resistances beyond the electrolyte path between measurement electrodes. Namely, the internal fill resistance and junction resistance of the reference electrode become important factors in the high frequency domain. For reference electrodes with a double-junction construction, an additional junction resistance and fill resistance would also contribute to the measured impedances.

The high frequency impedance of a reference electrode is usually dominated by the resistance of its isolation junction(s), which is often a porous frit made of an inert material. This junction separates the reference electrode’s internal filling solution from the test electrolyte. As previously discussed, a variety of junction types are used to construct reference electrodes, including ceramic frits, glass frits, polymeric frits, and asbestos threads. The Van London reference electrodes that are installed inside the Hanford double-shell tanks are of a single-junction construction and contain a polymeric (Kynar™) frit as the isolation junction. A slow flow of the filling solution through this junction is necessary for proper electrode operation. However, this slow flow creates a restricted flow path, which is why the junction often governs the HF impedance response of the reference electrode.

In a DNV study[94] involving the long-term performance of Van London reference electrodes in nonradioactive waste simulants, the high frequency impedance of the electrodes was monitored for approximately 1000 days. Figure 5-1 contains the potentials versus time (lower plot) and the high frequency impedances versus time (upper plot) of the reference electrodes that were exposed to various tank simulants. With the exception of one tank simulant (AW-105), it was found that the reference electrode potentials deviated significantly from the theoretical half-cell potential at some point during the test. Most of the electrodes "failed" by exhibiting a sudden, large drop in potential that that was hundreds of millivolts from the theoretical value. However, in the AY-101 tank simulant, the reference electrode deviation occurred in a more gradual manner in which the potential drifted upward with time.

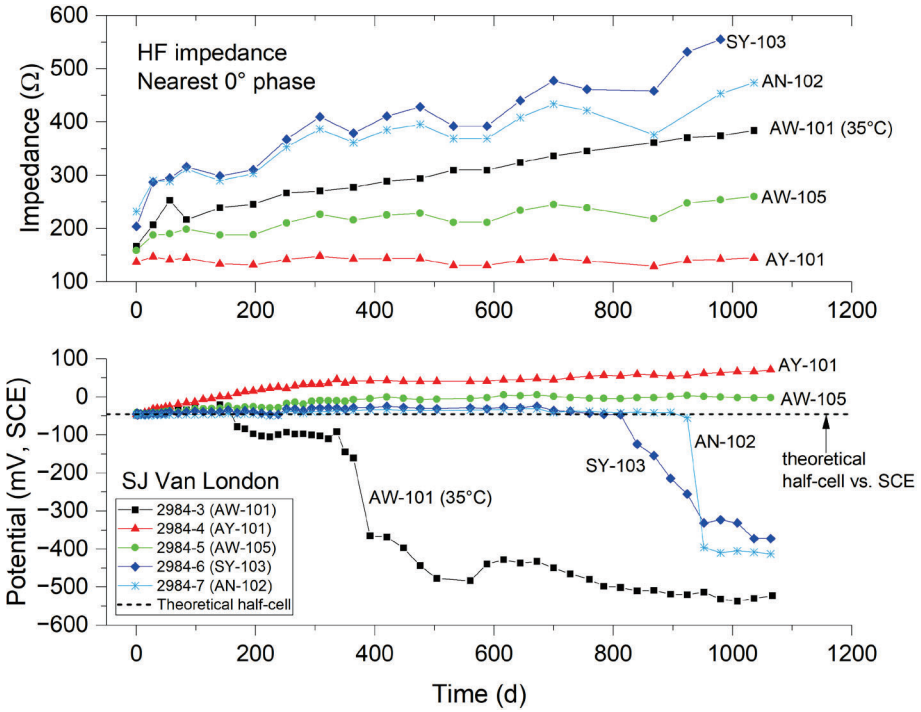

Figure 5-1. Results from 2018 study involving long-term exposure of Van London reference electrodes to various tank waste simulants: potentials vs. time (lower plot) and HF impedance vs. time (upper plot).[94]

As shown in the upper plot of Figure 5-1, the HF impedance of the reference electrodes either remained flat or increased slightly with time. It was presumed that the increases in HF impedance were related to changes in the internal fill resistance, although increases in the frit resistance were not ruled out. Regardless of the exact cause, there were no correlations between HF impedance behavior and the timing of electrode failures. Despite these shortcomings, the HF impedance can still serve as a good diagnostic tool to verify that the reference electrode fill or frit is still functioning properly and providing adequate communication with the Ag/AgCl element.

[94] S. Chawla, et al., RPP-RPT-63781, FY2021 DST Chemistry Testing Report, Prepared by DNV GL USA, Inc. for Washington River Protection Solutions, LLC, May 2022.

5.2.2 Low Frequency (LF) Impedance Response

The low frequency response in most electrochemical systems consists of Faradaic processes, which involve charge-transfer resistances and mass-transfer resistances (Warburg impedances) at a conducting electrode interface. More specifically, for the Van London reference electrodes installed in Hanford double-shell tanks, the charge-transfer and mass-transfer resistances are associated with the Ag/AgCl wire element in contact with the internal fill. Since reference electrodes should ideally behave as non-polarizable electrodes, redox systems with facile kinetics or low charge-transfer resistances are desired. The Ag/AgCl redox system fulfills this characteristic by having low impedances at the low frequency end of the spectrum. Figure 5-2 shows an example of an impedance spectrum for an exemplar Van London electrode placed in 4 M KCl. The low frequency (2 mHz) impedance magnitude is around 2 kΩ, which is considered relatively small compared to the charge-transfer resistances associated with passive electrodes.

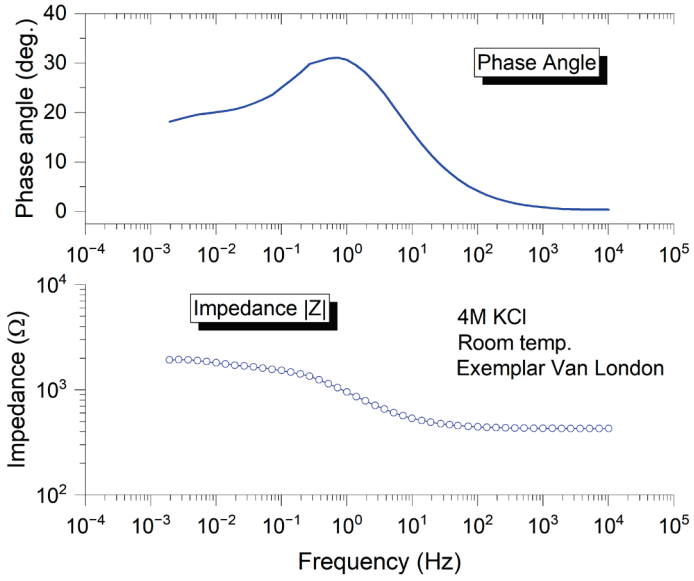

Figure 5-2. Impedance spectrum obtained on exemplar Van London reference electrode in 4 M KCl.

An increase in the impedance in the low frequency region has shown promise as a means of verifying reference electrode failure. This was demonstrated in a separate study[95] involving the long-term exposure of Van London reference electrodes in AW-101 simulant at 35°C. Figure 5-3 *(left plot)* contains the potential versus time data that were collected on a Van London electrode (SJ) immersed in AW-101 simulant for ~1000 days. After about 175 days of exposure, the reference electrode exhibited a large negative shift in potential to near -650 mV (SCE). A full-spectrum EIS scan was collected on the electrode after 529 days, which is also shown in Figure 5-3 *(right plot)*. It is evident that the low frequency impedance was around 3 orders of magnitude higher compared to the exemplar electrode results. The large increase in LF impedance of the exposed reference electrode was attributed to the severe damage that was found on the

[95] S. Chawla, K. Evans, S. Feng, and N. Sridhar, *Long-Term Performance of Reference Electrodes in Alkaline Radioactive Waste Storage Environments*, Corrosion Journal, 2024, **80**(5), 472-488.

Ag/AgCl wire during post-mortem examination. The wire showed major thinning and almost complete loss of the AgCl layer, which was presumed to be due to interaction with the high hydroxide content of the waste simulant (calculated pH of 15.6).

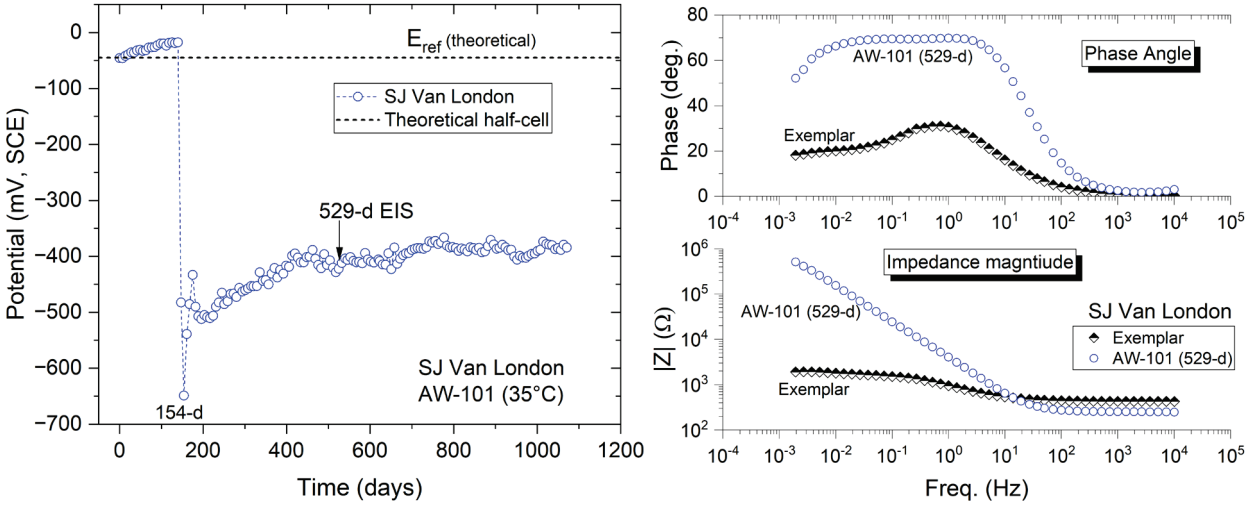

Figure 5-3. Long-term exposure of Van London reference electrode in AW-101 simulant at 35°C: Potential vs. time (left) and impedance spectrum of electrode after 529 days of exposure (right).[95]

6.0 Summary

Tank corrosion and SCC can be monitored by using electrochemical techniques such as measurement of the OCP of the tank. Attempts to measure the OCP in waste tanks have been made at both Hanford and SRS. A reference electrode is typically utilized for these measurements. Failures of the reference electrodes in the chemically and radiolytically harsh environment have occurred after relatively short-term exposures. Therefore, DOE-EM has undertaken a research program to develop reference electrodes that are capable of surviving the waste tank environment for longer periods of time, such that there is increase confidence in the systems performance.

This literature review provides the following key observations about the utilization and testing of reference electrodes:

- Measurement of the OCP provides a fundamental basis for predicting long-term performance of a waste tank. This approach provides a conservative estimate of the likelihood of failure modes such as pitting corrosion and SCC.
- Key characteristics of an effective reference electrode system include: lack of sensitivity to redox species in the waste, lack of sensitivity to pH, non-polarizability, resistance to other chemical species, low impedance, electrolyte communication, chemical and radiation resistance of the electrode body, and mechanical integrity.
- Long-term (~3 years) testing of commercial Ag/AgCl under laboratory conditions show that the degradation/failure modes can be broadly classified into two types: (1) monotonic positive drift from the initial potential, and (2) a sharp drop to negative

potentials after a period of relative stability. The degradation was attributable to diffusive intermixing of the internal fills of the Ag/AgCl reference electrodes with the external simulant solutions over time through the porous frit junctions leading to extensive KCl depletion and contamination of the fills.

- The potential drift trends were correlated to Cl^- activity changes in the fill and the effects of various contaminant species originating from the waste simulants.
- Long-term studies on SJ Ag/AgCl reference electrodes in actual supernatant waste samples drawn from various DSTs also indicated that degradation of electrodes was found to be primarily due to the intrusion of aggressive chemicals causing clogging, physical and chemical degradation of AgCl, and alteration of the internal electrolyte. Radiation had less impact on electrode degradation compared to chemicals, although radiolytic species like H_2O_2 and HNO_3 could possibly have contributed to Ag wire degradation.
- Reference electrodes have been utilized at both Hanford and SRS in the past to make instantaneous measurement and for long term monitoring of the corrosion behavior of tanks. However, reference electrode failures have typically occurred within 2-3 years of installation. Trends in the potential drift that were indicative of failure of an electrode during laboratory tests correlate with those observed in the field.
- Electrochemical noise systems, another electrochemical technique, were also deployed in Hanford waste tanks to monitor for localized corrosion and SCC. Although, the technique had modest success, the utilization of the system was discontinued due to many issues related to interpretation of noise signals and interference from ambient electrical noise. Stainless steel materials for the system were robust, however, they tended to fail at EPDM gaskets. The use of a fiber re-enforced plastic body for the system also suffered significant degradation.

This literature review provides the following recommendations on materials, design and testing of future reference electrodes:

- Alternate materials of construction for the internal fill of the reference electrode include solid state Ag/AgCl CNT thread reference electrode and a solid state reference electrode using carbon nanotubes.
- Alternate materials of construction for the reference electrode frit include ion-conducting composite, porous polymer frits, and Teflon frits.
- Alternate materials of construction for the body of the electrode include polymer composites doped with sizeable amounts of high atomic number (high-Z) materials, epoxy resins, non-oxide and oxide ceramics, and carbides of transition metals.
- Additive manufacturing can use several different materials of interest for the development of the reference electrode such as ceramics, metals, and thermoplastics. It can potentially reduce the cost because it can consolidate multiple parts into one and minimize material usage by building objects up rather than cutting, molding, and combining materials.
- Various type of alternative design concepts for reference electrodes have been discussed in the literature to overcome the limitations of traditional reference electrodes. These can be broadly classified into the following categories: reference electrodes with extended diffusion lengths, reference electrodes with improved liquid junction designs, reference electrodes with flowless junction designs, ionic liquid reference electrodes,

solid-contact reference electrodes, and Field Effect Transistor (FET) based reference electrodes.

- Reference electrode design development should focus on increasing the lifespan of reference electrodes by increasing the diffusion length of the internal and frit sections. Additive manufacturing may allow more flexibility and reproducibility to accomplish this objective.
- Testing protocols for the accuracy and functionality of the reference electrodes were presented. Electrochemical Impedance Spectroscopy (EIS) has been utilized in previous laboratory studies and may provide a baseline for comparison between the commercial electrodes and the newly developed electrodes.

Distribution:

SRNL

connie.herman@srnl.doe.gov

joseph.manna@srnl.doe.gov

morgana.whiteside@srnl.doe.gov

charles.james@srnl.doe.gov

pavan.shukla@srnl.doe.gov

bruce.wiersma@srnl.doe.gov

benjamin.barkai@srnl.doe.gov

kiana.sykes@srnl.doe.gov

junhua.jiang@srnl.doe.gov

monica.phillips@srnl.doe.gov

camden02.chatham@srnl.doe.gov

drew.snelling@srnl.doe.gov

haley.jones@srnl.doe.gov

brandi.clark@srnl.doe.gov

matthew02.williams@srnl.doe.gov

michael.stone@srnl.doe.gov

DNV

Sandeep.Chawla@dnv.com

nsridhar@mcconsult.com

John.Beavers@dnv.com

Kenneth.Evans@dnv.com

Kathleen.Sherer@dnv.com

DOE

em-labcall@em.doe.gov

ming.zhu@em.doe.gov

Kalee.Fenker@em.doe.gov

WRPS

jason_s_page@rl.gov

shawn_t_campbell@rl.gov

jason_r_gunter@rl.gov

kayle_d_boomer@rl.gov

melinda_r_fagundes@rl.gov

Records Administration (EDWS)

Savannah River National Laboratory®

We put science to work.™

Improvements to Waste Tank Reference Electrode Materials and Design

SRNL-MS-2025-00158

K. Sykes, and B. J. Wiersma

Environmental and Legacy Management

4/10/2025

Agenda

- Overview
- Reference Electrode Components
- Van London Reference Electrodes
  - Components
  - Analysis
- H-Cell Testing
- Path Forward

Overview

- Purpose: Improve in-tank reference electrode performance by recommending advanced materials of construction and design features.
- Functional Requirement: Accurate open circuit potential measurements for 10+ years.
  - Reference electrode indicates tank wall passivity in chemically compliant wastes
  - Reference electrode detects localized corrosion on tank wall due to chemically non-compliant wastes.
- Collaboration between SRNL/DNV

Reference Electrode Overview

Reference Electrode Components

- Redox system (half-cell reaction)
- Transducer element, with electrical connection
- Buffered internal electrolyte (fill), with constant activities of redox species
- Junction/bridge/frit for completing circuit to external solution
- Casing/housing

- Nonpolarizable
- High buffering capacity
- Reliable liquid junction
- Robust construction

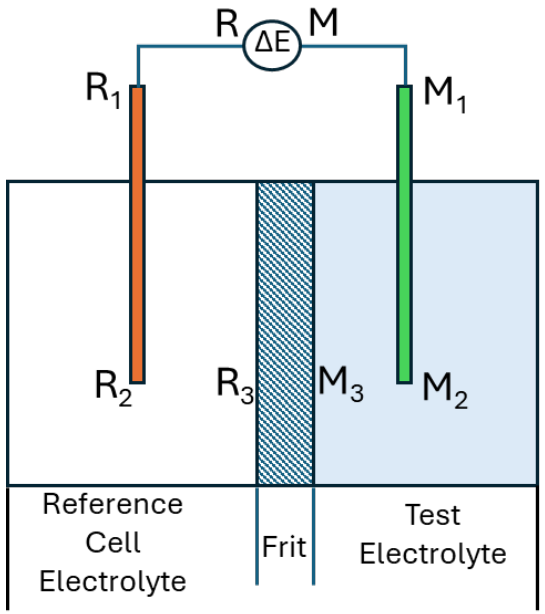

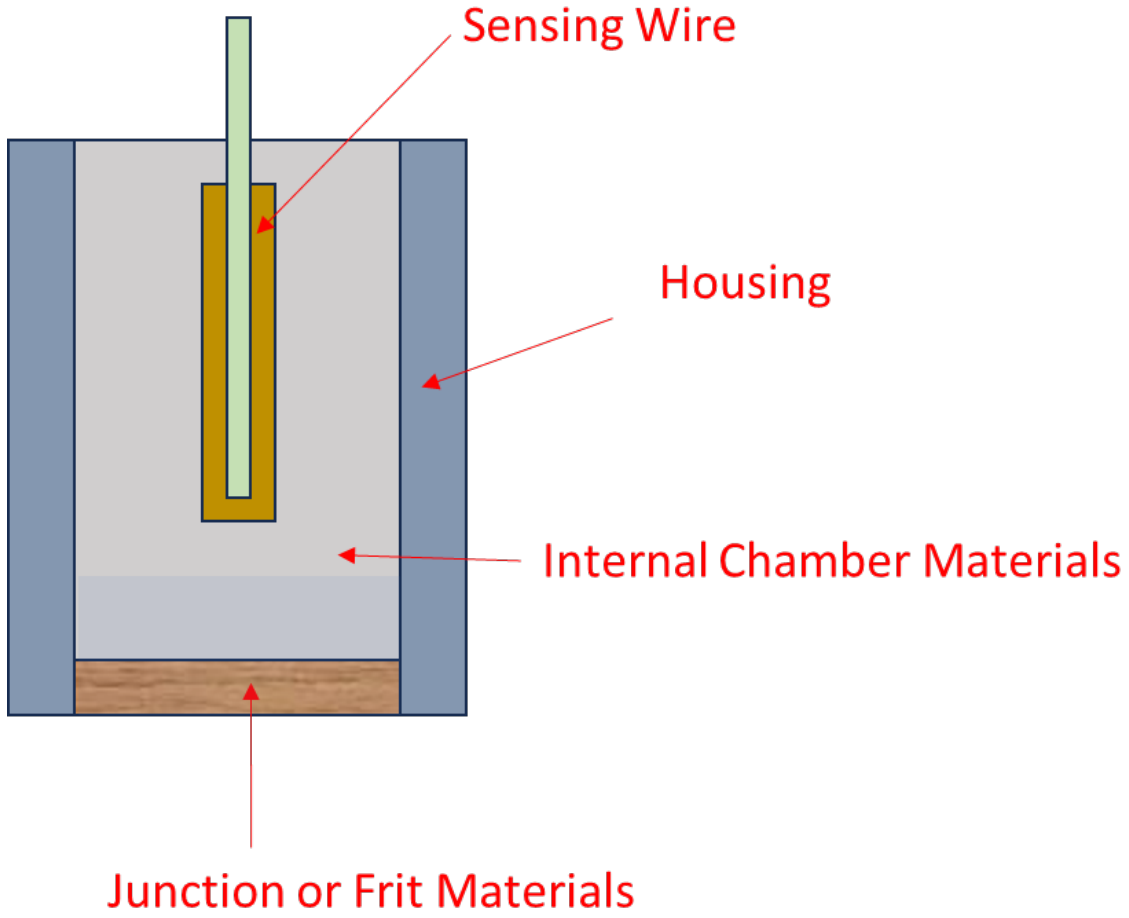

Reference Electrode Open Circuit Potential

- The fundamental basis for predicting long-term performance is the tank E_{corr} (also called Open-circuit Potential, OCP).
- The onset of localized corrosion or SCC occurs when the OCP exceeds the repassivation potential for localized corrosion (E_{rp}) or the critical cracking potential for SCC (CCP), respectively, in the same tank waste.

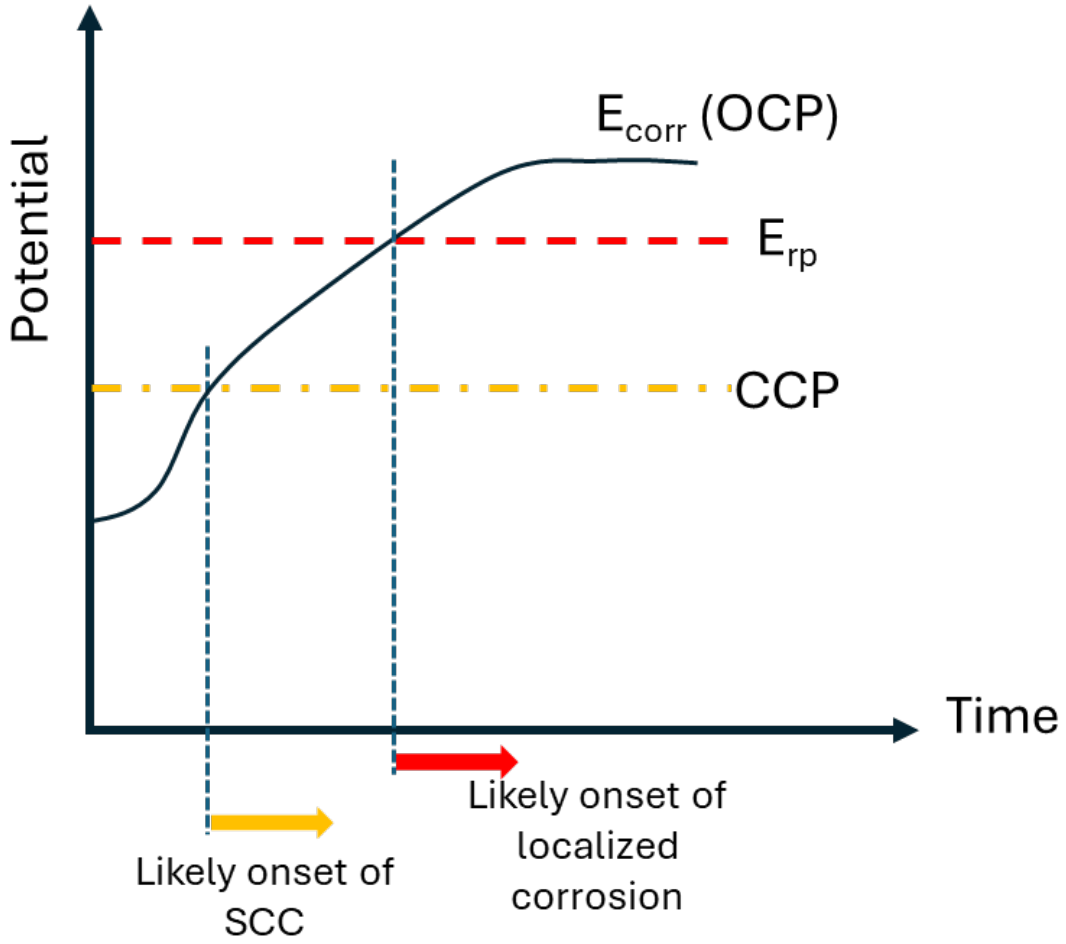

Failure Modes Observed in Long Term Studies

- Degradation was attributed to diffusive intermixing of the internal fills of the Ag/AgCl reference electrode and the external simulant solutions overtime.
- Gradual positive drift (top
  - Decrease in a_{Cl}
  - Modification of Nernstian response by Interferent species: OH^- (main), CO_3^{-2}, SO_4^{-2}, PO_4^{-3}, $C_2O_4^{-2}$, etc
- Sharp drop to negative potentials (bottom)
  - Thinning and loss of AgCl layer in very high pH simulants
  - Accompanied by large increase in polarization resistance

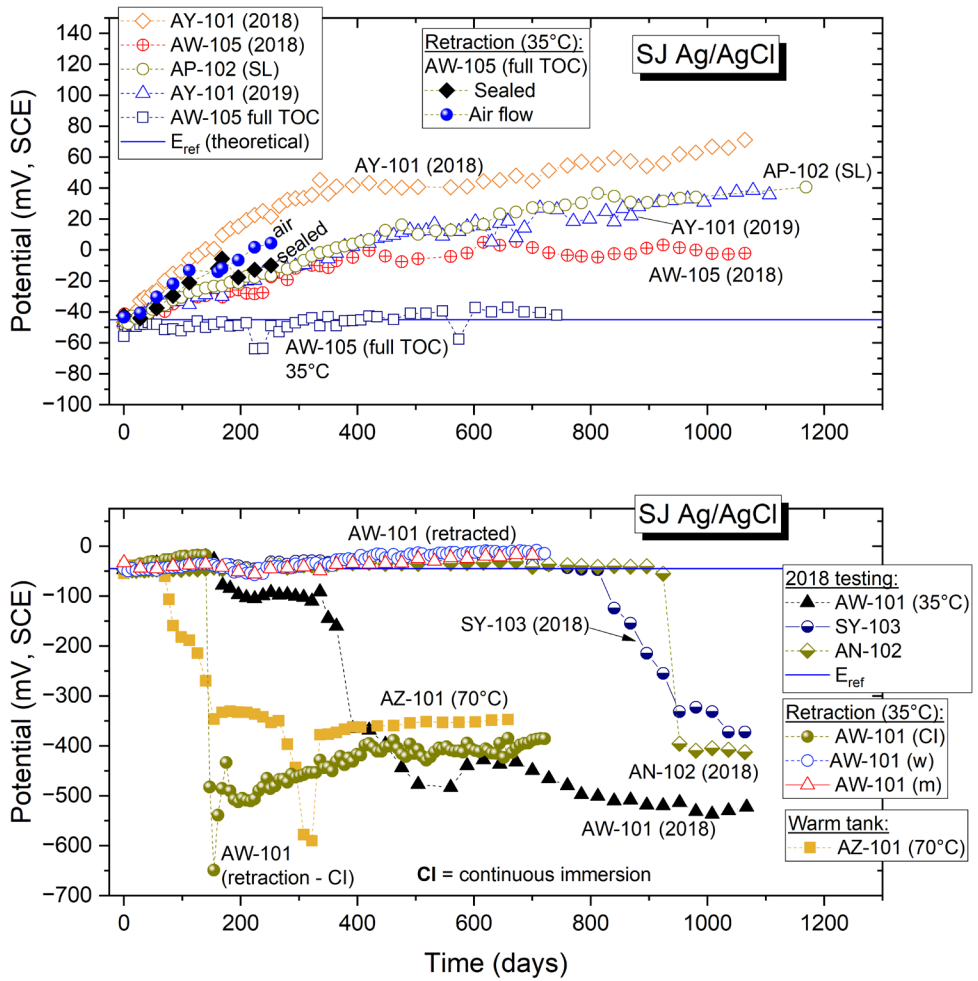

Van London Reference Electrodes

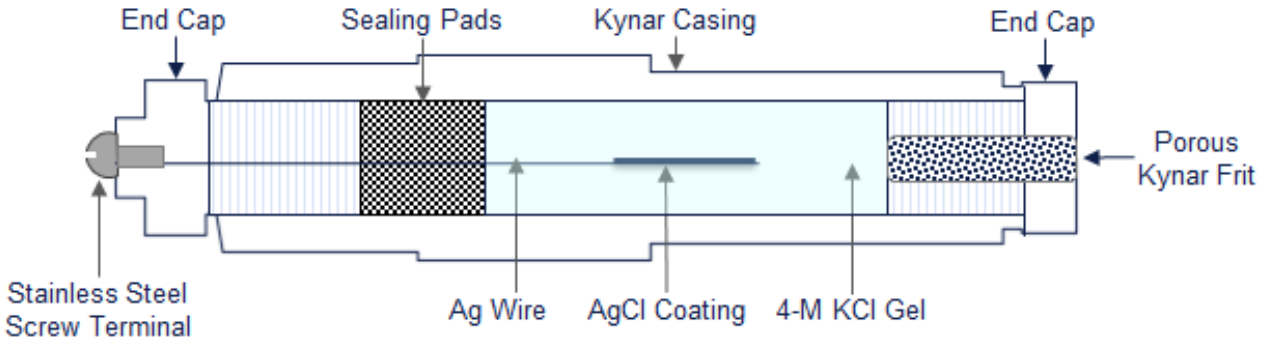

	Tank	Average Lifetime Ag/AgCl (months)
RCMP	AW-105 #1	9
	AW-105 #2	15
	SY-101	66
	AY-101	19
	AP-102	13
	AP-106	NA
	AZ-101	11

Reference Electrode	
Manufacturer/Supplier	Van London Co.
Part No./Model	8604201
Approx. Length x Diameter	4-in. x 0.75-in.
Electrode Type	Sealed Ag/AgCl
Electrode Body Material	Polyvinylidene fluoride (PVDF, Kynar)
Fill Type	4-M KCl (Gel)
Junction	Single*
Junction Type	Porous Frit
Junction Material (Proprietary)	Kynar
Comments	Incumbent electrode in DST RCMPs

Keyence Images Van London Reference Electrode Frit

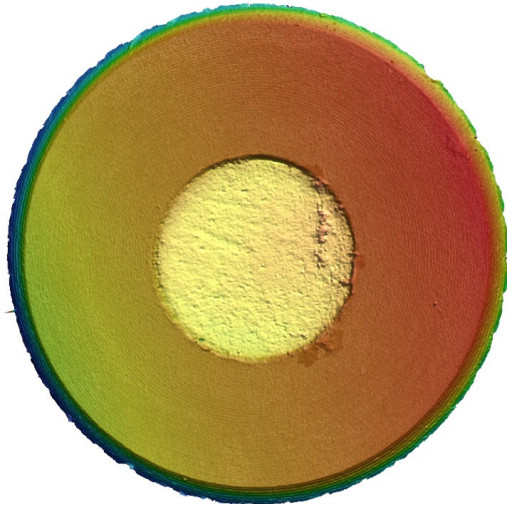

50x
Van London Reference Electrode Frit
520R 8604201

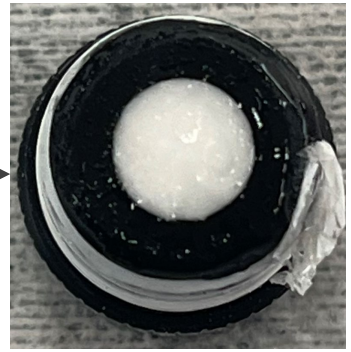

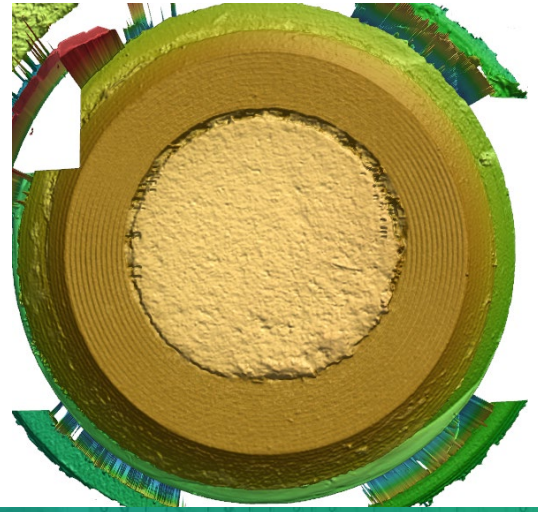

Fourier Transform Infrared Spectroscopy (FTIR)

- Infrared light is pass through or reflected off the sample.
- Different molecules absorb specific frequencies of infrared light.

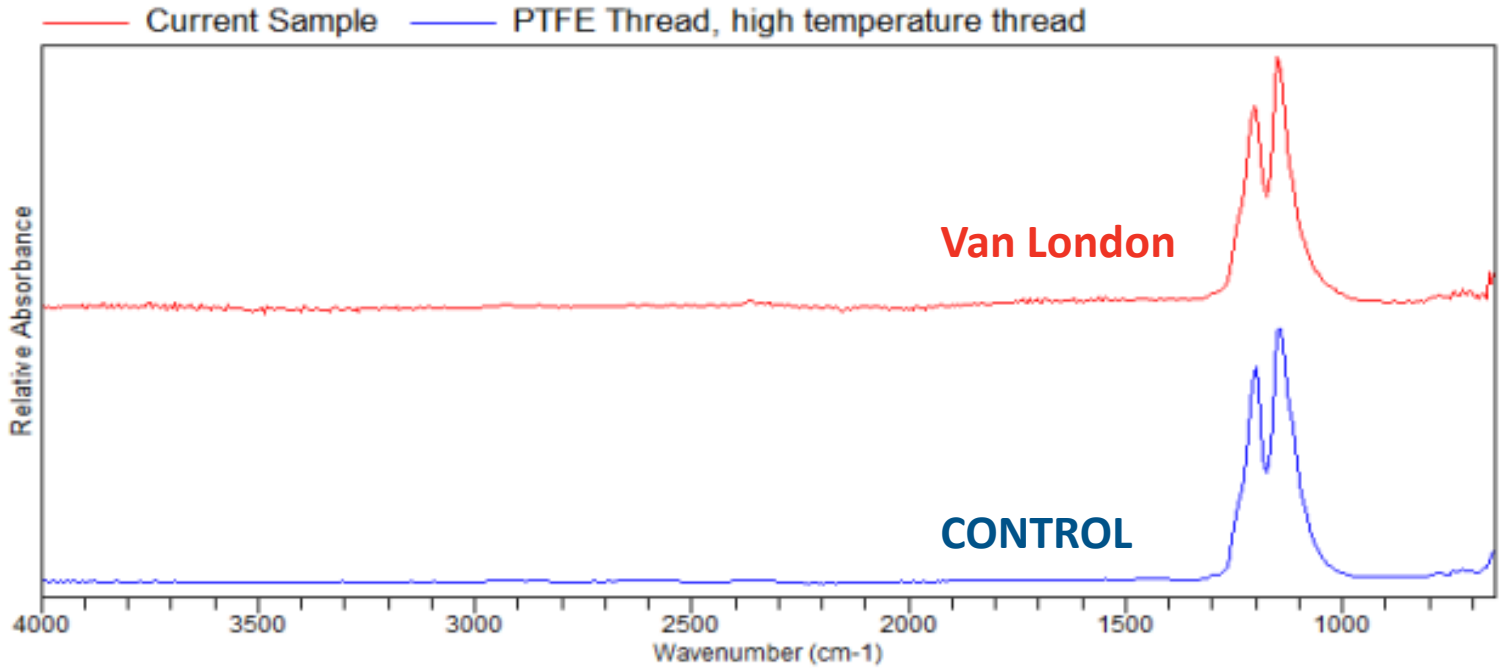

Fourier Transform Infrared Spectroscopy (FTIR)

- Infrared light is pass through or reflected off the sample.
- Different molecules absorb specific frequencies of infrared light.

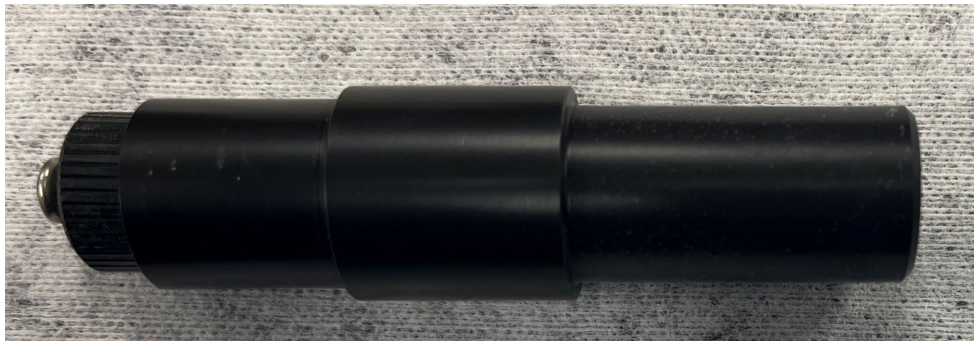

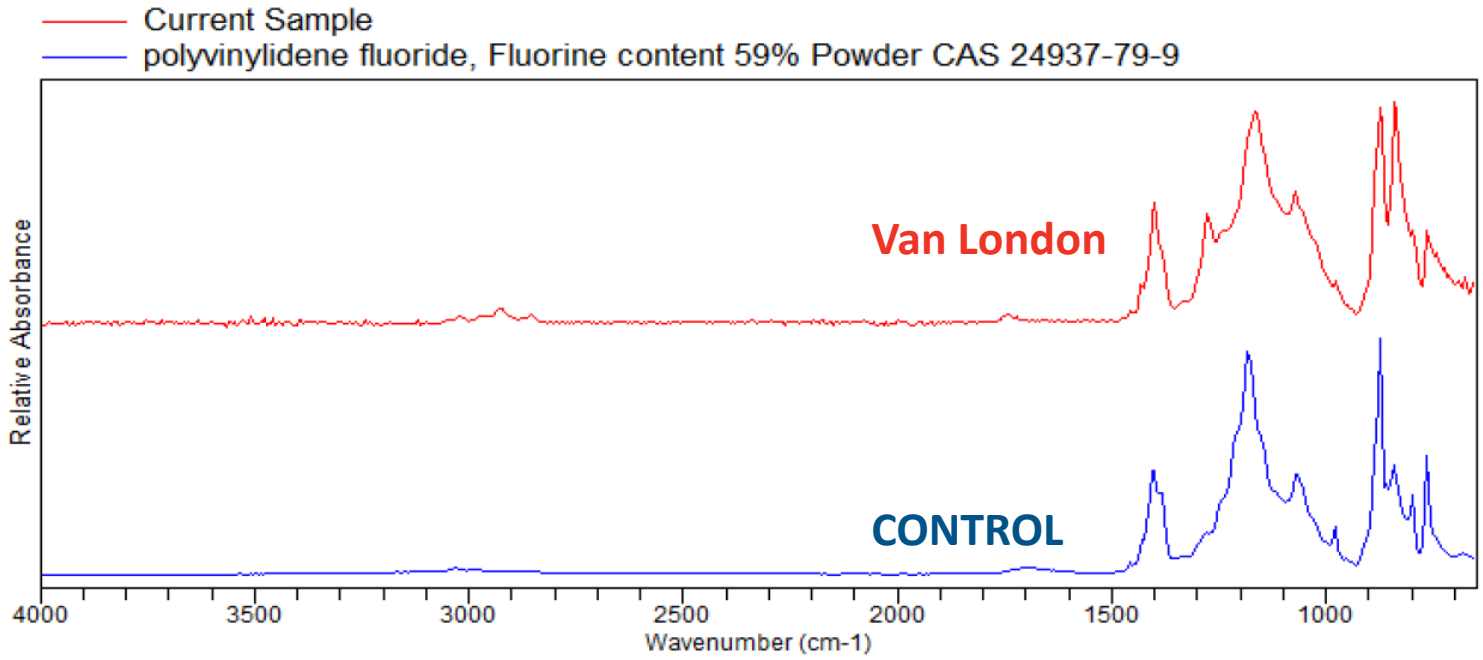

Scanning Electron Microscopy (SEM)

Sample was scraped onto carbon sticky tape on an aluminum stub and carbon coated to reduce charging.

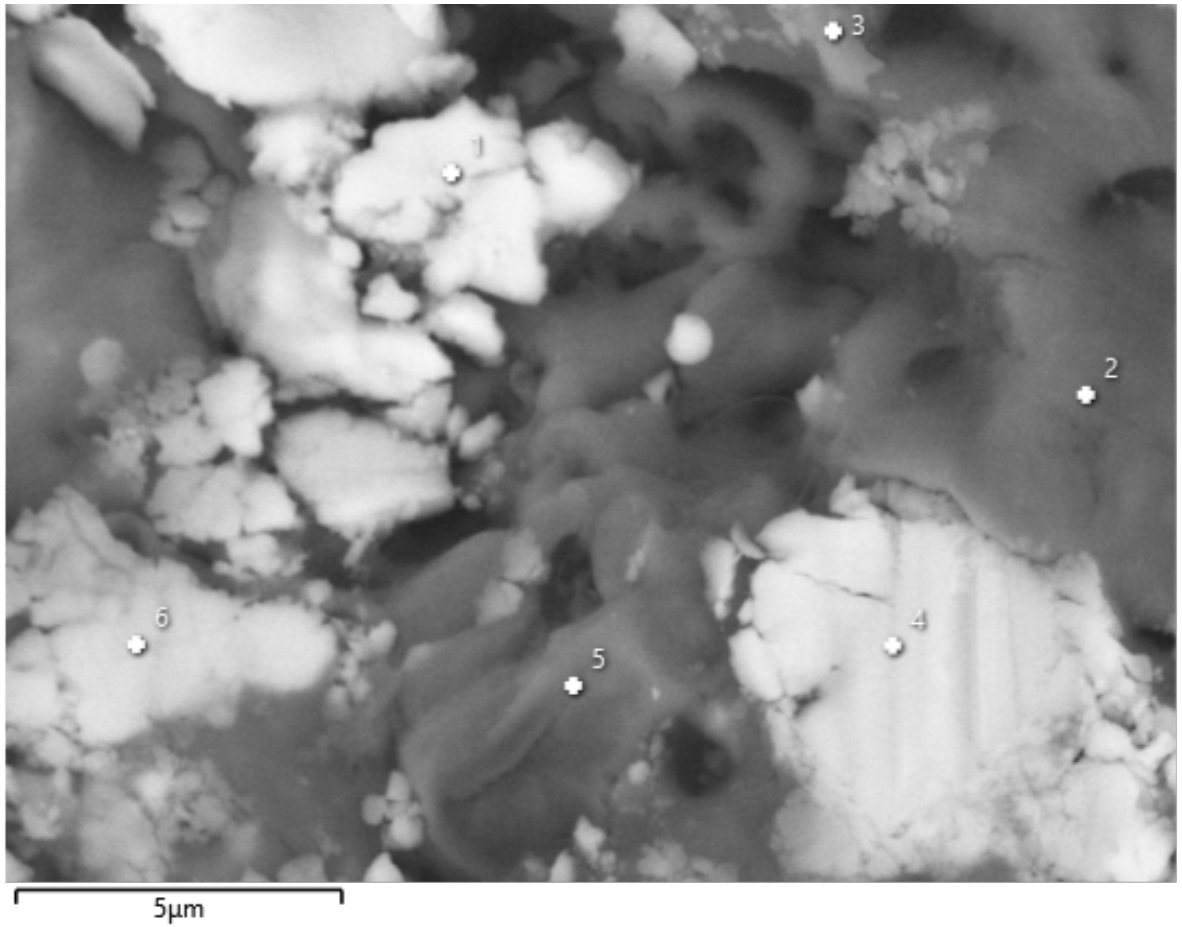

Energy Dispersive X-ray Spectroscopy (EDS)

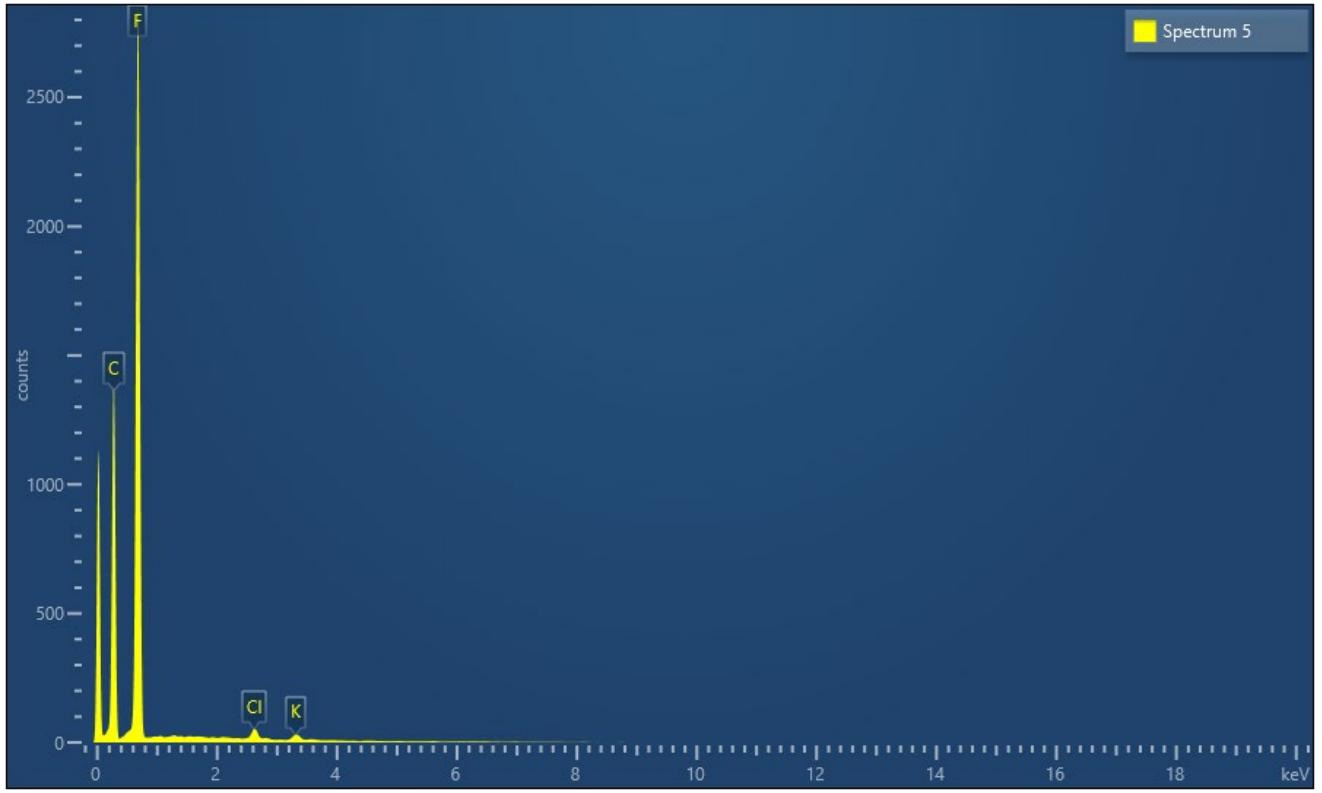

Scanning Electron Microscopy (SEM)

Sample was scraped onto carbon sticky tape on an aluminum stub and gold coated to reduce charging.

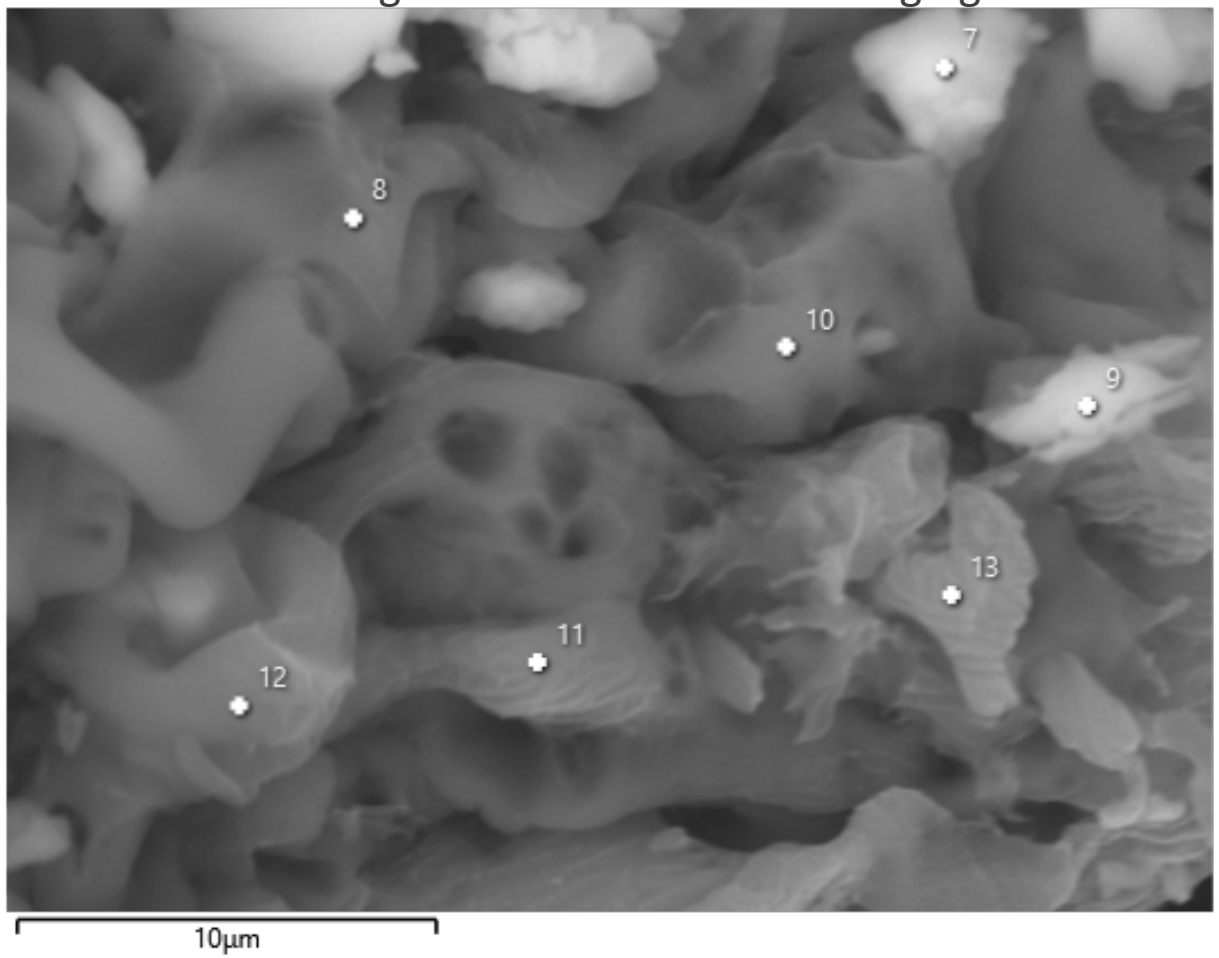

Energy Dispersive X-ray Spectroscopy (EDS)

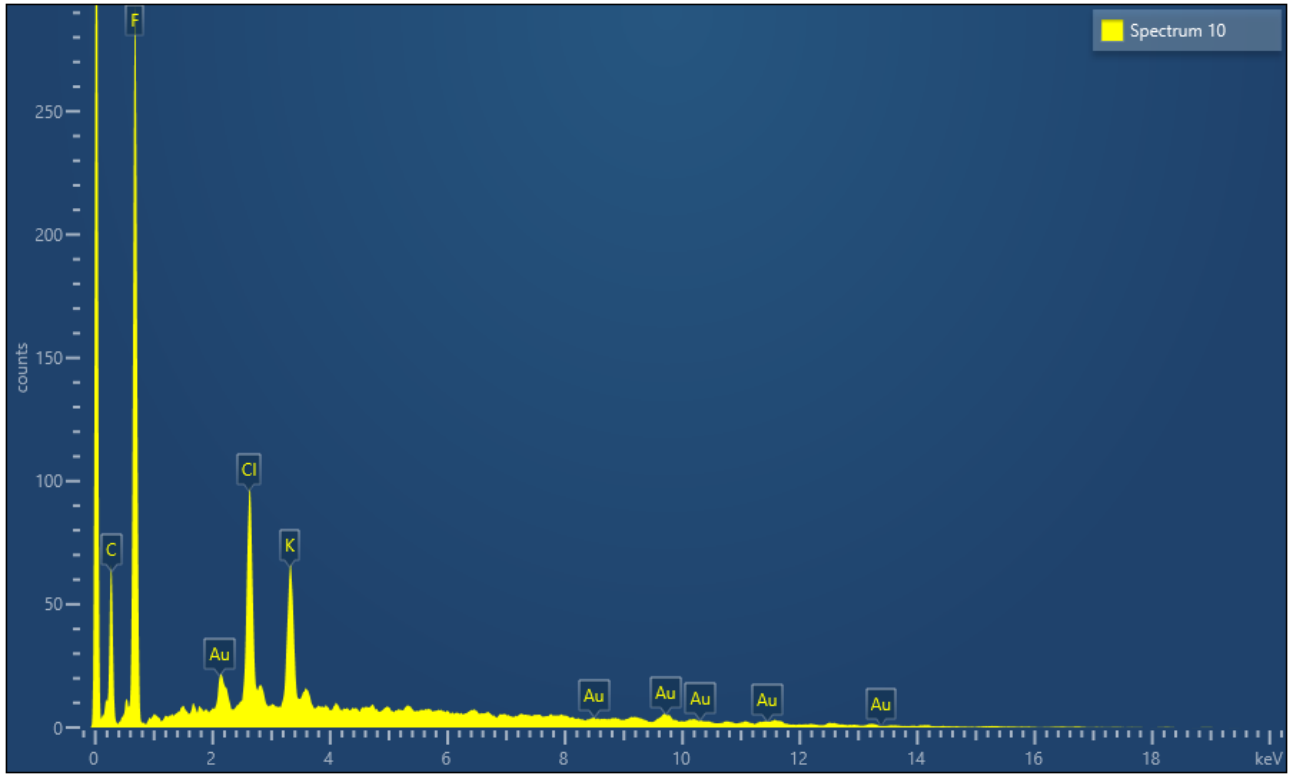

H-Cell Test Matrix

Material Matrix

- Nafion
- NASICON
- High Performance Grout
- Porous Teflon (Van London)
- Porous Kynar
- Borin Frit Materials

Additive Manufacturing Material Matrix

- PEEK
- PEEK Ionomer
- Kynar

Testing at Room Temp and 70°C

- pH
- Conductivity
- Permselectivity

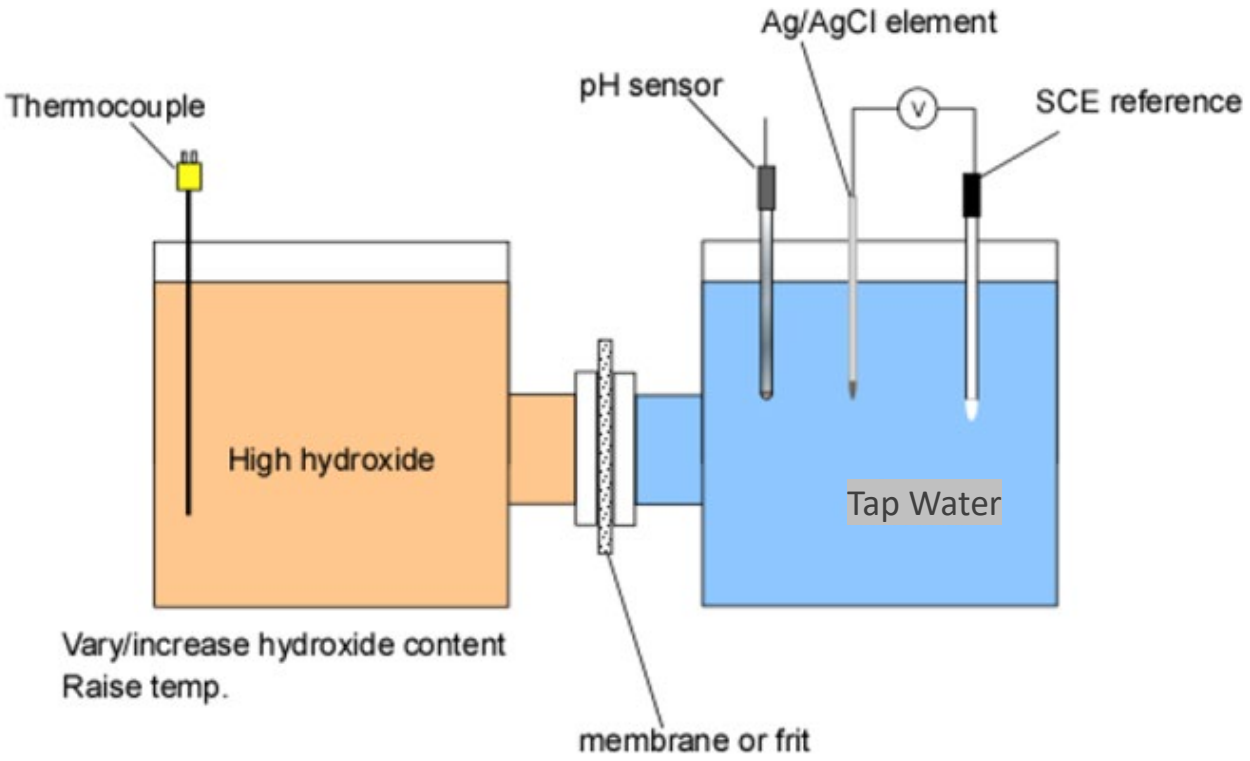

Chemical Exposure Testing

- The waste chemistry envelope for the Hanford Double Shell Tanks was employed to develop waste chemistry limits for pitting corrosion.
- A similar chemistry envelope that was used for for these tests, can be utilized to investigate the behavior of reference electrode materials.
- Objective: Define a set of materials that are robust over the entire DST chemistry envelope.
- A combination of a statistical design of experiments, along with the experience fro long-term testing in waste simulants (DNV) and actual waste (HLMI), will be utilized to define the test matrix for the chemistries.

Entity	Minimum	Maximum
Hydroxide (M)	0.0001	6.0
Nitrate (M)	0.0	5.5
Nitrite (M)	0.0	3.0
Chloride (M)	0.0	0.4
Fluoride (M)	0.0	0.3
Sulfate (M)	0.0	0.2
TIC (M)	0.0	1.0
Temperature (°C)	25	75

Note: Red indicates change from the Pitting Factor Statistical Matrix

Materials Paired with Design Changes

Implementation of a tortuous path

- To increase the distance between containments and the Ag/AgCl wire.
- Gypsum has shown promising results in increasing the longevity of the reference electrode. (Borin reference electrodes)

Additive Manufacturing

- ability to manufacture the body with the torturous path in 1 piece.

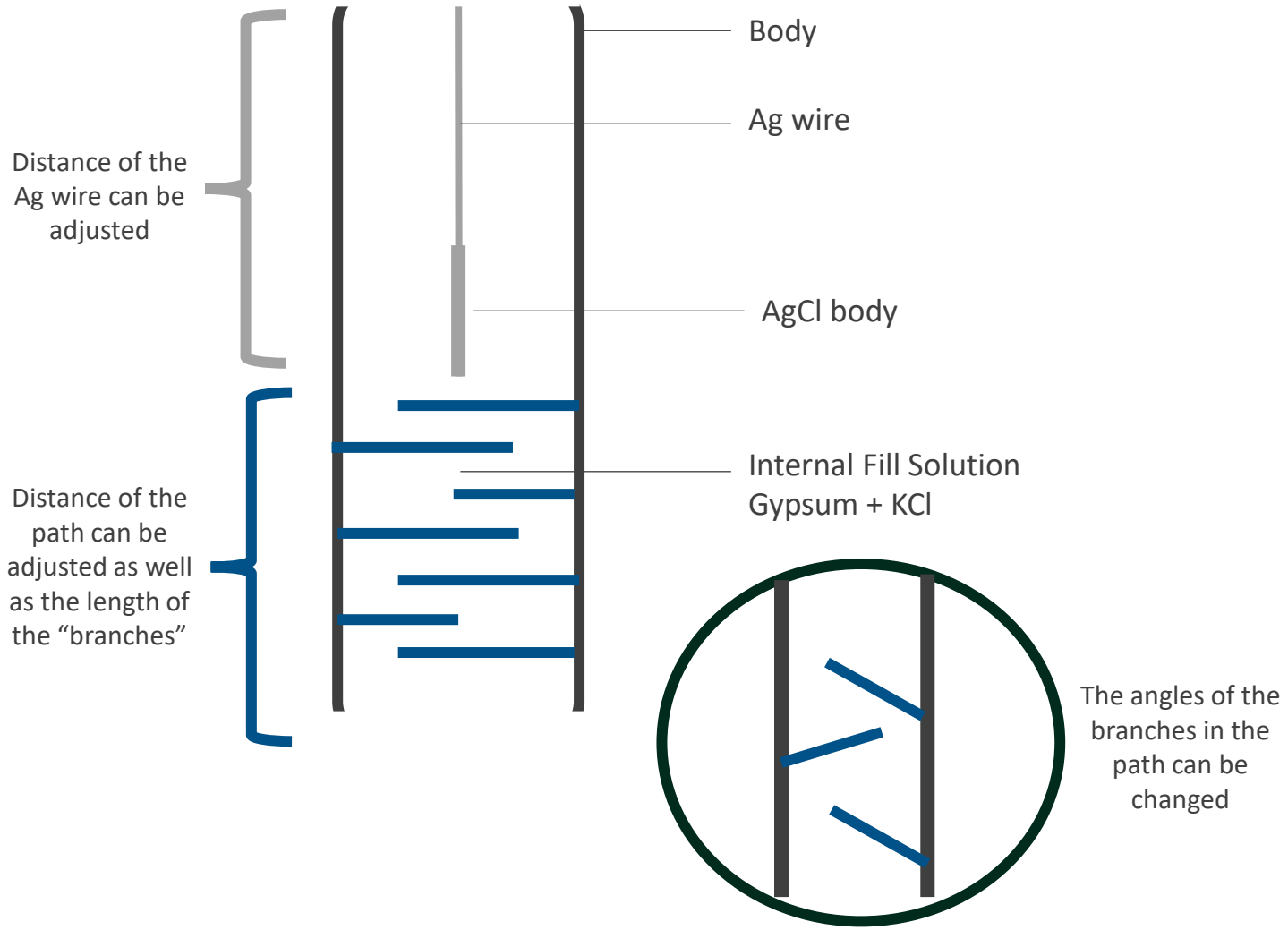

Path Forward

- Start the preparation of the porous Kynar.
- Begin the H cell testing.
- Determine which materials are feasible to move forward with further testing.
- Materials stability test

- Back-up Slides

Reference Electrode Usage and Performance

- Double Shell Tanks (DSTs) representative of different waste types were selected OCP monitoring.
- On average the reference electrodes fail within 3 years after installation.
- A closer look at an individual tank indicates that there is significant variability in the failure times for the reference electrodes.
  - Due to reference electrode fabrication consistency.
  - Due to waste type

Waste type	Tank(s)
High nitrate	AN-102, AN-107
High carbonate	AY-102
Retrieved SST sludge	AY-101
Retrieved SST supernatant	SY-101
High fluoride	AW-105
High hydroxide	AW-104
Higher temperature	AZ-101

SST = single-shell tank.

Tank AY-101

Electrode	Status	Failure Date	Lifetime (months)
SP-AGCL	Failed	Oct-22	37
SP-AGCL	Operational	NA	54+
SP-AGCL	Operational	NA	54+
SP-AGCL	Failed	Sep-19	0

Tank AW-104

Electrode	Status	Failure Date	Lifetime (months)
SP-AGCL	Failed	Jan-11	6
SP-AGCL	Failed	Jan-11	6

A U.S. DEPARTMENT OF ENERGY NATIONAL LAB • SAVANNAH RIVER SITE • AIKEN, SC • USA

Hanford Tank Waste R&D Year 1 Report

Portion of Award #277993 "Improvements to Waste Tank Reference Electrode Materials and Design"

Kiana Sykes

Bruce Wiersma

April 2025

SRNL-RP-2025-00647, Revision # 0

DISCLAIMER

Printed in the United States of America

Prepared for
U.S. Department of Energy

SRNL-RP-2025-00647
Revision 0

Keywords: Corrosion, Waste Tank Integrity, Corrosion Monitoring

Retention: Permanent

Hanford Tank Waste R&D Year 1 Report

Portion of Award #277993: "Improvements to Waste Tank Reference Electrode Materials and Design"

Kiana Sykes

Bruce Wiersma

April, 2025

Savannah River National Laboratory is operated by Battelle Savannah River Alliance for the U.S. Department of Energy under Contract No. 89303321CEM000080

Reviews and Approvals

AUTHORS:

KIANA SYKES (Affiliate) Digitally signed by KIANA SYKES (Affiliate)
Date: 2025.04.30 12:50:13 -04'00'

K. S. Sykes, SRNL/Research Scientist Date

BRUCE WIERSMA (Affiliate) Digitally signed by BRUCE WIERSMA (Affiliate)
Date: 2025.05.05 20:03:17 -04'00'

B.J. Wiersma, SRNL/Advisor Engineer Date

TECHNICAL REVIEWER:

RODERICK FUENTES (Affiliate) Digitally signed by RODERICK FUENTES (Affiliate)
Date: 2025.04.30 13:14:52 -04'00'

R. Fuentes, SRNL/Principal Engineer Date

APPROVAL:

PAVAN SHUKLA (Affiliate) Digitally signed by PAVAN SHUKLA (Affiliate)
Date: 2025.05.01 13:50:33 -04'00'

P. K. Shukla, SRNL/Advisor Engineer, Lead Principal Investigator Date

MORGANA WHITESIDE (Affiliate) Digitally signed by MORGANA WHITESIDE (Affiliate)
Date: 2025.04.30 07:58:26 -04'00'

M. Whiteside, SRNL/Manager, Materials Science and Disposition Date

JOSEPH MANNA (Affiliate) Digitally signed by JOSEPH MANNA (Affiliate)
Date: 2025.05.03 22:20:38 -04'00'

J. Manna, SRNL/Director, Materials Technology and Energy Sciences Date

MICHAEL STONE (Affiliate) Digitally signed by MICHAEL STONE (Affiliate)
Date: 2025.05.05 15:13:46 -04'00'

M. Stone, SRNL/DOE-EM Program Manager Date

Table of Contents

List of Tables

List of Figures

List of Abbreviations

OCP	Open Circuit Potential
AM	Advanced Manufacturing
DST	Double Shell Tank
NDA	Non-Disclosure Agreement
H2C	Hanford Tank Waste Operations and Closure
M	Molar
SRNL	Savannah River National Laboratory
WM2025	Waste Management 2025 Conference
NaOH	Sodium Hydroxide
FFF	Fused Filament Fabrication

1.0 Introduction

Reference electrodes are utilized to measure the open circuit potential (OCP) of a metal immersed in an electrolyte solution. The OCP provides a metric for assessment of the corrosion behavior (e.g., passivity, localized attack, etc.) of the material in each environment. Since 2008, the Hanford tank farm facility has utilized reference electrodes to monitor the tank material OCP [1]. Tank potential monitoring is an integral part of the Hanford tank farm facility structural integrity program [2]. One of the underlying challenges with reference electrodes in the waste chemistry environment is long term stability. Failures have been noted within 2-3 years of service due to ingress of contaminants from the tank waste into the internal components of the reference electrode via the junction material, thus, altering the potential readings. These failures limit the effectiveness of the reference electrode approach. The objective of this Year End Report is to highlight the delivery of milestones and technical achievements for the Hanford Tank Waste R&D Year 1 portion of award #277993 "Improvements to Waste Tank Reference Electrode Materials and Design." Within this report the year 1 milestones are discussed in detail along with technical details on the materials to be tested, and the design of the development of a prototype reference electrode. The following are the year 1 milestones.

1) Complete literature review to identify weaknesses in reference electrode materials.
2) Complete identification of candidate materials, and test protocols.
3) Start the development of a prototype reference electrode.

2.0 Delivery of Year 1 Milestones

The first activity in this program was to perform a comprehensive literature review to identify weaknesses in the reference electrode materials and designs that lead to these premature failures [3]. SRNL collaborated with its industry partner DNV, USA to examine the performance of the current reference electrode utilized at Hanford and based on these observations provide recommendations for alternate materials and designs. The literature review provided the following: 1) Defined the ideal performance of a reference electrode, 2) Evaluated the performance of previous reference electrodes installed in waste tanks at Hanford and SRS to determine average and range of service life, 3) Assessed laboratory testing of reference electrodes in simulated wastes and in actual wastes to investigate failure modes for the reference electrodes, 4) Reviewed the literature for alternate materials of construction for key components of the reference electrode (e.g., junction materials), 5) Examined alternate designs for reference electrode components that will enhance service lifetime, and 6) Recommended verification tests that will demonstrate that the new materials and design are superior to the current reference electrodes.

After the completion of the literature review, a workshop was conducted at DNV headquarters in Columbus, OH to review the literature review and discuss the next steps in the reference electrode development. Attachment 1 in the Appendix shows the agenda for the workshop. The major outcomes from the workshop were to define the primary failure modes, the candidate materials and designs for the reference electrode, and the test protocols for functional verification. The key component that resulted in failure was identified to be the junction material that is at the interface between the waste and the inner chamber of the reference electrode (see Figure 1). The reference electrode junction allows ionic transport between the internal and external solutions to allow for the potential measurements. Therefore, finding a material that can allow the ionic transport, but also prevent intrusion of contaminants from the waste, such as hydroxide ions, will increase the longevity of the reference electrodes.

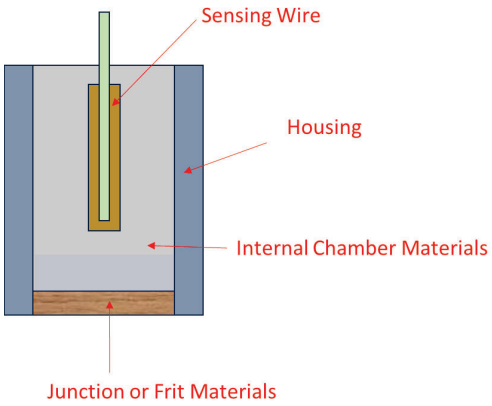

Figure 1. Reference electrode schematic showing various components, including the junction.

The following materials have been selected to undergo testing for the junction material of the new reference electrode.

Nafion

Nafion is a perfluoro sulfonic acid polymer and is a known proton exchange membrane. Nafion was selected as a proof of concept for using ion exchange membranes as a reference electrode junction. Nafion is one of the most used ion exchange membranes and properties are well known. It exhibits excellent resistance to chemicals in a caustic environment [4].

NASICON

NASICON, sodium super ionic conductor, membranes are a ceramic material that allows exchange of sodium ions. NASICON has been shown to have excellent resistance to chemicals. NASICON has been known to have ion conductivity and high interfacial resistance [5].

Porous Kynar

Kynar is fluoropolymer called polyvinylidene fluoride, it has been shown to be stable in a wide range of pHs, temperatures and chemicals [6].

Porous Teflon

The Van London reference electrode utilizes porous Teflon junctions, which will serve as a baseline comparison for new materials. The Van London reference electrodes are what is currently being utilized in the tanks. Teflon has good chemical compatibility but is known to have poor radiation resistance [7].

Borin Reference Electrode Frit (proprietary)

Borin is a supplier of a reference electrode that is being tested as a potential replacement for the Van London. DNV has conducted several tests with Borin reference electrodes, and they show promising results in terms of stability when compared to the Van London reference electrodes [8].

High Performance Grout

High performance grout, which has restricted porosity, will also be tested as a possibility for the junction material [9].

The workshop also identified reference electrode design as a significant means for reference electrode improvement. SRNL is exploring utilization of Advanced Manufacturing (AM) or 3D printing, specifically, using fused filament fabrication (FFF). FFF is commonly used in 3D printing for the fabrication of polymer-based materials, such as Kynar [3]. Advanced manufacturing is advantageous in that it will allow the fabrication process of the reference electrode casing and baffles to be formed with one piece instead of welding multiple pieces together. Additionally, AM will be used to increase the distance between the junction materials and the sensing wire. Placing overlapping baffles such as those shown in Figure 2, is a potential alternative. Advanced manufacturing will also be employed to allow for consistent fabrication of the reference electrode.

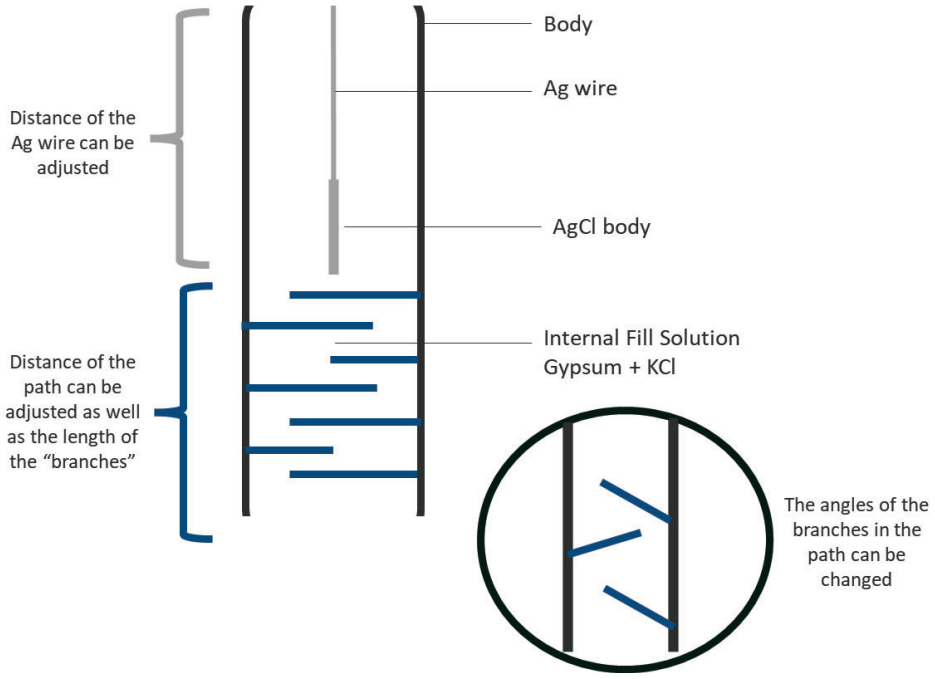

Figure 2. Baffle design for interior chamber of reference electrode

3.0 Laboratory Testing of Materials

The first set of laboratory tests are being performed to assess the performance of the junction materials. An H-cell set up will be employed to evaluate conductivity, permselectivity, and pH changes across these candidate materials. Some key considerations that determine a good junction material include the minimization of the junction potential, a steady flow rate, and chemical inertness. The liquid junction potential occurs when different ions with varying mobilities come into contact, this leads to a potential difference at the junction. Therefore, the best material will minimize the potential difference. Secondly, the junction must allow a steady but slow flow of the reference electrodes electrolyte into the test solution, this is required for the electrode to maintain a stable potential. Additionally, the junction material should be chemically inert and not react with the test solution. A H-cell will be employed using 3 M NaOH on one side and tap water on the other (Figure 3). This will allow the passing of hydroxide ions through the material to be monitored.

The next series of laboratory tests will involve chemical exposure of all reference component materials (i.e., housing, junction, internal chamber fill and sensing wire) to waste simulants. This test will assess the chemical durability of the materials. Table 1 shows the range of anion concentrations and

temperatures that will be tested. These are representative of the waste environment in the Hanford Double Shell Tanks (DST). A statistical design of experiments that involves random compositions within the envelope will be utilized to assess the performance of the various materials. Coupons of each material will be exposed for four months.

These activities have been presented in two external venues. A paper was prepared for Waste Management 2025, which was presented at a poster session [10]. Secondly, a presentation was made to the H2C Tank and Pipeline Integrity Group, which implements the reference electrode in the tank farm integrity program [11].

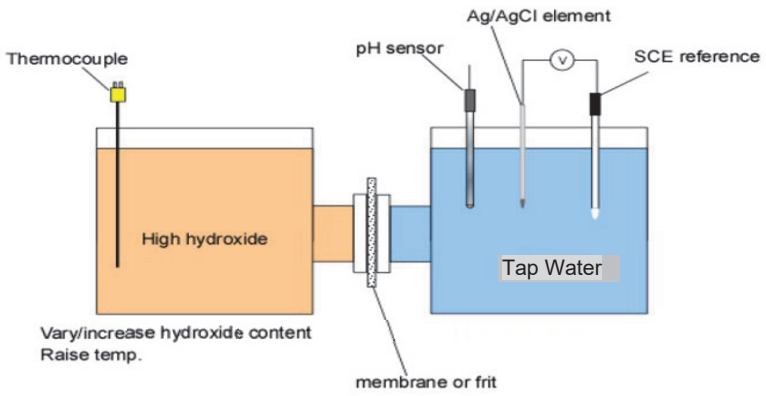

Figure 3. H-cell set-up

The final step will be to fabricate a prototype of the new reference electrode. To that end, SRNL has entered into a Non-Disclosure Agreement (NDA) with Borin Manufacturing, a leading producer of reference electrodes. Borin will provide expertise in assembling the electrode with the new materials and new design.

Table 1. Envelope of DST Waste Chemistry and Temperatures

Entity	Minimum	Maximum
Hydroxide (M)	0.0001	6.0
Nitrate (M)	0.0	5.5
Nitrite (M)	0.0	3.0
Chloride (M)	0.0	0.4
Fluoride (M)	0.0	0.3
Sulfate (M)	0.0	0.2
TIC (M)	0.0	1.0
Temperature (°C)	25	75

References

1. M. M. Dahl and R. J. Crosswhite, RPP-RPT-51766, Rev. 41, *Corrosion Probe Monitoring Systems: January through March 2024 Quarterly Report*, May 2024.
2. C. L. Girardot, RPP-7574, Rev. 8, "Double-Shell Tank Integrity Program Plan", August 10, 2021.
3. K. S. Sykes, J. Jiang, B. J. Wiersma, S. Chawla, N. Sridhar, K. Evans, and J. A. Beavers, "Design and Materials of Reference Electrodes for Radioactive Waste Tank Service – A Literature Review," SRNL-STI-2024-00539, Rev. 0, November 2024.
4. Y. Feng, J. Xie, G. Zhao, X. Li, J. Wang, W. Ding, Z. Wei, "Degradation study and diagnostic technology for Nafion membrane, *Journal of Power Sources*, 613, 234880, 2024.
5. J. Wolfenstine, W. Go, Y. Kim, J. Sakamoto, "Mechanical properties of NASICON: a brief review", *Ionics 29*, 1-3, 2023.
6. P. Saxena, P. Shukla, "A comprehensive review on fundamental properties and applications of poly (vinylidene fluoride) (PVDF), *Advanced Composites and Hybrid Materials*, 4, 8-26, 2021.
7. V. Saisnith, V. Fridrici, "A study of the wear damage of a PTFE coating: The effects of temperature and environment on its mechanical and tribological properties", *Wear,* 480-481, 203946, 2021.
8. S. Chawla, et al., DNV Test Plan & Status Report- 04102024, WRPS FY2024 Hanford Waste Chemistry and Corrosion Testing (10475418), Tank Integrity Expert Panel Corrosion Subgroup Meeting (Virtual), April 10, 2024.
9. N. Valdes, "Task Technical Plan for Hanford Tank Bottom Refurbishment Using Grouts", Technical Report *SRNL-RP-2025-00379*, March 2025.
10. B. Wiersma, J. Jiang, K. Sykes, S. Chawla, J. Beavers, and N. Sridhar, "Robust Reference Electrode Design and Testing Approaches for Application in Aggressive Chemical and Radiation Environments," Paper 25301, WM2025 Conference, March 9-13, 2025, Phoenix, AZ.
11. K. S. Sykes and B. J. Wiersma, "Improvements to Waste Tank Reference Electrode Materials and Design," SRNL-MS-2025-00158, Presentation to H2C Tank and Pipeline Integrity Group, Nashville, TN, April 10, 2025.

Appendix A. Reference Electrode Workshop Agenda

Attachment 1: Agenda for Reference Electrode Workshop

Date: January 13-14, 2025

Place: DNV, Dublin, OH

Connection: TEAMS link available

January 13, 2025

Morning (8:30-12)

Introductions and Administration	8:30-8:40
Background on EM Roadmap Integrity Program (P. K. Shukla)	8:40-9:00
Reference Electrode Basics (J. Beavers or S. Chawla)	9:00-9:30
Functional Requirements for Reference Electrode (B. Wiersma)	9:30-10:15
Break	10:15-10:30
Failure Mode, Effects and Analysis (B. Wiersma)	10:30-12:00
Lunch	12:00-1:00
Optional Tour	1:00-1:30

Afternoon (1:30-5:00)

Proposed Materials of Construction

Polymer Composites (J. Jiang)	1:30-2:15
Additive Manufacturing (H. Jones)	2:15-3:00
Break	3:00-3:15

Materials Testing

Chemical and Radiation Exposures	3:15-4:00
(B. Wiersma)	
Characterization	4:00-4:45
(K. Sykes/H. Jones)	
Summary of the Day	4:45-5:00
(B. Wiersma)	

January 14, 2025

Morning (8:30-12:00)

Design and Fabrication

Polymer Composites	8:30-9:15
(J. Jiang)	
Additive Manufacturing	9:15-10:00
(H. Jones)	
Break	10:00-10:15

Reference Electrode Verification

Comparison with Standard Electrodes	10:15-10:35
(S. Chawla/K. Evans)	
Impedance	10:35-10:55
(S. Chawla/K. Evans)	
Accelerated Tests	10:55-11:15
(S. Chawla/K. Evans)	
Approaches to Modeling Reference Electrode Performance	11:15-12:00
(J. Beavers/N. Sridhar)	
Lunch	12:00-1:00

Afternoon (1:00-2:00)

Schedule and Plans	1:00-1:30
(B. Wiersma)	
Summary of Day and Workshop	1:30-2:00
(B. Wiersma)	

Appendix C: Task 3 Deliverables — SRNL-STI-2024-00435 and SRNL-STI-2025-00209

A U.S. DEPARTMENT OF ENERGY NATIONAL LAB • SAVANNAH RIVER SITE • AIKEN, SC • USA

A General Overview of Cathodic Protection in Reinforced Concrete

Benjamin Barkai

September 2024

SRNL-STI-2024-00435, Revision 0

DISCLAIMER

Printed in the United States of America

Prepared for
U.S. Department of Energy

SRNL-STI-2024-00435
Revision 0

Keywords: Cathodic Protection, Reinforced Concrete

Retention: *Permanent*

A General Overview of Cathodic Protection in Reinforced Concrete

Benjamin Barkai

September 2024

Savannah River National Laboratory is operated by Battelle Savannah River Alliance for the U.S. Department of Energy under Contract No. 89303321CEM000080.

REVIEWS AND APPROVALS

AUTHOR:

BENJAMIN BARKAI (Affiliate) Digitally signed by BENJAMIN BARKAI (Affiliate)
Date: 2024.08.30 11:16:09 -04'00'

Benjamin Barkai, Materials Science and Disposition Date
Savannah River National Laboratory

TECHNICAL REVIEWERS:

KIANA SYKES (Affiliate) Digitally signed by KIANA SYKES (Affiliate)
Date: 2024.08.30 11:50:49 -04'00'

Kiana Sykes, Materials Science and Disposition Date
Savannah River National Laboratory

APPROVAL:

PAVAN SHUKLA (Affiliate) Digitally signed by PAVAN SHUKLA (Affiliate)
Date: 2024.08.30 11:59:35 -04'00'

Pavan Shukla, Materials Science and Disposition Date
Savannah River National Laboratory

MORGANA WHITESIDE (Affiliate) Digitally signed by MORGANA WHITESIDE (Affiliate)
Date: 2024.08.30 12:06:58 -04'00'

M. Whiteside, Manager, Materials Science and Disposition Date
Savannah River National Laboratory

JOSEPH MANNA (Affiliate) Digitally signed by JOSEPH MANNA (Affiliate)
Date: 2024.08.30 12:17:07 -04'00'

J. Manna, Director, Materials Technology and Energy Sciences Date
Savannah River National Laboratory

EXECUTIVE SUMMARY

Corrosion of reinforcement steel in concrete is a prevalent issue in infrastructures worldwide, with the direct costs of repair estimated to be $1 trillion annually. Treatment options are complicated by the concrete's role in the corrosion process. Ordinary, modern-day cement is so alkaline that it maintains a thick passive layer on the steel surface, reducing corrosion to inconsequential rates. However, environmental contaminants in the form of carbon dioxide or chlorides may cause a breakdown in the passive layer, exposing the steel surface to corrosion. Galvanic cells will be free to form due to potential differences along the rebar, and anode sites will create dissolved iron ions that cannot travel far through the still concrete. Thus, rust products will accumulate directly onto the steel/concrete interface. Iron oxides have a much higher volume relative to steel, and even a miniscule amount of rust can produce enough volumetric stress to cause cracking, spalling and delamination of the surrounding concrete, increasing the risk of structural failure. Safeguards and inhibiting technology exist to limit the chances of corrosion initiation by either species, but cracking of the concrete cover and gradual accumulation of contaminants means that corrosion is unavoidable in certain environments and will initiate, given enough time.

Corroded sections in a structure may be repaired or cleaned, but the corrosion process cannot be terminated until the contaminants are removed from the concrete. In structures that have been severely contaminated, this may not be realistic, as replacing large sections of concrete is neither cost-effective nor safe in terms of structural integrity. Cathodic protection (CP) of concrete became a major solution: by polarizing the reinforcement using a current, the steel becomes cathodic to an external anode, and rust products are unable to form. Initial field trials of CP occurred in 1959 in the San Francisco Bay, and since then, concrete CP has been adopted by agencies and companies worldwide, extending the lifespan of structures by decades.

Concrete CP systems may be split into two major categories, impressed current (ICCP) and galvanic (GCP) systems. Both operate by establishing a circuit with the reinforcement steel using the concrete as an electrolytic medium, but major differences lie in their choice of anode material and current source. ICCP systems use an inert anode attached to a DC power source to apply a current from the anode into the steel, while GCP systems electrically connect a less noble metal to the steel, generating a natural current. Deciding which CP system to use, as well as the anode's geometry, is dependent on factors such as concrete parameters, contamination levels, and structure conditions.

Potential measurements may be the most important indicator for determining CP performance. Compared to conventional CP systems that reduce the steel's potential to the immunity region, concrete CP systems aim for the passivity region, which requires smaller potentials. The high voltages or current needed to enter the immunity region may cause hydrogen embrittlement of the steel, in addition to degradation of the concrete. Absolute potential value criteria exist for CP, but because reference electrodes may drift over time and corrosion in reinforcement steel is likely to be heterogenous, polarization shifts are typically considered to be the better criterion. If a potential difference of at least 100 mV is visible after a CP system is powered on or off, the structure is considered protected. The polarization shift criterion has an additional advantage of requiring less current to fulfill, which reduces the risk associated with high currents. Over time, as the structure stays polarized, chemical changes in the concrete will reduce the working current requirements.

Other treatment systems exist for concrete rehabilitation alongside ICCP and GCP. These include hybrid cathodic protection (HCP), realkalization, and electrochemical chloride extraction (ECE). HCP is a two-phase treatment that attempts to combine the strengths of both ICCP and GCP while overcoming their individual weaknesses. Realkalization and ECE, while not true CP systems, operate by near-identical principles, establishing an ICCP circuit.

TABLE OF CONTENTS

LIST OF TABLES

LIST OF FIGURES

LIST OF ABBREVIATIONS

CP	Cathodic Protection
ICCP	Impressed Current Cathodic Protection
GCP	Galvanic Cathodic Protection
HCP	Hybrid Cathodic Protection
ECE	Electrochemical Chloride Extraction
FHWA	Federal Highway Administration

1.0 Corrosion of Reinforced Concrete

Under most ambient conditions, reinforcement steel in intimate contact with concrete has excellent corrosion resistance, owing to a naturally forming passive film. Concrete has high alkalinity, with pH values roughly around 14, and its alkalies are able to react with the surfaces of rebar to form a stable passive layer made up of metal oxides, hydroxides and cement minerals [1]. In most cases, no additional corrosion protection is needed because of this interaction, but certain environmental factors can breakdown the steel's passivity, leaving the surface vulnerable to corrosion. Anodes along the rebar will produce iron ions, and because concrete is a stagnant medium, the dissolved iron cannot travel far from its origin and rust products will accumulate at the metal/concrete interface. Iron oxides have a much higher volume relative to steel, and a small amount of rust can create sufficient stress to cause cracking, spalling and delamination of the concrete, threatening structural integrity [1-3].

Two main sources of reinforcement corrosion are recognized: carbonation and chloride-contamination. Both processes contaminate the concrete and destabilize the passive layer, exposing the steel surface to corrosion.

1.1 Carbonation

When carbon dioxide encounters water, such as the pore water trapped in concrete, it will react to form carbonic acid. This acid does not dissolve the concrete or steel, but neutralizes the concrete's alkalinity, causing a pH drop and a decrease in the available amount of hydroxides [4]. As carbon dioxide diffuses deeper into the concrete from the surface, it will create a pH gradient or "carbonation front" that will creep towards the reinforcement steel over time. At the rebar, a pH drop below 11 will cause corrosion products to begin developing, but carbonation can cause pH to fall lower than 8, at which point passivity is unstable and general corrosion will proceed [1-4].

Factors that influence gas diffusion, such as material parameters and environmental conditions, affect the carbonation rate. Concrete acts as a barrier to diffusion, but if the cover layer is too small, the water/cement (w/c) ratio is too high, or porosity is excessive, carbonation will be accelerated. These characteristics are controllable, and carbonation can be easily hindered by increasing concrete compactness or the concrete cover, which extends the distance to the rebar in the latter case. Humidity and temperature also factor into carbonation rates: higher temperatures speed up diffusion, but moisture slows it. Carbon dioxide diffuses by orders of magnitude faster in airy, dry concrete, but the low water content means that carbonic acid is unable to form. The highest rates of carbonation have been reported to occur at 60% humidity [3]. Carbonation is also accelerated by wet/dry cycles, as the dry periods allow rapid ingress of carbon dioxide, while the wet periods provide the moisture required for carbonic acid generation [4].

Historic structures were usually made with poor quality concrete that had high porosity and w/c ratios, increasing the chances of carbonation. Concrete that follows modern standards and procedures should not experience excessive ingress of carbon dioxide [4]. This does not mean that good quality concrete is impervious: aged structures will have higher concentrations of carbon dioxide, as well as structures in areas with higher emissions of carbon dioxide such as cities. [2, 3].

1.2 Chloride-Contamination

Although many species of electrolytes can harm concrete, the ones most commonly responsible are chlorides. Modern standards place limits on the allowable chloride content in cement mixtures, with values around 0.06% to 0.40% of cement mass [3], but concrete's porosity gives it capillary properties, which can draw ions out of the environment [2]. As a result, environments with a high concentration of chlorides will contaminate concrete structures over time. Chloride contamination is commonly caused by sea spray and

deicing salts, but can also be sourced from waterways, industrial brines, or chloride admixtures (common in older concrete variants as accelerants) [2, 3, 5].

At low concentrations, chloride ions bind to concrete, forming a mineral salt that poses little danger to the steel. Past a certain binding capacity, excess chloride ions remain dissolved and are transported throughout the concrete. If the free ions reach the steel surface, they will compromise the passive layer in the form of pits [3]. The definite mechanism of attack is unclear, but appears to be a combination of several processes: chlorides are able to create ionic defects in the passive layer, compete with passivating hydroxide ions over reaction sites, and form small amounts of hydrochloric acid [2]. Regardless of the process, the end result is that chlorides act as a catalyst for localized corrosion. Corrosion does not initiate until the pits have stabilized, as existing hydroxide ions continually repair any damaged sections of the passive layer. Corrosion will begin only once pitting growth exceeds the repair rate [6]. A high $[Cl^-]/[OH^-]$ ratio can indicate that a structure is actively corroding, with a commonly cited value of 0.6. However, a pH drop reduces the binding capacity of cement and increases the concentration of available chlorides, so the threshold for the content ratio is mutable [1, 3]. While chlorides may create localized acidic spots on the steel, they do not affect the pH of the bulk concrete. Carbonation encourages the formation of free ions, so it is possible for the two corrosion mechanisms to occur simultaneously.

2.0 Cathodic Protection

The corrosion of reinforced concrete has been recognized as a significant problem in structures worldwide, with annual repair costs estimated to be around $1 trillion [7]. Various barrier technologies have been developed to improve corrosion resistance of reinforcement steel, such as epoxy-coated rebar or corrosion inhibitors mixed into the cement, but they are useless once corrosion has initiated or if severe contamination has occurred [8]. In addition, weathering effects and service loads means that cracking of concrete is inevitable, which drastically increases the rate of contaminant ingress into the interior layers near the rebar [9]. In susceptible environments, all concrete structures will eventually corrode and require repairs.

Corroded sections can be cleaned and repaired, but practice has shown that repairs on contaminated structures are ineffective in the long run. Ordinarily, whenever a concrete structure shows signs of deterioration, patch repairs are performed on the immediate areas of concern. Concrete is scooped out, the reinforcement is cleaned if corrosion indicators are spotted, and the area is refilled with fresh mortar or concrete [10]. However, the repairs cannot arrest corrosion; chemical differences between the fresh concrete and old, contaminated concrete recreate galvanic cells, as shown in Figure 1. This “incipient” anode effect leads to premature failure of patch repairs, sometimes as fast as in the span of a few months [10]. The concentration gradient also means that in time, the chlorides from the preexisting concrete will diffuse and infest the fresh patch [9]. Potholes in concrete bridge decks became an enormous problem in North America as a result, as the only possible way to prevent the anode effect from occurring was the removal of the contaminated concrete, an unfeasible task for large structures. A cost-effective solution for concrete was developed in the mid-20th century in the form of cathodic protection (CP) [5]: by creating an electrical circuit with an external anode, the steel reinforcement is negatively polarized and becomes cathodic, limiting and minimizing any corrosion cells present. Not only does CP successfully protect the steel from corroding, but it is the only rehabilitation technique that does not require removal of any contaminated concrete except for areas that have spalled or delaminated [8, 11]. Since the first 1959 field tests of CP on bridge substructures [5], research into CP systems has spread into countries such as the UK, Italy, Australia, Switzerland, the Netherlands, and Saudi Arabia. The Federal Highway Administration (FHWA) has made official statements over the years endorsing CP, claiming that it is the only rehabilitation technique proven to stop corrosion in salt-contaminated bridge decks regardless of the chloride content [11, 12].

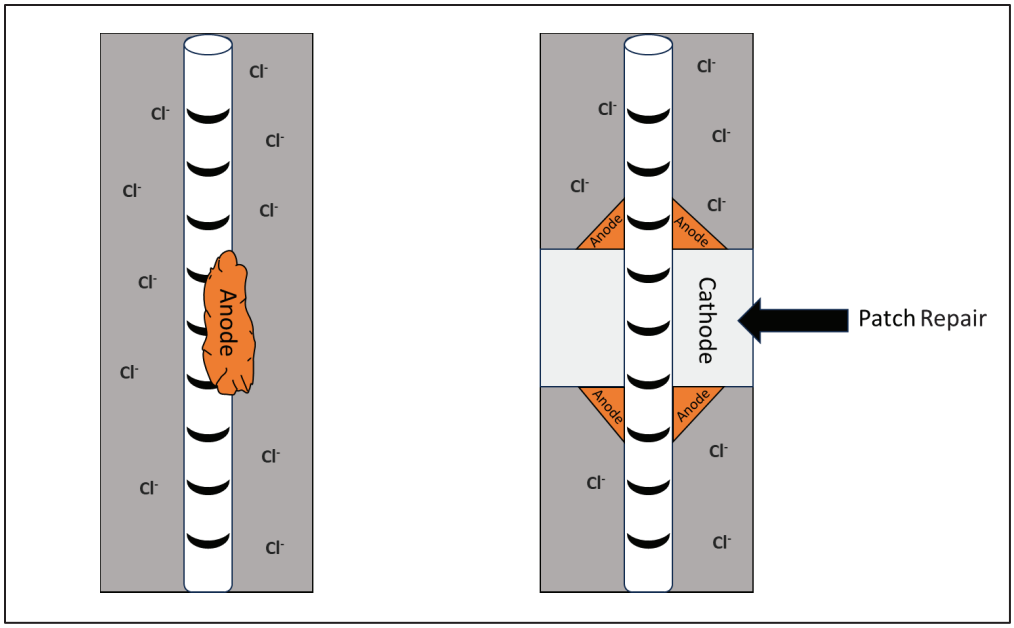

Figure 1. Patch repair to remove corrosion products from rebar. Fresh mortar is cathodic to the existing concrete, leading to the creation of new anodes along the steel. Redrawn from [5].

Modern-day concrete CP systems can be grouped into two categories: impressed current CP (ICCP) and galvanic CP (GCP). In either system, a protective current is generated that keeps the steel cathodic. These systems should sound familiar to those well-versed with CP systems in soil, as their basic principles of operation are near identical. In fact, certain comparisons can be made between the two CP media: concrete and soil are both porous but stagnant; ions and water are not homogenously distributed in either; and the media act as an obstacle for diffusion processes, which can delay the corrosion stages of steel [1, 7]. The principles are not fully interchangeable, and concrete has a much more active role in CP. While soil CP tries to reach steel's immunity region on the Pourbaix diagram, depicted in Figure 2, CP in concrete works with the medium to restore the steel back to its passive region. The low potentials needed for the immunity region may cause severe degradation in a concrete structure, so concrete CP designs set conservative limits on the CP system current. The higher dependence on the medium also means that concrete CP systems do not have fixed potential threshold values, and the performance criteria are based on empirical evidence [11].

The selection of a CP system for an arbitrary concrete structure depends on several design considerations, which include but are not limited to environment, size, and contamination levels. CP system lifespans are linked to their anode's lifespan; environmental factors and service loads should be considered during anode selection, as high consumption rates could cause premature failure of the system [8]. In addition, compared to soil systems, concrete systems have much less medium to work with, so anode placement is more critical for good system performance [7].

The impact of concrete CP systems can be split into "primary" electrokinetic and "secondary" electrochemical effects. When steel is polarized, the cathodic and anodic rates of reaction are shifted to favor cathodic development at the expense of the anodic rate. Simultaneously, the current in the CP system causes chemical changes in the concrete: chlorides are attracted towards the external anode away from the reinforcement, and new hydroxides are created at the steel surface by the cathodic oxidation of water [1, 7]. Under the kinetic interpretation, corrosion is only stopped once the steel potential is reduced to the immunity region in Figure 2, but in practice, CP can arrest corrosion under much smaller current densities

due to repassivation by the newly formed hydroxides [7]. Some evidence suggests that the secondary effects are the driving mechanism behind CP's success. Poorly installed systems with subpar current densities for polarization have been shown to still achieve protection [13]. Also, whenever an ICCP system is powered on or off, time must pass before a change in CP is registered, a delay that is attributed to time-dependent changes in the concrete's chemistry. The delay has one important implication: CP can continue to remain active if the protective current is temporarily interrupted, making it flexible around unintended power outages or inspections that require depowering [7, 13].

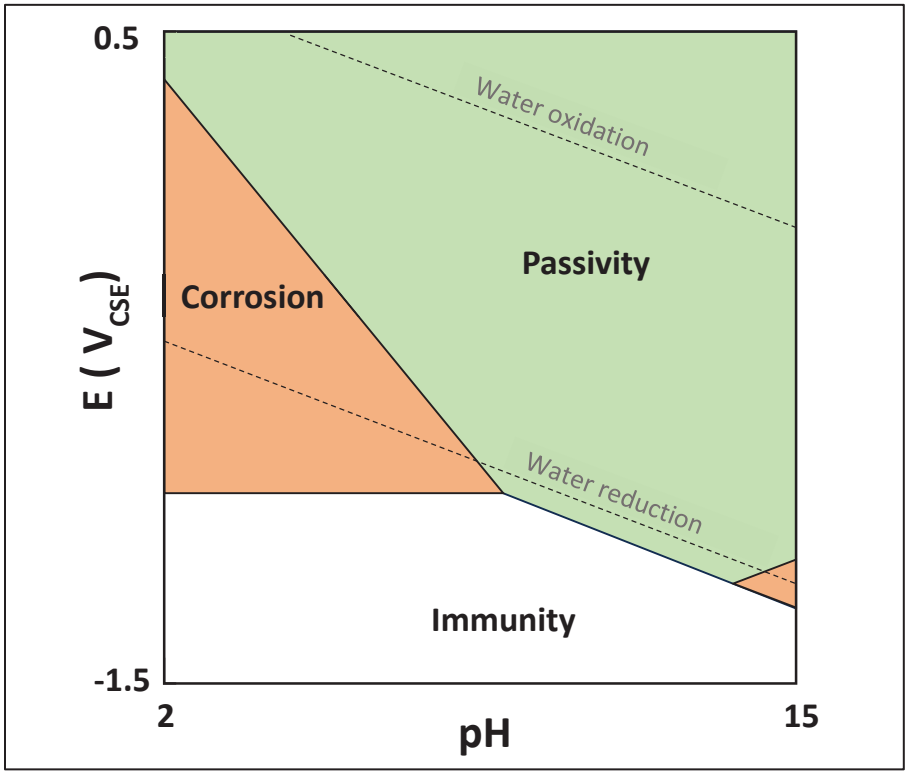

Figure 2. Pourbaix diagram of steel. Passive region occurs at high pH and relatively positive potentials. Under most ordinary circumstances, water is oxidized at the cathode to form [OH^-], but at sufficiently low potentials, water is reduced to monatomic H. Redrawn from [3].

A vital strategy of CP system design is sectioning parts of the structures into predefined zones. A single, all-encompassing anode system may experience setbacks in current output, spread and control. Factors that can affect zone selection include [5]:

- Structure size and its influence on current spread
- Discrete DC power output levels (e.g. 1 or 10 amps)
- Variations in steel density within the structure, higher densities requiring more current
- Exposure conditions of different subareas e.g. bridge columns in coastal tidal zones versus splash zones

Every zone will have an independent CP system with its own anode, electrical connections, monitoring system and power source (if necessary). If a rectifier is present, a control card can be used to split and isolate electrical parameters to each zone [8]. Designs must find a good balance in the number of zones based on the structure. Too few may lead to under or oversupply of current, producing insufficient protection or concrete deterioration. Too many can overcomplicate the design and run up costs [14].

Installation of CP systems should be done with supervision from qualified, certified individuals. Commercial vendors can offer guidance towards CP designs, but caution is advised for novel anodes. Most of the time, data over the long-term performance of specific anodes is nonexistent, and so marketed anode performance is usually supported by sales figures. Frequency of installation could quell fears of poor anode performance, but past cases exist where a new anode was pushed into the market (e.g. copper/polymer mesh), only to deteriorate rampantly after a few years [1, 8].

2.1 Impressed Current Cathodic Protection (ICCP)

ICCP connects the reinforcement steel to the negative terminal of a DC power source (usually a rectifier), and an inert anode to the positive terminal, establishing a permanent impressed current in the structure. This current negatively polarizes the reinforcement steel, terminating the steel's anodic reaction [8]. Figure 3 shows a typical layout of an ICCP system.

Anodes can be split into four generic groups [5]:

- Mesh with cement overlays
- Ribbons grouted into slots
- Probe anodes, grouted into holes
- Coatings applied directly to the concrete

A wide variety of material options exist for anodes, as the impressed current maintains polarity even if the anode candidate is more noble to the steel. Three of the most common in America are MMOTi, thermally-sprayed zinc and conductive paints [8]. MMOTi, a sintered alloy that prefers to form oxygen at the anode over acidic chlorine gas, is typically applied as a mesh or in ribbon form [5, 8]. Thermally-sprayed zinc and conductive paints are applied to substructure elements, but are only suitable for land structures that are occasionally exposed to de-icing salts. In marine environments, saltwater proves to be too aggressive, and will destroy the coatings prematurely. Mesh or bulk ICCP anodes are used instead in coastal areas, often surrounded in cement with optional protective fiberglass jackets [8]. Conductive paints, despite their poor resilience, are attractive because of their ease of installation and repairs, and can be combined with other anodes, such as platinum wire, to improve current distribution.

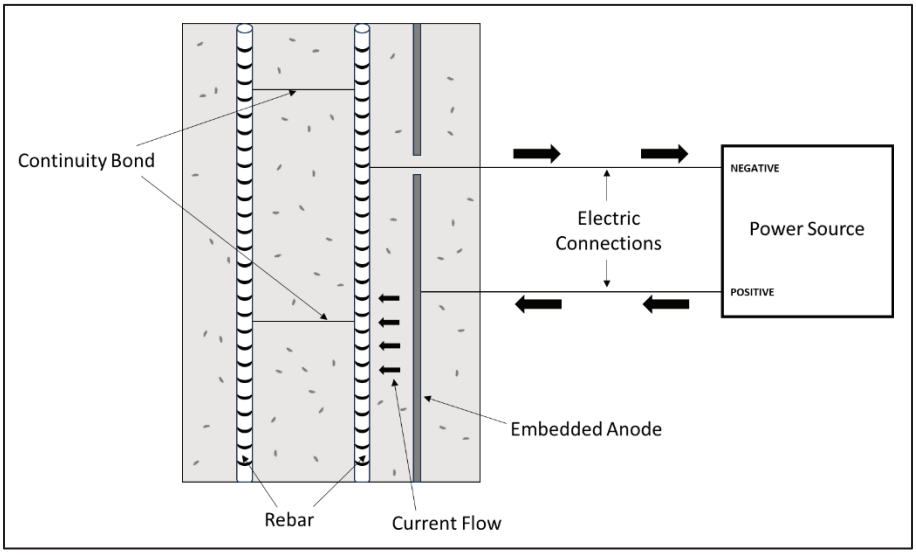

Figure 3. A simple schematic of an embedded ICCP system. Current flows through the concrete media from the anode to the steel. Electric connections complete the circuit. Inert anodes can be naturally cathodic to the steel, but the power source reverses the polarity. Redrawn from [8].

The two biggest advantages of ICCP systems are their lifespan and ability to control current output. The requirements of every single project are unique, and ICCP system parameters are easily adjustable with a large voltage range. This enables ICCP to work in a wide variety of conditions, including extreme ones where excess chloride requires higher voltages than possible in GCP systems. In addition, out of the many possible CP system anodes, the highest theoretical lifespan is achievable with ICCP, and can be up to 50 or 75 years [15]. Long-term studies conducted by the FHWA showed that actual working lifespans of installed ICCP systems are anywhere from 15 to 25 years, and though the lifespan falls short of the projected numbers, it is still much higher compared to GCP alternatives [12]. In fact, ICCP systems are able to last for so long that usually the electronic components are the first to fail [5, 15]. Electrical systems can be somewhat delicate, and improper installation may impact the performance or lifespan of the system. Asymmetrical connections between the rectifier and the steel can lead to nonuniform current distribution that will not fully protect the structure [16]. Shorts could disable entire zones if anodes are extremely conductive and improperly connected, which can occur with MMOTi ribbons and thermally-sprayed zinc [5]. Circuitry wiring may cause dissimilar metals to be in close proximity to each other, so insulation must be used to keep them from corroding [5, 17]. Proper attention and care of electrical systems can reduce the chances of underperformance and ensure that the lifespan of ICCP systems lasts for decades.

The current demand in ICCP systems is small; ISO 12696 states that CP in most concrete structures will operate at 2 – 20 mA/m^2 [6], and the voltage required for the system can be less than 10 volts, a fraction of the energy required to power a lightbulb [1]. However, the driving voltage of ICCP systems is relatively high compared to GCP, and very negative potentials can develop in the steel interface. This can have disastrous consequences: water will be reduced to monoatomic hydrogen at the cathode and gather within the steel's defects, increasing the risk of failure by embrittlement in prestressed concrete or high-strength steels [1, 18]. Many sources advise caution when using ICCP on prestressed structures for this reason [2, 5, 8]. Hydrogen evolution may be controlled by limiting the minimum potential value relative to a reference electrode (e.g. -900 mV vs. Ag/AgCl/0.5MKCl [6]), but the threshold value is dependent on the steel's condition, and hydrogen might still form if pitting or crevices exist on the reinforcement surface [1, 5]. Some restrictions exist on anode current density as well: if values reach close to 110 mA/m^2, the anode/concrete interface could experience acid attack, either by the oxidation of water into $[H^+]$ and/or chlorine evolution [1, 8]. Long-term application of a current could also deteriorate the concrete, causing issues such as bond degradation of the steel-concrete interface, concrete softening, porosity changes and micro-cracking [3, 19]. As previously mentioned, in the event that ICCP is switched off, CP effects are still retained thanks to induced chemical changes in the structure [13], so plausible designs exist where ICCP is intermittently toggled on and off, protecting the steel while avoiding the negative side effects associated with a constant current [3, 19].

All descriptions of ICCP paint it as extensive, robust and reliable. In practice, the complexity of ICCP has made it fall out of favor in recent decades. Surveys done with state agencies have revealed a mixed reception towards ICCP, largely due to inexperience, difficulty in handling ICCP, and poor past performance [5, 8]. Monitoring, maintenance, and control is the greatest concern; ICCP systems must be frequently monitored and adjusted to changes in current demand based on seasons, weather, and time. For example, NACE-recommended standard practice requires monthly inspection of power sources, annual surveys that verify protection criteria, and thorough inspections that check for "electrical shorts, ground connections, meter accuracy, rectifier efficiency, and circuit resistance" [20]. Power systems are the weakest link in ICCP systems; rectifiers are prone to damage by lightning strikes and vandalism, and it is to be expected that maintenance will be needed at least once each year [8]. Repairs can be a nuisance, but manageable as long as the damaged component is accessible; embedded parts are much more difficult to fix [8]. Wet environments are also problematic, as water could damage power supply units and junction boxes [14]. Surveys performed in the 90s by the Strategic Highway Research Program have shown that even when ICCP received enthusiastic feedback by state agencies, systems that were thought to be properly working had been switched off or broken for an unknown duration of time [21]. Despite these issues, ICCP systems

are still essential in contaminated structures that require both high voltages and current control, so planned installations should anticipate and devise strategies against potential setbacks during operation.

2.2 Galvanic Cathodic Protection (GCP)

Unlike ICCP, GCP systems connect a less noble metal to the reinforcement and use the resulting natural current to satisfy the requirements for cathodic protection. Over time, the anode will be consumed to produce the current, effectively "sacrificing" itself for the sake of the reinforcement steel. No external power source is needed [8], which immediately makes GCP much more desirable than ICCP. Figure 4 depicts a GCP system.

Typical GCP anode materials are zinc, magnesium and aluminum, though zinc is preferred as aluminum and magnesium can chemically alter the concrete surface [1]. Other anodic metals do exist relative to steel, but their current output is too low to enable cathodic protection [17]. Like ICCP, many different anode configurations exist, and zinc can be applied as a mesh, sheet, foil, ribbon, bulk or thermally-sprayed anode. Zinc does not have a good lifespan. A long-term study by the FHWA showed that many anodes failed after 5-15 years, but because these anodes are not always embedded into the concrete, they are easily replaceable [8].

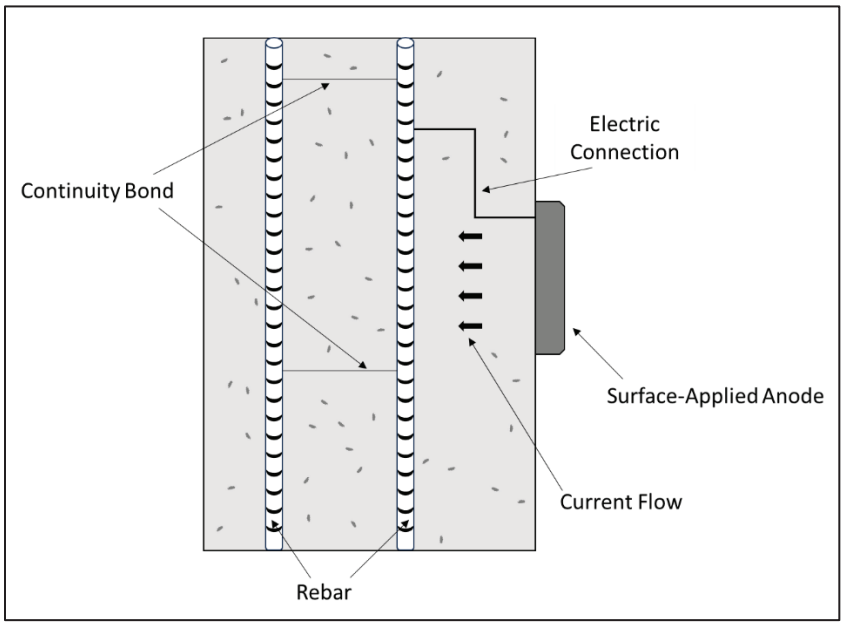

Figure 4. A simple schematic of a surface applied GCP system. Current flows through the concrete media from the anode to the steel. Electric connections complete the circuit. No power source exists, anode is consumed over time. Redrawn from [8].

Current output is influenced by the concrete's resistivity and anode passivation. GCP has a low driving voltage compared to ICCP, a concurrent benefit and drawback. Associated side effects of high current output, such as microstructural changes, hydrogen embrittlement, and acid attack, are near impossible to occur with GCP, so they can be used with high-strength steels and prestressed structures without worry [3, 5, 6]. On the other hand, the low voltage is more sensitive to concrete resistivity, and dry concrete could hinder the protective current. In addition, unlike the inert anodes of ICCP, zinc can form its own oxide layer, slowly becoming passive over time and crippling its ability to maintain a current [8, 22]. Passivity is favored by conditions that have low ion concentrations, such as the concrete surface where zinc anodes are frequently installed. Considering that wet conditions are needed to keep concrete's resistivity low, and a

high concentration of ions is needed to keep the anode active, marine structures experience the greatest frequency of GCP installations [8]. Innovations have boosted GCP's ability to function in non-ideal environments; humectants may be used to improve absorption and retention of moisture, and alternative materials such as Al-Zn-In exist that have reduced passivation and higher driving voltages [8]. GCP anodes have also found home in patch repairs because of their simplicity and small protection radius. Although monitoring is nonexistent and long-term effectiveness is inconclusive, GCP is perceived as a perfect countermeasure for incipient anode effects. [1, 14].

Controlling the current output in GCP is impossible, which could be a potential cause of concern in structures that have heterogeneous or highly variable distributions of contaminants. Surprisingly, environmental changes have a smaller impact, as the GCP system can adapt to fluctuations in moisture and temperature. In wet seasons or zones, current output will increase due to changes in conductivity, enabling the anode to maintain cathodic protection under sudden bursts of corrosion-favorable conditions, such as floods [17, 23]. GCP systems also self-adjust to chloride content, though higher ion concentrations could intensify consumption rates [23]. The responsiveness of GCP means that monitoring can be performed at a far lesser frequency compared to ICCP systems, though standards advise against operating GCP systems without any monitoring procedures in place.

2.3 Hybrid Cathodic Protection (HCP)

ICCP may be unavoidable for certain prestressed structures, but the risk of hydrogen embrittlement is ever-present, especially if a constant current is involved. One novel alternative combines the concept of both ICCP and GCP to create a hybrid cathodic protection (HCP) method. In this two-phase treatment, an impressed current is run at elevated levels through an external anode for a few weeks, restoring the steel's passive layer. After sufficient time has passed, the power source is disconnected, and galvanic anodes maintain passivity for the remainder of the service life [14]. Figure 5 shows a diagram of a fusion anode that can be used in HCP treatments, capable of switching between the two phases. This process combines the benefits of both CP systems while sidestepping their weaknesses; the ICCP phase has a strong driving voltage, and the galvanic phase prevents hydrogen embrittlement & reduces maintenance of the system. At the time of writing, no written standards are available for HCP methods; ISO 12696 recognizes that they exist but offers little guidance, so present-day installations require extra scrutiny.

First phase treatments usually use high current densities to restore the reinforcement area rapidly. This enables the second phase to operate at much lower current densities, a "cathodic prevention" current regime that maintains passive conditions and impedes chlorides from getting close to the steel. The galvanic phase uses prevention criterion found in ISO 12696 (0.2 – 2 mA/m^2), but the ICCP phase typically uses charge criteria not found in any standard, instead sourced from literature. Successful installations have been performed where the first phase produced charge densities of 50 kC/m^2 [24] or current densities of around 20 – 60 mA/m^2 [25]. Debate has yet to reach a consensus as to what level of charge densities are required. An upper limit of 500 kC/m^2 is suggested by one source, though they state that most structures are unlikely to require more than 100 kC/m^2. Another source argues that charge densities are underestimated and reports a system in the UK that used 300 kC/m^2, but polarization readings showed that the minimum CP criteria had been surpassed [15, 26]. Ultimately, the required charge density will be derived from the chloride content and steel potential readings of the structure [26]. First phase treatments are expected to last for a few months, though the duration of time depends on whether an external or integrated power supply is used. Because most of the treatment duration will be spent in Phase 2, HCP lifespans are comparable to GCP systems but are expected to last longer, as the galvanic phase operates with significantly reduced current demands and consumption rates [15].

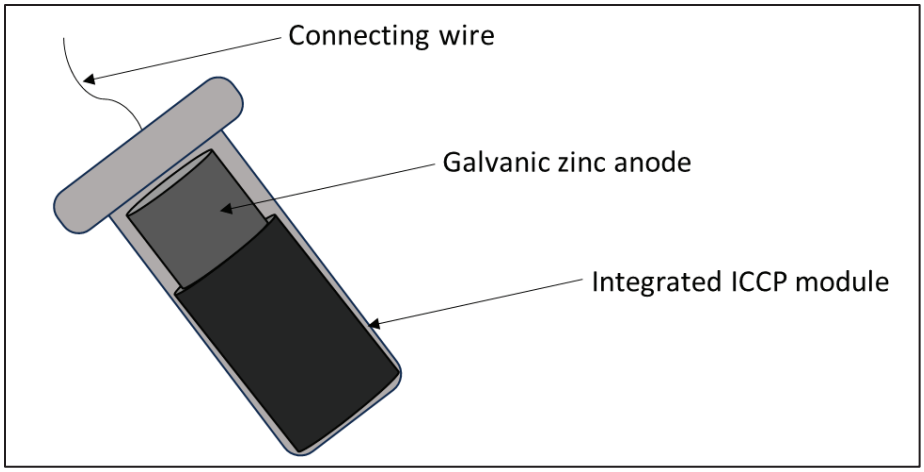

Figure 5. Fusion anode comprising of ICCP and GCP phases. ICCP system runs temporarily during the first phase, the zinc maintains protection for the rest of the anode lifespan. Redrawn from [24].

2.4 Electrochemical Chloride Extraction and Realkalization

Recognizing the fact that the concrete environment has a large effect on cathodic protection, electrochemical chloride extraction (ECE) and realkalization treatments attempt to restore the passive layer via the concrete's chemistry, either by focusing on chloride removal or hydroxide generation respectively. While they may not technically be considered cathodic protection strategies, the setup is near identical to ICCP systems [3, 4].

ECE uses a large current to attract chlorides towards an external anode away from the reinforcement steel while simultaneously generating hydroxides to repair the passive layer. Unlike ICCP, which is built to last for decades, ECE is meant to be a temporary remedy, usually for structures that are irregularly exposed to chlorides such as de-icing salts. Treatment may last as soon as a few weeks. However, for the chloride extraction to be thorough, ECE employs current densities that are three orders of magnitude higher than ICCP. Possible risks related to current output, such as hydrogen evolution; changes in concrete microstructure; and debonding, are exacerbated. Anode selection also becomes more important; the high current will consume anodes faster, and a high conductivity material is required to handle the current requirements [3]. Chloride extraction is extensive, with yields of anywhere from 50% to 90% removed, and insufficient removal may still terminate corrosion thanks to the simultaneous generation of hydroxides [1]. Some research suggests that similar to intermittent ICCP, intermittent ECE can avoid the associated side effects of a constant current, while improving efficiency of extraction by giving bound chlorides some time to equilibrate and free themselves [3].

Realkalization works exactly as ECE, but it is targeted towards carbonated structures. Restoring pH is the priority, and realkalization focuses solely on generating hydroxides, although the treatment can extract chlorides. Though they both technically produce the same electrochemical effects, ECE and realkalization have some differences because of their target contaminant. In realkalization, certain electrolytes can be used that push carbonates into the concrete, which can neutralize carbon dioxide and make the structure more resistant to further carbonation [1, 4]. Compared to ECE, realkalization is performed for only a few days and at lower current densities, so damage risks associated with current are reduced. The current is still high relative to normal ICCP, so treatment should be done with great care for prestressed structures. However, carbonation of properly constructed prestressed concrete is unusual. If sufficient carbonation on a

prestressed structure has occurred, it is likely that the concrete has significant pre-existing issues with its quality and porosity [1, 4].

3.0 Buried and Submerged Structures

Most of the research on concrete CP systems have been performed on bridges, although the same procedures have been easily transferred to other atmospherically exposed structures such as tunnels, parking garages, swimming pools, etc. [8]. This has some long-lasting implications on the way CP is understood and handled, and much of the discourse related to concrete CP assumes atmospheric exposure. Surprisingly, the working criteria for buried and submerged structures have been shown to be similar to atmospheric ones, but new quirks are introduced because of the change in environment [6, 27]. As an example, the chances of chloride contamination in these two environments are higher, as seawater naturally has a high concentration of chlorides, and soil could be seeped in ions originating from salts or runoff [2]. A much more significant difference lies in oxygen. In atmospherically-exposed structures, low potentials are associated with high corrosion rates, but if oxygen has been depleted in a water-saturated environment, low potentials will be seen alongside low corrosion rates [9]. The slowed rates also means that CP current requirements are reduced, though structures that are only partially saturated and actively corroding would still require current densities similar to atmospherically exposed ones [6]. Reference electrodes are also affected, as they will falsely suggest that steel is actively corroding when in reality no corrosion is taking place [1].

If an immersed concrete structure has one face that is exposed to air, a differential aeration cell will be created between the immersed face and the air-exposed face. Such cases be seen in tunnels, underground storage tanks, and coastal bridge columns. Low concrete thickness could encourage development of the aeration cell. If a cell does form, the immersed face of the structure will require a higher current density, and it is advisable to split the faces into zones [6].

Non-atmospheric structures offer one advantage in that anodes need not be directly attached to the concrete and can be placed some short distance away. Traditional CP systems for buried or submerged steel are applicable to concrete structures with few alterations. For example, submerged structures may use standoff galvanic anodes or remote ICCP anode sleds, while buried structures may use discrete galvanic anodes or ICCP anode beds. Seawater and soil enable CP from a distance because they are relatively homogenous media, but the addition of a second medium into the system means that resistivity will change with distance from the anode, which must be considered for proper anode selection [27].

4.0 Criteria and Implementation

Documentation for cathodic protection is extensive, with multiple standards in place. Table 1 lists several standards pertaining to cathodic protection of concrete. Note that this list is not comprehensive.

All CP projects must begin with an inspection of the structure. While this may be as simple as finding visual signs of corrosion (staining, cracking, delamination, etc.), a full grasp of the situation would require up-to-date drawings of the structure, as well as subsurface measurements. Concrete cracking may not be visible from the exterior, so techniques such as sounding or heat-imaging scans should be used to find hidden cavities that could impact the efficiency of CP [1]. If the structure is buried or immersed, visual surveys can still be performed via excavation or cofferdams [6]. Concrete cores can be drilled to identify contaminant species by testing for pH drops and elevated chloride levels. Concrete resistivity measurements are not mandatory, but highly recommended because of their impact on the CP current [6].

Installations of CP systems require careful anode placement. Concrete is stagnant with high resistivity, and heterogeneous corrosion is bound to occur in which some parts of the structure are more anodic than others

[1]. Anodes usually have a small area of effect due to their limited size and concrete's low conductivity; improper placement can attenuate their influence and reduce CP performance. To ensure that corroding structures are properly treated, zones must be configured such that the reinforcement is fully protected by the current. Up-to-date drawings of the structure can help determine the exact location of reinforcement within the concrete, as well as embedded pieces of miscellaneous material that could form discontinuities in the CP circuit. Metals that are isolated from each other may experience stray currents leaping between them, corroding the ends from which electricity is discharged. However, concrete's high resistivity and CP systems' low current outputs reduce the risk of stray currents in most cases. More significant hurdles associated with discontinuities are the fact that they will cause a non-uniform current distribution, leaving sections of the structure unprotected, and obfuscate system measurements that are required for fulfilling CP criteria [1]. As a result, electrical continuity is imperative, and must be verified early in the CP installation process. Continuity can be demonstrated by showing low variability in DC resistance, AC resistance, and/or half-cell potential [6]. These techniques are somewhat unreliable on their own; as an example, AC resistance measurements can give false readings by shorting across isolated pieces of rebar, so these three techniques are recommended to be used in tandem to ensure accuracy of verification [12].

Potential readings of the steel are likely the most crucial measurement for any CP system. The corrosion risk of any immediate area can be correlated to the steel potential of the spot, measurable using reference electrodes with relative simplicity [1, 3]. If enough potential readings are made, they may be used to generate contour or grip maps of the structure to distinguish areas of high and low risk [9]. Potential readings do require the electrode to be directly connected to the steel, which can be cumbersome because of the layers of concrete that have to be penetrated. An alternative approach uses two reference electrodes, requiring only one of them to be fixed. The other can be dragged along the concrete's surface, but potential readings are relative to the other probe and not to the steel interface [1, 3].

Potential readings are not infallible; some situations, such as when concrete resistivity is high or oxygen is depleted, can impact potential measurements and bring them into question [3]. Corrosion cannot always be verified visually, so corrosion rates are usually measured to dispel any uncertainty regarding potential readings [1]. The most common techniques to measure rates are linear polarization resistance (LPR) and electrochemical impedance spectroscopy (EIS). LPR is performed by slightly polarizing the reinforcement and measuring the resulting current with a counter electrode, while EIS is frequency-based, alternating potential at various frequences to measure an alternating current. The ratio between the potential change and current is called "polarization resistance," and can be converted into an instantaneous corrosion rate using the Stern-Geary equation. EIS generally supplies more information than LPR, such as concrete resistivity, presence of steel films, and steel/concrete interfacial reactions, but it is much more time-consuming and complex, so LPR is preferred for field measurements [3, 9]. Although beneficial, LPR and EIS should only be used as supplementary devices to potential measurements due to perceived difficulties with handling and accuracy [6]. LPR is sensitive to variations in temperature and moisture, and pits attract applied polarization currents, making readings somewhat unreliable. Guard rings may be employed to confine the current into a known area and keep neighboring anodic zones out of the measurement, but this requires an accurate potential mapping of the structure [1, 3]. For this reason, standards rely more on potential readings to get a feeling for CP performance, and corrosion rates, while beneficial, should not be relied upon solely.

After a CP system has been installed, successful termination of corrosion may be verified with one of two criteria. The first is borrowed from CP of exposed steel in soil or water, an instant-off potential measurement in the range of -720 mV to -850 mV which indicates that corrosion has been arrested [1, 6, 18]. The second criterion is a polarization shift, a change in potential whenever a CP system is switched on or off that should measure at least 100 mV. Either one can be used to show that CP is working, but polarization shifts are preferred because they can work with embedded reference probes that have lost calibration, and they could require less current compared to the other criterion [1, 18]. Since concrete has a temporary buffer period

where CP lingers after the current is interrupted, some time must pass for polarization evolve, which can last as long as a few days. However, the rate of change is dependent on oxygen, and in depleted conditions such as in buried or submerged environments, polarization could take weeks to fully evolve, which is impractical to measure. In oxygen-starved cases, ISO recommends using absolute potential measurements [6]. NACE acknowledges the potential criterion as an alternative for concrete structures as well, but states it could lead to polarization shifts greater than 100 mV [18].

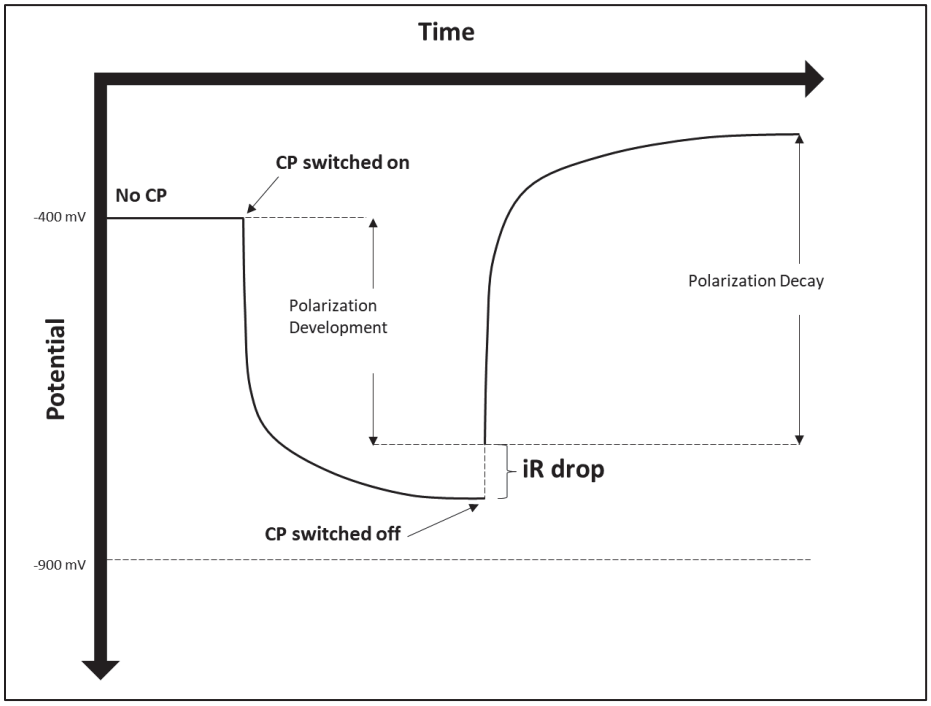

Figure 6. Polarization decay and development curves. Speed of polarization evolution is dependent on oxygen levels. Potentials readings after decay are more positive than pre-CP potential due to restoration of passive layer. Redrawn from [18].

Polarization shifts can be measured using decay or development curves, as seen in Figure 6. During development, the protective current is switched on, and instant-off measurements are recorded periodically. During decay, the CP current is switched off, and the potential drop is measured. The requirements for CP are satisfied when the potential difference between the initial and final readings is at least 100 mV, corrected for the iR drop [18].

An important footnote for CP criteria is that they are empirically based and generalized. Output current values are not set and will vary based on factors such as contamination levels, corrosion severity, or timing of CP installation. In fact, CP systems that are installed on newly built structures, dubbed “cathodic prevention” systems, can operate at significantly reduced current outputs, as it is much easier to shield and maintain a passive layer compared to rehabilitating a damaged one. Prevention appears to increase the critical chloride threshold needed to initiate corrosion, cathodic prevention studies done on salt ponded concrete slabs showed they were able to withstand corrosion despite having chloride concentrations as high as 2% [28]. Prevention systems are also suitable for prestressed structures because of the smaller electrical output, so ICCP systems have smaller risk if they are installed early in a structure’s service life [11]. ISO 12696 claims that cathodic protection systems will likely have current output in the 2 – 20 mA/m^2 range, or 0.2 – 2 mA/m^2 in the case of cathodic prevention, but current requirements are not confined to this range. In the island nation of Bahrain, multiple bridges were shown to have cathodic prevention current densities

of 5 mA/m^2, more than twice as high as the upper limit in ISO 12696 [5]. Over time, as chlorides are cleared from the structure and the passive layer is restored, reduced current requirements are anticipated. However, some CP systems are able to arrest corrosion, but have insufficient current to rebuild the passive layer, so current requirements will remain high for the duration of the service life [28]. Although the gradual change in requirements should not be an issue with the self-regulating current of galvanic systems, ICCP systems will require constant adjustment to avoid overprotection.

Table 4-1. List of standards related to cathodic protection of concrete.

ACI 222R	Guide to Protection of Reinforcing Steel in Concrete against Corrosion	• An in-depth report over concrete corrosion. • Does not focus on CP. Broad description of entire field, including corrosion science and corrosion barrier technology.
AMPP SP21520	Acceptance Criteria for Cathodic Protection of Steel in Concrete Structures	• Lists CP criteria. • No description of design elements
ASTM C876	Standard Test Method for Corrosion Potentials of Uncoated Reinforcing Steel in Concrete	• Describes corrosion potential mapping procedures
ISO 12696	Cathodic protection of steel in concrete	• In-depth checklist of required procedures and measurements • Applicable to every kind of concrete structure, except patch repairs.
NACE SP0290	Impressed Current Cathodic Protection of Reinforcing Steel in Atmospherically Exposed Concrete Structures	• Brief checklist of design elements and criteria for ICCP • Not applicable to pre-stressed structures
NACE SP0216	Galvanic Cathodic Protection of Reinforcing Steel in Atmospherically Exposed Concrete Structures	• Brief checklist of design elements and criteria for GCP • Applicable to pre-stressed structures
NACE SP0408	Cathodic Protection of Reinforcing Steel in Buried or Submerged Concrete Structures	• Brief checklist of design elements and criteria in non-atmospheric structures • Some overlap with NACE SP0290 and NACE SP0216

4.1 Monitoring and Control

The requirements for concrete CP systems are dynamic, affected by seasonal changes and gradual restoration of the concrete. Since ICCP cannot self-regulate its current output against these changes, monitoring and control systems are imperative. GCP systems are unable to be controlled, but monitoring equipment are still required by NACE and ISO standards [6, 29].

ICCP system output is set by their rectifiers, which can be remotely monitored and adjusted. Rectifiers are either voltage controlled or current controlled, though current controlled is the preferred option in most cases. A few rectifiers have potential control in order to directly fulfill CP criteria, best used for high-

strength steels or non-atmospheric structures [1, 8]. At the bare minimum, permanent reference electrodes should be installed to track the steel's potential [6, 8], though supplementary monitoring equipment are heavily recommended, such as LPR probes for measuring corrosion rate, or current/null probes for measuring current flow [5, 12]. Data logging has many options, ranging from manual systems in easily accessible areas, to remote systems that record measurements automatically for download or wireless transmission [1]. As decades passed, the monitoring systems for ICCP improved but became more complex, introducing additional possible avenues of failure. Simple systems may be preferable over more sophisticated ones due to this risk, and an optimal ICCP system could be sufficient with a basic power supply, a feature to take instant-off measurements, a data logger, and web-based monitoring [14].

5.0 Conclusion

Reinforced concrete builds a natural passive layer around rebar because of concrete's high alkalinity. Environmental contamination by chlorides or carbon dioxide can disrupt the passive layer, leaving it exposed to corrosion. Rust products have a greater volume than steel, and will apply volumetric stress to the concrete, leading to cracks and spalls. Contaminated concrete must be removed for structure repairs to be successful, as corrosion will be ongoing as long as contaminants exist. Cathodic protection systems can circumvent the removal of infested concrete and prevent the formation of rust on reinforcement steel. CP systems can be split into two main categories: ICCP and GCP. Both use an external anode to create a circuit with the steel, which polarizes the steel into the cathodic direction and chemically alters the concrete to restore the passive layer.

- ICCP systems use a DC power supply along with an inert anode. System lifespan is long, currents are high enough to handle severely contaminated structures, and rectifiers provide the means for control over system output. Power systems are the weakest link and require frequent repairs.
- GCP systems connect a less noble metal, typically zinc, to the steel. No external power supply is used, current is produced by the potential difference between the steel and anode. Low driving voltage makes it suitable for prestressed structures. Current output is sensitive to high resistivity, such as in dried concrete, so GCP sees most use in marine environments. Low maintenance can make it preferable to ICCP.
- Alternative treatment solutions exist in the form of HCP, which fuses ICCP and GCP systems, and ECE & realkalization, which use high current output to treat the concrete's chemistry and restore the passive layer.
- Evaluation of CP performance can be fulfilled by one of two criteria: either by showing that the potential is more negative than a threshold value versus a reference electrode, or by showing a polarization shift of 100 mV.
- Current requirements are not static and will vary with changes in temperature, moisture and chloride content.
- Most discussion around concrete CP is based on atmospherically exposed structures. The principles of CP in buried or submerged concrete are similar, but designs must recognize differences in resistivity, water saturation and oxygen availability.

6.0 References

1. Broomfield, J.P., *Corrosion of Steel in Concrete*. 2nd ed. 2007: Taylor & Francis.
2. *Guide to Protection of Reinforcing Steel in Concrete against Corrosion*. 2019, ACI.
3. Hu, J.Y., et al., *A review on corrosion detection and protection of existing reinforced concrete (RC) structures.* Construction and Building Materials, 2022. **325**.

4. *Electrochemical Realkalization of Steel-Reinforced Concrete— A State-of-the-Art Report*. 2020, NACE.
5. Broomfield, J.P., *A Historical Review of Impressed Current Cathodic Protection of Steel in Concrete.* Construction Materials, 2020. **1**(1): p. 1-21.
6. ISO, *Cathodic protection of steel in concrete*. 2022.
7. Angst, U.M., *A Critical Review of the Science and Engineering of Cathodic Protection of Steel in Soil and Concrete.* Corrosion, 2019. **75**(12): p. 1420-1433.
8. Sohanghpurwala, A.A., *Cathodic Protection for Life Extension of Existing Reinforced Concrete Bridge Elements*. National Academies of Sciences, Engineering, and Medicine. 2009, Washington, DC: The National Academies Press.
9. Bentur, A., S. Diamond, and N.S. Berke, *Steel Corrosion in Concrete: Fundamentals and Civil Engineering Practice*. 1st ed. 1997: Taylor & Francis.
10. Christodoulou, C., et al., *Diagnosing the cause of incipient anodes in repaired reinforced concrete structures.* Corrosion Science, 2013. **69**: p. 123-129.
11. Pedeferri, P., *Cathodic protection and cathodic prevention.* Construction and Building Materials, 1996. **10**(5): p. 391-402.
12. *Long-Term Effectiveness of Cathodic Protection Systems on Highway Structures*. 2001, Federal Highway Administration.
13. Christodoulou, C., et al., *Assessing the long term benefits of Impressed Current Cathodic Protection.* Corrosion Science, 2010. **52**(8): p. 2671-2679.
14. Cheaitani, A. and S. Cheytani, *New developments for corrosion protection of concrete structures in Australia.* MATEC Web of Conferences, 2019. **289**.
15. Brueckner, R., et al., *A review of developments in cathodic protection systems for reinforced concrete structures.* MATEC Web of Conferences, 2022. **361**.
16. Srinivasan, R., et al., *Design of Cathodic Protection of Rebars in Concrete Structures: An Electrochemical Engineering Approach.* 1996.
17. *Sacrificial Cathodic Protection of Reinforced Concrete Elements— A State-of-the-Art Report*. 2020, NACE.
18. AMPP, *Acceptance Criteria for Cathodic Protection of Steel in Concrete Structures*. 2023.
19. Koleva, D.A., et al., *Electrical resistivity and microstructural properties of concrete materials in conditions of current flow.* Cement and Concrete Composites, 2008. **30**(8): p. 731-744.
20. NACE, *Impressed Current Cathodic Protection of Reinforcing Steel in Atmospherically Exposed Concrete Structures*. 2019.
21. Broomfield, J.P. and J.S. Tinnea, *Cathodic Protection of Reinforced Concrete Bridge Components*. 1992, Strategic Highway Research Program: Washington, DC.
22. Troconis de Rincón, O., et al., *Galvanic Anodes for Reinforced Concrete Structures: A Review.* Corrosion, 2018. **74**(6): p. 715-723.
23. Stone, C., et al., *Case studies of hybrid and galvanic systems on bridge structures.* MATEC Web of Conferences, 2019. **289**.
24. Christodoulou, C. and R. Kilgour, *The world's first hybrid corrosion protection systems for prestressed concrete bridges.* 2013.
25. Krishnan, N., et al., *Hybrid Anodes for Accelerated Cathodic Protection of Corroding Concrete Structures.* Indian Concrete Journal, 2020.
26. Sergi, G., et al., *Long term control of corrosion of steel reinforcement by a two-stage cathodic protection method.* MATEC Web of Conferences, 2022. **361**.
27. NACE, *Cathodic Protection of Reinforcing Steel in Buried or Submerged Concrete Structures*. 2019.

28. Pedeferri, P., et al., *Cathodic protection and cathodic prevention in concrete: principles and applications.* Journal of Applied Electrochemistry, 1998. **28**: p. 1321-1331.
29. AMPP, *Galvanic Cathodic Protection of Reinforcing Steel in Atmospherically Exposed Concrete Structures*. 2023.

Distribution

em-labcall@em.doe.gov
ming.zhu@em.doe.gov)
Kalee.Fenker@em.doe.gov
justin_j_carter@orp.doe.gov
nicholas.machara@em.doe.gov
michelle.buchanan@science.doe.gov
john.vetrano@science.doe.gov
philip.wilk@science.doe.gov
bill.horak@hq.doe.gov
jenifer.shafer@hq.doe.gov
robert.ledoux@hq.doe.gov
christopher.crowley@em.doe.gov
rodrigo.rimando@em.doe.gov
john.moon@em.doe.gov
pavan.shukla@srnl.doe.gov
bruce.wiersma@srnl.doe.gov
alex.cozzi@srnl.doe.gov
joseph.manna@srnl.doe.gov
connie.herman@srnl.doe.gov
eric.skidmore@srnl.doe.gov
Richard.wyrwas@srnl.doe.gov
crystal_l_girardot@rl.gov
jason_s_page@rl.gov
michael.stone@srnl.doe.gov
Records Administration (EDWS)
robert_j_nelson@rl.gov
shawn_t_campbell@rl.gov
jason_r_gunter@rl.gov
kayle_d_boomer@rl.gov
melinda_r_fagundes@rl.gov

Savannah River National Laboratory®

We put science to work.™

Developing Cathodic Protection System for Underground Double Shell Storage Tanks

H2C Tank and Pipeline Integrity Program

SRNL-STI-2025-00209

Benjamin Barkai, Pavan Shukla, Andrew Nordquist, and Bruce Wiersma

Tank Integrity Expert Panel Corrosion Subgroup Meeting, April 10-11, 2025, Nashville, TN

Agenda

- Background
- Construction Details
- Resistivity Survey
- Existing CP
- Finite-Element Modeling
- Summary and Path Forward

Hanford DSTs

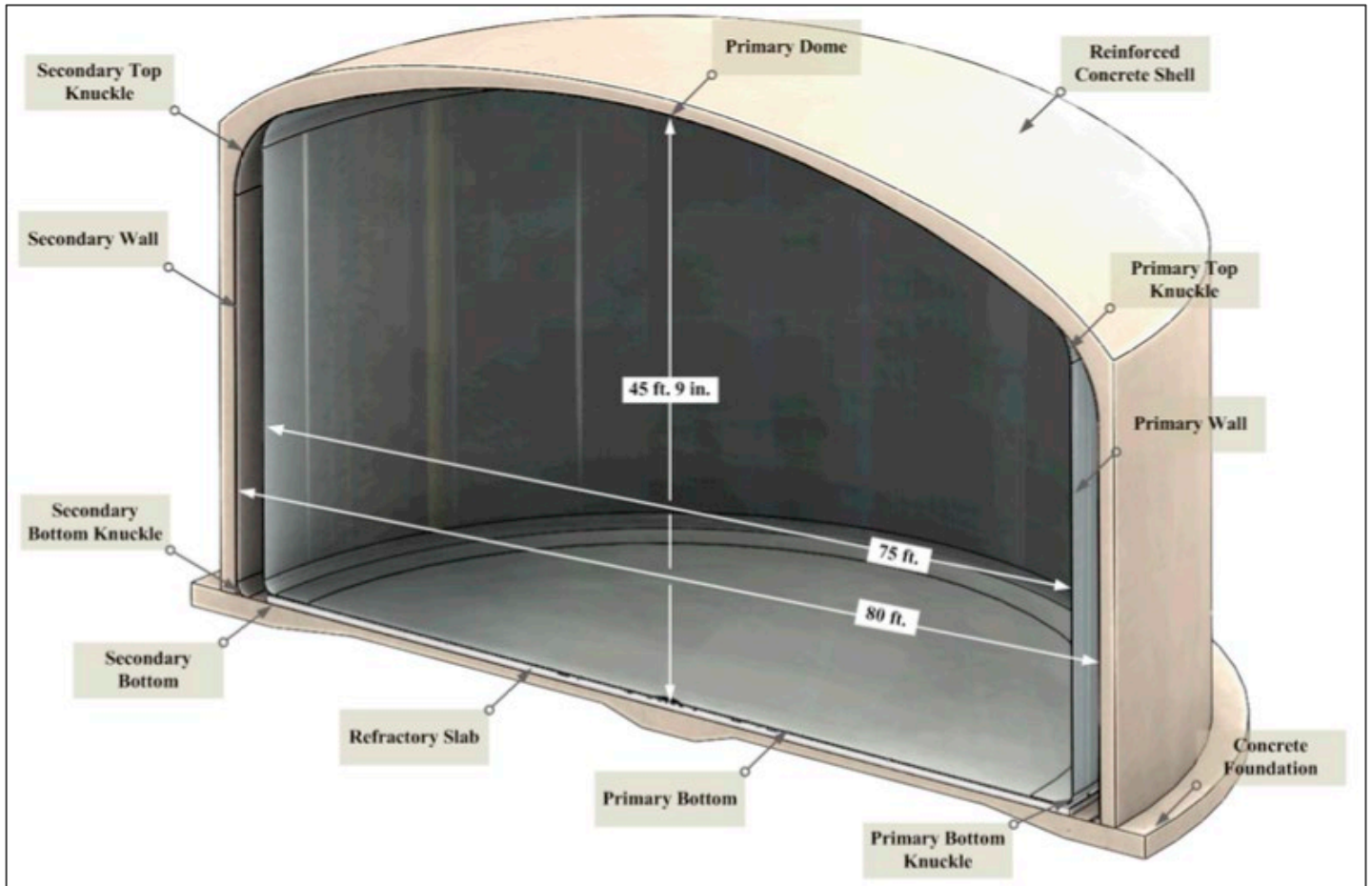

Figure A-2. Cross-Sectional Drawing of a Typical Double-Shell Tank

History

Table A-1. Double-Shell Tank Construction Details and Age as of 2024

Tank Farm	Number of Tanks	Construction Period	Construction Project	Year put into Service	Service Life	Current Age
AY	1	1968–1970	IAP-614	1971	40	53
AZ	2	1970–1974	HAP-647	1976	40[a]	48
SY	3	1974–1976	B-101	1977	50	47
AW	6	1976–1979	B-120	1980	50	44
AN	7	1977–1980	B-130, B-170	1981	50	43
AP	8	1982–1986	B-340	1986	50	38

[a]Determined in the 2006 IQRPE assessment to be equivalent to that of 241-AY tank farm (RPP-28538)

Corrosion of Hanford Tanks

- Degradation of Hanford components, including primary liners, secondary liners, and pipelines, can occur by several ways (RPP-PLAN-65866).
  1. Thinning of the steel walls by general corrosion (structural failure)
  2. Pitting of the walls (leaks)
  3. SCC and fatigue-induced flaw growth (leaks)
  4. LAI corrosion (accelerated thinning; pitting of walls)
- Ultrasonic testing (UT) of annulus floors has revealed troubling reduction in liner thickness.
  - Moisture accumulation is believed to be a culprit.

Thinning of DST Liner

Secondary Liner Ultrasonic Inspection Data			
DST	Year	Maximum Thinning (percent)	Area Examined (ft^2)
AN-101	2022	46.6	50
AN-102	2019	17.8	50
AN-103	2015	23.8	65
AN-104	2015	39.6	65
AN-105	1999	0.2	10
	2006	3.6	10
	2016	29.8	62
AN-106	2017	9.6	60
AN-107	1999	10.0	8
	2022	18.8	50
AP-101	2023	10.8	50
AP-102	2014	70.2	52
	2019	71.6	100
AP-103	2021	10.0	50
AP-105	2022	14	50
AP-106	2014	2.2	9.8
	2019	15.8	53
AP-107	2019	13.0	64
AP-108	2019	10.8	51

Objectives

- CorrPro
  - Develop closed-couple design for protection of DST exteriors
  - Conduct CP survey of a Hanford Tank Farm Facility
- Finite Element Expert
  - Develop finite element model for existing and newly designed CP systems
  - Develop a large-scale model for existing and newly designed CP systems.
- SRNL
  - Review design and develop an implementation plan for CP system.
  - Review large-scale model with industry expert.
  - Provide WRPS with an implementation plan for the individual tanks.

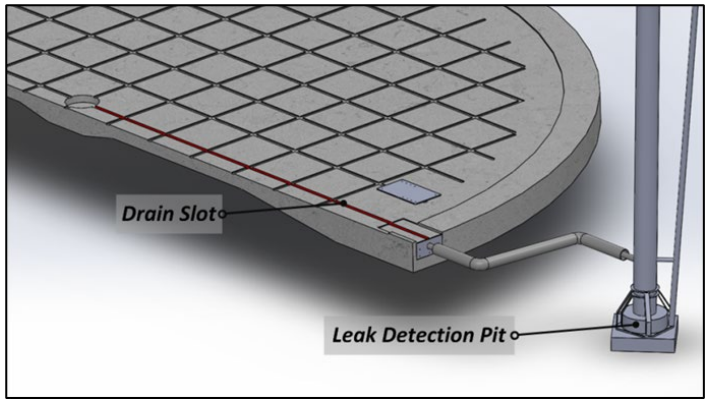

AP Tank Wall Configuration (RPP-RPT-55983)

- Youngest tank farm. Similar in construction to AN tank farms.
  - 8 DSTs total.

Table 3-1. Materials Comparison

Material	241-AY Tank Farm	241-AP Tank Farm
Concrete	3000 psi Type V for the walls Type III for the haunch and dome	4500 psi Type II for the foundations 5000 psi Type II for the walls, domes, and haunches
Reinforcing Bar	ASTM A432 for the walls, dome and haunch ASTM A15 for the foundation	A615, Grade 60, except #3 ties shall be Grade 40
Steel Plate	ASTM A515-65	ASTM A537-79, Class 1

AP Cement conformed to ASTM C150. General use with moderate sulfate resistance

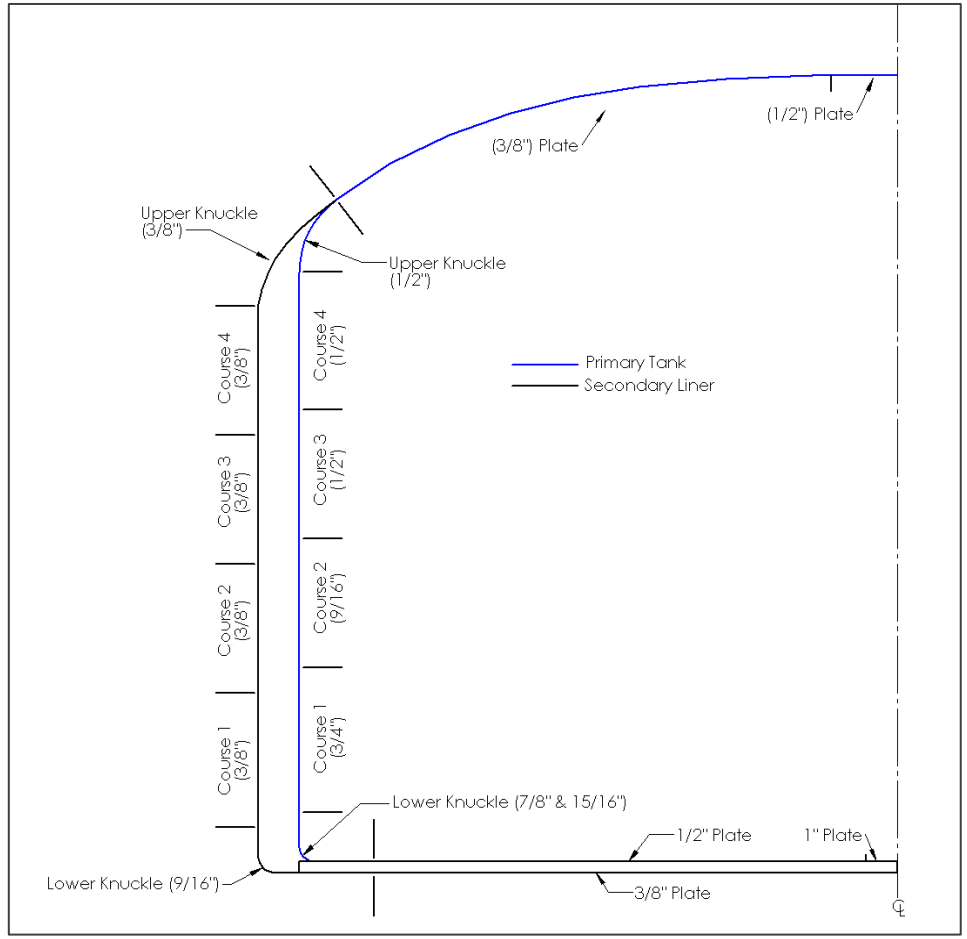

AP Concrete Shell (RPP-RPT-55983)

- Rebar was installed around the tank/dome before concrete was poured.
  - Secondary liner acted as the inner concrete form.
- Shell is about 1.5 feet thick. Rests on a slide and bearing plate supported by the foundation.

AP Reinforced Concrete Foundation (H-2-90439)

- Two rebar layers are installed.
  - Different rebar sizes are used depending on distance from center.
  - Central region – net formation
- Foundation thickness is not uniform, outer edges have an 8-in drop-off, creating a shoulder to resist lateral displacement caused by soil pressure.

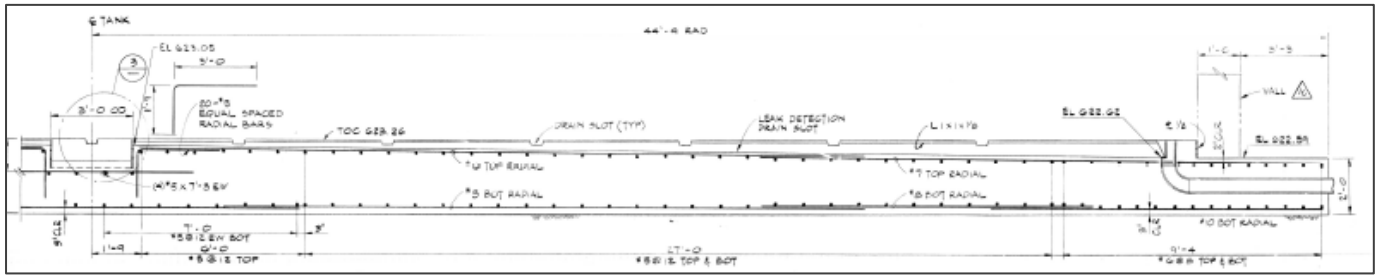

Rebar cross-sectional area represented by dots

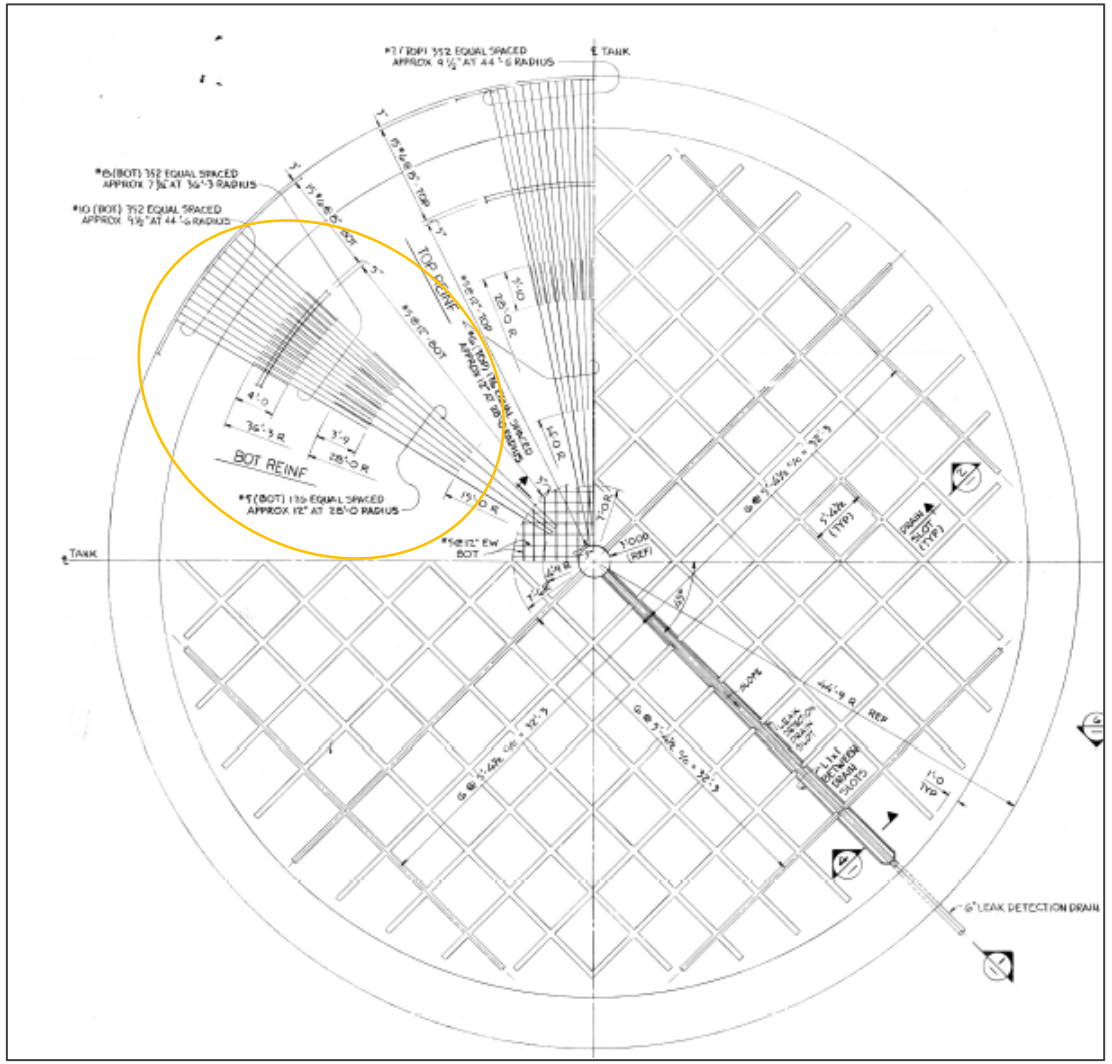

AP Concrete Dome (H-2-90441)

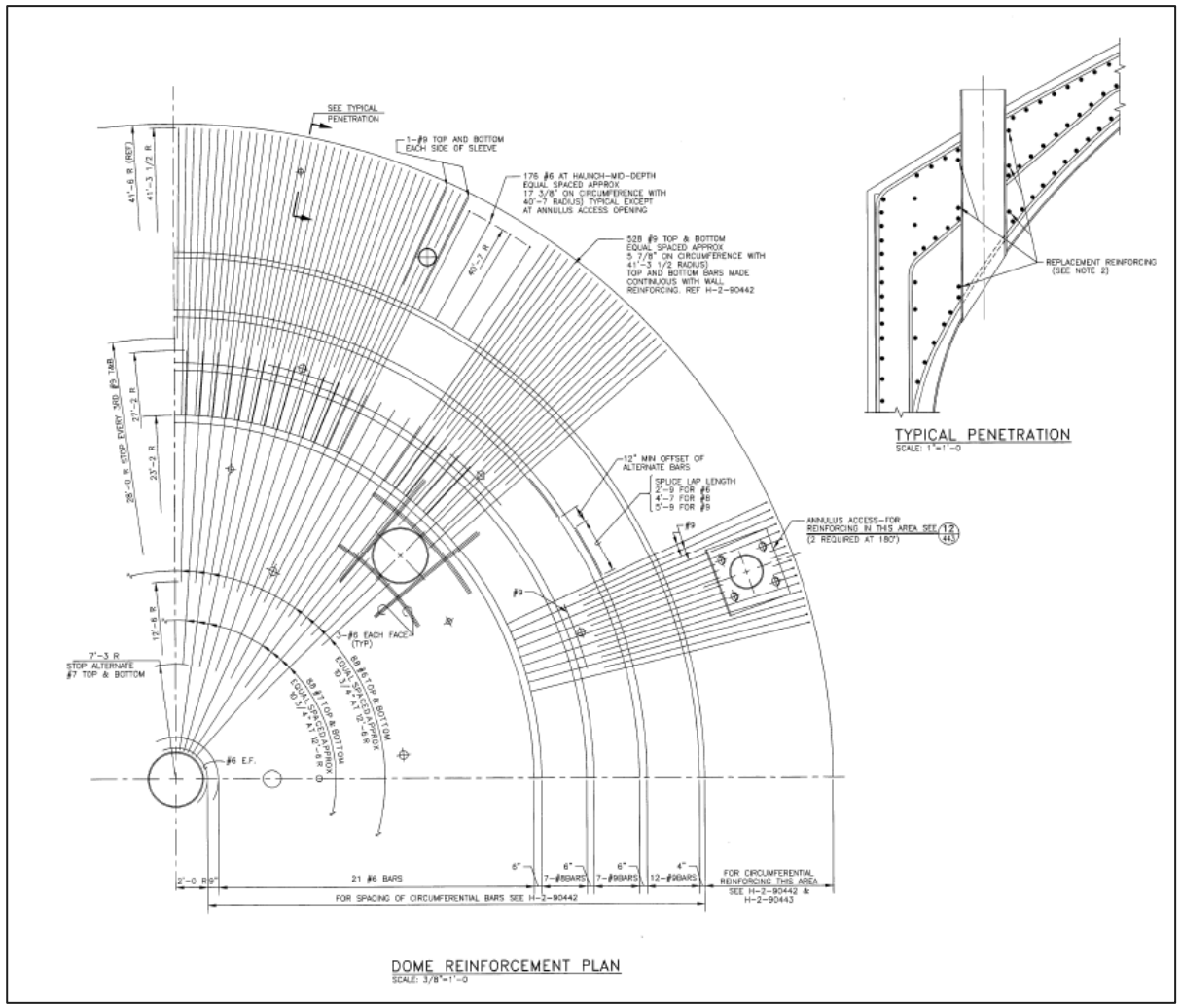

AP Concrete Specs (B-340)

Foundation (B-340-C3)

PART 2 - PRODUCTS

2.1 CONCRETE

2.1.1 Cement: ASTM C 150, Type II (Low Alkali)

2.1.2 Aggregates: ASTM C 33, maximum size 1-1/2 inch

2.1.3 Air-Entraining Admixture, Conforming to ASTM C 260: Sika Chemical Company "SIKA AER", Chem-Masters Corp "Adz-Air" or Protex Industries "Protex".

2.1.4 Properties

2.1.4.1 Minimum allowable compressive strength: 4500 psi at 28 days.

2.1.4.2 Slump: 4 inch maximum in accordance with ACI 301, Section 3.5.

2.1.4.3 Air content: In accordance with ACI 301, Table 3.4.1.

2.1.4.4 Proportions: In accordance with ACI 301, Section 3.8, Method 2.

2.1.5 Mixing: In accordance with ASTM C 94.

Concrete Shell construction specifications are found in B-340-C5

AN Tank Wall Configuration (RPP-RPT-55982)

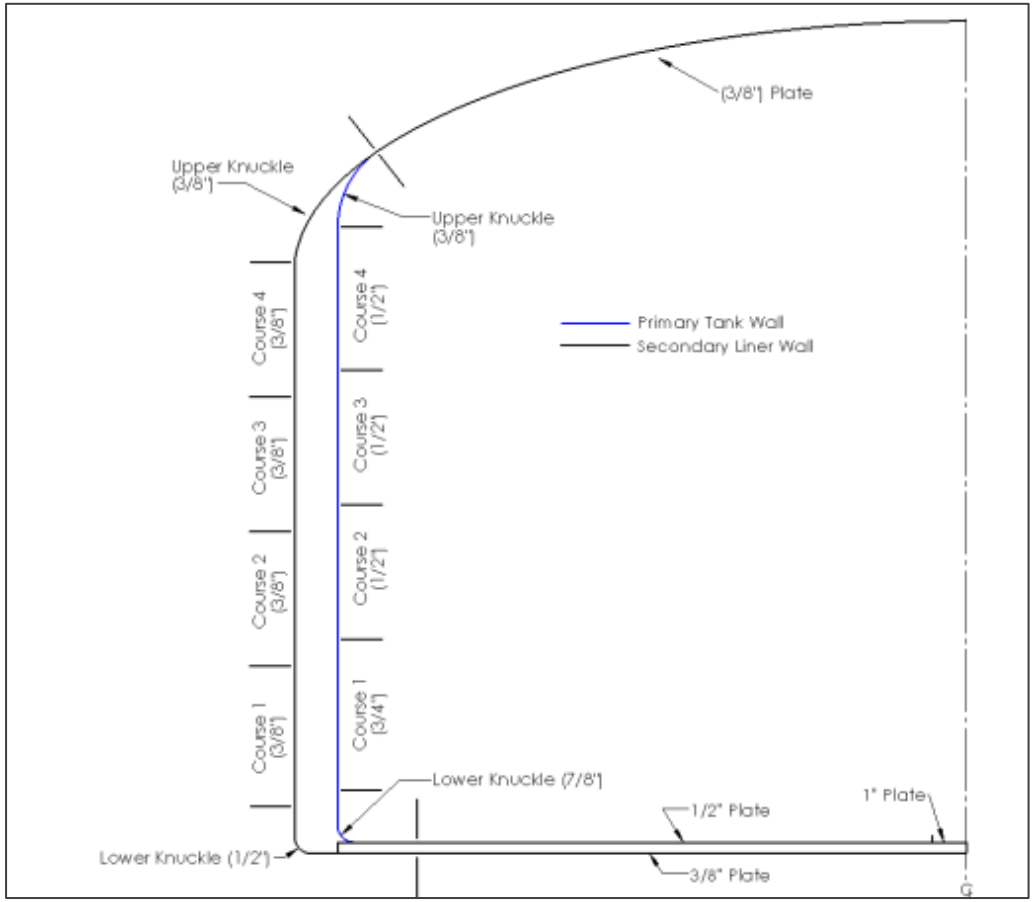

AN Tank Geometry

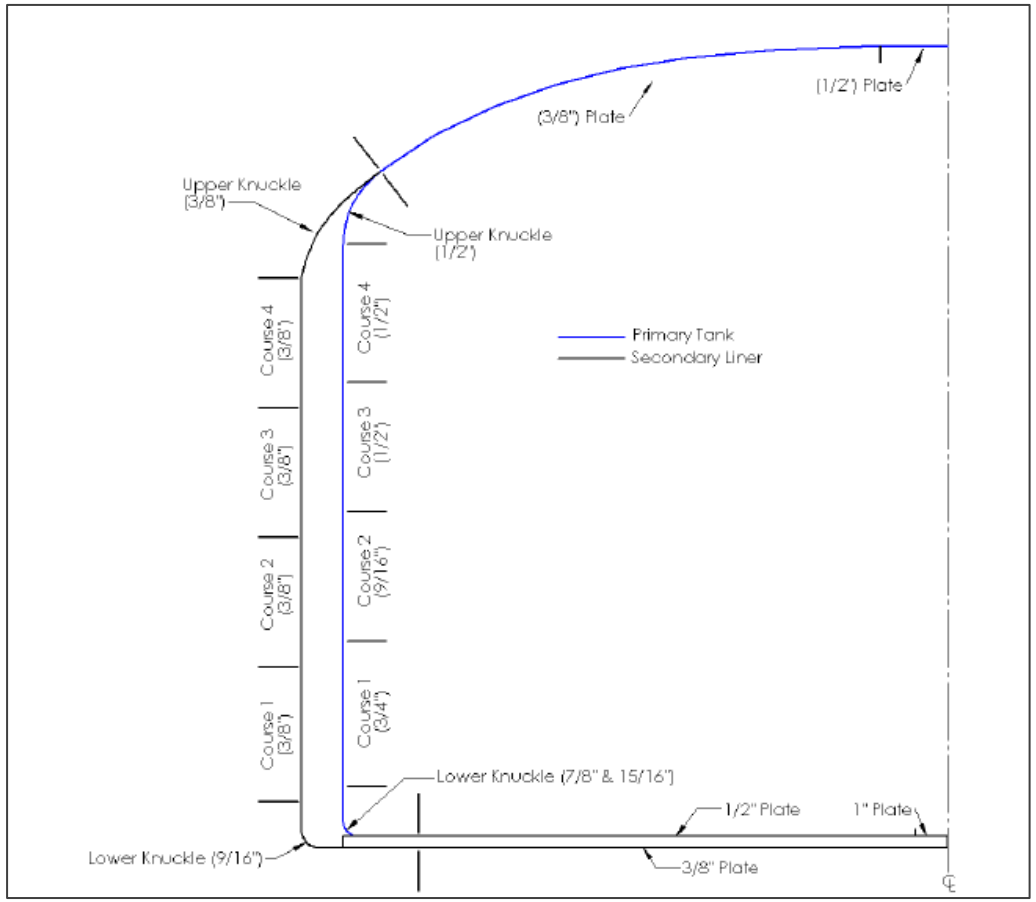

AP Tank Geometry

AN Tank Wall Configuration (RPP-RPT-55982)

Material	241-AY Tank Farm	241-AN Tank Farm
Concrete	3000 psi Type V for the walls Type III for the haunch and dome	4500 psi Type II for the foundations 5000 psi Type II for the walls, domes, and haunches
Reinforcing Bar	ASTM A432 for the walls, dome and haunch ASTM A15 for the foundation	A615, Grade 60, except #3 ties shall be Grade 40
Steel Plate	ASTM A515-65	ASTM A537-75, Class 1

Material	241-AY Tank Farm	241-AP Tank Farm
Concrete	3000 psi Type V for the walls Type III for the haunch and dome	4500 psi Type II for the foundations 5000 psi Type II for the walls, domes, and haunches
Reinforcing Bar	ASTM A432 for the walls, dome and haunch ASTM A15 for the foundation	A615, Grade 60, except #3 ties shall be Grade 40
Steel Plate	ASTM A515-65	ASTM A537-79, Class 1

Material selection for both tank farms were identical.

AZ Tank Farm (RPP-RPT-54818)

- One of the oldest farms, design similar to AY tanks.
  - Only two DSTs exist
  - Material choices are closer to the AY farms than the AP/AN farms, but the general design is similar.

Material	Tank Farm	
	241-AY	241-AZ
Concrete	3000 psi Type V for the walls; Type III for the upper haunch and dome	3000 psi Type V for the walls; Type III for the upper haunch and dome
Reinforcing Bar	A432	A615-60
Steel Plate	ASTM A515-65	ASTM A515-69

ASTM C150. Type III is high early strength cement. Type V is high sulfate resistant cement.

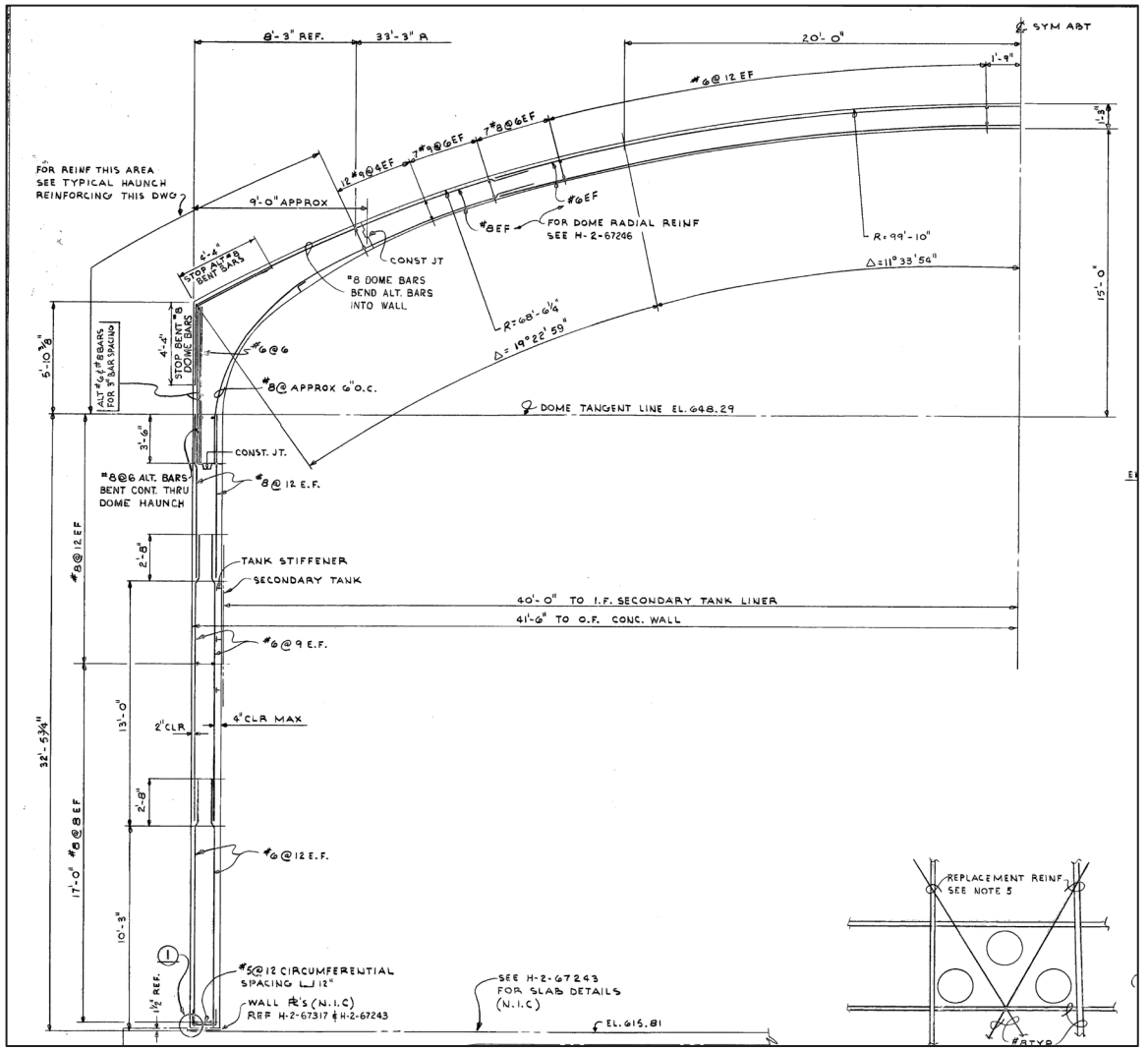

AZ Foundation (RPP-RPT-54818)

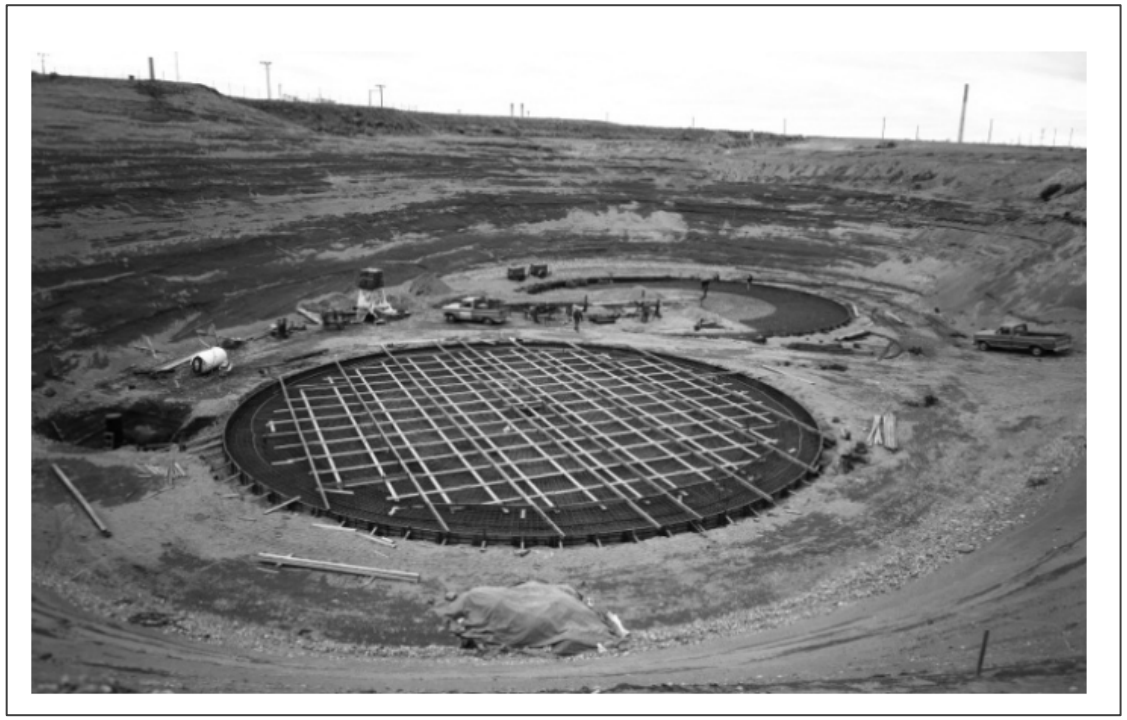

AZ Foundation (RPP-RPT-54818)

- Two rebar layers are installed.
  - Different rebar sizes are used depending on distance from center.
  - Central region – net formation
- Foundation thickness is not uniform, outer edges have an 8-in drop-off, creating a shoulder to resist lateral displacement caused by soil pressure.

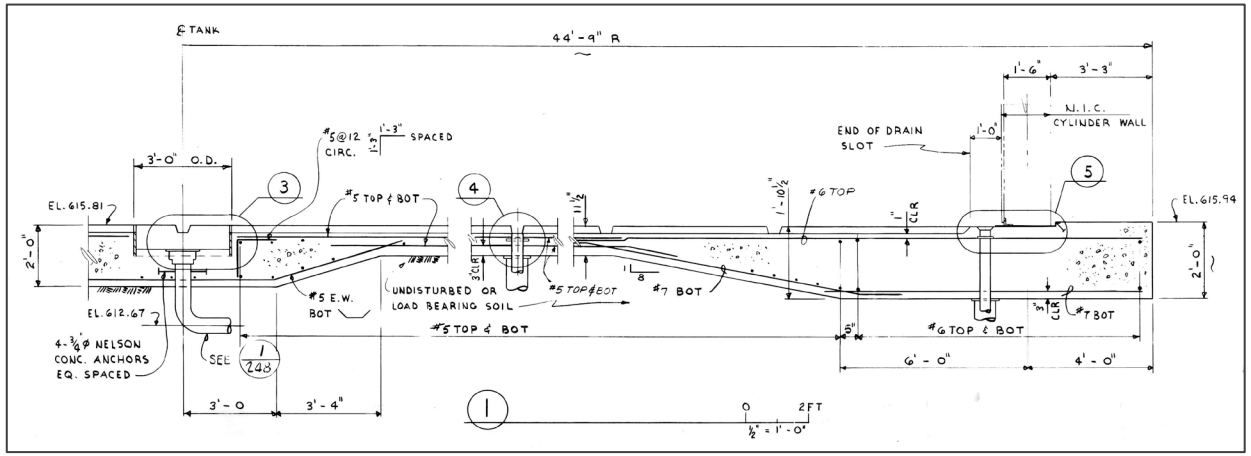

Change in thickness starts to occur about 6.5 ft from the center

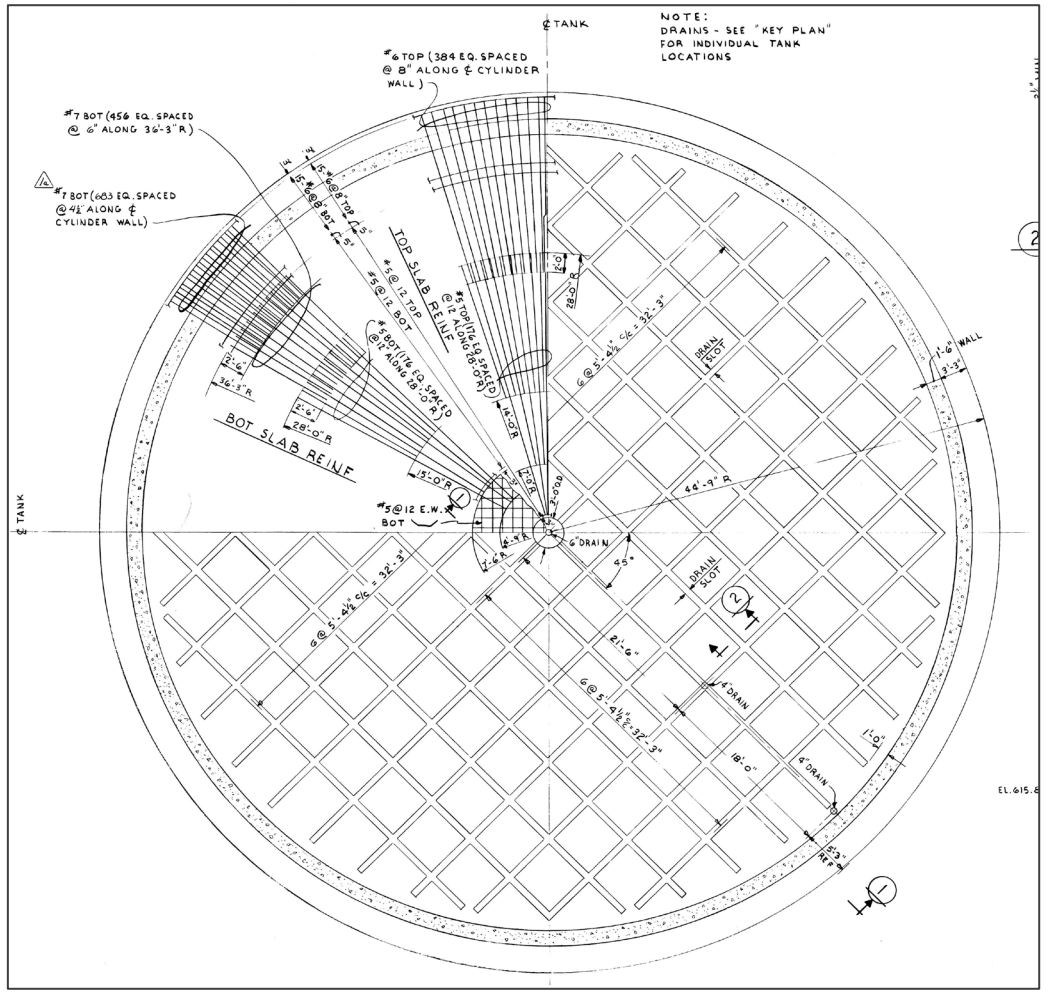

AZ Haunches (H-2-67425)

GENERAL NOTES:

1. ALL CONCRETE TO HAVE 3000 PSI COMPRESSIVE STRENGTH AT 28 DAYS.
2. REINFORCING STEEL SHALL HAVE A MINIMUM YIELD STRENGTH OF 60,000 PSI AND SHALL CONFORM TO ASTM A-615 SPECIFICATION FOR DEFORMED BILLET STEEL BAR FOR CONCRETE REINFORCEMENT WITH 60,000 PSI MINIMUM YIELD STRENGTH.
3. BAR SPLICES AND BENDS PER ACI 318-63.
4. ALL CIRCUMFERENTIAL REINFORCING IN DOME HAUNCH SPACED LESS THAN 6" O.C. SHALL BE MADE CONTINUOUS BY BUTT WELDING EXCEPT AS NOTED. ALL RADIAL REINFORCING IN DOME HAUNCH SHALL BE MADE CONTINUOUS BY BUTT WELDING EXCEPT AS NOTED.
5. WALL REINFORCEMENT INTERRUPTED BY PENETRATIONS SHALL BE REPLACED BY AN EQUIVALENT AREA OF REINFORCEMENT AND SHALL HAVE A MINIMUM LAP OF 30 DIAMETERS. SEE H-2-67314, H-2-67315 & H-2-67316 FOR WALL PENETRATIONS.

GENERAL NOTES: (CONTINUED)

6. CONCRETE PROTECTION FOR REINFORCING UNLESS OTHERWISE NOTED SHALL BE:

FOOTINGS:		3" CLEAR - BOTTOM & SIDES
WALLS & SLABS:	FACES EXPOSED TO EARTH OR WEATHER:	2" CLEAR #6 & OVER
		1-1/2" CLEAR #5 & UNDER
	INTERIOR OR UNEXPOSED FACES:	3/4" CLEAR
BEAMS - COLUMNS - GIRDERS:		1-1/2" CLEAR TO TIES, STIRRUPS, OR SPIRALS.

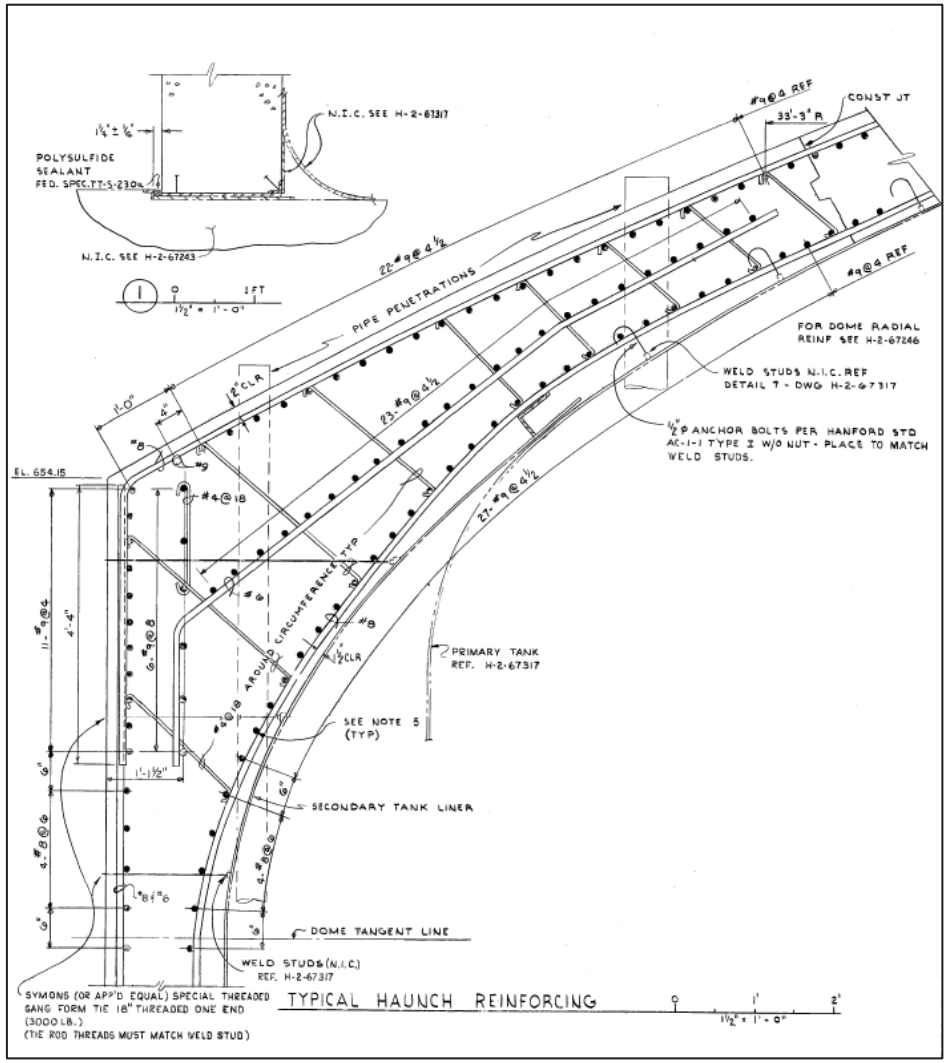

AN/AP/AZ Steel Comparison

Feature	AP	AN	AZ
Tank Foundation	A615 Grade 60 (#5 - #8, #10)	A615 Grade 60 (#5, #6, #8, #10)	A615 Grade 60 (#5-#7)
Wall/Domes	A615 Grade 60 (#6 - #10)	A615 Grade 60 (#4, #6, #9, #10)	A615 Grade 60 (#4, #6, #8, #9)
Secondary Plates	A537-79 3/8" thick	A537-75 3/8" thick	A515-69 3/8" thick

Primary Tank					
	Tank Bottom	Tank Lower Knuckle	Tank Wall	Tank Upper Knuckle	Tank Dome
AY	3/8 in. and 1 in.	7/8 in.	3/4 in. and 1/2 in.	3/8 in.	3/8 in. and 1/2 in.
AZ	1/2 in. and 1 in.	7/8 in.	3/4 in. and 1/2 in.	3/8 in.	3/8 in. and 1/2 in.
SY	1/2 in. and 1 in.	7/8 in.	3/4 in. and 1/2 in.	3/8 in.	3/8 in. and 1/2 in.
AW	1/2 in. and 1 in.	7/8 in.	3/4 in. and 1/2 in.	3/8 in.	3/8 in. and 1/2 in.
AN	1/2 in. and 1 in.	7/8 in.	3/4 in. and 1/2 in.	3/8 in.	3/8 in. and 1/2 in.
AP	7/8 in., 1/2 in., and 1 in.	15/16 in.	7/8 in., 9/16 in., 3/4 in. and 1/2 in.	1/2 in.	3/8 in. and 1/2 in.

Secondary Liner				
	Liner Bottom	Liner Lower Knuckle	Liner Wall	Liner Upper Knuckle
AY	1/4 in.	1/4 in.	1/4 in.	3/8 in.
AZ	3/8 in.	1/2 in.	3/8 in.	3/8 in.
SY	3/8 in.	1/2 in.	3/8 in.	3/8 in.
AW	3/8 in.	1/2 in.	3/8 in.	3/8 in.
AN	3/8 in.	1/2 in.	3/8 in.	3/8 in.
AP	3/8 in.	9/16 in.	3/8 in. and 1/2 in.	3/8 in.

Evaluation of Soil Corrosion/HW-33911 (1955)

- Soils across Hanford vary in physical characteristics, but chemical content and resistivities are similar (HW-33911).
- Soil Survey of Benton County, A.E. Kocher, Bureau of Soils, 1916
  - 200W – Soil make-up is 40% Ephrata **sandy loam** and 60% Winchester **fine sand.**
  - 200E – Soil make-up is 15% Ephrata **sandy loam**, 20% Ephrata **fine sandy loam**, 65% Winchester **fine sand.**
- HW investigation compared Hanford soil corrosivity to soil properties compiled by the National Bureau of Standards (NBS)
- Report conclusions state that **all stainless-steel buried installations should use CP**. Avoid using minerals that could decrease resistivity of surrounding soil to below 1500 ohm-cm.

Hanford Soil Properties (1955)

Fine sandy loam
-
-
Sandy loam
Fine sand

TABLE III

CHEMICAL PROPERTIES OF SOILS AT THE HANFORD PLANT

Soil Location*	pH	Total Acidity Mg-eq per 100 g of Soil	Resist-ivity at 60°F	Composition of Water Extract - Mg-eq/100 g of Soil							Soil Sample Number*
				Na+K as Na	Ca	Mg	CO_3	HCO_3	Cl	SO_4	
183-F	8.4	0.50	3000 to >100,000	0.21	0.08	0.09	<0.01	0.50	0.02	0.08	29
181-F	7.8	0.54	1500 to 44,000	0.41	0.05	0.22	<0.01	2.20	0.01	0.15	28
184-B	7.4	0.66	12,000	0.12	0.20	0.15	<0.01	2.30	0.01	0.02	21
183-B	8.1	1.28	6,300	0.32	0.01	0.12	<0.01	5.00	<0.01	0.15	22
241-A	8.6	0.60	4,500	0.38	0.01	0.12	<0.01	1.30	0.02	0.10	16A
Average Hanford Soil**	8.2	0.65	5,000	0.35	0.08	0.15	<0.01	2.00	0.01	0.10	

*See Table II for detailed location.
**Estimated from above data and miscellaneous unrecorded observations.

*Hanford soils **as a whole** are somewhat higher in solubles/alkalies than the NBS soils. Slight increase in corrosion risk.*

Comparison to NBS Soil (1955)

TABLE IV

CHEMICAL PROPERTIES OF SELECTED SOILS AT NBS TEST SITES COMPARED WITH TYPICAL HANFORD SOIL

NBS Soil No.	pH	Total Acidity Mg-eq per 100 g of Soil	Resist-ivity at 60°F	Composition of Water Extract - Mg-eq/100 g of Soil						
				Na+K as Na	Ca	Mg	CO_3	HCO_3	Cl	SO_4
12	7.1	2.5	3,190	0.39	0.50	0.16	<0.01	0.40	<0.01	0.14
20	7.5	1.5	2,870	0.25	0.48	0.20	<0.01	0.51	<0.01	0.15
26	7.3	2.6	2,980	0.27	0.50	0.31	<0.01	0.70	<0.03	0.12
32	7.3	0.5	5,700	0.23	0.70	0.12	<0.01	0.73	0.01	0.42
47	7.6	3.0	1,770	0.67	0.72	0.39	<0.01	0.88	0.06	0.48
Hanford Soil	8.2	0.65	5,000	0.35	0.08	0.15	<0.01	2.00	0.01	0.10

Comparison to NBS Soil (1955)

TABLE VI

CALCULATED DATA ON PIT DEPTHS AND LEAKS ON A CARBON STEEL PIPELINE

Length of Unit Section 1000 Ft, Dia of Pipe 8.625"
Thickness of Pipe Wall 322 Mils

Soil	Deepest Pit in 30 Years	Standard Error	Length of Pipe Per Puncture in 30 Yrs	Time for Puncture Per 1000' of Pipe	Remarks
12	215	284	1.7×10^4	670 Yr	Poorly Aerated
20	371	120	4.7×10^2	22 Yr	Poorly Aerated
26	262	125	5.5×10^3	49 Yr	Good Drainage
32	330	120	8.6×10^2	28 Yr	Good Drainage
47	270	84	2.1×10^3	54 Yr	Poorly Aerated
Highly Alkaline Reducing Soil	863	334	0.8	4 Yr	For Comparison
Neutral Leached Soil	75	20	2.4×10^7	∞	For Comparison
Hanford Plant	350	150	1×10^3	25 Yr	Estimated from Local Observations

A COMPARISON OF CORROSION RATES OF NBS SOILS ON VARIOUS MATERIALS WITH TYPICAL HANFORD SOIL

(10 to 12 Year Exposure)	Soil Type 12	20	26	32	47	Hanford*
Mild-Steel - Wrought Pipe Maximum Penetration - Mils	80	70	45	90	26	90
Galvanized Pipe - Weight Loss in oz/ft^2	0.40**	1.22	0.71	0.61	1.06	1.5
Commercial Lead Pipe Maximum Penetration - Mils	43	51	29	18	30	60

* Values in this column approximate, based on observations. See Table III.
** Only sheet samples available.

NBS data are based on small coupons. In practice, buried steel may experience pitting rates faster than listed due to oxygen depleted conditions.

Resistivity

- Soil resistivity may be measured to detect contaminants/leaks from tanks.
  - Soil surveys have been performed on SSTs to find anomalous patches of low resistivity/flow of contaminants through vadose region of soil.
  - DST farms were not the focus of investigations
- An early 1970s analysis on resistivity leak detection measured Hanford soil in an unspecified area (ARH-ST-127).
  - Hanford soil samples were tested for electrical conduction. Two samples were measured both wet & dry. A third sample, retrieved via dry suction, was measured as is.
  - No information over the location of origin of these samples. Implied to have been sampled in a pristine area.

TABLE A-I

HANFORD SOIL RESISTIVITY

Sample No.	Characteristic	Condition	Resistivity ohm-cm
1	Fine sand	Dry	5.5×10^6
1	Fine sand	+ 5% H_2O	2.8×10^4
2	Coarse sand	Dry	1.3×10^5
2	Coarse sand	+ 5% H_2O	4.4×10^3
3	Test site soil	As-received	1.0×10^5

CP System Experience (1992) (WHC-SA-0648-FP)

- 1950 Presentation by FJ Mollerus to American Institute of Electrical Engineering.
  - Underground stainless steel installations should be avoided due to pitting.
  - External voltage between sacrificial anode and steel (impressed current) provides absolute protection against corrosion.
- GU Udine (1952) published similar findings
  - Several Hanford waste lines failed before 1947.
  - External galvanic action caused failures.
  - Galvanic corrosion eliminated through application of CP.

CP System Experience (1992) (WHC-SA-0648-FP)

- CP used on underground waste lines for 40 years (1952)
- Original corrosion of 347 stainless steel pipes was caused by sulfuric acid produced by bacteria.
- CP system had successfully protected waste lines form leaks from 1947-1980. Post-1980, a newer version was installed and the older system in 200E and W was shut off.
  - Report document describes differences in both systems
- New CP system has 35 rectifiers, 1418 anodes, 529 test stations between East & West.
  - Old system used railroad rails/scrap iron anodes with salt-mixed backfills to improve conductivity. Annual inspections were performed.
- **CP system protects the underground piping ONLY, not the underground tanks.**

CP System Experience (1992) (WHC-SA-0648-FP)

- Hanford has a CP expert in house, with the NACE specialist responsible for the system.
- Test stations are located underground beneath a manhole cover so to not impede traffic.
- Single NACE acceptance criterion was adopted by Hanford site (-0.85 VCSE).
  - However, presence of concrete may require a separate criterion (100 mV shift).
- All underground ventilation lines are cathodically protected after early failures were experienced.

1997 Annual CP Survey Report (HNF-3379)

- Voltage data and continuity measurements of test stations at several areas:
  a) 242-A evaporator
  b) A-Farm, near valve pits
  c) AW-Farm, near AW valve pits, AW-101 and AW-102
- Operating criteria was evaluated using NACE "Corrosion Control of Underground Storage Tank Systems by Cathodic Protection".
  - Pipe-to-soil potential at least -0.85 V
  - 100 mV polarization difference.
- Rectifier spreadsheet data is provided in the report.
- Anodes are described as being high silicon, chromium iron material with a copper lead wire. Prepackaged in steel canisters with coke breeze backfill.

1997 Annual CP Survey Report (HNF-3379)

- A-Farm Valve Pit Area Test Stations
  - “Rectifier 18” system contributed the most to polarization, running at 19.3 amps (nameplate = 40 amps).
- AW-Farm
  - “Rectifier 19” system was running at 5.5 amps (nameplate = 12 amps).
- Evaporator Area
  - “Rectifier 18” (nameplate = 40 amps) and “Rectifier R1” (nameplate = 60 amps) were each running at ~20 amps.
- Test station data showed that many underground pipes had been polarized to values greater than NACE standard.
- If unprotected piping are not connected to the CP rectifier system, piping may draw stray currents and discharge.
- Resistance measurements at test stations can show if a piping is not connected to the rectifier.
  - Evaporator property had piping with resistance values in the Mohms. Polarization testing of piping also gave poor values. Note that these pipes were not designed for protection.

1997 Annual CP Survey Report (HNF-3379)

- Conclusions
  - All piping originating on evaporator property and A-Farm is protected by NACE/WAC standards.
  - Piping SN-650 originating from AP-Farm is protected by NACE/WAC standards.
  - All piping entering AW-Farm from the evaporator is protected.
  - Some piping were identified in the ionic current path from the underground anodes that were not bonded to the rectifiers, or were bonded but showed high resistance values.
    - Recommended to bond the stray piping to their respective test stations.

1997 Annual CP Survey Report (HNF-3379)

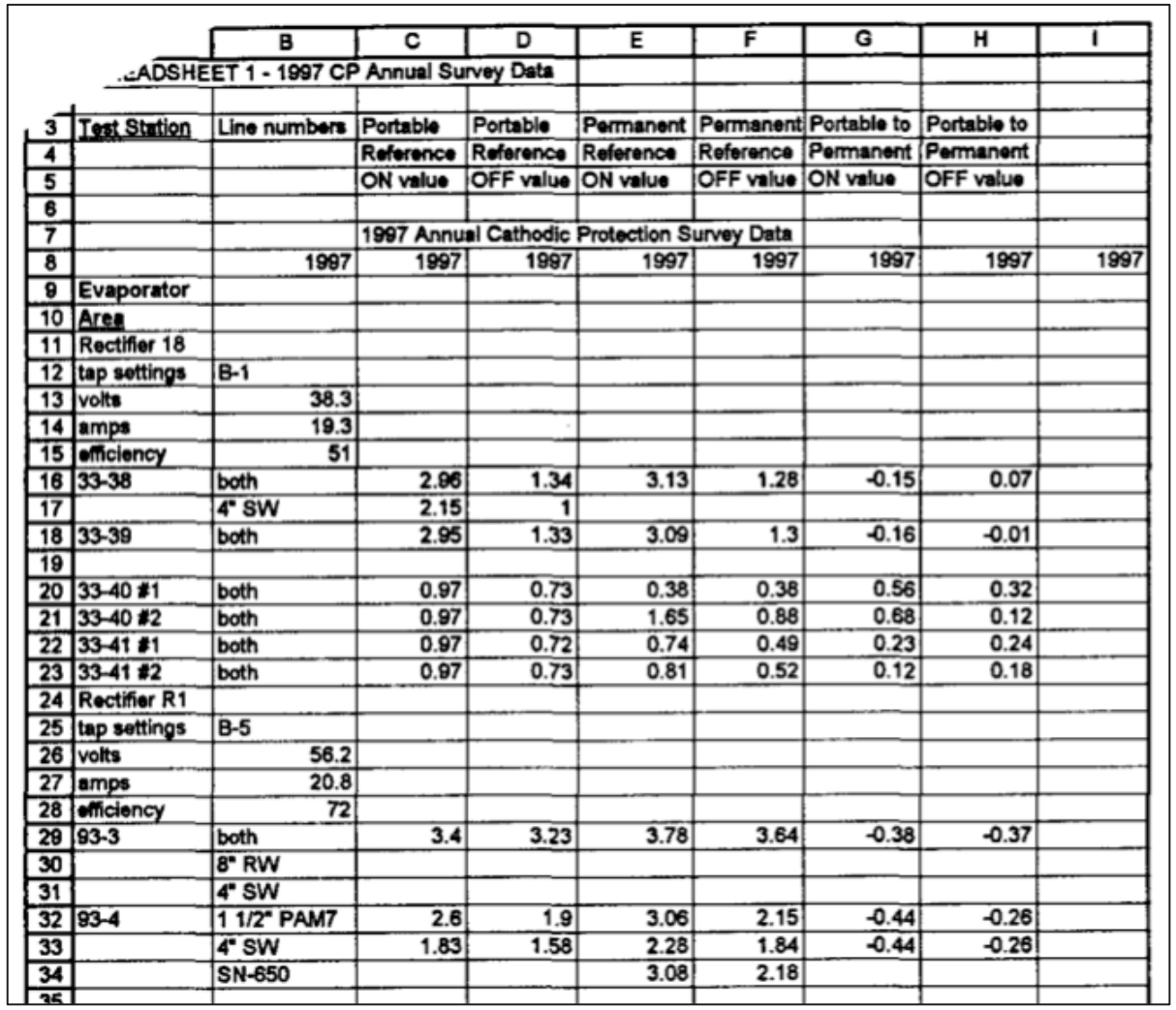

	B	C	D	E	F	G	H	I
	ADSHEET 1 - 1997 CP Annual Survey Data							
3	Test Station	Line numbers	Portable	Portable	Permanent	Permanent	Portable to	Portable to	
4			Reference	Reference	Reference	Reference	Permanent	Permanent	
5			ON value	OFF value	ON value	OFF value	ON value	OFF value	
6									
7			1997 Annual Cathodic Protection Survey Data						
8		1997	1997	1997	1997	1997	1997	1997	1997
9	Evaporator								
10	Area								
11	Rectifier 18								
12	tap settings	B-1							
13	volts	38.3							
14	amps	19.3							
15	efficiency	51							
16	33-38	both	2.96	1.34	3.13	1.28	-0.15	0.07	
17		4" SW	2.15	1					
18	33-39	both	2.95	1.33	3.09	1.3	-0.16	-0.01	
19									
20	33-40 #1	both	0.97	0.73	0.38	0.38	0.56	0.32	
21	33-40 #2	both	0.97	0.73	1.65	0.88	0.68	0.12	
22	33-41 #1	both	0.97	0.72	0.74	0.49	0.23	0.24	
23	33-41 #2	both	0.97	0.73	0.81	0.52	0.12	0.18	
24	Rectifier R1								
25	tap settings	B-5							
26	volts	56.2							
27	amps	20.8							
28	efficiency	72							
29	93-3	both	3.4	3.23	3.78	3.64	-0.38	-0.37	
30		8" RW							
31		4" SW							
32	93-4	1 1/2" PAM7	2.6	1.9	3.06	2.15	-0.44	-0.26	
33		4" SW	1.83	1.58	2.28	1.84	-0.44	-0.26	
34		SN-650			3.08	2.18			
35									

Example of spreadsheet data. Other rectifiers surveyed. Data exists for 1994 through 1997.

1997 Annual CP Survey Report (HNF-3379)

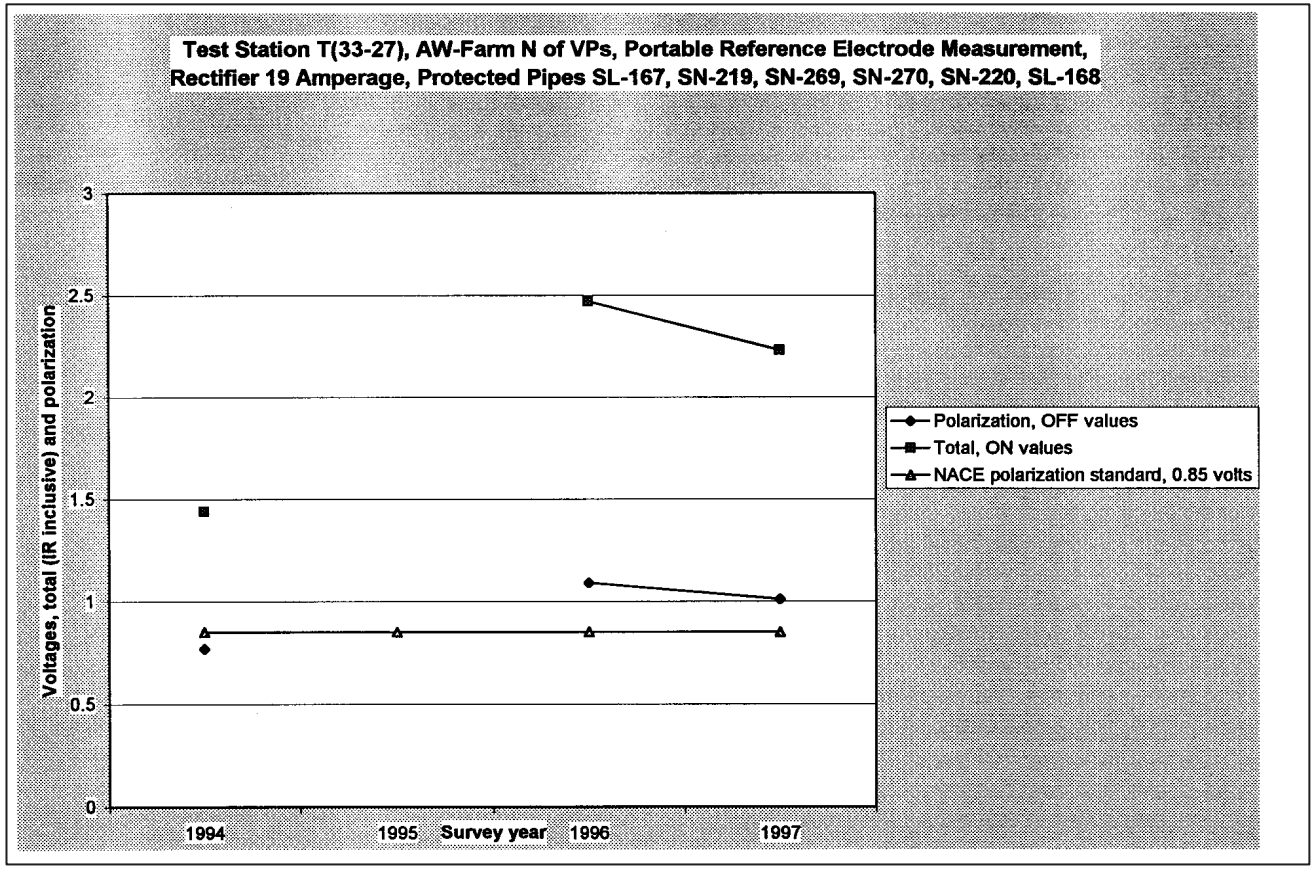

Sample plot of reference electrode data at a test station.

1999 Annual Cathodic Protection Survey Report (HNF-7099)

- Data for PFP property.
- Resistance testing show that all piping was continuous.
- Protection of piping varied. Some piping were unable to reach the -0.85V standard, but were able to show 100 mV polarization shift.
  - Some piping showed neither. Although corrosion was not terminated, report states that the CP system would slow down the rate.

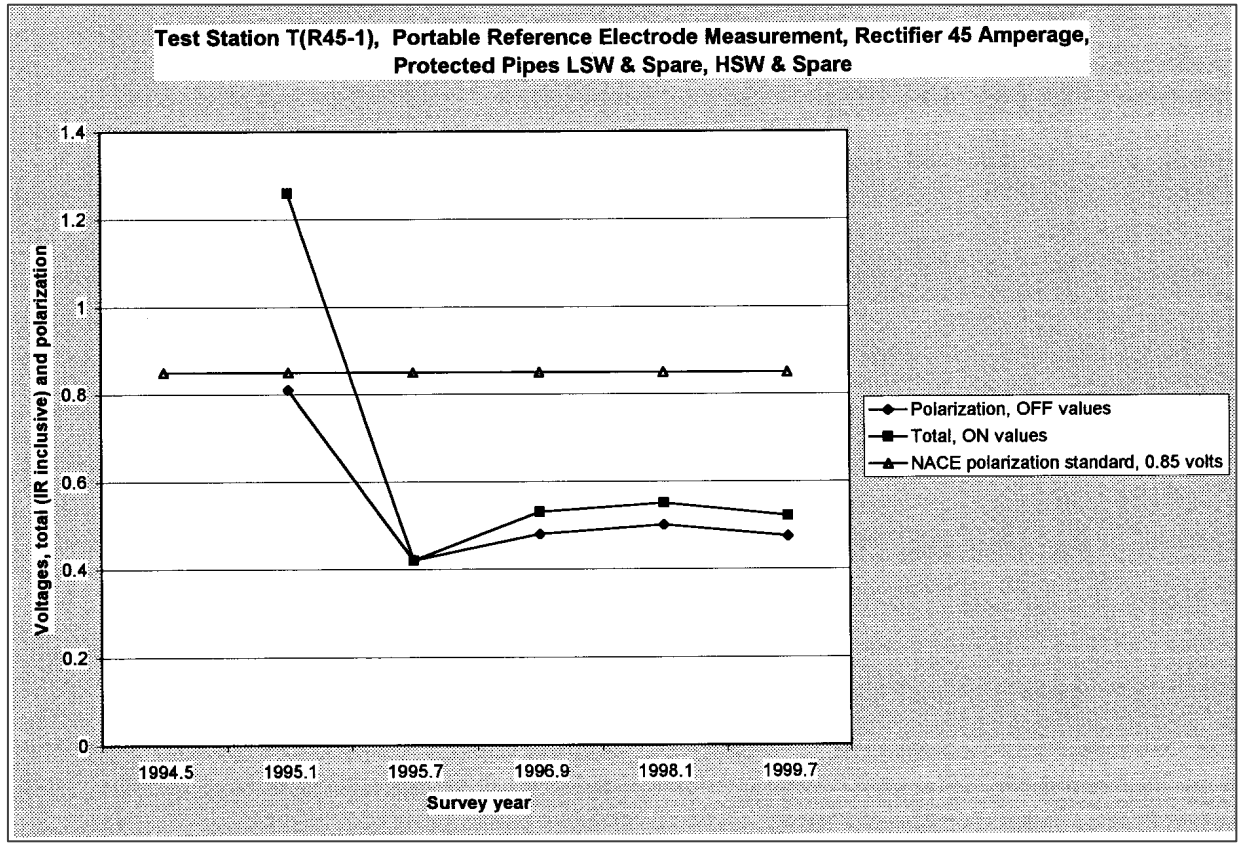

1999 Annual Cathodic Protection Survey Report (HNF-7099)

TABLE 1 Polarization Voltages at PFP test stations

Test Stations on PFP property	Polarization Voltage	Native potential voltage, A(assumed) and M(measured)	NACE Standard 4.2.1.2 achieved (YES/NO); 0.85 volts of polarized potential	NACE Standard 4.2.1.3 achieved (YES/NO); minimum of 100 mVolts of polarization gain	Corrosion Rate Reduction, Assuming decade of current reduction Per 100 mV of polarization gain
PFP Rectifier 45 system					
T(R45-1)	.475	.42 (M)	NO	NO	55 mV gain, 354% rate reduction
T(R45-2)	.469	.42 (M)	NO	NO	49 mV gain, 309% rate reduction
T(R45-3)	.744	.35 (M)	NO	YES	8.7E5% red.
T(R45-4)	.678	.42 (A)	NO	YES	3.8E4% red.
T(R45-5)	.801	.42 (A)	NO	YES	6.5E5% red.
T(R45-6)	.649	.42 (A)	NO	YES	2.0E4% red.
T(R45-7)	.758	.42 (A)	NO	YES	2.4E5% red.
T(R45-8)	.578	.42 (A)	NO	YES	3.8E3% red.
West area Rectifier No. 23 (TX241-CATH-RECT-102) system					
T(19-1)	.819	.42 (A)	NO	YES	9.7E5% red.
West area Rectifier No. 22 system					
T(18-11)	.91	.42 (A)	YES	YES	Insignificant corrosion
T(18-9)	.904	.42 (A)	YES	YES	Insignificant Corrosion

Polarization data from test stations. Note that the first two test stations were unable to reach CP criteria, but corrosion rate was reduced by 300%

Existing CP of Transfer Lines (2007) (RPP-25299-Rev_1)

- Volume 4 of System Integrity Assessment examined buried lines.
  - Ensure that CP system has proper health and is being adequately managed.
- CP has 31 rectifiers, 1418 anodes, 529 test stations
  - Assessment examined only 14 rectifiers and 179 stations
- Anodes are installed evenly along piping throughout the tank farms.
  - Away from tanks, anodes are vertical. Above the tanks, anodes are laid horizontally.
  - Anodes can be disconnected if needed to improve current distribution, or eliminate stray currents or overprotection.

Existing CP of Transfer Lines (2007) (RPP-25299-Rev_1)

- Design specifications:
  - Anodes are limited to 30 mA above the DSTs and 500 mA away from the DSTs
  - Negative cathodic structure potentials (-0.85 VCSE)
  - Soil resistivity is assumed to be 40,000 ohm-cm
  - Anodes are closely coupled along the piping
  - Rectifiers are independent of adjacent systems and are placed outside tank farms.
  - Anodes are packaged with low resistivity backfill
  - Rectifiers are oil cooled
  - Test stations are placed above protected piping
  - Anode leads terminate in distribution boxes in DST areas
- Early operational criteria included a 300 mV potential gain criterion. AP Tank Farm included this criterion

Existing CP of Transfer Lines (2007) (RPP-25299-Rev_1)

- CP Projects W-020H/W-314 continued the design features but with some changes:
  - Soil resistivity assumption varied from 20,000 to 40,000 ohm-cm
  - 300 mV potential gain criterion was discarded
  - NACE Standards for underground piping corrosion control (RP0169 & RP0285) were employed as acceptance specifications (Criteria 1, 2, or 3).
  - Eventual changes to polarization measurements meant that NACE Criterion 1 was no longer used after 1996.
- NACE Criteria:
  1. Negative cathodic potential of 0.85 V while CP is applied (CSE)
  2. Negative polarized potential of 0.85 V (CSE)
  3. 100 mV polarization shift

Existing CP of Transfer Lines (2007) (RPP-25299-Rev_1)

- CorrPro had made several comments about the proximity of the DSTs to the piping during 1994 field survey work:
  - Commissioning report for AP Tank Farm shows electrical continuity between the piping and the tanks.
  - All the tanks indicated electrical continuity to the piping. Electrical continuity with rebar is more difficult to determine without excavating/destructive sampling of the concrete.
  - Survey work showed that tested tanks were receiving some protection from the buried CP system.
- CorrPro recommendations for rectifiers:
  - Rectifier R1 (241-AP tank farm) – Set rectifier output near 31V, 18A. **Projected amp/anode** = 0.369 A
  - Rectifier R2 (241-AP tank farm) – Set rectifier output near 95V, 22A. **Projected amp/anode** = 0.547 A
  - Rectifier 11 (241-AZ tank farm) – Set rectifier output near maximum amperage (either 50V or 6A). **Projected amp/anode** = 0.158 A
  - Rectifier 13 (241-AN tankAmp/anode = 0.158 farm) – Set rectifier output near maximum ampere output (12A). **Projected amp/anode** = 0.129 A
  - Rectifier 31 (241-AY tank farm) – Set rectifier output near maximum amperage (6A). **Projected amp/anode** = 0.058 A
- Projected anode outputs were considerably higher than the 0.030 A parameter. Values were lowered closer to 30.

Anode Output (RPP-25299-Rev_1)

Table 10-1. Double-Shell Tank Farms Cathodic Protection System Survey Average Anode Outputs (December 2004 to February 2005) (2 Sheets).

	Rectifier	Shunt Conv. Factor*	Volt Range	Tap Setting	Survey Millivolts	Max. Millivolts
ET-08184	36	1	17-21	C-3	2	16
ET-05618	13	0.3	6.3-8.3	A-4	15.3	40
ET-08777	R1	1.6	25-30	A-5	6.6	37.5
ET-08778	R2	1.6	42-48	B-3	5	37.5
ET-08779	19	0.3	6.5-9.5	A-4	11.2	40
ET-05625	31	1	6.5-9.5	B-2	5.1	12
ET-05616	11	1	7-11	B-2	2.6	12

Anode Output (RPP-25299-Rev_1)

Table 10-1. Double-Shell Tank Farms Cathodic Protection System Survey Average Anode Outputs (December 2004 to February 2005) (2 Sheets).

	Rectifier	Survey Volts	Survey Calc. Amps	Survey Taps		Average mAmps/Anode
ET-08184	36	18.43	2	C-3		33.9
ET-05618	13	4.45	4.49	A-4		45.4
ET-08777	R1	27.1	10.56	A-5		162.5
ET-08778	R2	44.8	8	B-3		125
ET-08779	19	7.9	3.4	A-4		33
ET-05625	31	8.47	5.1	B-2		36.7
ET-05616	11	8.84	2.6	B-2		30.6
Rectifier 19	Anodes	Total		Rectifier 13	Anodes	Total
H-14-105346, sht. 1	7			H-14-104405, sht. 1	6	
H-2-91033, sht. 2	96	103		H-2-91040, sht. 2	93	99
Rectifier R1				Rectifier 31		
H-2-76933, sht. 1	10			H-2-818708, sht. 1	6	
H-2-94082	15			H-2-91041, sht. 15	41	
H-2-94081	13			H-2-131378, sht. 3	31	
H-2-94080	16			H-2-91042, sht. 2	61	139

Anode Output (RPP-25299-Rev_1)

Table 10-2. Voltage Gradient of Vertical and Horizontal Arrangements of Individual Anodes.

Vertical Anode	**V,x = 0.038*Amp*resistivity/PI/Y* log [(y + sqrt (y^2 + x^2) / x]**					
Ground Anode Current, Amps	**Y, length of anode in earth in feet**		**X, distance from ground anode in feet**		**Resistivity ohm-cm**	**V,x volts**
0.03	8		10		40,000	**0.58**
0.18	8		10		40,000	**3.46**
Horizontal Anode	**V,xy = 0.012*Amp*resistivity/L* log { [sqrt((x+L/2)^2 + y^2 + D^2) + X + L/2] / [sqrt((x-L/2)^2 + y^2 + D^2) + X - L/2] }**					
Ground Anode Current, Amps	**L, length of anode in earth in feet**		**vertical distance Y, distance from ground anode in feet**			
0.03	8		10			
0.18	8		10			
		lateral distance X, distance from center lie of anode		**D Depth, ft**	**resistivity ohm-cm**	**V,xy volts**
		0		4	40,000	**0.57**
		0		4	40,000	**3.41**

Source: Peabody [2001], Ebasco [1983a].

CP Assessment (RPP-25299-Rev_1)

- Out of 246 pipelines, 91 designed to be protected, 51 inadvertently protected, 100 not connected to test stations and are unprotected.
- Following the NACE criteria, 33% of test stations met #1, 90% met #2.
  - 21 test stations had no data.
- No data analysis reports appear to exist for bi-monthly rectifier inspections or annual surveys.
- CP is effective only when the current can contact the surfaces of buried piping. It is not clear the extent of protection provided to piping covered in bubble wrap/insulation.

NACE SP0290 – ICCP Systems (Concrete)

- Concrete and soil have similar physical properties, ionic current can travel between the two electrolytic media.
  - Concrete alkalinity encourages passivity in steel.
  - Buried anode beds can be utilized for underground concrete structures.
- Information useful for selecting and designing an impressed current cathodic protection system includes:
  - ❖As-built drawings of the concrete structure
  - ❖Condition survey (in accordance with ACI(2) 2019)
  - ❖Potential survey (in accordance with ASTM C876)
  - ❖Chloride analysis of the concrete
  - ❖Electrical continuity of the embedded metal
  - ❖Repair, maintenance history and service life requirements
  - ❖Concrete cover to the reinforcing steel
  - ❖AC power availability (rectifier to convert to DC power)
  - ❖**Concrete resistivity data**

Activity Status

- Work Status
  - Compilation of the soil-resistivity data, initial assumption of 5000 Ω-cm.
  - Preliminary model is being developed.
  - CP system is being designed that such that current is predominantly delivered to the soil-side bottom of the secondary shell.
  - Rebar corrosion is being evaluated.
  - Implementation of the detailed construction drawing in the model.
  - Laboratory-scale experiment to understand rebar corrosion.
  - Additional discussions are being planned during the AMPP week.

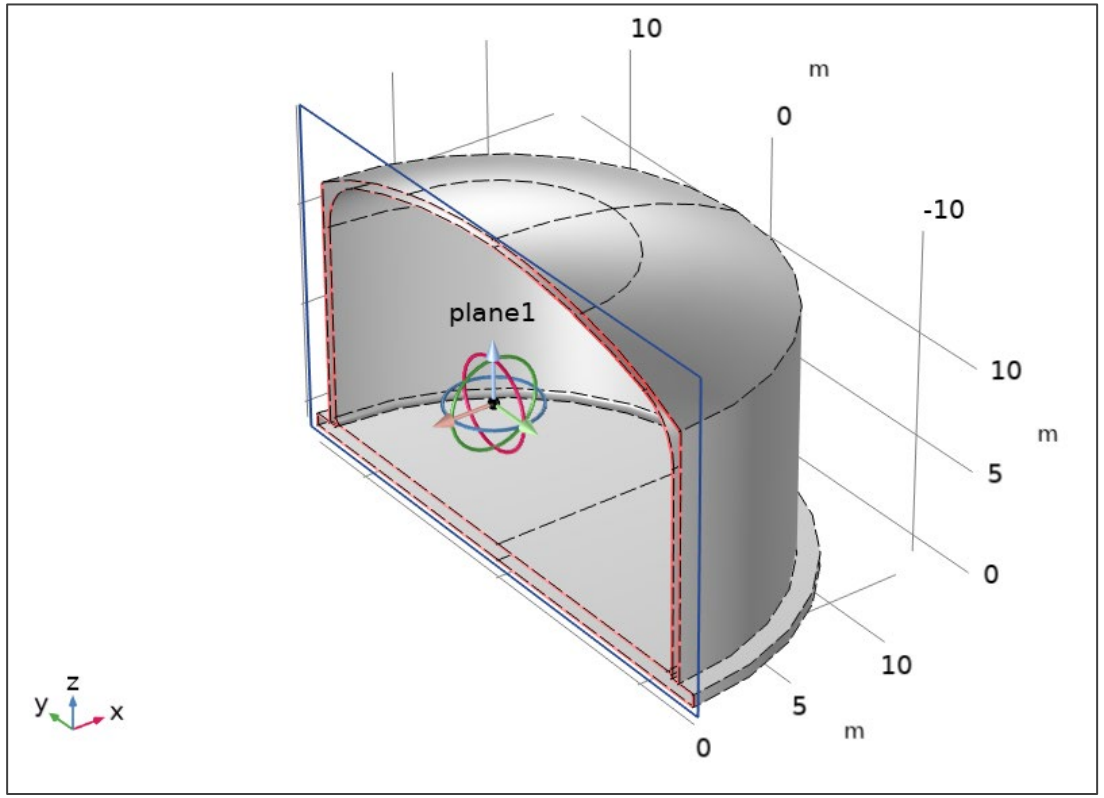

Tank Farm CP Model – Initial assumptions

- Tanks in AY, AZ, AP, and AN farms are similar.
  - ❖ Differences in rebar sizes and placement exist, but distribution is similar.
- Piping and CP systems differ between Tank Farms, based on their age and design function
- Modeling six tanks plus piping plus CP system with about 100,000 linear feet of rebar reinforcement per tank would be unwieldy.
- Try to model pertinent rebar on each tank as a metallic shell, with a fraction of the CP current of a solid metal shell.
- Shell has low resistivity, yet CP current passes through it.
- Volume Fraction of combination rebar/concrete shell is 0.0904
- Rebar shell “Parallel Resistors” resistivity is 2.2E-6 ohm-m

Tank Geometry – Concrete Shell and Slab

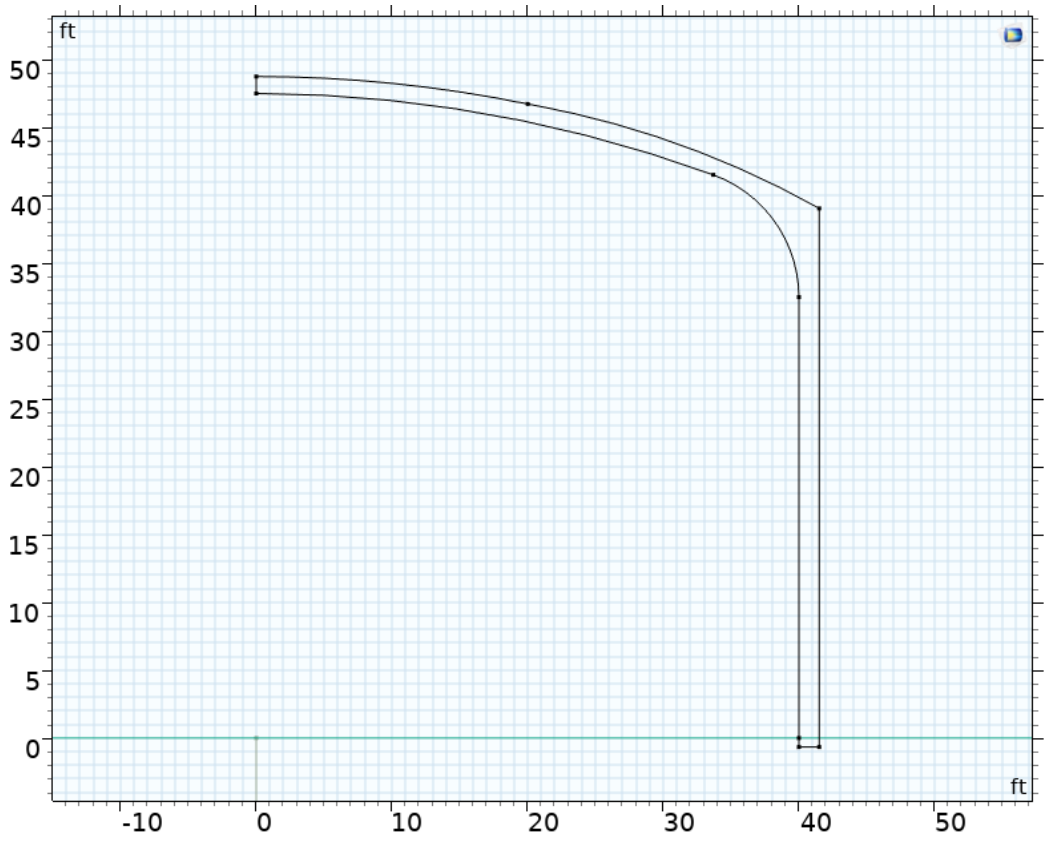

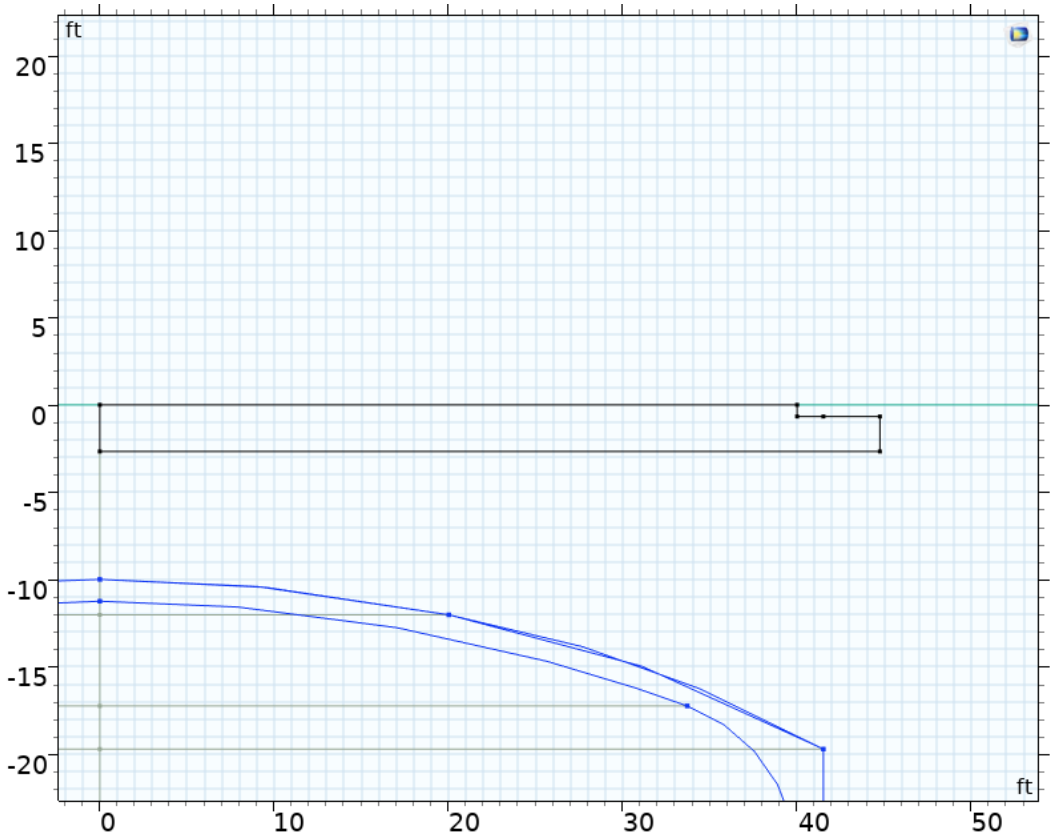

Tank Geometry – Concrete and “Plug”

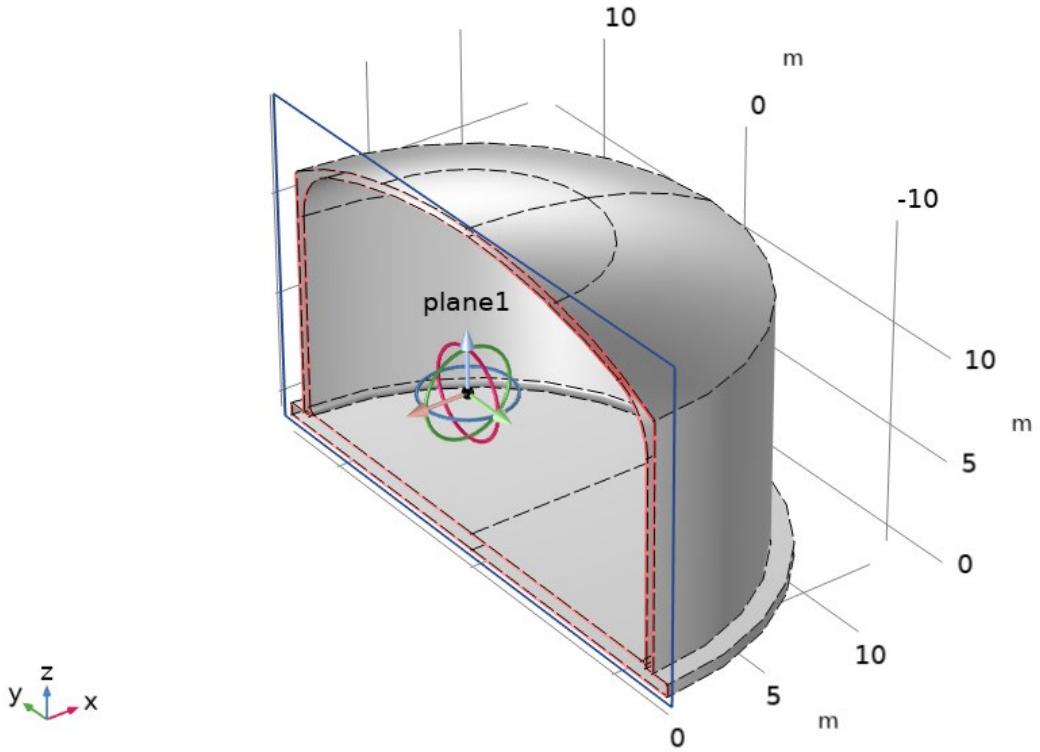

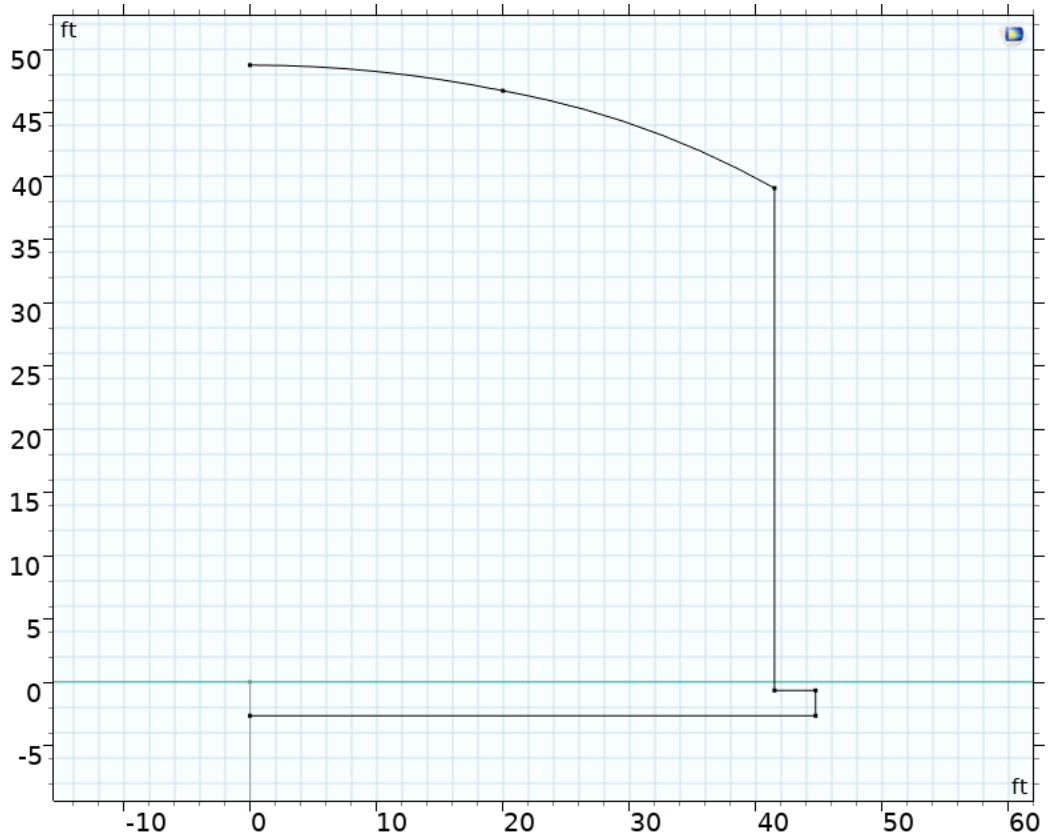

Tank CP Model – Full Shell (Iteration 1)

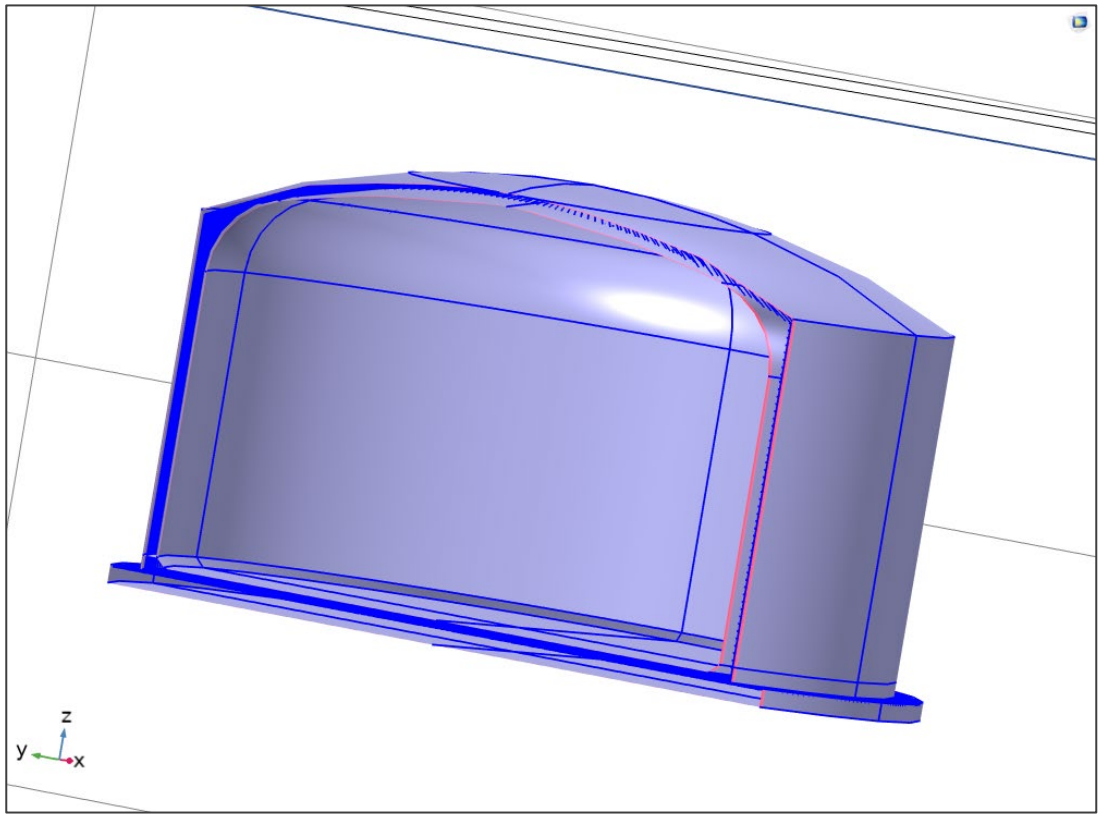

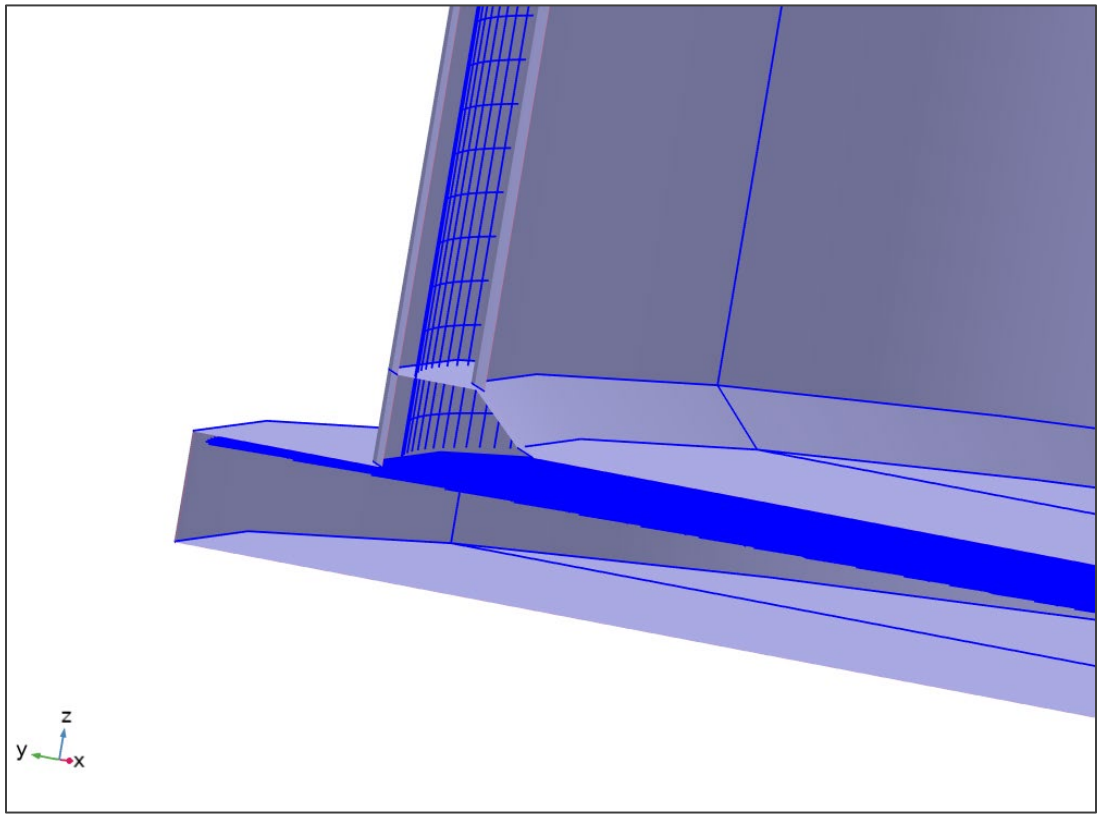

264 vertical rebar in wall, horizontal rebar every 0.8 ft. Rebar in slab, bonded to tank steel.

Tank CP Model – Foundation Excluded (Iteration 2)

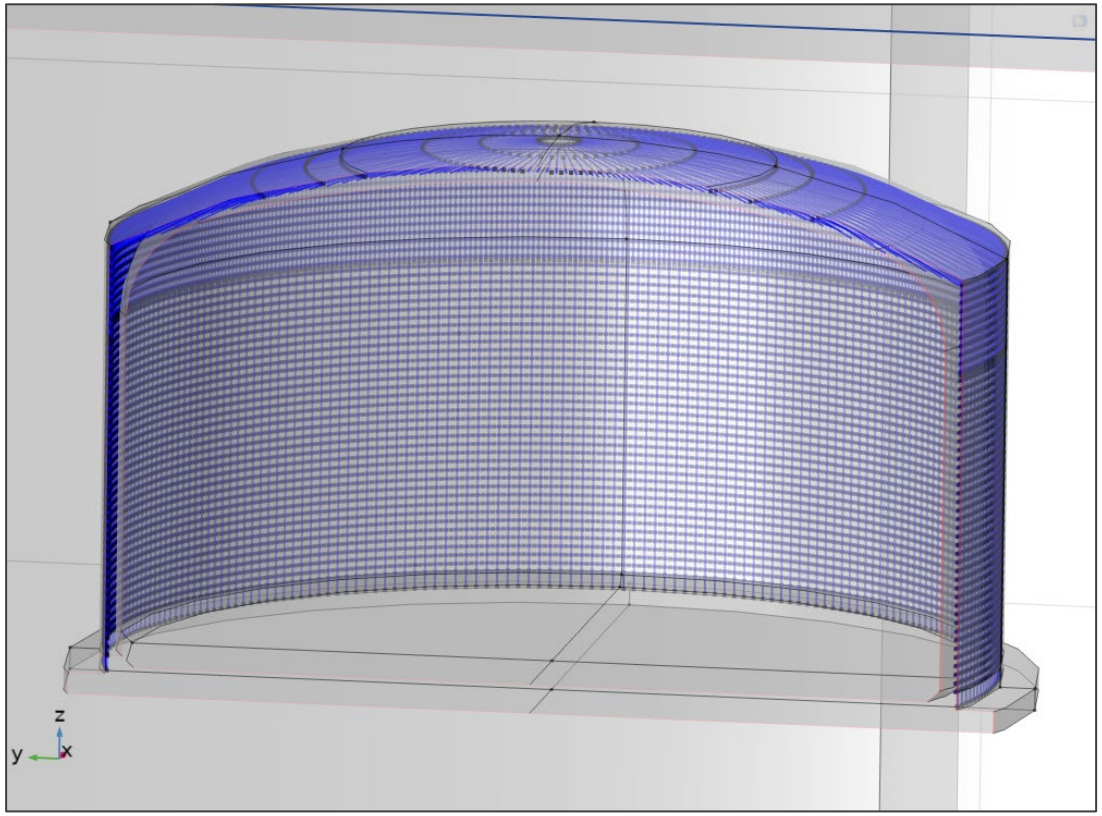

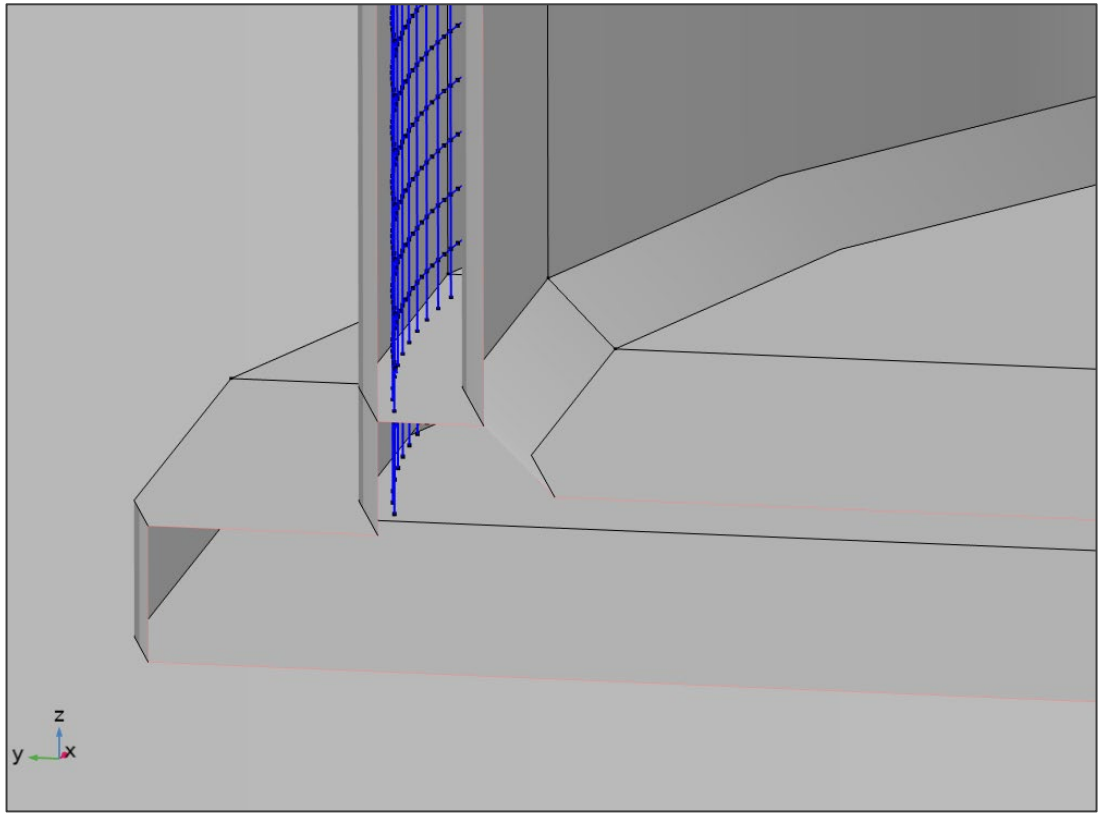

Tank CP Model – Rebar as a shell element (Iteration 3)

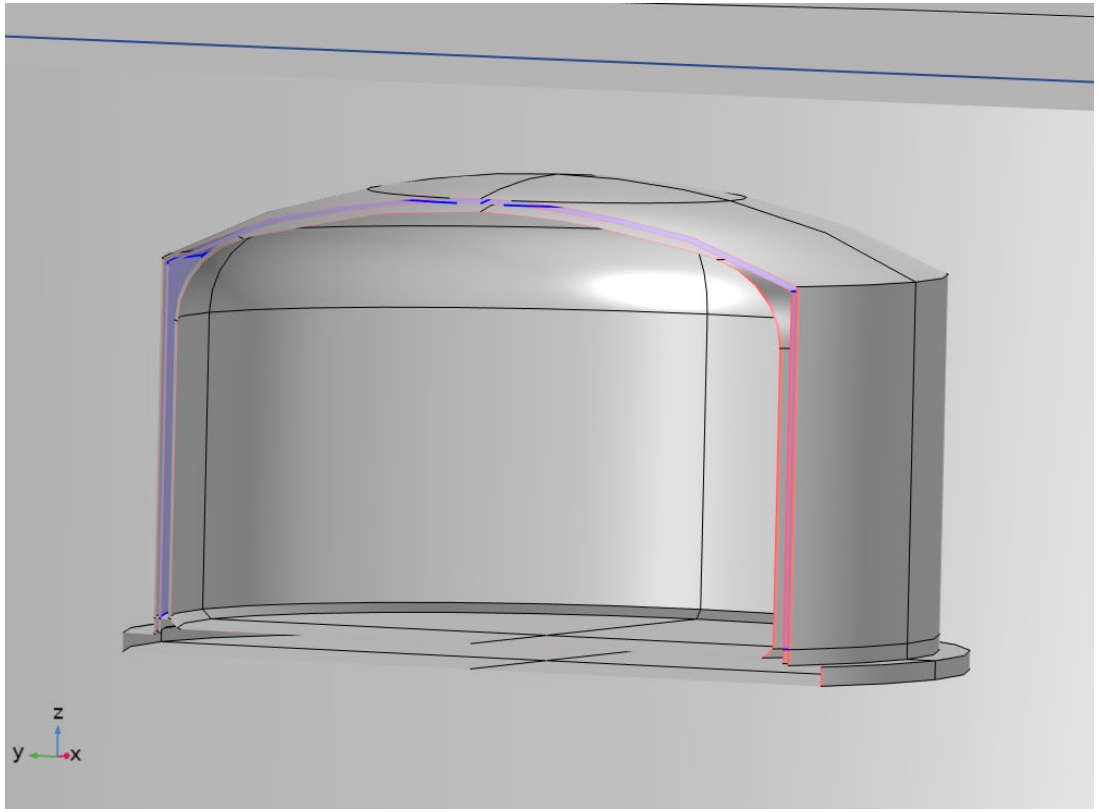

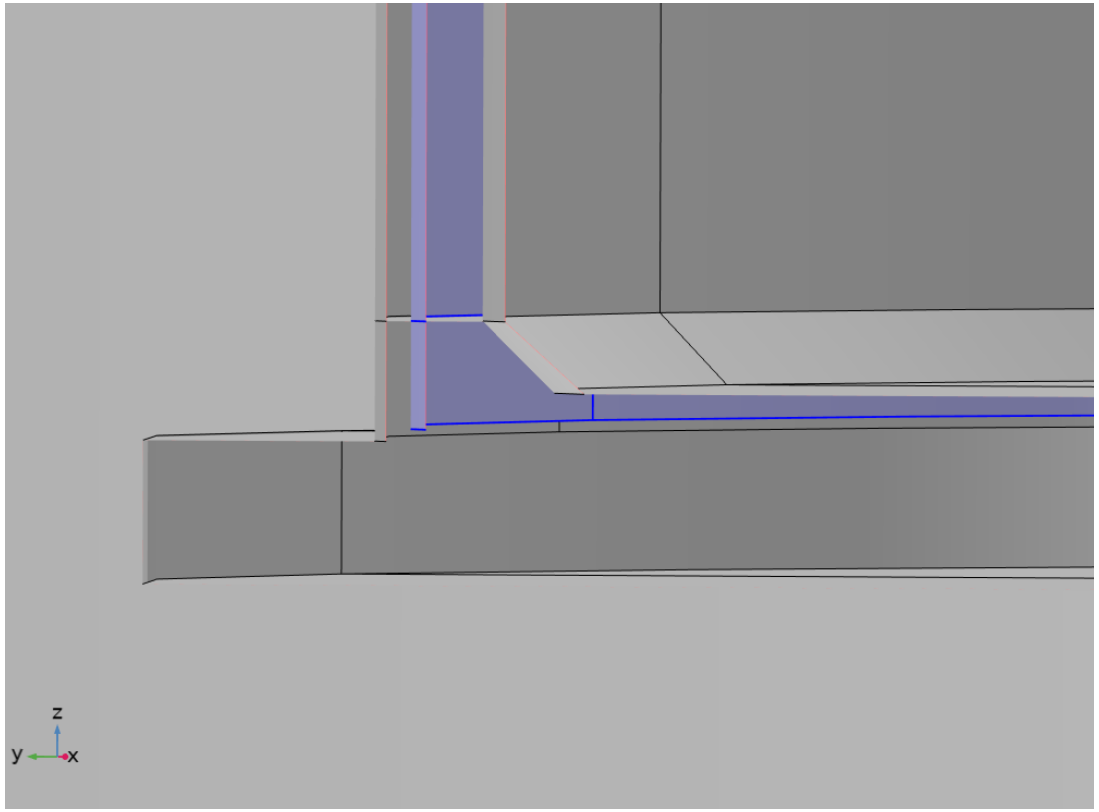

DST CP Model – Table of Results

Brief Results table, corrected rebar model, progression comparison												
10 Amps impressed current, unless otherwise noted						Typical anode voltage is ~18.5V						
Rebar modeled as shell element, 0.5" thick, volume fraction rebar/concrete = 0.0904												
	ohm-cm	RB Rp	Integrated Amps					Amps/ft^2 (outgoing)			Resources	
CaseID	Rebar ρ	Fraction	I-steel	I-bottom	I-walls	I-dome	I-rebar	max i_btm	min i_btm	Remarks	DOF	time, sec
lt. 1	--	1	1.4080	0.4207	0.6926	0.2955	8.5912	-0.055	-0.213	Corrected rebar in walls, slab & shell bonded	1557683	224
lt. 2	--	1	4.8352	3.0713	1.2231	0.5607	5.1448	0.324	2.510	Rebar only on shell, no slab rebar	619280	127
lt. 2 (new)	**--**	**1**	**3.9969**	**2.8713**	**0.8346**	**0.2909**	**6.0031**	**-0.323**	**-2.16**	**Corrected rebar in walls, BENCHMARK**	**655543**	**126**
RBshell10	2.20E-06	1	3.0468	2.6667	0.5259	0.2142	6.5932	-0.322	-1.82	Corrected rebar shell, parallel resistors	412998	64
RBshell11	2.20E-06	1.5	3.7762	2.7321	0.7397	0.3043	6.2238	-0.322	-1.93			
RBshell12	**2.20E-06**	**2**	**4.1023**	**2.785**	**0.9317**	**0.3856**	**5.8977**	**-0.322**	**-2.01**			
	ResRebar	Resistivity of rebar shell, ohm-cm										
	Fraction	Fraction of i_steel current density applied to rebar shell										
	I-steel	Current Density integrated over all tank steel										
	I-bottom	Current Density integrated over tank bottom										
	I-walls	Current Density integrated over tank walls										
	I-dome	Current Density integrated over tank dome										
	I-rebar	Current Density integrated over rebar, assume 0.5" diameter										
	max i_btm	Maximum value of current density on tank bottom										
	min i_btm	Minimum value of current density on tank bottom										
	DOF	Degrees of Freedom to solve for model										
	time, sec	Elapsed time used to solve model										

Tank-Soil CP – 10A on Anode; Potential and Field Lines

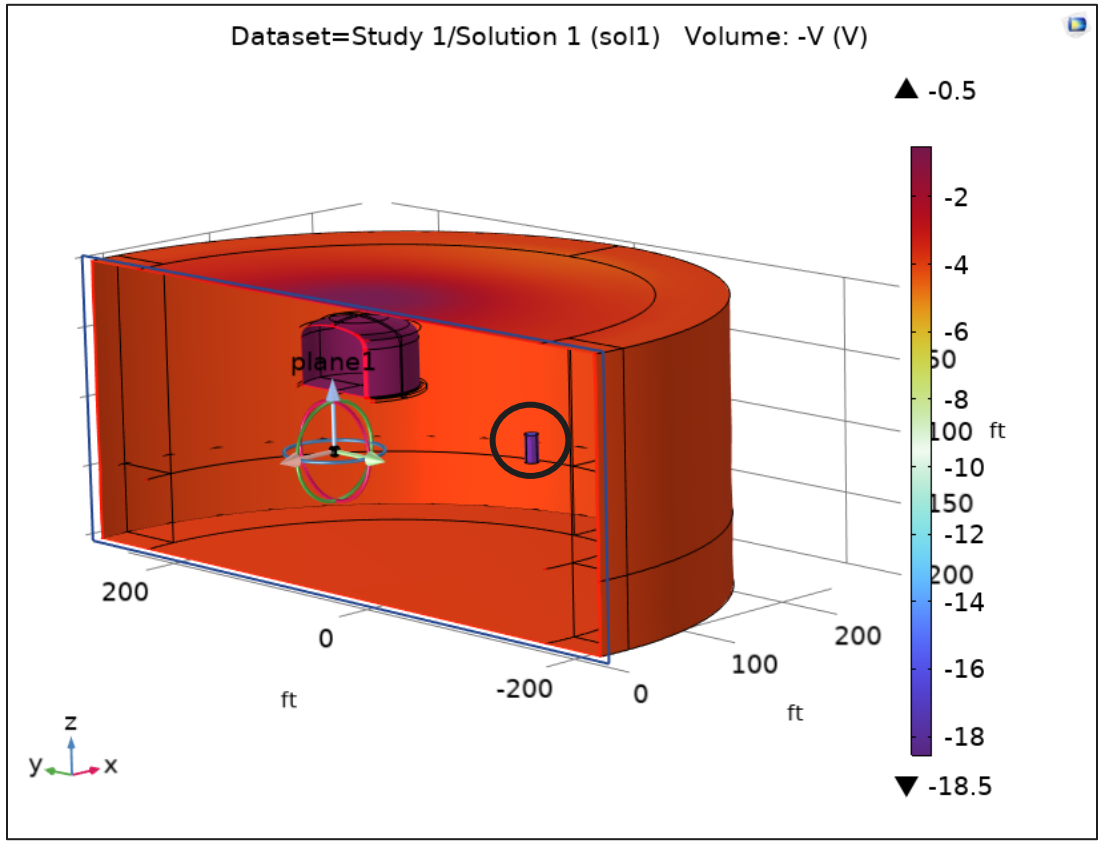

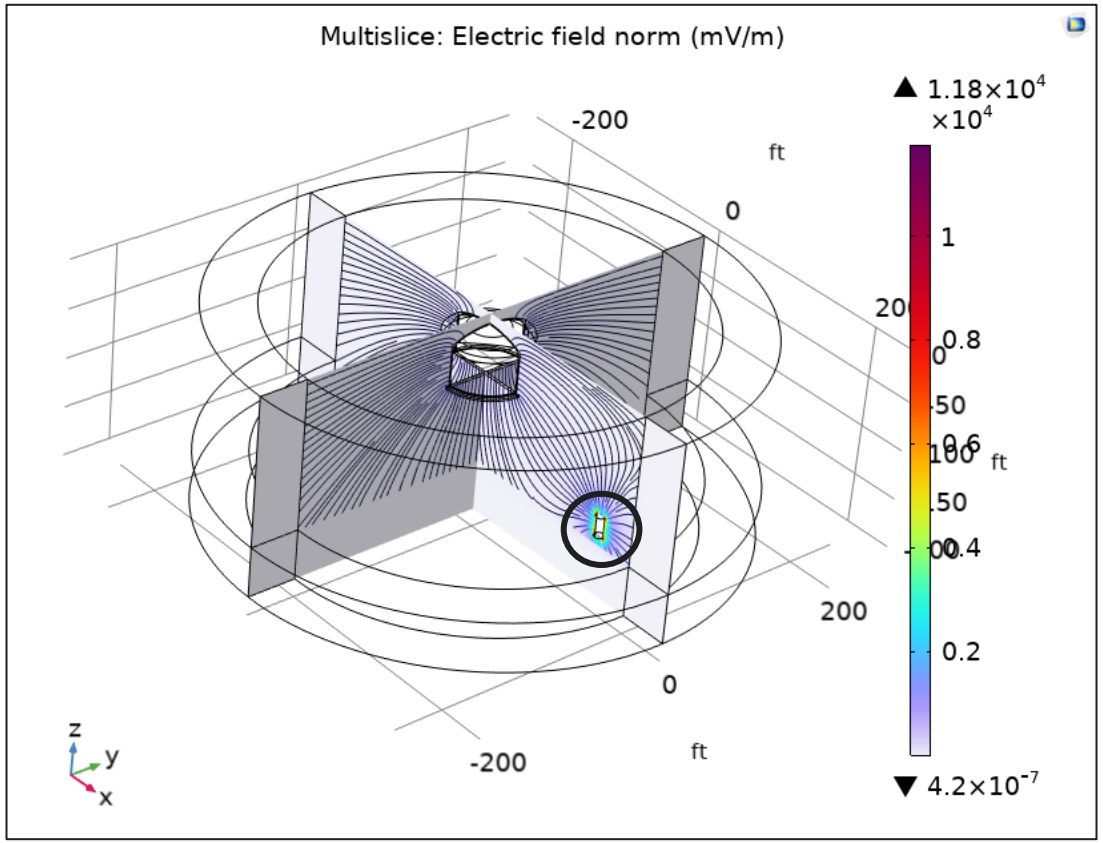

Tank CP Solution – Current Density on Bottom (Anode on the right)

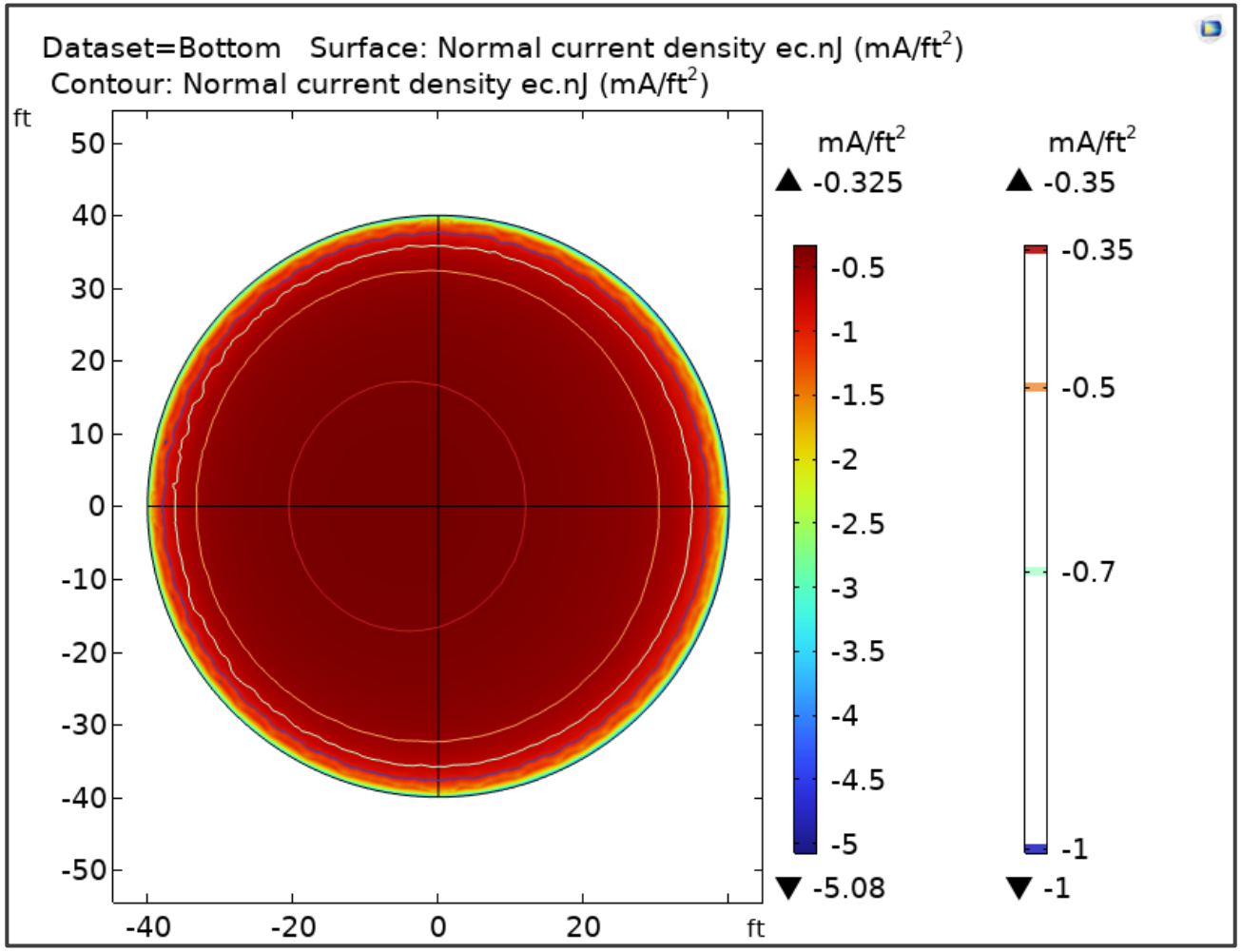

Maximum current density at bottom. Sharp corner?

Tank CP Solution – Current Density on Walls (Anode below, right +x)

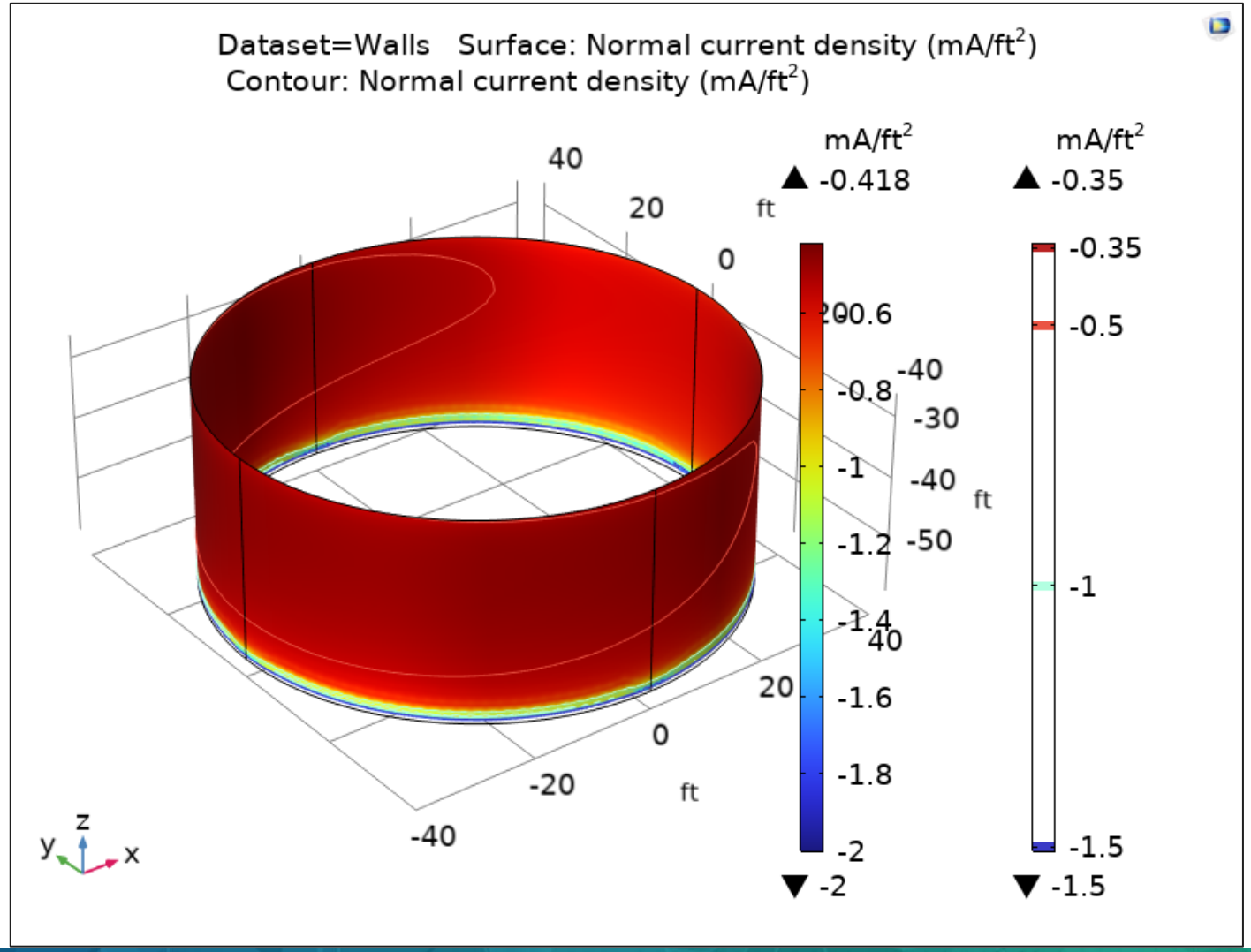

Tank CP Solution – Current Density on Dome

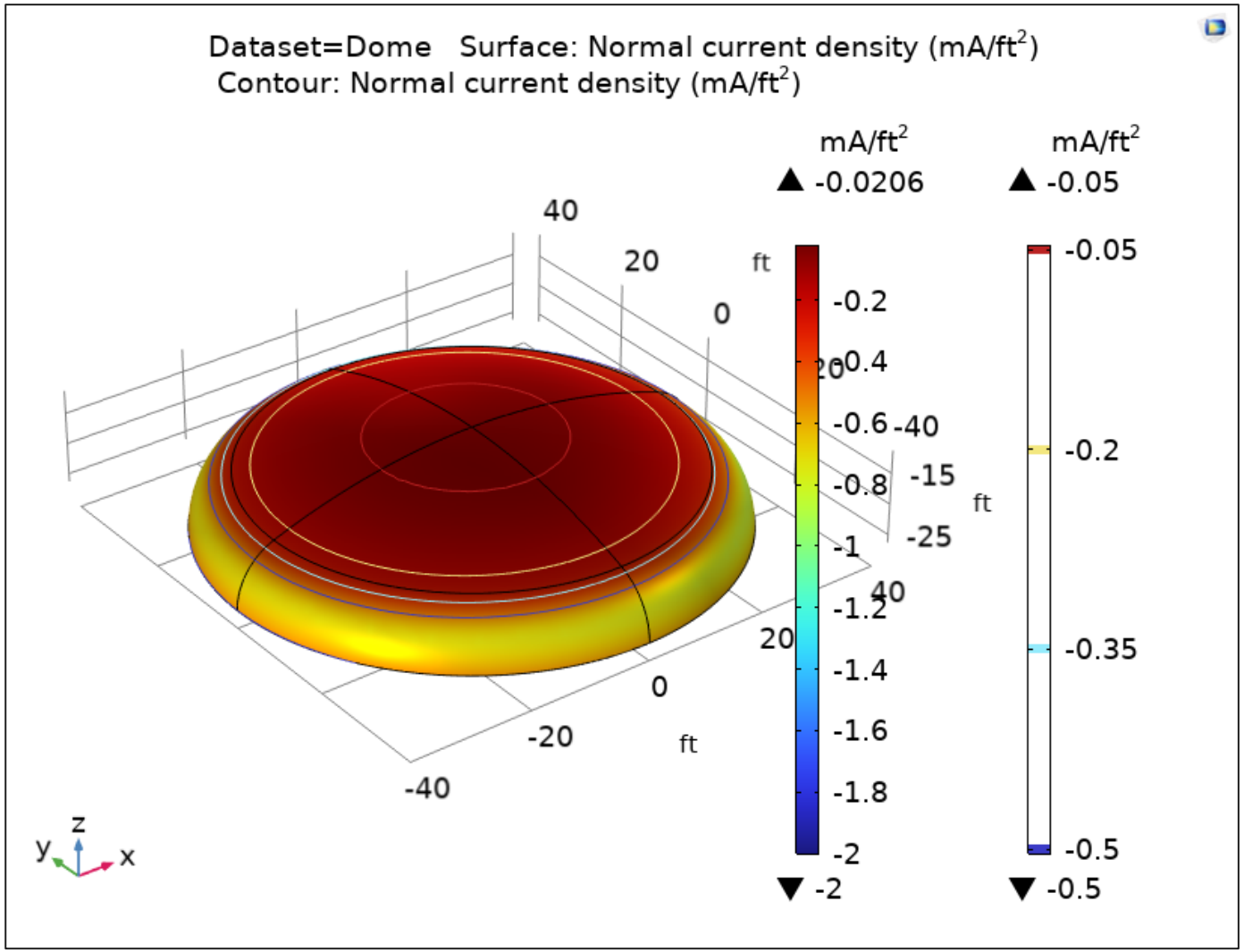

Tank CP Solution – Current Density on Steel

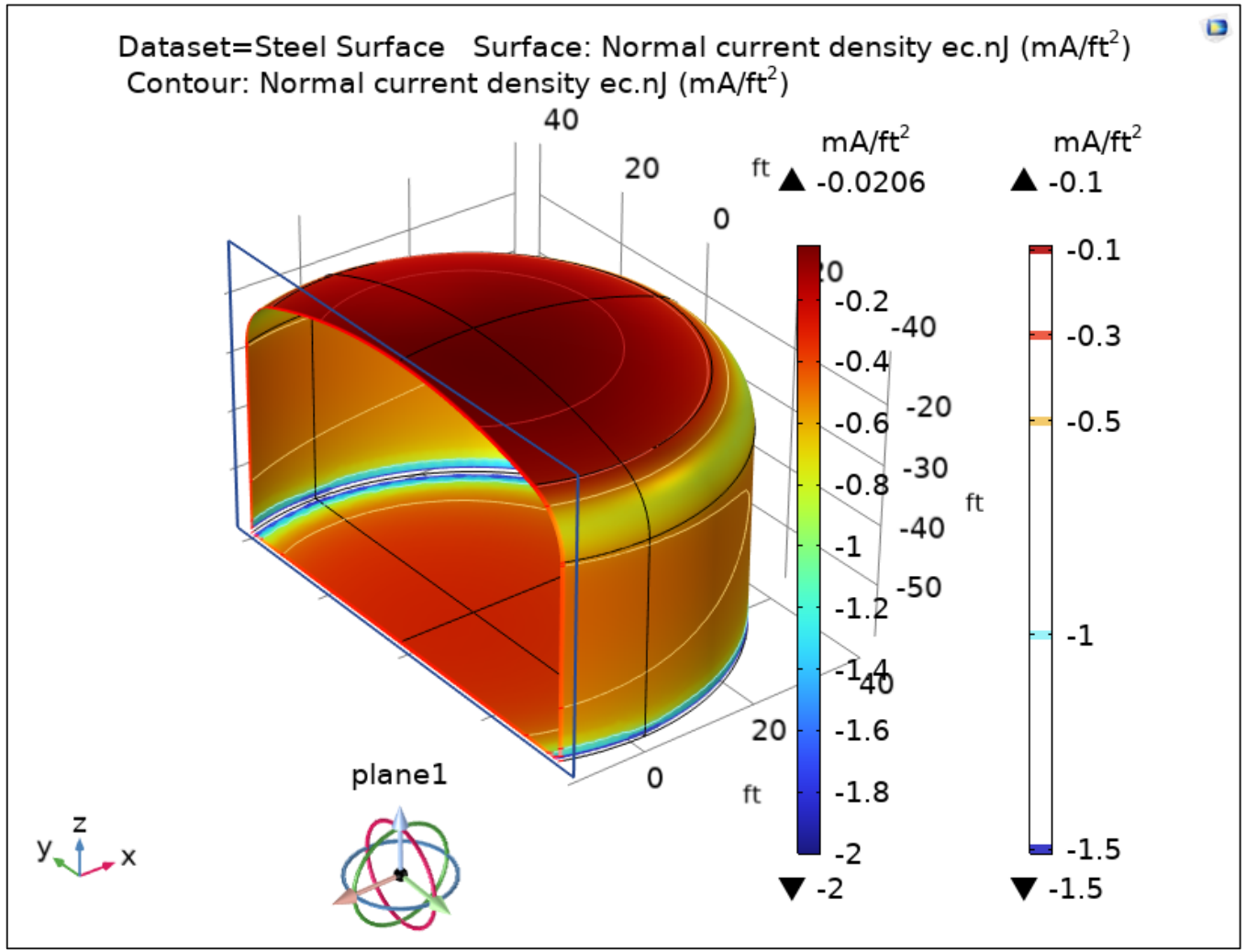

Tank CP Solution – Current Density on Bottom (Chamfer on corner)

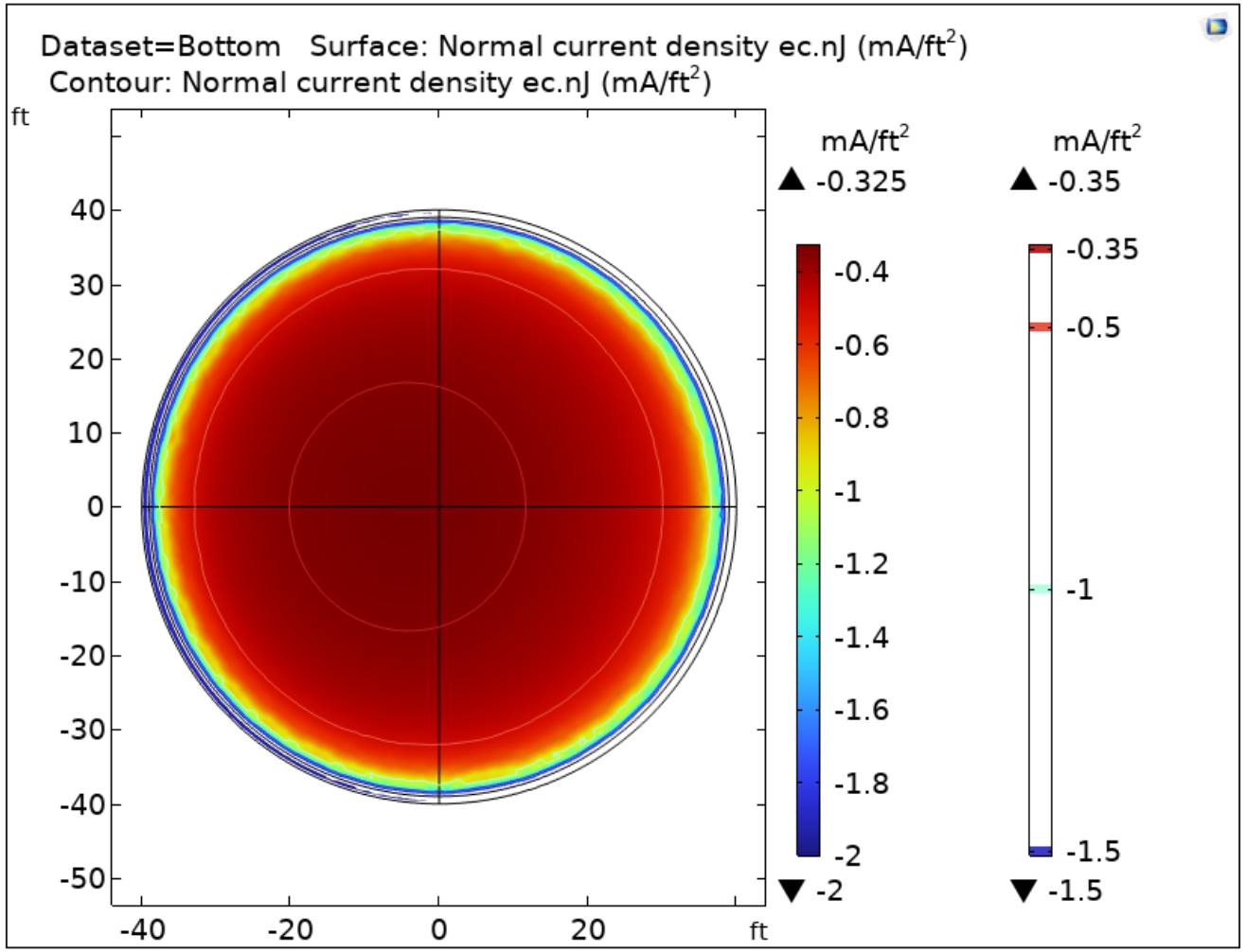

Maximum CD on bottom reduced from 5 to 3 A/ft²

Tank Geometry – Rebar and Concrete

1-layer rebar “birdcage” on left, rebar inside concrete on right

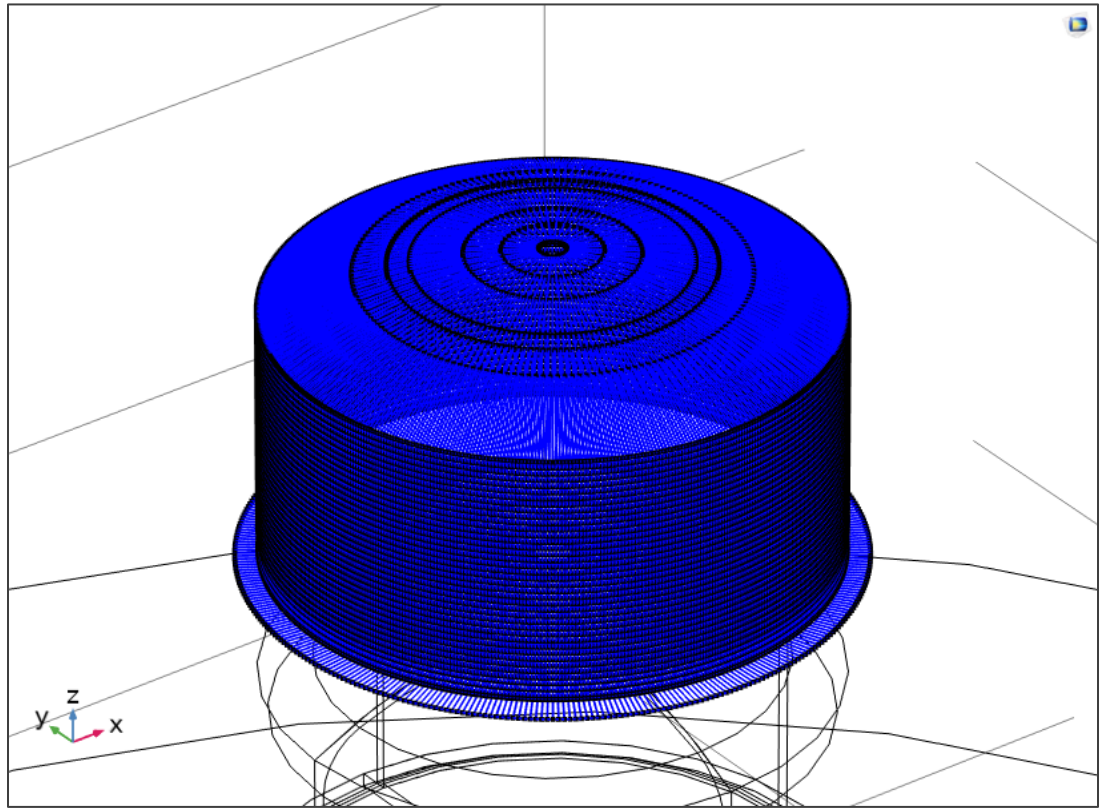

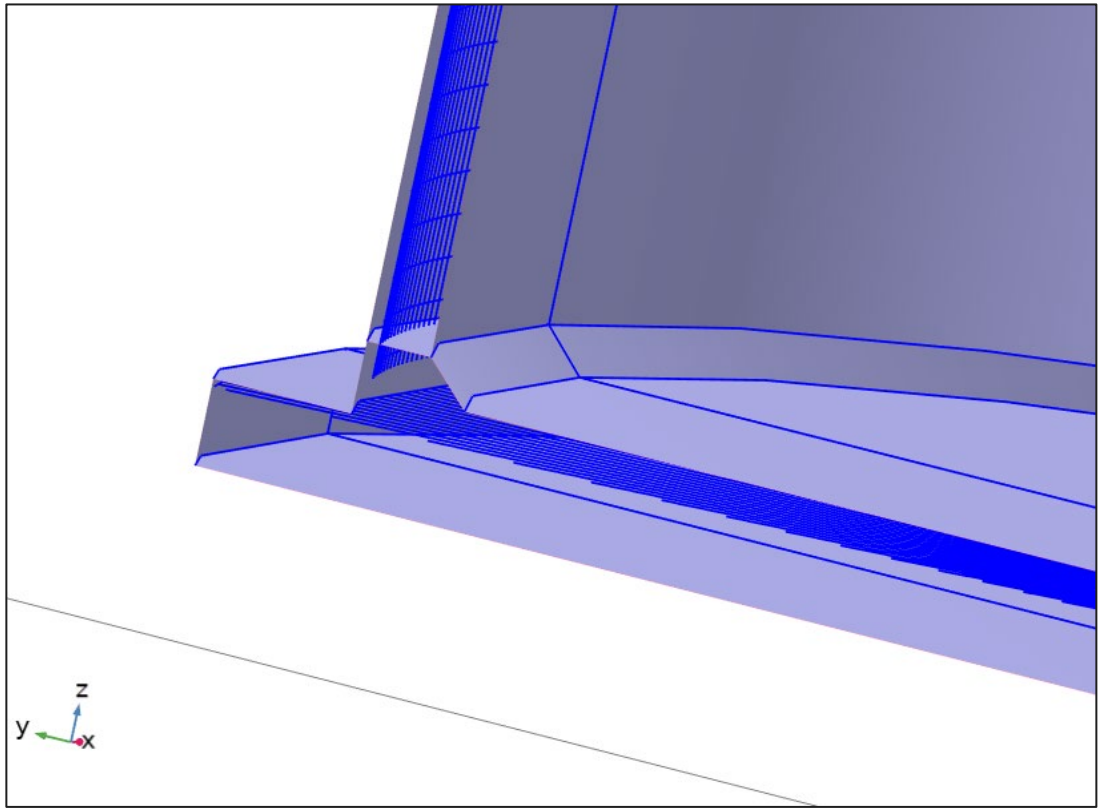

Tank CP Solution – Current Density on Bottom (Rebar & Chamfer)

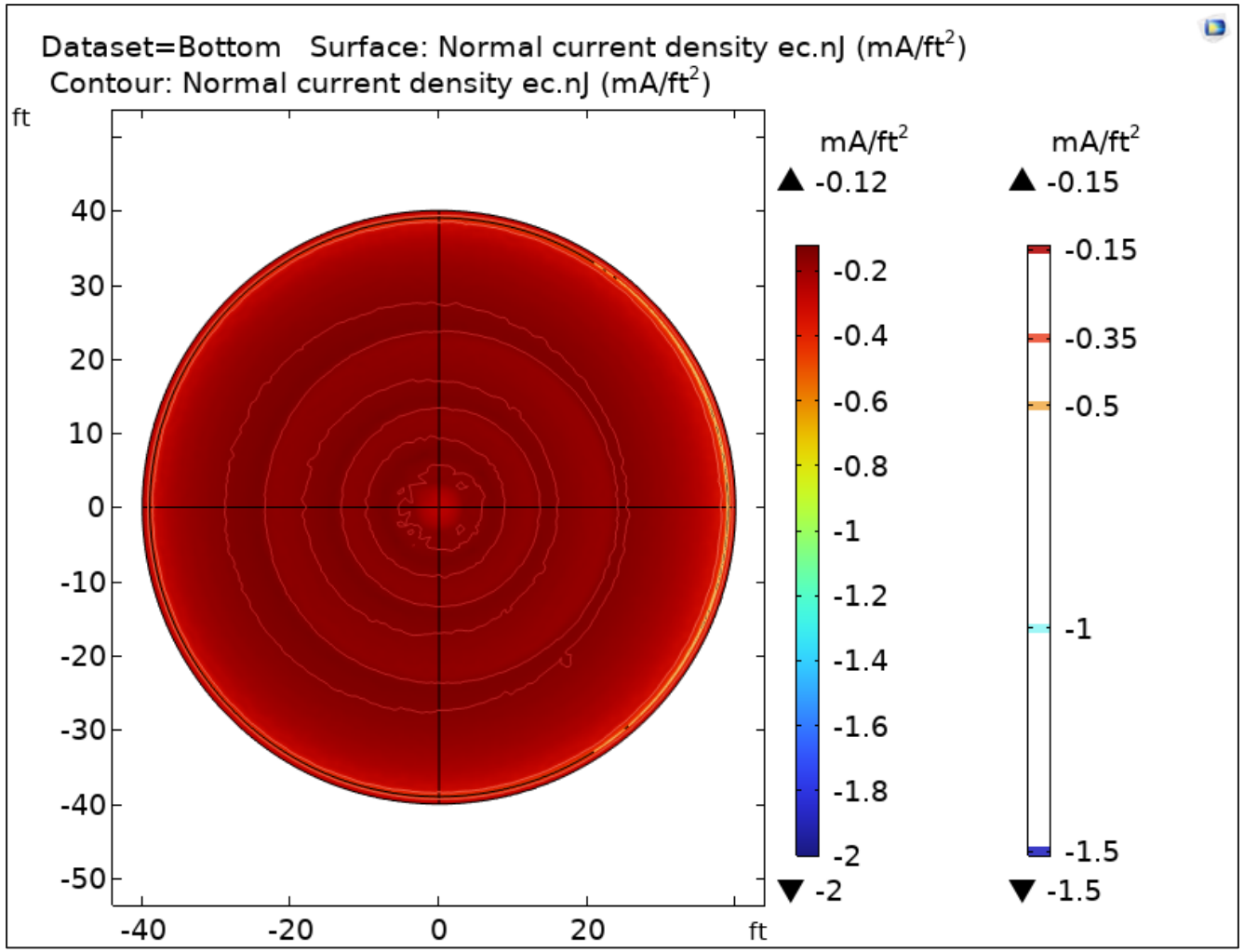

Maximum CD on bottom reduced from 3 to 0.5 A/ft²

Tank CP Solution – Current Density on Steel (Rebar & Chamfer)

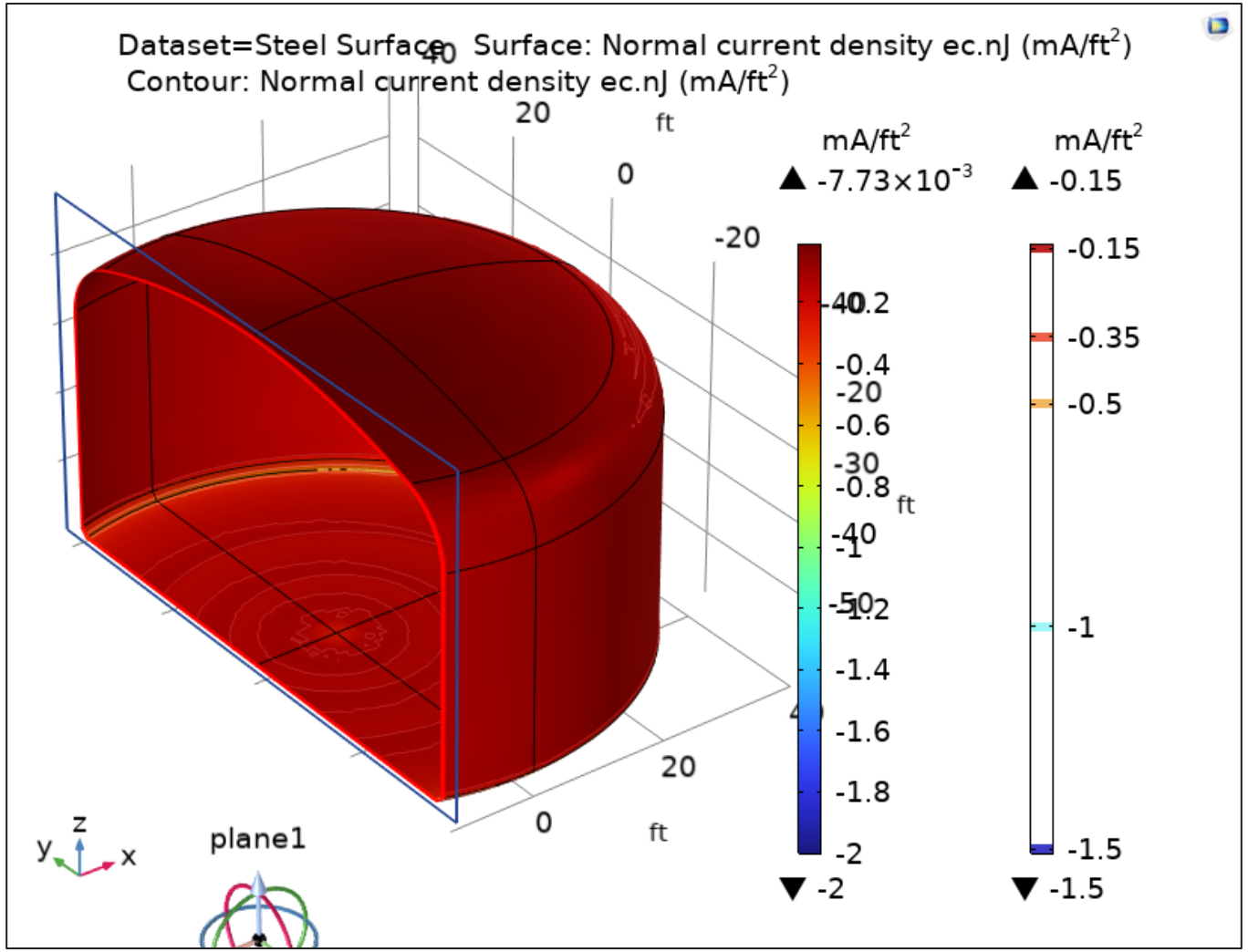

Tank CP Solution – Current Density on Walls (Rebar & Chamfer)

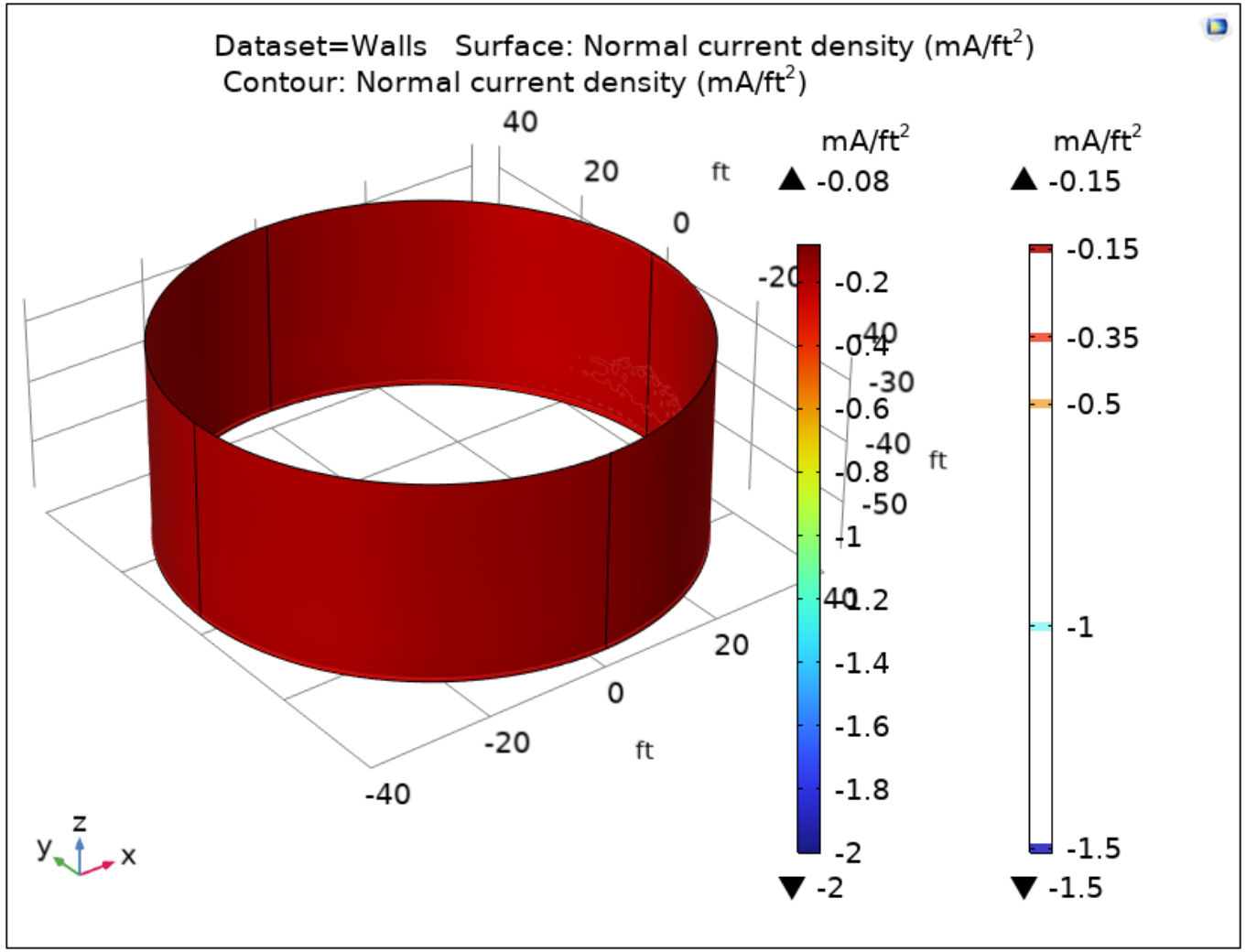

Tank CP Solution – Current Density on Dome (Rebar & Chamfer)

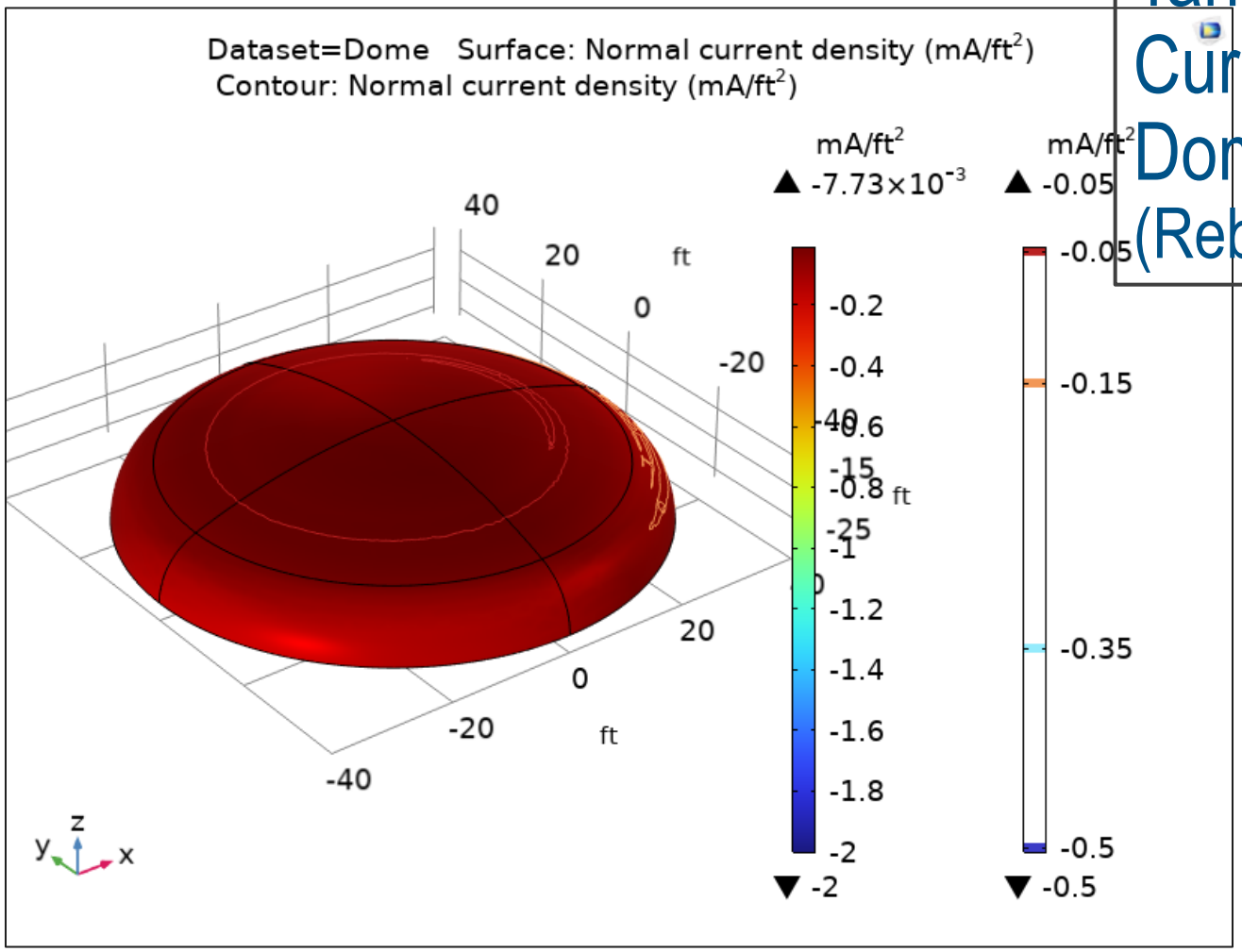

Tank CP Solution – Current Density on Bottom (Rebar, Chamfer, Hoops)

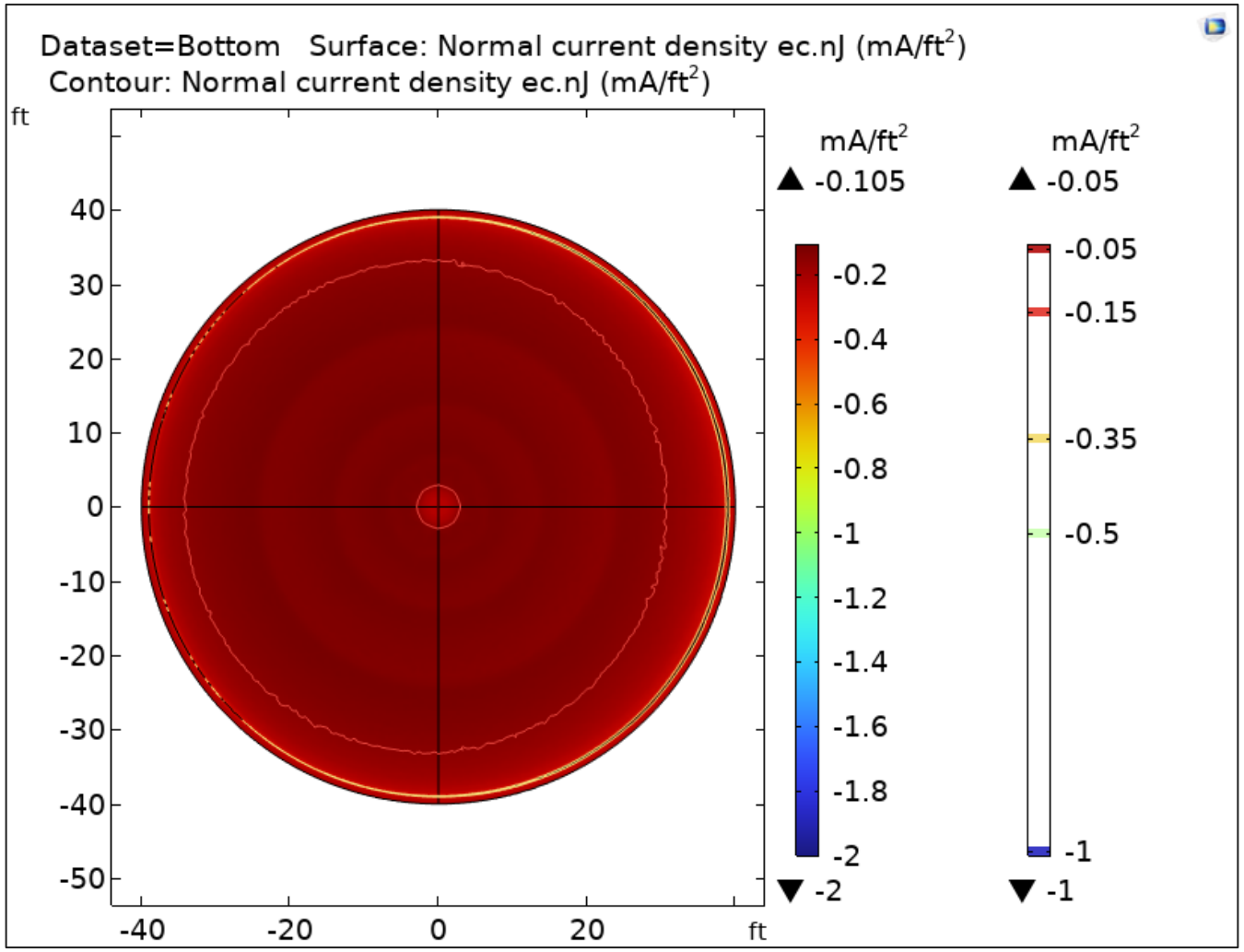

Maximum CD on bottom reduced from 3 to 0.4 A/ft²

Brief Results table, model progression comparison

10 Amps impressed current, unless otherwise noted						Typical anode voltage is ~18.5V
Rebar modeled as linear current source (sink), 0.5-in diameter						
	Amps			Amps/ft^2 (-implied, outgoing)		
CaseID	I-shell	I-rebar	I-bottom	max i_btm	min i_btm	Remarks
Simple	6.9347	--	3.065	0.325	5.080	Simple case, no rebar, sharp corner
Chamfer	6.565	--	3.435	0.327	3.020	Simple case, no rebar, 1x1-ft concrete chamfer on corner
Rebar1	1.3863	7.6577	0.956	0.120	0.835	Add 1 layer of rebar to concrete shell & slab, circular hoops in wall only
~~Rebar1~~	6.938	--	3.062	0.326	4.840	Model check - turn off rebar current, sharp corner
Rb-chamfer	1.5465	7.4304	1.0181	0.124	0.561	Change sharp corner at bottom of shell to 1-ft by 1-ft concrete chamfer
Rebar1c	1.6083	7.6327	0.759	0.104	0.620	Add circular hoops to bottom rebar, every 1-ft R from 3-ft to 44-ft
Rebar1cc	1.5821	7.6209	0.797	0.105	0.439	Add concrete chamfer to Rebar1c model
~~Rebar1cc~~	6.565	--	3.435	0.327	3.060	Turn off rebar current in Rebar1cc model
Rebar2	1.7839	5.1448	3.0713	0.324	2.510	Remove rebar from slab (floating); keep chamfer
Rebar2a	1.5631	4.5381	3.8988	0.552	2.39	same as Rebar2, except move anode to x=0
	I-shell	current on dome and walls				
	I-rebar	current on all rebar in model				
	I-bottom	current on bottom, including chamfer if any				
	max i_btm	max current density on bottom (least negative)				
	min i_btm	min current density on bottom (most negative)				

Spatial Distribution of Stray Currents

- Electrically-disconnected reinforcement may attract stray currents. Areas of discharge will produce corrosion.
- Y. Peng *et al.*, Spatial characteristics of stray current corrosion of reinforcing bars in pseudo concrete. *Structural Concrete*. **24**, 374–388 (2022).
  - Concerned with predicting discharge regions/stray current path in rebar.
- Current density of steel surface predicted by Tafel equations.

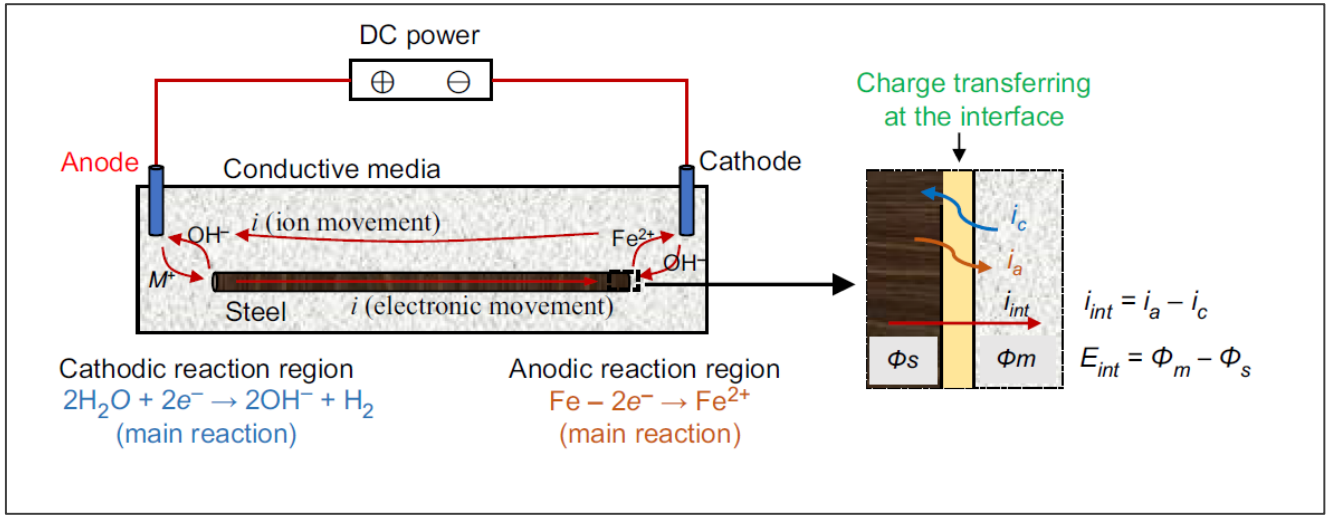

$$i_a = i_{ao} * \mathrm{e}^{2.303\left(\frac{\Phi_m - \Phi_s - E_{ao}}{\beta_a}\right)}$$

$$i_c = i_{co} * \mathrm{e}^{2.303\left(\frac{\Phi_m - \Phi_s - E_{co}}{\beta_c}\right)}$$

Spatial Distribution of Stray Currents

- Replication of Peng et al. model would provide confidence that stray current physics are being accurately modeled in the DST.

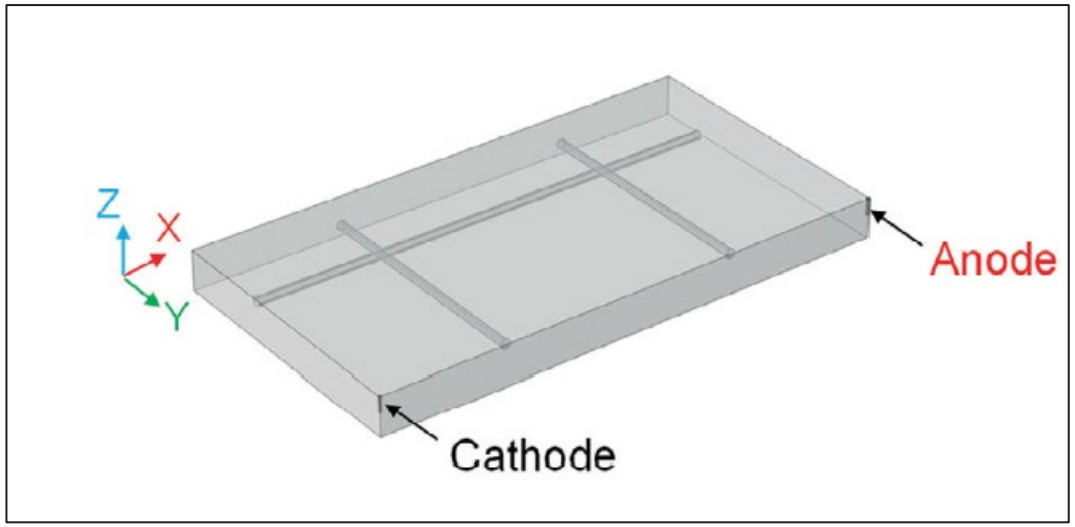

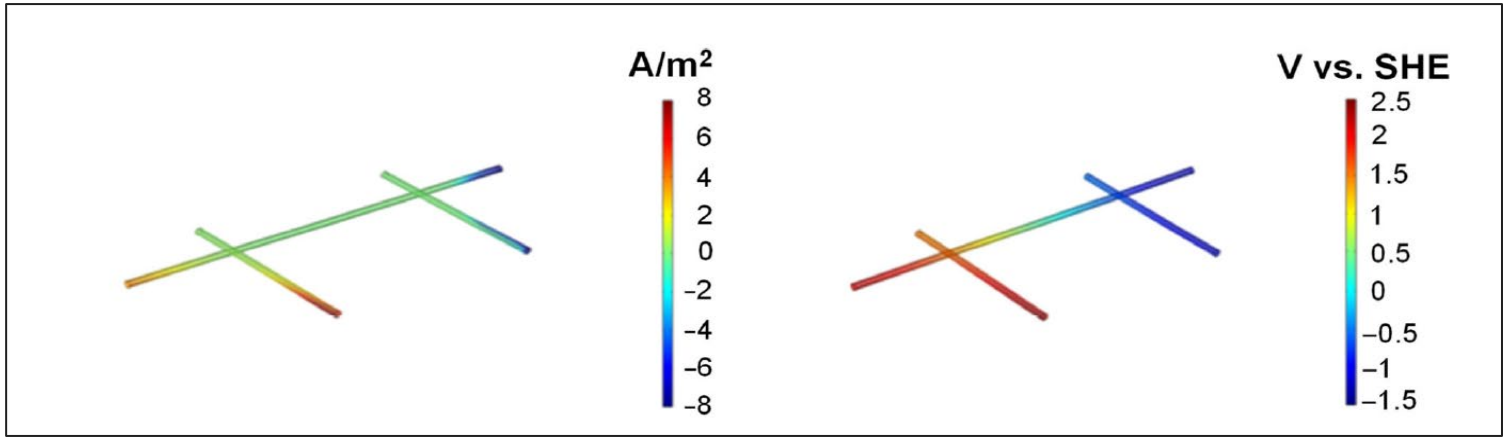

Spatial Distribution of Stray Currents

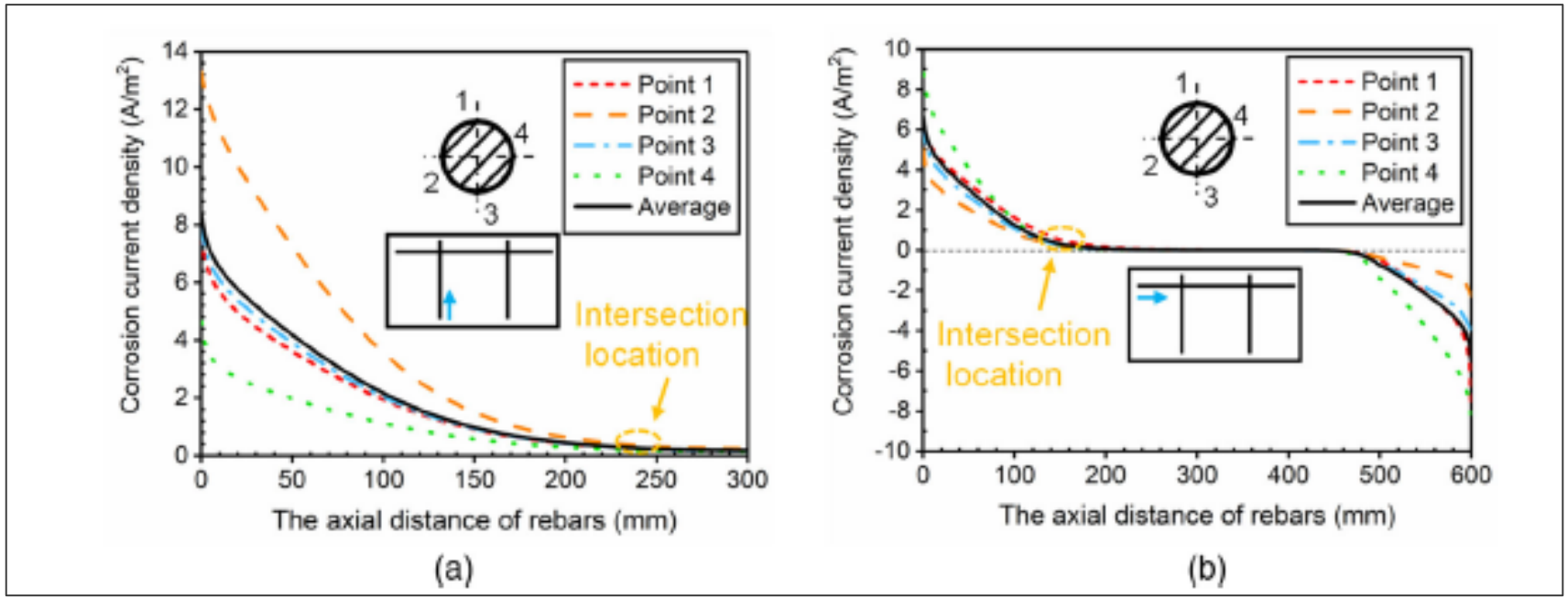

Current density vs. distance along rebar.
Higher values represent discharge.

Spatial Distribution of Stray Currents

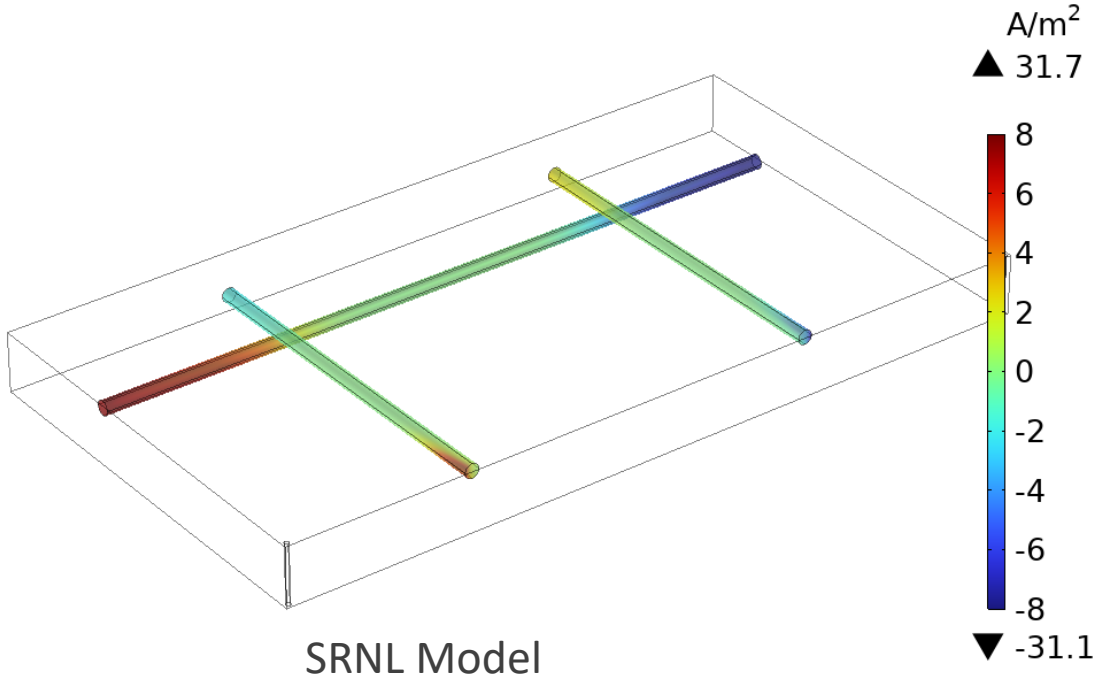

SRNL Model

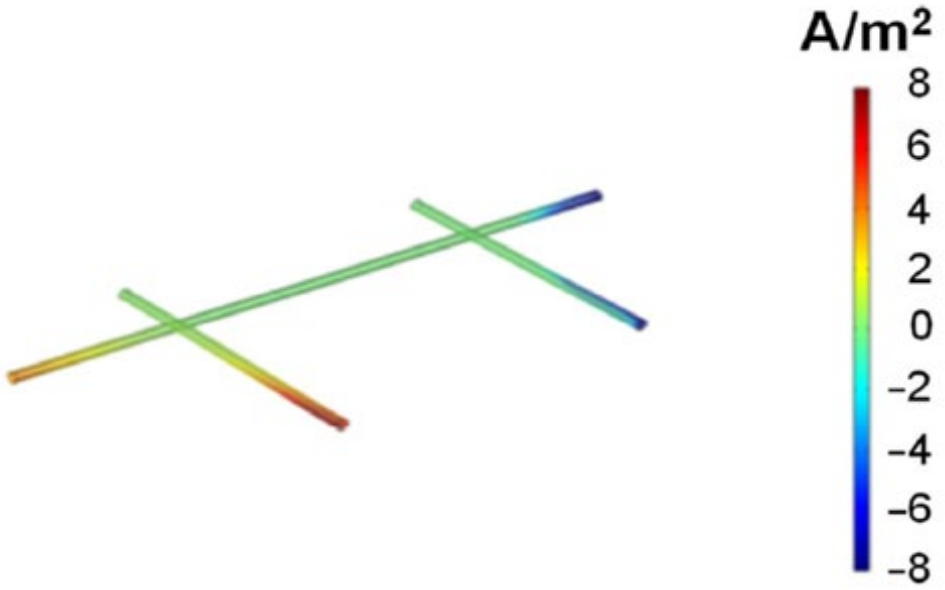

Peng et al. paper

Summary and Path Forward

- Information compilation
  - DST construction details
  - Tank farm buried structure layout
  - Existing CP system layout and associated data
- Modeling
  - DST CP modeling
  - Stray current effect
  - Close-coupled CP system
- Overall integration and CP effect study
- Laboratory-scale experiment
- Establishment of the proof of concept

Appendix D: Task 4 Deliverables — SRNL-STI-2025-00235

A U.S. DEPARTMENT OF ENERGY NATIONAL LAB • SAVANNAH RIVER SITE • AIKEN, SC • USA

Evaluation of Hanford Supernatant Waste Evaporation

B. Barkai

September 2025

SRNL-STI-2025-00235, Revision 0

DISCLAIMER

Printed in the United States of America

Prepared for
U.S. Department of Energy

SRNL-STI-2025-00235
Revision 0

Keywords: Double shell tanks, vacuum evaporation, OLI Studio, LDR organic compounds

Retention: Permanent

Evaluation of Hanford Supernatant Waste Evaporation

B. Barkai

September 2025

Savannah River National Laboratory is operated by Battelle Savannah River Alliance for the U.S. Department of Energy under Contract No. 89303321CEM000080.

REVIEWS AND APPROVALS

AUTHOR:

BENJAMIN BARKAI (Affiliate) Digitally signed by BENJAMIN BARKAI (Affiliate)
Date: 2025.09.18 10:52:31 -04'00'

B. Barkai, Materials Science & Disposition Date

TECHNICAL REVIEWER:

CHRISTOPHER MARTINO (Affiliate) Digitally signed by CHRISTOPHER MARTINO (Affiliate)
Date: 2025.09.18 11:12:09 -04'00'

C. Martino, Advanced & Energy Materials Date

APPROVAL:

PAVAN SHUKLA (Affiliate) Digitally signed by PAVAN SHUKLA (Affiliate)
Date: 2025.09.18 11:55:10 -04'00'

P. Shukla, Lead PI, Materials Science & Disposition Date

MORGANA WHITESIDE (Affiliate) Digitally signed by MORGANA WHITESIDE (Affiliate)
Date: 2025.09.18 11:58:14 -04'00'

M. Whiteside, Manager, Materials Technology & Energy Sciences Division Date

JOSEPH MANNA (Affiliate) Digitally signed by JOSEPH MANNA (Affiliate)
Date: 2025.09.18 12:29:36 -04'00'

J. Manna, Director, Materials Technology & Energy Sciences Division Date

MICHAEL STONE (Affiliate) Digitally signed by MICHAEL STONE (Affiliate)
Date: 2025.09.18 14:30:06 -04'00'

M. Stone, Program Manager, Environmental and Legacy Management Date

ACKNOWLEDGEMENTS

The author acknowledges the U.S. Department of Energy-Environmental Management (DOE-EM) for the funding and support to conduct this research. The investigation of evaporative treatment as an alternative to tank space construction is under the umbrella of a program that was initiated as part of the "R&D Roadmap for Hanford Tank Waste Mission Acceleration" (NNLEMS-2022-00005). The title of the awarded program within the roadmap is, "Integrity Monitoring and Assessment, Prediction, Repair, and Corrosion Control of the Hanford Storage Tanks" (Award #277993). The Principal Investigator for the program is Dr. P.K. Shukla of the Savannah River National Laboratory. The calculations documented in this report are preserved in the SRNL Scientistic Notebook M9313-00792.

The author thanks R. S. Skeen and Z. B. Smith from Hanford Tank Waste Operations & Closure (H2C) for providing additional information concerning Hanford operations and tank waste that assisted in structuring this report. The author acknowledges Dr. Ming Zhu of DOE-EM for supporting and providing programmatic direction for this work.

EXECUTIVE SUMMARY

Storage space within Hanford's double shell tanks is running low, with only an approximate 4.1 Mgal of space remaining. Construction of additional storage space is not a pursuable option, but treatment of the waste via vacuum evaporation may be used to reduce the waste volume and increase the available amount of free space. However, without proper care and consideration, concentrating the waste may lead to harmful effects such as excessive solids generation, growth in liquid density and ionic concentration, and development of aggressive properties in the solution. OLI Studio was used to simulate a subset of DSTs using BBI ionic concentrations to generate recipes of every tank's supernatant layer. Vacuum evaporation was performed by taking each simulated solution and bringing it to 50°C under a pressure of 60 Torr, after which the vapor phase was removed from the simulation, and the solution was brought back to ambient temperature and pressure. Several million gallons of space were created, and only about 100-200 kgal of solids were precipitated during evaporation. Minimal changes to the solution's pitting factor occurred, and no solution is expected to develop aggressive characteristics due to evaporation. Although a theoretical result is provided, it is unique to the specific temperature and pressure value chosen for the simulation, and future transfers of waste are expected to cause changes in waste properties, which would cause the OLI recipes to lose accuracy. Though the results are not anticipated to be used as a target value or a guide, as an exercise, they show that the extent of volume gains could be equivalent to the construction of new DSTs.

Pre-treatment of LDR organics may be required when waste is immobilized into grout under the SLAW program, and a majority of these organics are expected to be treatable by vacuum evaporation. What is less certain is the extent of removal that each compound could experience. After a suitable TSCR pre-treated waste recipe was selected, individual simulations of every potentially present LDR organic were created. Not every compound could be simulated in OLI, but compounds that were successfully inputted generally agreed with anticipated volatility. A few volatile compounds that were simulated showed nonvolatile behavior, and when investigated further, the Henry's law constants of the discrepant compounds were smaller in the simulations compared to recorded literature values. Although the percent removal of each attempted compound is reported, additional work is needed to verify that OLI is accurately simulating the behavior of each organic in the waste solution.

TABLE OF CONTENTS

LIST OF TABLES

LIST OF FIGURES

LIST OF ABBREVIATIONS

ALARA	As Low as Reasonably Achievable
AQ	Aqueous
BBI	Best Basis Inventory
DFLAW	Direct Feed Low Activity Waste
DST	Double Shell Tank
H2C	Hanford Tank Waste Operations & Closure
LAW	Low Activity Waste
LDR	Land Disposal Restriction
MSE	Mixed solvent electrolyte
PF	Pitting Factor
RCRA	Resource Conservation and Recovery Act
SLAW	Supplemental Low Activity Waste
SpG	Specific Gravity
SRNL	Savannah River National Laboratory
SST	Single Shell Tank
TSCR	Tank-Side Cesium Removal
WAC	Waste Acceptance Criteria

1.0 Introduction

Hanford's 200 East and West areas contain a total of approximately 56 million gallons of waste, of which a large portion is held inside the site's double-shell tanks (DSTs). In future Hanford waste processing, the DSTs will have two purposes: storage for the waste that originates from the legacy single shell tanks (SSTs) and other sources, and as feed preparation and staging tanks for waste treatment. Over the past few decades, the available amount of free space inside the DSTs has shrunk to 4.1 million gallons, roughly 13% of their total maximum capacity of 31.7 Mgal. It is paramount that additional storage space is created. The construction of new tanks would create a few additional Mgal of space, but it is undesirable due to the high cost of construction, the duration of time it would take to construct a new farm, and the burden that opening new tanks would place on the Hanford mission goals of complete DST closure. Some insight into the costs is provided in a 2011 RPP System Plan, in which a rough-order estimate cost of $683 million is provided for the design, construction and permitting of a new tank farm. In addition, the report provides an estimated cost of the 241-AP Tank Farm to be $230 million in 2011 [1]. When adjusted for inflation to 2025 using the consumer price index, the cost range could be from $300 million to upwards of about $1 billion. Aboveground storage may be a cheaper and more flexible option in the form of additional temporary interim or mobile storage, but may run into regulatory hurdles due to the greater risk of personnel radiation exposure, necessitating ALARA PPE. Because the construction of new space is undesirable, an alternative treatment method is required to increase the available amount of storage space inside the tanks.

Waste inside Hanford's DSTs stratifies into separate phases, with insoluble sludge and soluble saltcake settling at the bottom, and a water-rich, supernatant appearing above the solid layers. Figure 1 shows that the supernatant layer generally contributes the most to the waste volume. About 27.5 million gallons of waste exist inside the DSTs, and 21.2 million gallons (77%) of that total is present as supernatant. Because this liquid layer is primarily water, targeting this layer with vacuum evaporation would be relatively simple to employ compared to other volume reduction methods, and great gains are anticipated because of the large fraction of space that the supernatant occupies. Hanford has employed vacuum evaporation since the inception of the 242-A Evaporator in 1977, making the methodology fairly mature. Outside of storage needs, vacuum evaporation has also been considered as a treatment option for removal of organics from the waste, particularly for organics that fall into the Resource Conservation and Recovery Act (RCRA) hazardous Land Disposal Restricted (LDR) category. However, not every LDR organic is treatable by evaporation, and each compound's removal efficiency from the waste is not yet well fully understood.

Although practical, volume reduction can change the physical characteristics of the waste in a manner that impacts site operations, including but not limited to changes in density, total solids, or corrosivity. Furthermore, it is unknown if the amount of storage space that is made available through vacuum evaporation will justify the labor and time that is required. In order to understand the limits of supernatant evaporation, such as the extent of gains in storage space and organic removal, the waste must be simulated to see how it may evolve with changes in pressure and temperature. Using OLI Studio, simulations of vacuum evaporation were performed on solutions mimicking the supernatant layer to generate a rough estimate of concentrated waste characteristics.

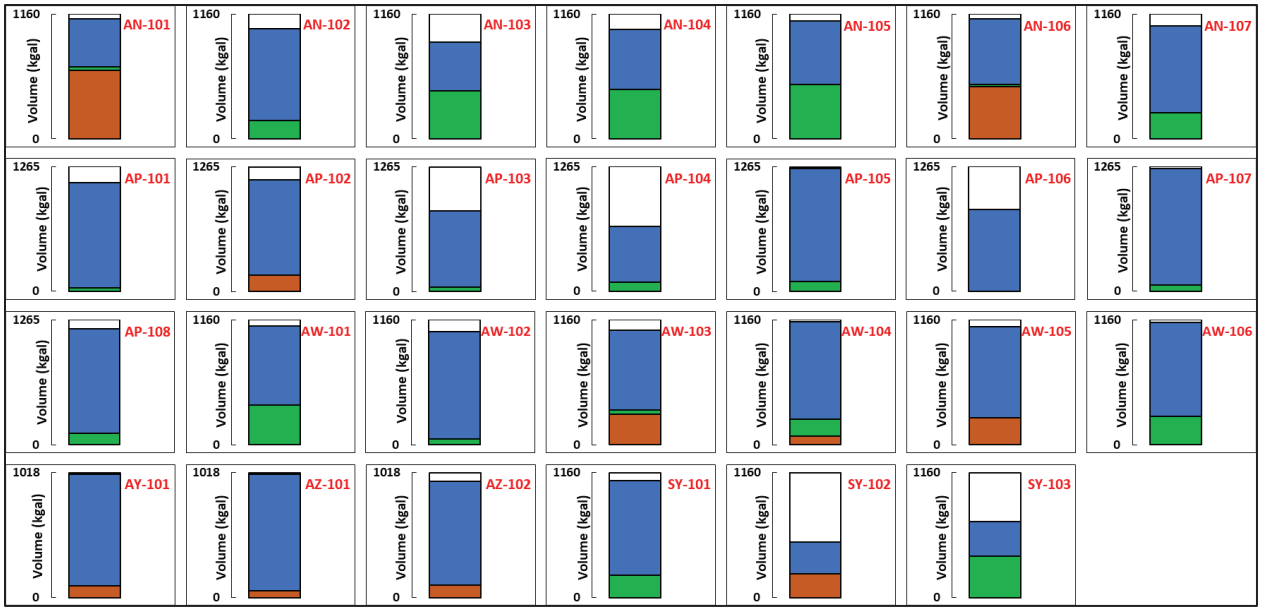

Figure 1. Tank waste volume for each DST on site. Brown layers represent sludge, green represents saltcake, and blue represents supernatant. Waste phases were calculated using BBI data obtained from PHOENIX on April 10th, 2025.

2.0 Discussion

2.1 Storage

Currently, the direct-feed low-activity waste (DFLAW) program is used to treat the low-activity waste (LAW) inside the DSTs, a pathway in which waste is pretreated to filter out radioactive Cs-137/Sr-90 using the Tank Side Cesium Removal system (TSCR) before it is sent to the Waste Immobilization and Treatment Plant (WTP) to be vitrified into solid glass [2, 3].

An original assumption for the OLI waste simulations was that the stored waste must fall beneath TSCR's waste acceptance criteria (WAC) over the entirety of its evolution. The TSCR WAC has several major limits: the incoming waste must match the site definition of a supernatant (specific gravity (SpG) value below 1.35 & insoluble solids account for <5% by mass or volume), and the waste stream's potassium & sodium content must fall beneath a 0.16 M and 6 M concentration threshold respectively, as these ions can impact TSCR's ion-exchange columns and filters at higher concentrations [2]. Using the BBI data for each DST, Table 1 shows that almost every DST currently exceeds at least one of these criteria. Taking density as an approximation for SpG, only 13 of the 27 tanks have supernatants that meet the TSCR WAC, and only 6 meet both the SpG and ion concentration criteria. Vacuum simulations in OLI Studio were performed on the remaining six WAC-complying tanks to see if any meaningful volume reduction is possible without concentrating the waste above the WAC criteria of density and ion concentrations.

Table 1. Tank Densities and Ion Concentrations. Values in red have exceeded the TSCR WAC.

Tank	Density (g/mL)	Na^+ (M)	K^+ (M)
SY-102	1.20	3.69	0.011
AW-102	1.20	4.22	0.103
AW-103	1.22	4.64	0.267
AP-102	1.24	4.64	0.151
AN-101	1.25	5.41	0.075
AP-107	1.25	5.41	0.089
AP-106	1.27	5.78	0.084
AN-106	1.28	6.31	0.059
AZ-102	1.29	6.01	0.065
AP-108	1.30	6.31	0.162
AW-105	1.32	5.83	0.579
AY-101	1.33	6.17	0.087
AP-101	1.33	7.38	0.101
AZ-101	1.35	7.92	0.155
AW-104	1.37	8.58	0.148
AP-103	1.39	8.79	0.135
AW-106	1.40	9.72	0.165
AN-104	1.40	11.28	0.173
AP-104	1.41	9.01	0.153
AN-107	1.42	8.58	0.045
AN-105	1.42	10.73	0.168
AP-105	1.42	8.69	0.193
AN-102	1.45	10.70	0.069
AW-101	1.47	10.13	0.900
SY-103	1.48	10.25	0.120
AN-103	1.48	11.74	0.426

The waste data suggests that even if a tank currently has density and cation concentrations that meet the WAC limits, they are close enough to the WAC limits to prohibit meaningful volume reduction. In order to increase the overall volume reduction and the number of tanks that could qualify for evaporation, the supernatant waste is expected to require exceeding the WAC. Communication with H2C personnel has revealed that additional factors could also make a tank ineligible for evaporation, as shown in Table 2. Waste Group A status is a major concern, indicating that the tank has a high risk of experiencing flammable buoyant displacement gas release events [2]. Tanks that are designated as Waste Group A are a safety risk, and the status must be remediated before any further work could take place. Waste Group A status is determined by several factors, but a major contributor is the total amount of solids that are present in the tank.

Table 2. Tanks ineligible for evaporation

Tank	Limitation
AN-105, AN-103, AW-101, AN-104, SY-103	Waste Group A
AN-102, AN-107	Complexant Tanks (high organic concentration)
AN-106, AN-107, AP-104, AP-105, AP-106, AP-107	Feed tanks
SY Tank Farm	Cross-site transfer required
AZ-101	High radioisotope activity
AW-105	Excess phosphate

To develop a practical candidate list for the OLI simulations, DSTs with low supernatant densities were considered (utilizing the WAC threshold of 1.35 as an arbitrary cut-off point), as tanks with lower densities would be easier to dilute for retrieval after they have been concentrated. Only 13 tanks have an SpG below 1.35, and five from that set are ineligible for evaporation. The remaining eight tanks, listed in Table 3, were simulated in OLI Studio to see the extent of volume reduction possible and the total amount of solids that are generated.

Table 3. Candidate tanks for evaporation

Tank	BBI Density (g/mL)
AN-101	1.25
AP-101	1.33
AP-102	1.24
AP-108	1.30
AW-102	1.20
AW-103	1.22
AY-101	1.33
AZ-102	1.29

When waste is evaporated, the reduction in volume will increase the concentrations of all chemical species found in the waste. Simultaneously, solids will precipitate and will remove specific ions from the solution. If the concentration of corrosion-promoting ions grows too high with respect to the concentration of corrosion-inhibiting ions, the supernatant can develop aggressive characteristics and lead to pitting corrosion of the steel tank walls. The pitting factor (PF) of Hanford waste may be measured as a weighted ratio of corrosion-inhibiting ions to corrosion-promoting ions using the following equation [4]:

$$\text{Pitting Factor} = \frac{8.06\,[\mathrm{OH^-}] + 1.55\,[\mathrm{NO_2^-}]}{[\mathrm{NO_3^-}] + 16.7\,[\mathrm{Cl^-}] + 5.7\,[\mathrm{F^-}]}$$

PF values above 2 indicate that pitting is unlikely to occur, while values below 1 indicate that pitting is highly likely to occur. Values between 1 and 2 indicate a moderate chance of pitting, with lower values indicating elevated risk. Even if other tank properties permit substantial volume reduction, a decrease in PF is undesirable, and possible changes in PF must be simulated to see if the tank waste becomes more corrosive after evaporation has been performed.

2.2 Organic Vaporization

The WTP is predicted to not have the capacity to treat roughly 50% of the existing LAW during the DFLAW mission. To ensure full immobilization of the waste, a supplemental LAW (SLAW) program is required. The SLAW pathway is identical to the DFLAW program, but with a key difference in the method of immobilization: DFLAW vitrifies the waste, but SLAW will grout the aqueous waste into a cementitious form. Grouting is a favorable methodology because it is quick to implement and fairly inexpensive compared to alternatives [3], but the supernatant waste may require additional pre-treatment to comply with federal regulations.

As part of the 1984 Hazardous and Solid Waste Amendments to the RCRA, the Land Disposal Restrictions (LDR) for Hazardous Waste program specifies that land disposal of untreated hazardous waste is prohibited, and the EPA must set concentration limits for hazardous compounds which are required to be met prior to

disposal. When waste is vitrified, operating temperatures can reach above 1000 °C, which is considered sufficient to destroy any hazardous organic compounds that could be present in the waste [3]. Grouting does not involve such high temperatures, and the solidified waste may retain LDR organics that exceed the concentration limits. The organic chemistry in the Hanford tanks has not been fully characterized, and information about the compounds inside the tanks, including the expected concentrations, is limited. Sampling of Hanford waste for the specific LDR organics has not been extensive, and only a few DSTs have been sampled in the past few decades. Out of the 207 LDR organic compounds, 132 have been identified as potentially present in the Hanford waste [5], but not all of them are expected to vaporize.

LDR concentration limits are set in units of mg/kg (ppm) and the sampling data, although not fully extensive, shows that few organics have been detected above the limits [6]. Because the organics are so dilute, they are expected to follow Henry's law, which states that the partial pressure of an organic vapor above a solution is proportional to the amount of that same organic dissolved in the solution. The proportionality constant, H_v, can be interpreted as an indicator for whether an organic compound is volatile or not; greater H_v values mean that a compound has a greater tendency to vaporize. If a semi-volatile compound with a low H_v can be shown to vaporize under vacuum conditions, then it can be assumed that any compound with a higher H_v value is vaporizable under those same conditions. Experimental studies done in 2023 showed that N-nitrosomorpholine, which has the one of the lowest H_v values among the LDR organics, is treatable by vacuum evaporation, and is the current theoretical threshold of volatility [7]. The relative amount of removal that each organic can experience in a waste solution is not yet fully understood.

2.3 OLI Frameworks

Two available frameworks were used in the OLI simulations: Mixed-solvent electrolyte (MSE) and the older Aqueous (AQ) framework. Both frameworks calculate the activity coefficients of present species in the simulation, but vary in their approach for the calculations: a description of how these models are calculated may be found elsewhere [8]. In more qualitative terms, the AQ framework assumes that the solvent in the simulation is water, and erroneous results may occur if the simulation has high values of solute concentration, ionic strength, temperature or pressure. The MSE framework is not limited to water as a solvent, and as a result, has less limitations in solution parameters. OLI Systems recommends the use of the MSE framework over AQ, but because MSE is more recent, its provided chemical database contains less entries compared to the AQ framework, especially for organic species [9]. For the volume reduction simulations, the MSE framework was used, but for the organic evaporation simulations, the AQ framework was used.

Simulations were performed in OLI's Stream Analyzer software, which assumes and calculates steady-state equilibria for multi-phase solutions. Although the 242-A evaporator behaves as a continuous system, the surveys performed in OLI studio were performed as a batch system, in which the entire volume of the solution was brought to a final pressure and temperature. Steady-state vapor phases that formed were subsequently excluded from the solution, and the concentrate was then brought back to the initial temperature and pressure conditions.

3.0 Methodology

Recipes of DST supernatant phases were created using version 12.0 of OLI Studio. The Best Basis Inventory (BBI) for each tank was downloaded from PNNL's PHOENIX Gallery on April 10, 2025. Simulant recipes were generated by inputting the ions with the greatest concentrations into OLI's Water Analysis tool under the MSE framework, listed in Table 4. Although waste temperatures inside the DSTs

may vary, a simplifying assumption was made that the initial temperature condition of every supernatant was 25 °C (77 °F).

Table 4. List of major ion species used in OLI supernatant recipes.

Ion
Na^{+1}
NO_3^{-1}
NO_2^{-1}
TIC as CO_3^{-2}
Free OH^{-1}
Al^{+3} as $Al(OH)_4^{-1}$
SO_4^{-2}
K^{+1}
Cl^{-1}
PO_4^{-3}
TOC as $C_2H_3O_3^{-1}$
F^{-1}
$C_2O_4^{-2}$

A few adjustments to the BBI ion information were required when input into OLI. The cation and anion concentrations are likely to experience charge imbalance, a result of trace waste ions being excluded from the simulation and sampling measurements containing unavoidable noise. For the recipe to be generated, the imbalance must be first reconciled by adjusting species molarity. Sodium was chosen to be reconciled in each recipe due to it having the highest concentration in the waste (minimizing percent change in molarity) and because of the smaller impact it would have on the calculated pitting factor. Note that while sodium is entered into the water analysis tool as a free ion concentration, the generated output recipe will split the total amount of sodium between free ions in solution, aqueous compounds containing Na^+, and solid compounds. Concentrations of sodium and potassium ions that appear in this report indicate the total aqueous content.

Although BBI provides CO_3^{-2} as a representative ion for TIC, no such ion is provided for TOC. A generic TOC value cannot be entered into OLI, and although TOC represents a mixture of organics, as an enabling step, glycolate was selected to be a single representative ion. Despite oxalate appearing as a separate entry in the BBI, the TOC amount was not adjusted to account for the oxalate concentration, as both compounds appear in such minute concentrations that it is unlikely to affect the physical properties of the solution.

In the extremely alkaline conditions of the supernatant, with pH values approximately 13-14, aluminum tends to stabilize into hydroxyaluminate ($Al(OH)_4^{-1}$). If Al^{+3} is entered into OLI's recipe generator alongside OH^-, the two ions will immediately react with each other and become depleted. OH^- is needed for the pitting factor calculations, and it is crucial that the recipe's free OH^- concentration matches the information provided in the BBI. As a result, Al^{+3} is entered into the recipe generator in the form of $Al(OH)_4^{-1}$ without any changes to its molarity, which gives greater stability to the entered OH^- values in the simulation, but causes the output concentration of free hydroxide to become slightly elevated in the generated recipes. To balance the free hydroxide concentration with the BBI data, the OH^- molarity was lowered manually in the recipe input until the generated output matched the BBI concentration to four decimal places. Removal of anions from the simulation will affect the degree of charge imbalance and reconciliation, causing the "reduced hydroxide" recipes to have a smaller sodium content relative to the "unmodified" recipes.

Although the reduced hydroxide recipes provide more accurate OH^- values, the supernatant density and sodium concentration decreases – neither recipe version ("reduced" or "unmodified") is a perfect representation of the waste that exists inside the tanks, so simulation results for both versions are provided in this report. Differences in properties between the two OLI recipe versions are shown in Appendix A.

3.1 Volume Simulations

For the six WAC-complying tanks, supernatant recipes were temperature surveyed in intervals of 0.05 °C under a pressure of 60 Torr, as demonstrated by Figure 2. After a temperature was reached that caused a physical property to exceed the WAC, the vapor phase was ejected from the simulation, and the resulting concentrated solution was brought back to 25°C and 760 Torr. Ion concentration and density will increase slightly when the solution is returned to ambient conditions, so temperatures below the initial stopping temperature were sampled in decreasing order until an evaporation temperature gave WAC-agreeable values after the concentrated waste was brought back to 25°C and standard pressure. This temperature was recorded as the maximum vaporization temperature. Changes in liquid volume and density were recorded.

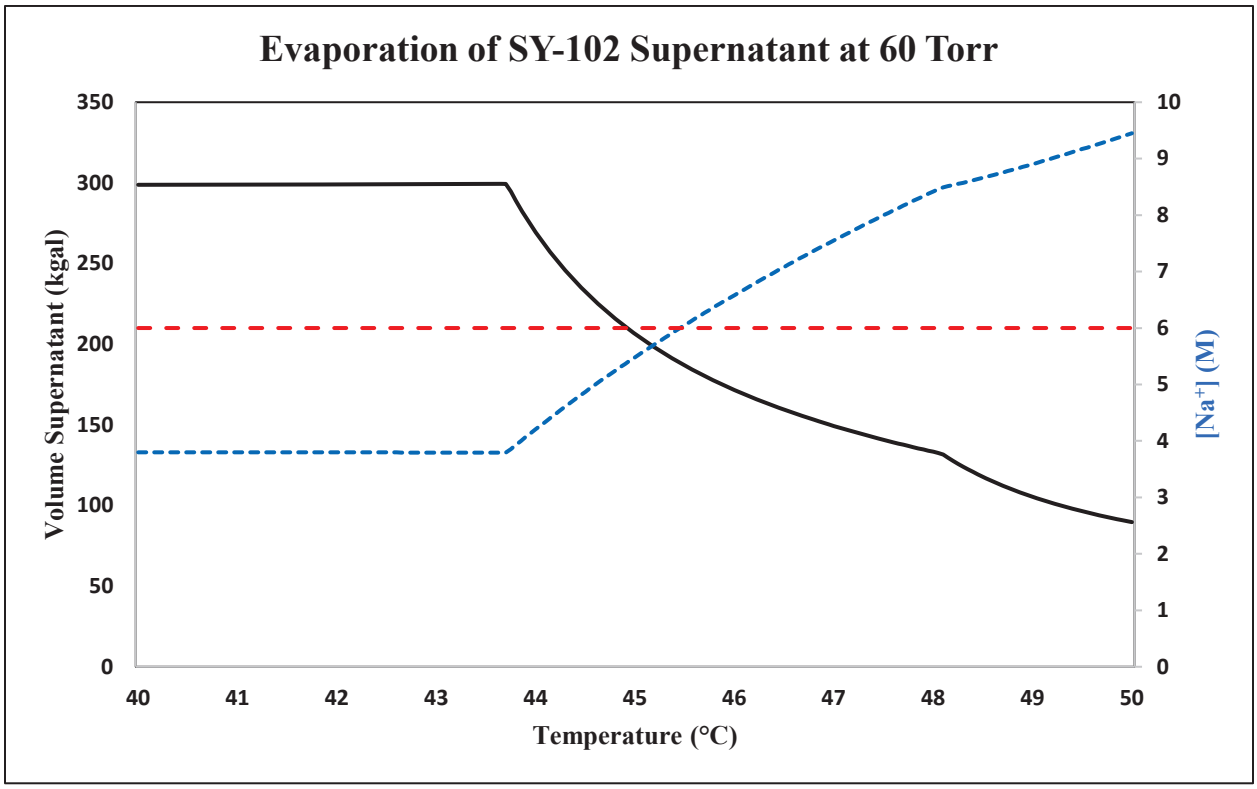

Figure 2. Calculated changes in the volume and $[Na^+]$ concentration of SY-102's supernatant with respect to temperature. 6 M limit (shown in red) is reached at approximately 45.4 °C.

For the eight candidate tanks, similar temperature surveys were performed under pressure conditions of 60 Torr, but in intervals of 1°C. Each survey was brought to 50°C, which produced an approximate final density of 1.40 g/mL in all supernatants. The vapor phase was ejected, and the concentrated waste was brought back to atmospheric pressure and 25°C. Changes in liquid volume, solid volume and the concentration of corrosion-affecting ions were recorded.

3.2 Organic Vaporization

An assumption was made that the LDR organic pre-treatment would occur after the waste has been processed through TSCR and before it is immobilized. Thus, a supernatant recipe is required that would reflect post-TSCR characteristics of a waste stream. For the SY-farm located in West Area, the 2024 200W Preliminary Flowsheet uses GCALC to predict characteristics of every waste feed at every step along the DFLAW/SLAW process, using TWINS data that was downloaded on 7/15/2024. From this flowsheet, West Waste Feed-1 was selected, representing a blended supernatant feed from SY-101 and SY-102, and its ionic concentrations were extracted from Stream 5, representing the feed after it has been pre-treated through TSCR and transferred into an interim low-activity waste storage tank (ILST) [2]. Ions selected for the OLI recipe were identical to the ones in Table 4. The recipe was generated under the AQ framework due to the greater amount of organic compounds in the database compared to the MSE framework. Sodium was chosen to be reconciled for charge imbalance. Although natroxalate precipitated out in the recipe, aluminum content was low and did not form any solids, which kept the free hydroxide concentration identical to the entered amount. Only a single recipe version was created, with ion concentrations listed in Table 5.

Table 5. Projected ionic concentration of pre-treated SY supernatant. Addition of reconciled amount shown for sodium.

Ion	Concentration (M)
Na^{+1}	5.1538 (+0.2771)
K^{+1}	0.032517
Free OH^{-1}	1.41434
NO_2^{-1}	1.11947
NO_3^{-1}	1.55217
Cl^{-1}	0.110352
F^{-1}	0.012961
SO_4^{-2}	0.037644
PO_4^{-3}	0.061537
CO_3^{-2}	0.363769
$C_2O_4^{-2}$	0.012058
$Al(OH)_4^{-1}$	0.152549
$C_2H_3O_3^{-1}$	0.089991

At a pressure of 60 Torr, temperatures of 45.31°C, 45.53°C, 45.84°C and 46.21°C were selected that would simulate a volume reduction of 1%, 5%, 10% and 15% in the 718 kgal of solution (equivalent to a liquid volume loss of 7 kgal, 36 kgal, 72 kgal and 108 kgal respectively). Copies of the recipe were generated, each having an addition of single LDR instance at 100 mg/L, until every one of the 132 potentially present LDR compounds had been simulated. Under the AQ framework, OLI calculates the vapor-liquid equilibria using the Soave-Redlich-Kwong equations of state, but unanticipated results may arise if interaction parameters are missing from the database [7, 9].

4.0 Results

In total, 11 different tank supernatants were investigated, with six tanks being selected for evaporation that would not breach the WAC, and a second set of eight “candidate tanks” being selected due to their low densities (Table 3). Three DSTs were eligible for both conditions, lowering the expected total of simulations

from 14 to 11. Table 6 shows the starting densities of each generated recipe. Between the candidate tanks, 7 Mgal of supernatant volume exist, and between the WAC tanks, 4.7 Mgal of supernatant exist.

Table 6. Volume and density of DST supernatants

Set	Tank	Supernatant Volume (kgal)	PHOENIX BBI Density (g/mL)	OLI BBI Recipe Density (g/mL)	OLI Reduced Hydroxide Density (g/mL)
Candidate	AW-103	745	1.22	1.232	1.228
Candidate	AZ-102	846	1.29	1.279	1.265
Candidate	AP-108	1060	1.30	1.325	1.313
Candidate	AP-101	1071	1.33	1.332	1.316
Candidate	AY-101	909	1.33	1.283	1.276
WAC	SY-102	296	1.20	1.187	1.183
WAC	AP-107	1182	1.25	1.244	1.235
WAC	AP-106	831	1.27	1.257	1.248
WAC/Candidate	AW-102	999	1.20	1.190	1.181
WAC/Candidate	AP-102	972	1.24	1.214	1.208
WAC/Candidate	AN-101	448	1.25	1.241	1.234

A drop in density occurs when the input concentration of hydroxide is reduced, which is expected since $[OH^-]$ and $[Na^+]$ are removed from the solution. Tank densities were not far off from the PHOENIX Gallery BBI values for each supernatant, with a displacement of about ±0.03 g/mL. However, AY-101 experienced significant deviation, being 0.05 g/mL lower than the BBI value. Appendix A shows that the removal of ions during the AY-101's reconciliation is comparable to the other tank formulas, so the dramatic drop-off in density cannot be fully explained by changes to the ion concentration. Although this could suggest the presence of inaccuracies in the BBI data, the density difference in OLI may have also resulted from the choice of ions in the recipe list. Only the major ion constituents were simulated, and ions that were excluded could have had an impact on the density (applicable to every tank).

4.1 Volume Reduction

For the six WAC-complying tanks, the volume change in the supernatant phase as a result of evaporation is shown in Table 7. This volume change does not factor in the volume change of solids. As previously stated, the supernatants are close to the WAC limits, and were not anticipated to experience drastic volume reduction. Ion concentrations were shown to be the primary limiting factor, and tank supernatants reached the concentration limits first before the SpG limits. For volume change, only tanks AW-102 and SY-102 experienced a large percent change in supernatant volume, with the remaining four tanks experiencing a percent change in the range of 4-15%.

Table 7. Simulated volume reduction as a result of vacuum evaporation in WAC-complying tanks

a) Unmodified Recipe

Tank	AN-101	AP-102	AP-106	AP-107	AW-102	SY-102
Volume (kgal)	448	972	831	1182	999	296
Density (g/mL)	1.25	1.24	1.27	1.25	1.20	1.20
OLI Density (g/mL)	1.241	1.214	1.257	1.244	1.190	1.187
Evaporation Temp. (°C)	45.95	44.8	45.85	45.95	46.00	45.45
Limit	Na^+	K+	Na^+	Na^+	Na^+	Na^+
Limiting Concentration (M)	5.955	0.158	5.991	5.990	5.958	5.974
OLI Final Density (g/mL)	1.260	1.223	1.268	1.270	1.267	1.271
Volume Evaporated (kgal)	36	43	39	127	314	106
Volume Change (%)	-8.1	-4.4	-4.7	-10.7	-31.4	-35.7

b) Reduced OH Recipe

Tank	AN-101	AP-102	AP-106	AP-107	AW-102	SY-102
Volume (kgal)	448	972	831	1182	999	296
Density (g/mL)	1.25	1.24	1.27	1.25	1.20	1.20
OLI Density (g/mL)	1.234	1.208	1.248	1.235	1.181	1.183
Evaporation Temp. (°C)	45.90	44.65	45.80	45.90	45.95	45.40
Limit	Na^+	K+	Na^+	Na^+	Na^+/K^+	Na^+
Limiting Concentration (M)	5.956	0.1597	5.979	5.978	5.957/0.1599	5.957
OLI Final Density (g/mL)	1.262	1.218	1.269	1.271	1.270	1.271
Volume Evaporated (kgal)	52	50	73	174	357	111
Volume Change (%)	-11.7	-5.2	-8.8	-14.7	-35.7	-37.3

The total volume reduction between all six tanks is small. With the original unmodified recipes, only about 664 kgal of supernatant are expected to be vaporizable, and this sum is increased with the reduced hydroxide recipes to 816 kgal. Because the reduced hydroxide recipes lower the initial concentration of sodium, it can be assumed that the 816 kgal is an upper estimate of volume change, and the 664 kgal a lower estimate. Not only is this amount smaller than the ~1 Mgal capacity of a single DST, but it accounts for only a 14-17% reduction in the 4.7 million gallons of supernatant that is inside these six tanks. If every DST onsite is considered, this volume reduction represents only ~3-4% of the overall supernatant waste.

For the eight candidate tank supernatants, Table 8 shows the volume reduction and physical properties of the aqueous supernatant phase after each tank was brought to 50 °C. This volume change does not factor in

the volume change of solids as a result of precipitation. Density values hovered around 1.40 g/mL for each evaporated supernatant. Ion concentrations were somewhat variable, but the average concentrations for sodium and potassium were ~9.4 and ~0.25 M respectively. Tanks that had a larger initial density experienced smaller percent reduction in the volume. The greatest amount of volume reduction occurred in tanks AW-102, AP-102 and AY-101. Because AY-101's OLI density is much lower than the BBI density, the amount of volume reduction is overrepresented. If the overall volume loss is summed, about 3 Mgal of supernatant is evaporated in each recipe version, which accounts for a 41-46% removal of supernatant, and a 14-15% reduction of the total combined supernatant volume of all 27 DSTs.

Table 8. Simulated volume reduction as a result of vacuum evaporation for eight candidate DSTs

a) Unmodified Recipe

Tank	AN-101	AP-101	AP-102	AP-108	AW-102	AW-103	AY-101	AZ-102
Initial Density (g/mL)	1.241	1.332	1.214	1.325	1.190	1.232	1.283	1.279
Initial Volume (kgal)	448	1071	972	1060	999	745	909	846
Final Volume (kgal)	252	786	397	858	428	382	495	510
Volume Reduction (%)	-43.8	-26.6	-59.1	-19.0	-57.1	-48.7	-45.5	-39.7
Volume Removed (kgal)	196	284	575	201	571	363	414	336
Final Density (g/mL)	1.393	1.409	1.404	1.395	1.408	1.406	1.413	1.405
$[Na^+]$ (M)	9.31	9.59	9.34	9.23	9.46	9.02	9.59	9.58
$[K^+]$ (M)	0.134	0.137	0.371	0.200	0.240	0.520	0.160	0.107

b) Reduced OH Recipe

Tank	AN-101	AP-101	AP-102	AP-108	AW-102	AW-103	AY-101	AZ-102
Initial Density (g/mL)	1.234	1.316	1.208	1.313	1.181	1.228	1.276	1.265
Initial Volume (kgal)	448	1071	972	1060	999	745	909	846
Final Volume (kgal)	236	713	370	807	388	368	466	455
Volume Reduction (%)	-47.3	-33.4	-62.0	-23.8	-61.1	-50.6	-48.8	-46.3
Volume Removed (kgal)	212	358	602	253	610	377	443	392
Final Density (g/mL)	1.397	1.414	1.408	1.402	1.414	1.411	1.415	1.410
$[Na^+]$ (M)	9.38	9.66	9.39	9.37	9.54	9.11	9.62	9.68
$[K^+]$ (M)	0.142	0.152	0.398	0.213	0.264	0.540	0.170	0.120

4.2 Solids

Between all eight candidate tanks, seven solid species are predicted to appear with OLI Studio, listed in Table 9. Not all species appeared in every tank: NaF was only simulated in the waste of AW-103, and burkeite only appears in AZ-102, AY-101 and AP-101. Table 10 shows the mass of solids inside the eight candidate tanks after the waste was concentrated by vacuum evaporation.

Table 9. List of solid species detected between all eight evaporated DST supernatants.

Mineral Scale	Formula
Thermonatrite	$Na_2CO_3 \cdot 1H2O$
Gibbsite	$Al(OH)_3$
Natrophosphate	$Na_7F(PO_4)_2 \cdot 19H2O$
Kogarkoite	$Na_2SO_4 \cdot NaF$
Burkeite	$2Na_2SO_4 \cdot Na_2CO_3$
Natroxalate	$Na_2C_2O_4$
Villiaumite	NaF

Table 10. Mass and distribution of solids in the concentrated supernatant of candidate DSTs

a) Unmodified Recipe

Tank	AN-101	AP-101	AP-102	AP-108	AW-102	AW-103	AY-101	AZ-102
Solids Weight (Mg)	56.04	327.72	272.96	118.58	86.13	75.44	309.66	250.12
Thermonatrite (mass %)	25.42	36.43	60.85	-	3.06	-	71.08	36.10
Gibbsite (mass %)	48.34	47.31	19.94	98.38	86.44	40.09	20.80	42.47
Natrophosphate (mass %)	10.48	-	11.88	-	7.02	8.83	3.28	1.25
Kogarkoite (mass %)	12.83	3.44	4.65	-	0.69	20.51	3.24	3.10
2Na2SO4.Na2CO3 (mass %)	-	4.28	-	-	-	-	0.78	8.31
Natroxalate (mass %)	2.93	8.55	2.68	1.62	2.79	5.85	0.82	8.76
Villiaumite (mass %)	-	-	-	-	-	24.71	-	-

b) Reduced OH Recipe

Tank	AN-101	AP-101	AP-102	AP-108	AW-102	AW-103	AY-101	AZ-102
Solids Weight (Mg)	68.36	381.11	293.83	132.50	115.82	79.32	334.71	296.30
Thermonatrite (mass %)	31.31	38.78	61.14	-	19.00	-	69.86	37.60
Gibbsite (mass %)	45.66	44.30	20.34	98.55	70.81	41.92	20.38	39.73
Natrophosphate (mass %)	9.61	0.57	11.60	-	7.26	9.03	4.12	3.28
Kogarkoite (mass %)	11.02	2.91	4.43	-	0.85	19.87	2.76	2.15
2Na2SO4.Na2CO3 (mass %)	-	6.09	-	-	-	-	2.12	9.85
Natroxalate (mass %)	2.40	7.35	2.49	1.45	2.08	5.57	0.76	7.40
Villiaumite (mass %)	-	-	-	-	-	23.61	-	-

The ion concentrations taken from the BBI were associated with the supernatant phase, but when the initial recipes were generated in OLI, gibbsite and natroxalate had high scaling factors and were predicted to appear in every simulated supernatant. A third initial species appeared in AW-103 in the form of villiaumite. The weights of the initial supernatant solids are listed in Table 11. Table 12 shows the distribution of aluminum and oxalate between the liquid and solid phases. Virtually all oxalate in the initial recipes is present as solid natroxalate, with only AW-102 having a significant portion (approximately 25%) remaining in the aqueous phase. Most of the aluminum is precipitated as well, but compared to oxalate, a greater fraction will exist in the liquid phase.

Table 11. Weights of initial supernatant-associated solids

a) Unmodified Recipe

Tank	Volume	Gibbsite (Mg)	Natroxalate (Mg)	Villiaumite (Mg)
AN-101	448	29.244	1.546	-
AP-101	1071	151.252	27.999	-
AP-102	972	52.455	6.761	-
AP-108	1060	116.555	1.899	-
AW-102	999	71.872	1.806	-
AW-103	745	28.421	4.242	2.814
AY-101	909	59.740	2.493	-
AZ-102	846	104.771	21.868	-

b) Reduced OH Recipe

Tank	Volume	Gibbsite (Mg)	Natroxalate (Mg)	Villiaumite (Mg)
AN-101	448	32.068	1.535	-
AP-101	1071	163.576	27.997	-
AP-102	972	56.446	6.704	-
AP-108	1060	128.414	1.896	-
AW-102	999	77.668	1.690	-
AW-103	745	30.721	4.232	1.808
AY-101	909	63.703	2.489	-
AZ-102	846	114.030	21.858	-

Table 12. Distribution of supernatant Al^{+3} and oxalate ions between the liquid and solid phases

a) Unmodified Recipe

	Aluminum		Oxalate	
Tank	**Liquid (mol %)**	**Solid (mol %)**	**Liquid (mol %)**	**Solid (mol %)**
AN-101	37.92	62.08	5.96	94.04
AP-101	18.98	81.02	0.05	99.95
AP-102	27.10	72.90	7.48	92.52
AP-108	32.67	67.33	1.02	98.98
AW-102	22.52	77.48	24.93	75.07
AW-103	38.92	61.08	3.91	96.09
AY-101	20.49	79.51	1.95	98.05
AZ-102	20.84	79.16	0.25	99.75

b) Reduced OH Recipe

	Aluminum		Oxalate	
Tank	**Liquid (mol %)**	**Solid (mol %)**	**Liquid (mol %)**	**Solid (mol %)**
AN-101	31.92	68.08	6.65	93.35
AP-101	12.38	87.62	0.05	99.95
AP-102	21.56	78.44	8.26	91.74
AP-108	25.82	74.18	1.16	98.84
AW-102	16.28	83.72	29.76	70.24
AW-103	33.97	66.03	4.14	95.86
AY-101	15.22	84.78	2.11	97.89
AZ-102	13.85	86.15	0.29	99.71

Although the mass of the solids is high, with some supernatant recipes having more than 100 Mg of initial solids, the volume that is contributed by the solids is small relative to the supernatant layer. Table 13 provides the volume of the initial solids that form during OLI's recipe creation, the volume of generated solids that form during evaporation, and the total volume of solids that are associated with the final concentrated supernatant. No single tank had more than 50 kgal of solids associated with the supernatant even after evaporation had occurred, and the highest amount of generated solids occurred in AY-101, with 32 kgal formed in the reduced hydroxide recipe. The combined volume of solids between the unmodified and reduced hydroxide versions is 170 kgal and 193 kgal respectively, three orders of magnitude smaller than the total supernatant volume that had been evaporated during the simulation.

Table 13. Volume of supernatant associated solids

a) Unmodified Recipe

Tank	Initial Supernatant Volume (kgal)	Total Initial Volume of Supernatant Solids (kgal)	Generated Solids (kgal)	Final Volume of Supernatant Solids (kgal)
AN-101	448	3.34	3.04	6.38
AP-101	1071	19.53	16.98	36.51
AP-102	972	6.44	25.90	32.34
AP-108	1060	12.83	0.01	12.84
AW-102	999	7.98	1.62	9.60
AW-103	745	3.82	4.25	8.07
AY-101	909	6.75	29.11	35.86
AZ-102	846	13.81	14.13	27.94
Total	-	74.50	95.05	169.55

b) Reduced OH Recipe

Tank	Initial Supernatant Volume (kgal)	Total Initial Volume of Supernatant Solids (kgal)	Generated Solids (kgal)	Final Volume of Supernatant Solids (kgal)
AN-101	448	3.64	4.16	7.81
AP-101	1071	20.87	21.72	42.59
AP-102	972	6.87	27.92	34.79
AP-108	1060	14.11	0.24	14.35
AW-102	999	8.60	4.49	13.09
AW-103	745	3.97	4.54	8.51
AY-101	909	7.18	31.66	38.83
AZ-102	846	14.81	18.56	33.37
Total	-	80.05	113.29	193.34

4.3 Pitting Factor

In the eight candidate tanks, the supernatant's PF was calculated at each temperature step using the weighted ratio of corrosion-affecting ions from Section 2.1. Figure 3 shows the PF of every DST's supernatant as they are heated to 50 °C, have their vapor phase ejected, then cooled back down to 25 °C at a constant pressure of 60 Torr. A drop in pitting factor is visible at approximately 45 °C, the point at which the supernatant typically begins to evaporate. At these higher temperatures, the existing solid gibbsite deposits appear to react with free hydroxide ions in the solution to form hydroxyaluminate ions, temporarily reducing the pitting factor by consuming OH^-. Once the solution is cooled, the hydroxyaluminate ions will dissociate back into gibbsite and OH^-, restoring the pitting factor. Three of the precipitating solids that appear in Table 8 contain fluoride, and as these solids form, aqueous fluoride is depleted and pitting factor will increase. This occurrence is most visible in AW-103, which has the highest concentration of fluoride compared to the other tanks. Figure 3 and Table 14 show that little change occurs to the supernatant PF as the waste is concentrated in seven of the tanks, but a large jump in PF is visible in AW-103 as fluoride

drops out of the solution and all three of the fluoride-containing solids are formed. The results of both OLI recipes are shown, but the reduced hydroxide version is likely to be more accurate because the free OH^- concentration of the generated recipes conform to the BBI data.

As OLI only provides the steady-state results for the solution, the reaction kinetics are not immediately evident, and the waste may exist at a lower PF for an extended period of time. However, it is unlikely that the supernatant would develop a PF that is lower than the minimum predicted value from the simulations. Table 15 shows the lowest calculated PF of each DST supernatant simulation. Tanks AP-101, AW-102, AW-103 and AY-101 develop a PF between 1 and 2 at some point during the temperature survey, but the minimum PF is closer to 2 than 1, indicating only a slight increase in pitting chance. Of the four tanks, AY-101 would have the greatest chance for pitting, and only if the precipitation/dissolution kinetics require a long timespan for stabilization.

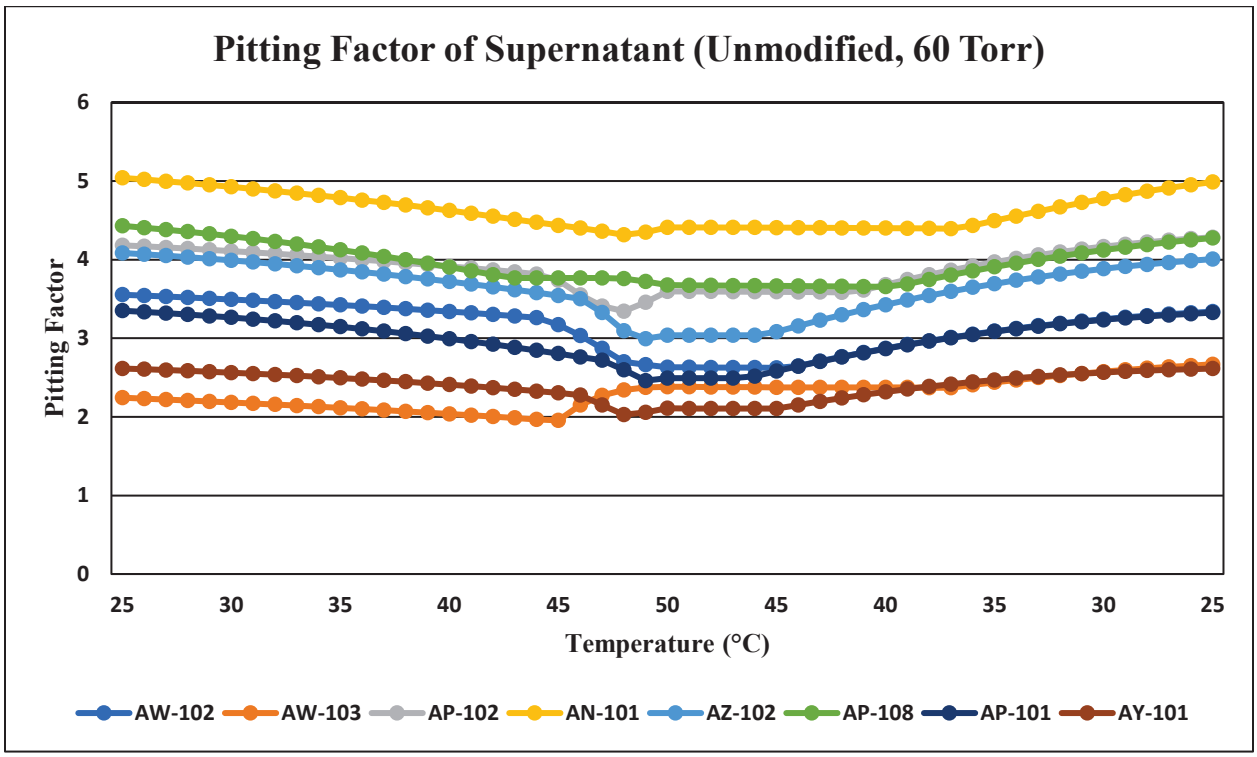

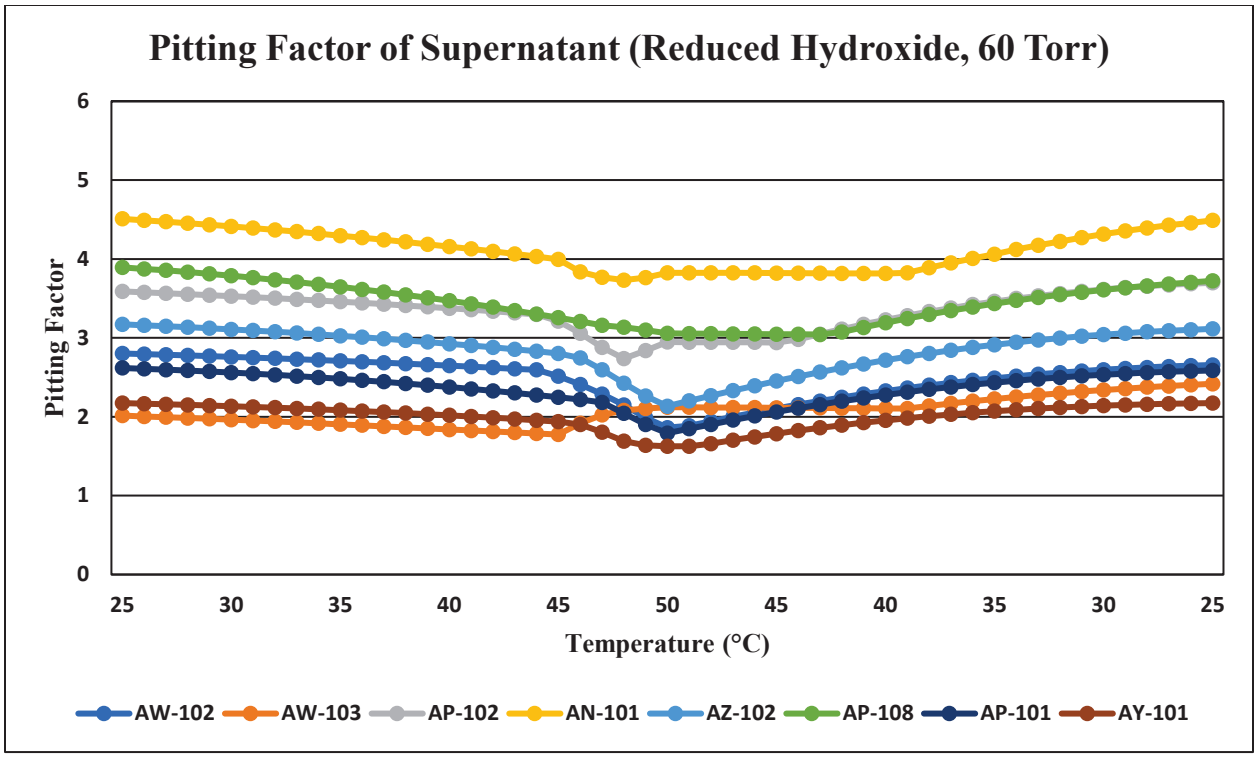

Figure 3. PF of candidate tank supernatants during the evaporation cycle

Table 14. Pitting factor of tank supernatant at 25°C, 760 Torr, before and after vacuum evaporation

a) Unmodified Recipe

Tank	Initial PF	Evaporated PF
AN-101	5.04	4.98
AP-101	3.35	3.32
AP-102	4.18	4.28
AP-108	4.43	4.28
AW-102	3.55	3.34
AW-103	2.24	2.67
AY-101	2.61	2.61
AZ-102	4.09	4.00

b) Reduced OH Recipe

Tank	Initial PF	Evaporated PF
AN-101	4.51	4.49
AP-101	2.62	2.59
AP-102	3.59	3.70
AP-108	3.89	3.72
AW-102	2.80	2.66
AW-103	2.01	2.42
AY-101	2.17	2.17
AZ-102	3.17	3.12

Table 15. Minimum pitting factor of each supernatant during evaporation

a) Unmodified Recipe

Tank	Minimum PF
AN-101	4.32
AP-101	2.46
AP-102	3.34
AP-108	3.66
AW-102	2.62
AW-103	1.96
AY-101	2.03
AZ-102	2.99

b) Reduced OH Recipe

Tank	Minimum PF
AN-101	3.73
AP-101	1.79
AP-102	2.74
AP-108	3.04
AW-102	1.86
AW-103	1.77
AY-101	1.63
AZ-102	2.13

4.4 Organic Vaporization

Appendix B shows the full list of the 132 organics that are potentially present, as well as the percent removal in concentration after each one was individually simulated into the recipe. Not every organic could be entered into OLI: 22 of the LDR organic CAS numbers do not exist in OLI's AQ framework, and 21 of the

LDR organics are expected to be untreatable with a vacuum due to having low pKa values. As a result, only 89 compounds could be simulated in OLI.

The least volatile LDR organic compound that previous experimental testing has shown to be vaporizable from a waste solution is N-nitrosomorpholine, setting an H_v threshold value [7]. Out of the 89 simulated compounds, only one is theorized to be nonvolatile, and the remaining 88 are expected to vaporize. OLI Studio supported the prediction for all but six compounds: discrepancies arose in the LDR organics listed in Table 16, which includes the simulated compound suspected to be nonvolatile (dibenzo[a,h]anthracene).

Table 16. Organic compounds with discrepancies in anticipated volatility

Organic	CAS	H_v (atm-m3 / mol)	OLI H_v at 1% volume reduction (atm-m3 / mol)
Anthracene	120-12-7	6.50E-05	1.15E-07
1,4-Dinitrobenzene	100-25-4	2.27E-07	3.08E-08
bis(2-Chloroethoxy)methane	111-91-1	3.76E-07	3.17E-09
Di-n-octyl phthalate	117-84-0	5.48E-06	5.13E-11
Butyl benzyl phthalate	85-68-7	1.26E-06	4.14E-11
Dibenzo[a,h]anthracene	53-70-3	1.48E-08	1.39E-05

OLI does not automatically provide Henry's law constants for every organic compound, but the value can be calculated using the simulated organic's partial pressure and concentration in the solution. For the first five organics in the table, their H_v values are several orders of magnitude smaller than the theoretical values, causing them to behave as a nonvolatile when volatility is expected. Likewise, dibenzo[a,h]anthracene's H_v is several orders of magnitude higher in OLI than expected, causing it to behave as a volatile in the simulation.

Without further verification, it is difficult to determine the cause of these discrepancies, as most organic compounds only exist in the AQ framework. As an example, anthracene is one of the few compounds that exist in both OLI's MSE and AQ frameworks. When 0.01 M of anthracene was simulated in DI water, the AQ framework gave H_v values in the order of 10^{-7} - 10^{-8}, but the MSE framework provided values around 10^{-4} - 10^{-5}, more closely aligned with the literature. When 5 M of NaCl was added to the solution, anthracene in the AQ framework experienced little change in H_v, but displayed a significant reduction in solubility in the MSE framework, a result of simulated ionic effects on the organic solubility.

5.0 Conclusions

OLI simulations of vacuum evaporation of DST waste were performed after generating recipes using the ionic concentrations found in the supernatant BBI data. Tanks that had characteristics below the TSCR pre-treatment WAC were first considered, but because the existing waste is high in both density and Na^+/K^+ concentrations, the WAC will limit the amount of volume reduction that would occur. An exercise was performed to show that only six DSTs are eligible for evaporation, and the total volume reduction will be under 1 Mgal, less than the capacity of a single tank. Ion concentrations are more of a limiting factor than supernatant density and will breach the WAC sooner.

When only density was considered and after excluding tanks that are ineligible for evaporation (due to factors listed in Table 2), a list of eight DSTs was created. Under conditions of 60 Torr and 50 °C, an approximate theoretical total of 3 million gallons of supernatant can be reduced, a volume equivalent to the construction of 2-3 double shell tanks. The theoretical total is not an optimized number: volume could be further reduced at lower pressures and higher temperatures, but will lead to further growth in the

supernatant density and the Na^+/K^+ concentrations to levels that would be difficult to manage even outside of an existing WAC.

Generating the supernatant recipes for each DST revealed that much of the aluminum and oxalate content is expected to scale, but the volume of these "initial supernatant solids" is small relative to the supernatant volume (albeit in units of kgals). Evaporation of the supernatant did simulate the formation of seven unique solid compounds, but the amount generated is not significant compared to the few million gallons of liquid that is removed. Although additional analysis would be needed, the amount of solids formed is not expected to push a tank into Waste Group A status. The OLI simulations are not able to suggest how the solids would be distributed through the waste; assuming every solid species settles to the bottom waste layers without any changes to density, Figure 4 visualizes the volume changes to the liquid and solid waste layers inside the tanks after evaporation has occurred.

Corrosivity of the tanks was analyzed by performing pitting factor calculations with the concentrations of corrosion-inhibiting and corrosion-encouraging ions. As the waste is heated, PF is expected to initially decrease, but rise once the solution is cooled. Precipitation of solids will consume free OH^- and F^- ions, which creates a decrease and increase in PF respectively. Most tanks experienced very little change to PF, but a dramatic increase was visible in AW-103 as the high concentration of fluoride lead to a greater precipitation of fluoride-containing minerals, causing the concentrate to become less corrosive. No supernatant is expected to develop a greater risk of pitting as a result of these specific evaporation conditions.

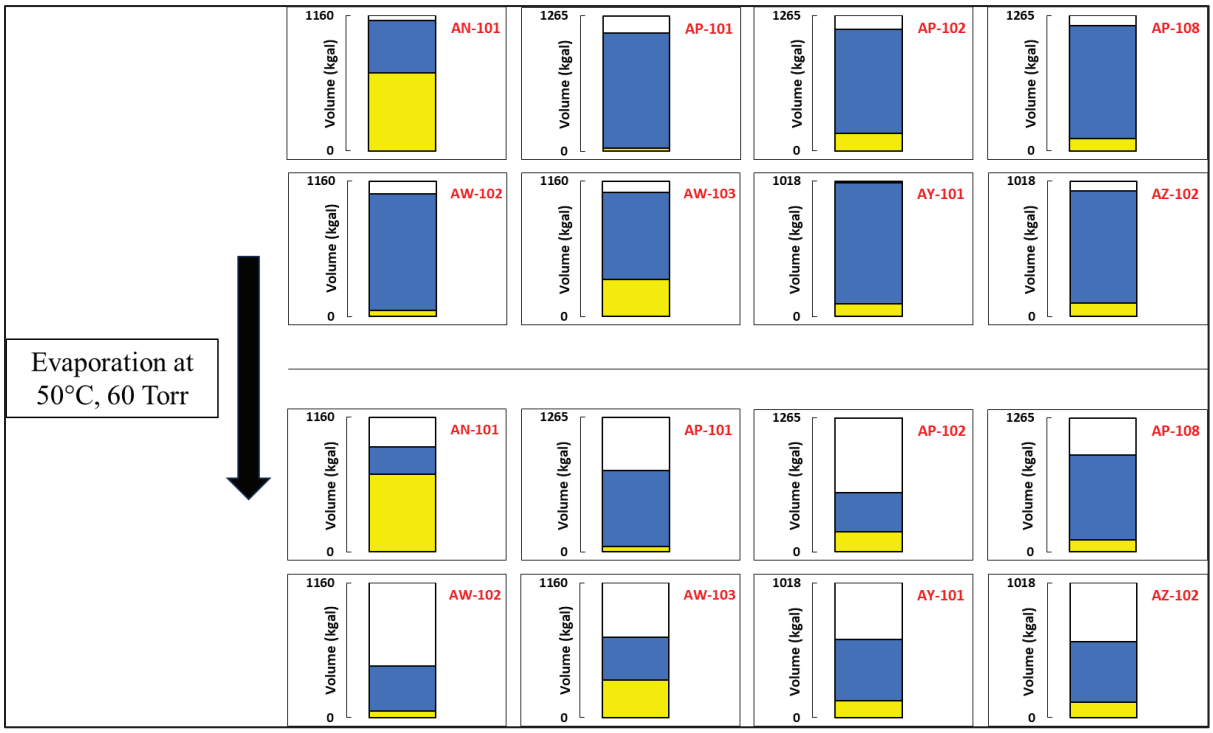

Figure 4. Tank waste volume before and after vacuum evaporation. Blue layers represent the liquid supernatant, yellow layers represent non-supernatant waste.

Analysis of organic vaporization was done on a single blended supernatant recipe from SY farm. In contrast to the volume simulations, the organic vaporization simulations were done under the AQ framework due to its larger chemical databank supporting a greater range of organics. Only 89 of the 132 potentially present LDR organics exist within the OLI AQ library. Virtually all of the 89 organics that were simulated in OLI

were predicted to be volatile, but discrepancies between the expected behavior and simulated behavior were visible in a few compounds. When the Henry's law constant was calculated using OLI's simulated values, they were found to be much smaller than what is reported in the literature. Appendix B lists the compounds in order of volatility (obtained from literature), but the percent change in each compound is scattered, and it is not clear if any unexpected removal rates are a result of simulated salting effects or possible shortcomings in the OLI calculations. A significant factor in this uncertainty is the solvent that is used: literature values for H_v are often reported with water as a solvent and at 25 °C, but the simulation uses a concentrated salt solution with temperatures above 40 °C; the resultant impact that the solvent difference has on solubility is uncertain. Additional work is needed to verify that the calculated Henry's law constants are accurate for each attempted compound, and to determine if OLI is correctly simulating both vapor-liquid equilibria, organic partitioning between phases, and ionic interactions.

Communications with H2C has revealed that evaporation campaigns were being considered for the eight candidate tanks even before the writing of this report, and are expected to begin in the near future. Although the results in this simulation predict a 3 Mgal gain in space, this value is specific only to the temperature and pressure parameter utilized in this report, and actual yields will vary based on the true number of tanks that are evaporated, the exact temperature and pressure values used for each tank, and the potential presence of other limiting factors that could reduce the volume yield. Note that future tank transfers are also likely to occur. By the time an evaporation campaign will begin, transfers will have caused the BBI data to change, and the OLI simulations created for this report will not precisely represent the waste characteristics in the future. Although the simulation results are likely to become out-of-date over time, they may still be used as a proof of concept, revealing that significant gains in storage space are possible with minimal adverse effects on solid formation and corrosivity.

6.0 References

[1] P. J. Certa, P. A. Empey and M. N. Wells, *River Protection Project System Plan*, ORP-11242 Rev. 06, 2011
[2] J. W. Templeton and V. C. Nguyen, *Preliminary 200 West Area Flowsheet*, RPP-RPT-64319 Rev. 01, 2024
[3] *Follow-on Report of Analysis of Approaches to Supplemental Treatment of Low-Activity Waste at the Hanford Nuclear Reservation*, SRNL-STI-2023-00007, Volume I, Revision 0, 2023
[4] B. J. Wiersma, R. E. Fuentes and L. M. Stock, *Chemistry Envelope for Pitting and Stress Corrosion Cracking Mitigation*, SRNL-STI-2019-00217, 2019
[5] R. S. Skeen, *Tank Waste LDR Organics Data Summary for Sample-and-Send*, RPP-RPT-63493 Rev. 1A, 2022
[6] R. S. Skeen, *Distribution of LDR Organic Compounds in Hanford Tanks Waste and The Implications to LAW Treatment by Cementitious Solidification/Stabilization*, RPP-RPP-64064 Rev. 00, 2022
[7] J. R. Dekarske, S. C. Hunter, M. J. Siegfried, F. F. Fondeur, T. L. White, L. N. Oji and R. S. Skeen, *Organic Evaporation, Oxidation, and Hydrolysis Testing in Support of Hanford Sample-and-Send*, SRNL-STI-2023-00596 Rev. 01, 2024
[8] Z. Jaworski, M. Czernuszewicz and Ł. Gralla, *A Comparative Study of Thermodynamic Electrolyte Models Applied to the Solvay Soda System,* Chem. Process Eng., 32(2):135-154, 2011
[9] *Selecting an OLI thermodynamic framework for oil and gas production,* OLI Systems Inc., 2017

Appendix A. OLI Recipe Reconciliation

			OLI Recipe Output OH^- Concentration [M]		OLI Recipe Density (g/mL)	
Tank	Initial OH^- [M]	Reduced OH^- [M]	No Reduction	With Reduction	No Reduction	With Reduction
AN-101	1.37017	1.1582	1.55516	1.37014	1.24114	1.23356
AP-101	1.093850	0.63695	1.48079	1.09383	1.33172	1.31567
AP-102	0.747555	0.5705	0.90578	0.747535	1.21416	1.20781
AP-106	0.716274	0.45886	0.947288	0.716275	1.25689	1.24787
AP-107	0.810509	0.56299	1.0335	0.810503	1.24362	1.23489
AP-108	1.759100	1.4203	2.0419	1.75915	1.32463	1.31269
AW-102	0.695126	0.43975	0.927778	0.695135	1.18988	1.18052
AW-103	0.936514	0.8119	1.04845	0.936515	1.23171	1.22759
AY-101	0.647804	0.441875	0.828157	0.647802	1.28299	1.27578
AZ-102	1.025850	0.60472	1.39258	1.0258	1.27937	1.26455
SY-102	0.311808	0.20106	0.412962	0.3118	1.18652	1.18254

		Reconciliation Amount [M]		Reconciled Na^+ [M]	
Tank	Initial Na^+ [M]	No OH^- Reduction	With OH^- Reduction	No OH^- Reduction	With OH^- Reduction
AN-101	5.4147	0.071019	-0.14095	5.485719	5.27375
AP-101	7.38369	0.333829	-0.12307	7.717519	7.26062
AP-102	4.64396	0.0724903	-0.104564	4.71645	4.539396
AP-106	5.78303	-6.05E-02	-0.31787	5.722573	5.46516
AP-107	5.41286	-0.0586956	-0.306215	5.354164	5.106645
AP-108	6.31149	1.17187	0.83307	7.48336	7.14456
AW-102	4.22203	-0.127378	-0.382754	4.094652	3.839276
AW-103	4.64444	0.275905	0.151291	4.920345	4.795731
AY-101	6.17054	0.185073	-0.0208564	6.355613	6.149684
AZ-102	6.01413	0.467871	0.0467452	6.482001	6.060875
SY-102	3.69455	0.293244	0.182496	3.987794	3.877046

Appendix B. Organic Removal

The list of 132 potentially present LDR compounds, in addition to their CAS numbers, is shown below. Each compound began with an arbitrary 100 mg/L starting point in the simulation. "DNE" entries are for compounds that do not have representative data in OLI. "pKa" entries indicate compounds that would fully dissociate and are untreatable by evaporation. Organic compounds that deviated from their expected behavior under vacuum are highlighted in red. Compounds are listed in decreasing order of Henry's law constants, beginning with the most volatile compound.

			Concentration Change (%)			
Number	Compound	CAS	45.31°C	45.53°C	45.84°C	46.21°C
1	1,1,2-Trichloro-1,2,2-trifluroethane	76-13-1	-100.00	-100.00	-100.00	-100.00
2	Trichlorofluoromethane	75-69-4	-99.99	-100.00	-100.00	-100.00
3	Carbon tetrachloride	56-23-5	-99.97	-99.99	-99.99	-100.00
4	Vinyl chloride	75-01-4	-99.96	-99.98	-99.99	-99.99
5	1,1-Dichloroethylene	75-35-4	-99.99	-100.00	-100.00	-100.00
6	1,1,1-Trichloroethane	71-55-6	-99.95	-99.98	-99.99	-99.99
7	Tetrachloroethylene	127-18-4	-99.96	-99.99	-99.99	-100.00
8	Hexachlorocyclopentadiene	77-47-4	-99.95	-99.98	-99.99	-99.99
9	Hexachlorobutadiene	87-68-3	-99.99	-100.00	-100.00	-100.00
10	Chloroethane	75-00-3	-99.95	-99.98	-99.99	-99.99
11	Trichloroethylene	79-01-6	-99.92	-99.97	-99.98	-99.99
12	Chloromethane	74-87-3	-99.98	-99.99	-100.00	-100.00
13	2-Chloroethyl vinyl ether	110-75-8	-98.95	-99.59	-99.79	-99.87
14	3-Chloropropylene	107-05-1	-99.97	-99.99	-99.99	-100.00
15	Ethyl benzene	100-41-4	-99.91	-99.96	-99.98	-99.99
16	Toluene	108-88-3	-99.88	-99.95	-99.97	-99.98
17	1,1-Dichloroethane	75-34-3	-99.85	-99.94	-99.97	-99.98
18	Benzene	71-43-2	-99.86	-99.94	-99.97	-99.98
19	Chloroform	67-66-3	-99.77	-99.91	-99.95	-99.97
20	Hexachloroethane	67-72-1	-99.95	-99.98	-99.99	-99.99
21	trans-1,3-Dichloropropylene	10061-02-6	-99.48	-99.80	-99.90	-99.93
22	Chlorobenzene	108-90-7	-99.69	-99.88	-99.94	-99.96
23	1,3-Dichlorobenzene	541-73-1	-99.80	-99.93	-99.96	-99.98
24	cis-1,3-Dichloropropylene	10061-01-5	-99.86	-99.95	-99.97	-99.98
25	1,2,4,5-Tetrachlorobenzene	95-94-3	-99.99	-100.00	-100.00	-100.00
26	1,1,1,2-Tetrachloroethane	630-20-6	-99.70	-99.89	-99.94	-99.96
27	Methylene chloride	75-09-2	-99.79	-99.92	-99.96	-99.97
28	1,2,4-Trichlorobenzene	120-82-1	-99.76	-99.91	-99.95	-99.97
29	1,4-Dichlorobenzene	106-46-7	-99.77	-99.91	-99.95	-99.97
30	1,2-Dichlorobenzene	95-50-1	-99.74	-99.90	-99.95	-99.97
31	1,2-Dichloroethane	107-06-2	-99.13	-99.66	-99.82	-99.89
32	1,1,2-Trichloroethane	79-00-5	-99.14	-99.67	-99.83	-99.89
33	Ethyl Ether	60-29-7	-99.32	-99.73	-99.86	-99.91
34	1,2-Dibromoethane/Ethylene dibromide	106-93-4	-98.79	-99.54	-99.76	-99.85

35	Naphthalene	91-20-3	-99.07	-99.64	-99.81	-99.88
36	Aldrin	309-00-2	-68.00	-85.63	-92.17	-95.06
37	Nitrobenzene	98-95-3	-52.41	-74.87	-85.19	-90.18
38	1,1,2,2-Tetrachloroethane	79-34-5	-98.74	-99.52	-99.75	-99.84
39	2-Chloronaphthalene	91-58-7	-98.94	-99.60	-99.80	-99.87
40	4-Methyl-2-pentanone	108-10-1	-99.80	-99.92	-99.96	-99.97
41	Ethyl acetate	141-78-6	-95.61	-98.24	-99.08	-99.42
42	Methacrylonitrile	126-98-7	-96.53	-98.58	-99.25	-99.53
43	Acenaphthene	83-32-9	-97.75	-99.15	-99.56	-99.73
44	Acrolein	107-02-8	-94.73	-97.79	-98.82	-99.25
45	4-Bromophenyl phenyl ether	101-55-3	-97.23	-98.97	-99.47	-99.67
46	Acenaphthylene	208-96-8	-96.51	-98.67	-99.31	-99.57
47	Acrylonitrile	107-13-1	-93.21	-97.12	-98.46	-99.02
48	Anthracene	120-12-7	-	-	-	-
49	Fluorene	86-73-7	-97.16	-98.92	-99.43	-99.64
50	2-Butanone	78-93-3	-88.78	-95.26	-97.46	-98.39
51	Acetone	67-64-1	-76.26	-89.07	-93.97	-96.12
52	Phenanthrene	85-01-8	-87.22	-94.84	-97.28	-98.28
53	p,p′-DDE	72-55-9	-66.16	-84.57	-91.56	-94.67
54	Heptachlor epoxide	1024-57-3	-3.41	-7.45	-13.71	-21.51
55	Acetonitrile	75-05-8	-77.85	-89.54	-94.19	-96.24
56	Fluoranthene	206-44-0	-85.24	-94.07	-96.90	-98.08
57	bis(2-Chloroethyl)ether	111-44-4	-76.47	-89.73	-94.41	-96.43
58	bis(2-ethylhexyl)phthalate	117-81-7	-10.86	-24.85	-39.84	-52.66
59	Pyrene	129-00-0	-73.91	-88.55	-93.75	-96.01
60	p,p′-DDT	50-29-3	-99.96	-99.99	-99.99	-100.00
61	p,p′-DDD	72-54-8	-1.34	-1.82	-3.56	-7.04
62	Isobutyl alcohol	78-83-1	-97.22	-98.87	-99.40	-99.61
63	Dieldrin	60-57-1	-54.53	-77.15	-86.99	-91.65
64	alpha-BHC	319-84-6	-98.76	-99.54	-99.76	-99.85
65	Cyclohexanone	108-94-1	-50.01	-72.90	-83.87	-89.28
66	n-Butyl alcohol	71-36-3	-70.12	-85.94	-92.16	-94.95
67	Pyridine	110-86-1	-29.49	-52.95	-68.43	-77.59
68	Acetophenone	98-86-2	-50.45	-73.40	-84.22	-89.53
69	Di-n-octyl phthalate	117-84-0	-	-	-	-
70	3-Methylcholanthrene	56-49-5	-10.76	-24.62	-39.50	-52.27
71	Chrysene	218-01-9	-95.46	-98.30	-99.13	-99.47
72	delta-BHC	319-86-8	-95.49	-98.30	-99.12	-99.45
73	Methanol	67-56-1	-44.23	-66.79	-79.31	-85.92
74	1,4-Dioxane	123-91-1	-38.83	-63.09	-76.72	-84.04
75	Benz(a)anthracene	56-55-3	-87.56	-95.11	-97.47	-98.44
76	gamma-BHC	58-89-9	-82.86	-92.98	-96.24	-97.60
77	N-Nitrosodimethylamine	62-75-9	-1.08	-1.20	-2.76	-6.48

78	Indeno(1,2,3-c,d) pyrene	193-39-5	-36.34	-61.60	-76.13	-84.04
79	Butyl benzyl phthalate	85-68-7	-	-	-	-
80	Benzo(b)fluoranthene	205-99-2	-39.34	-64.55	-78.34	-85.64
81	Benzo(k)fluoranthene	207-08-9	-39.37	-64.57	-78.36	-85.66
82	di-n-Butyl phthalate	84-74-2	-13.63	-30.14	-46.11	-58.65
83	bis(2-Chloroethoxy)methane	111-91-1	-	-	-	-
84	beta-BHC	319-85-7	-99.84	-99.94	-99.97	-99.98
85	Diethyl phthalate	84-66-2	-3.37	-7.32	-13.41	-20.96
86	1,4-Dinitrobenzene	100-25-4	-	-	-	-
87	Benzo(g,h,i)perylene	191-24-2	-71.29	-87.41	-93.22	-95.76
88	Dimethyl phthalate	131-11-3	-2.05	-3.75	-7.02	-11.90
89	Dibenzo(a,h)anthracene	53-70-3	-18.53	-38.80	-55.96	-68.00
90	Xylene(m,p,o)	1330-20-7	DNE	DNE	DNE	DNE
91	Hexachlorobenzene	118-74-1	DNE	DNE	DNE	DNE
92	Pentachloronitrobenzene	82-68-8	DNE	DNE	DNE	DNE
93	N-Nitroso-di-n-butylamine	924-16-3	DNE	DNE	DNE	DNE
94	Aroclors	1336-36-3	DNE	DNE	DNE	DNE
95	Isodrin	465-73-6	DNE	DNE	DNE	DNE
96	Ethyl cyanide/Propanenitrile	107-12-0	DNE	DNE	DNE	DNE
97	Endrin aldehyde	7421-93-4	DNE	DNE	DNE	DNE
98	N-Nitrosodiethylamine	55-18-5	DNE	DNE	DNE	DNE
99	2,4-Dimethylaniline (2,4-xylidine)	95-68-1	DNE	DNE	DNE	DNE
100	N-Nitroso-di-n-propylamine	621-64-7	DNE	DNE	DNE	DNE
101	N-Nitrosomethylethylamine	10595-95-6	DNE	DNE	DNE	DNE
102	4-Chloroaniline	106-47-8	DNE	DNE	DNE	DNE
103	N-Nitrosopiperidine	100-75-4	DNE	DNE	DNE	DNE
104	p-Cresidine	120-71-8	DNE	DNE	DNE	DNE
105	Benzo(a)pyrene	50-32-8	DNE	DNE	DNE	DNE
106	Diphenylamine	122-39-4	DNE	DNE	DNE	DNE
107	2-Naphthylamine	91-59-8	DNE	DNE	DNE	DNE
108	2-Nitroaniline	88-74-4	DNE	DNE	DNE	DNE
109	N-Nitrosopyrrolidine	930-55-2	DNE	DNE	DNE	DNE
110	N-Nitrosomorpholine	59-89-2	DNE	DNE	DNE	DNE
111	4-Nitroaniline	100-01-6	DNE	DNE	DNE	DNE
112	Cresols (m,p,o)	1319-77-3	pKa	pKa	pKa	pKa
113	Phthalic acid	100-21-0	pKa	pKa	pKa	pKa
114	2,4,5-Trichlorophenoxyacetic acid/2,4,5-T	93-76-5	pKa	pKa	pKa	pKa
115	2,4-Dinitrotoluene	121-14-2	pKa	pKa	pKa	pKa
116	2-Nitrophenol	88-75-5	pKa	pKa	pKa	pKa
117	2,4,6-Trichlorophenol	88-06-2	pKa	pKa	pKa	pKa
118	2-Chlorophenol	95-57-8	pKa	pKa	pKa	pKa
119	2,3,4,6-Tetrachlorophenol	58-90-2	pKa	pKa	pKa	pKa
120	p-Chloro-m-cresol	59-50-7	pKa	pKa	pKa	pKa

121	2,4-Dimethyl phenol	105-67-9	pKa	pKa	pKa	pKa
122	2,4,5-Trichlorophenol	95-95-4	pKa	pKa	pKa	pKa
123	2,4-Dichlorophenol	120-83-2	pKa	pKa	pKa	pKa
124	4,6-Dinitro-o-cresol	534-52-1	pKa	pKa	pKa	pKa
125	o-Cresol	95-48-7	pKa	pKa	pKa	pKa
126	m-Cresol (difficult to distinguish from p)	108-39-4	pKa	pKa	pKa	pKa
127	p-Cresol (difficult to distinguish from m)	106-44-5	pKa	pKa	pKa	pKa
128	Pentachlorophenol	87-86-5	pKa	pKa	pKa	pKa
129	2-sec-Butyl-4,6-dinitrophenol/Dinoseb	88-85-7	pKa	pKa	pKa	pKa
130	Phenol	108-95-2	pKa	pKa	pKa	pKa
131	2,4-Dinitrophenol	51-28-5	pKa	pKa	pKa	pKa
132	p-Nitrophenol	100-02-7	pKa	pKa	pKa	pKa

Distribution:

SRNL
connie.herman@srnl.doe.gov
joseph.manna@srnl.doe.gov
morgana.whiteside@srnl.doe.gov
pavan.shukla@srnl.doe.gov
bruce.wiersma@srnl.doe.gov
benjamin.barkai@srnl.doe.gov
kiana.sykes@srnl.doe.gov
chris.martino@srnl.doe.gov
charles.james@srnl.doe.gov
michael.stone@srnl.doe.gov
Records Administration (EDWS)

DOE
em-labcall@em.doe.gov
ming.zhu@em.doe.gov
john.t.kelly@em.doe.gov

H2C
jason_s_page@rl.gov
shawn_t_campbell@rl.gov
jason_r_gunter@rl.gov
kayle_d_boomer@rl.gov
melinda_r_fagundes@rl.gov
stephanie_r_doll@rl.gov
david_j_swanberg@rl.gov
rodney_s_skeen@rl.gov
zabrina_b_smith@rl.gov

Distribution:

SRNL
connie.herman@srnl.doe.gov
joseph.manna@srnl.doe.gov
morgana.whiteside@srnl.doe.gov
pavan.shukla@srnl.doe.gov
bruce.wiersma@srnl.doe.gov
benjamin.barkai@srnl.doe.gov
kiana.sykes@srnl.doe.gov
chris.martino@srnl.doe.gov
charles.james@srnl.doe.gov
michael.stone@srnl.doe.gov
Records Administration (EDWS)

DOE
em-labcall@em.doe.gov
ming.zhu@em.doe.gov
john.t.kelly@em.doe.gov

H2C
jason_s_page@rl.gov
shawn_t_campbell@rl.gov
jason_r_gunter@rl.gov
kayle_d_boomer@rl.gov
melinda_r_fagundes@rl.gov
stephanie_r_doll@rl.gov
david_j_swanberg@rl.gov
rodney_s_skeen@rl.gov
zabrina_b_smith@rl.gov